

NEW LOW COST AND GREEN COMPOSITE BINDER FOR
CONSTRUCTION

by
POZHHAN MOKHTARI

Submitted to Graduate School of Engineering and Natural Sciences
in partial fulfillment of
the requirement for the degree of
Doctor of Philosophy

Sabanci University

Spring 2019

NEW LOW COST AND GREEN COMPOSITE BINDER FOR
CONSTRUCTION

APPROVED BY:

Prof. Dr. Mehmet Ali Gulgun
(Dissertation Supervisor)



Prof. Dr. Cleve Ow-Yang



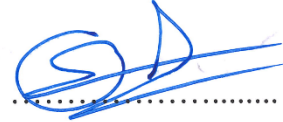
Assist. Dr. Zeynep Basaran Bundur



Prof. Dr. Melih Papila



Prof. Dr. Sedat Alkoy



DATE OF APPROVAL: 19.07.2019

TO MY WIFE AND DAD

© POZHHAN MOKHTARI 2019

All Rights Reserved

ABSTRACT

NEW LOW COST AND GREEN COMPOSITE BINDER FOR CONSTRUCTION

Pozhhan Mokhtari

Materials Sciences and Engineering, PhD Dissertation, 2019

Supervisor: Prof. Dr. Mehmet Ali Gulgun

Keywords: Supplementary Cementitious Materials, Calcined Schist, Calcined Carbonate, Pozzolanic Reactivity, Cement Substitution

One of the most promising ways to make cement and concrete more sustainable is to blend them with the proper supplementary cementitious materials (SCM). This study evaluates several schist type materials as partial replacement for ordinary Portland cement (OPC). Materials received from several mines in ground powder form were studied by X-ray diffraction, thermogravimetry (TGA), and scanning electron microscopy (SEM). According to the TGA results, the activation procedures for the candidate SCMs were determined. This dissertation includes two main phases. For the first step that is named as calcined clay cement (C^3), the virgin powders were heat treated in three different decomposition regimes (30%,

50% and 80% of the total weight losses during thermal decomposition). These regimes correspond to the activation level of the potential SCMs due to the de-hydroxylation of the clayey minerals within them. Pozzolanic reactivity (pozzolanicity) of untreated as well as treated powders were estimated via electrical conductivity measurements in calcium hydroxide solution. Blended cement pastes with 30 wt% of OPC substitution with calcined overburden clayey materials have developed mechanical properties equal to pure cement (100wt% OPC) paste after 28 days of setting time. Two blended cement pastes prepared with candidate SCMs were compared to 100% OPC (C) and OPC composite paste with Meta-Kaolinite (MK) which is regarded as literature standard. For the second phase of project is named as limestone calcined clay and carbonate cement (LC⁴), the same scenario by considering the best activation temperature is carried out. The results represent the possibility of reactivation of any kind of clay class for the ordinary Portland cement partial substitution and obtaining the compressive strength as well as OPC.

ÖZET

İNŞAAT İÇİN YENİ DÜŞÜK MALİYET VE YEŞİL KOMPOZİT BİNDER

Pozhhan Mokhtari

Malzeme Bilimleri ve Mühendisliği, Doktora Tezi, 2019

Tez Danışmanı: Prof. Dr. Mehmet Ali Gülgün

Anahtar Kelimeler: Yardımcı Çimento Malzemeleri, Kalsine Şist, Kalsine Karbonat, Pozolanik Reaktivite, Çimento İkame

Çimento ve betonu daha sürdürülebilir hale getirmenin en umut vaat eden yollarından biri, bunları uygun ek çimento materyalleri (SCM) karıştırmaktır. Bu çalışma sıradan Portland çimentosu (OPC) için kısmi ikame olarak çeşitli şist tipi malzemeleri değerlendirmektedir. Öğütülmüş toz formundaki birkaç mayından alınan malzemeler, X-ışını difraksiyonu, termogravimetri (TGA) ve taramalı elektron mikroskobu (SEM) ile incelenmiştir. TGA sonuçlarına göre, aday SCM'lerin aktivasyon prosedürleri belirlendi. Bu tez iki ana aşamadan oluşmaktadır. Kalsine killi çimento (C^3) olarak adlandırılan ilk adım için, ham tozları üç farklı ayrışma rejiminde (ısıl ayrışma sırasında toplam ağırlık kayıplarının % 30, % 50 ve % 80'i) ısıl işlem görmüştür. Bu rejimler, içlerindeki killi

minerallerin hidroksilasyonundan dolayı potansiyel SCM'lerin aktivasyon seviyesine karşılık gelir. İşlem görmemiş tozların yanı sıra işlenmemiş tozların puzolanik reaktivitesi (puzolanisite), kalsiyum hidroksit çözeltisindeki elektriksel iletkenlik ölçümleri ile tahmin edilmiştir. % 30 oranında OPC ikamesi ile kalsine edilmiş aşırı killi killi malzemelerle harmanlanmış harmanlanmış çimento pastaları, 28 gün ayar süresinin ardından saf çimento (% 100 ağırlıkça OPC) macununa eşit mekanik özellikler geliştirmiştir. Aday SCM'lerle hazırlanan iki harçlı çimento macunu, % 100 OPC (C) ve literatür standardı olarak kabul edilen Meta-Kaolinit (MK) ile OPC kompozit macun ile karşılaştırıldı. Projenin ikinci aşaması ise kireçtaşı kalsine kil ve karbonat çimentosu (LC⁴) olarak adlandırılır, aynı senaryo en iyi aktivasyon sıcaklığı dikkate alınarak gerçekleştirilir. Sonuçlar, sıradan Portland çimentosunun kısmi ikamesi için herhangi bir kil sınıfının yeniden aktifleştirilmesi ve OPC'nin yanı sıra basınç dayanımının elde edilme olasılığını temsil eder.

ACKNOWLEDGMENT

Foremost, I would like to express my sincere gratitude to Prof. Dr. Mehmet Ali Gulgun for giving me the chance to work in exceptional condition. Thank you for supervising my research, your support, comments to streamline my work. Thanks for your dynamism, energy and flexibility toward my attitude. I profoundly recommend working with him for any university professors and researchers to know how to grow up the graduate student.

My special thanks go to Prof. Dr. Melih Papila, Prof. Dr. Cleva Ow. Yang and Dr. Zeynep Basaran for their subtle and firm support during my PhD.

More generally, I would like to thank AkcanSA cement manufacture for their financial support during my PhD and the R&D office members. We always had very good interactions between Ismail Gokalp, Yasin Engin, Caglar Geven and Irfan Akikol.

I would like to thank the members of the jury for reading of my dissertation and for their useful comments and helped to improve the final document: Prof. Dr. Cleva Ow. Yang, Prof. Dr. Melih Papila, Prof. Dr. Sedar Alkoy, Assist. Prof. Dr. Zeynep Basaran.

I would like to thank my friends at sabanci university. However, I must emphasize mainly thanks to Sorour Semsari Parapari, Kosar HassanNezhad, Noyan Ozkan, Sezen Donmez, Yasemin (Cafer) Akyol and Sirous (Hamid) Khabbaz Abkenar for their helps during my research work.

Finally, my deepest gratitude goes to my caring and supportive wife and family for their love and strength they give me. I have lost my dad during my PhD, but his encouragement is always with me when the times go rough. He is always with me....!

TABLE OF CONTENT

ABSTRACT5
ÖZET7
ACKNOWLEDGMENT9
TABLE OF CONTENT10
LIST OF FIGURES15
LIST OF TABLES25
Glossary30
CHAPTER 131
INTRODUCTION31
1.1 General31
1.2 Objectives of Study34
1.3 Materials and Methods35
1.3.1 Materials35
1.3.1.1 Schist-minerals as possible supplementary cementitious materials (SCMs)35
1.3.1.2 Schist-type materials Studied35
1.3.1.3 Reference Kaolinite and Carbonate Source36
1.3.1.4 Used Ordinary Portland Cement36
1.3.2 Methods37
1.3.2.1 Chemical phase composition analysis37
1.3.2.1.1 X-ray powder diffraction37
1.3.2.1.2 Quantitative Phase Analysis by Rietveld Method37
1.3.2.2 Microstructure Evaluation38
1.3.2.2.1 Imaging with secondary electrons in a scanning electron microscope (SEM)	38
1.3.2.2.2 Elemental Distribution maps with Energy Dispersive Spectroscopy (EDS)	38
1.3.2.3 Thermal Analysis for Determining Activation Process Parameters38
1.3.2.4. Activation of schist-type SCMs by heat-treatment40
1.3.2.4.1 Virgin and Carbonate-Modified SCM alternatives40

1.3.2.5 Calcination Process	40
1.3.2.6 Pozzolanicity Measurement	40
1.3.2.7 Evaluation Compressive Strength of Cement Containing Schist-Type SCM Alternatives	41
1.3.2.7.1 Paste Preparation	41
1.3.2.7.2 Test Specimen Preparation	42
1.3.2.7.3 Compressive Strength Test.....	42
1.3.2.7.4 Measure Strength Data Analysis	42
CHAPTER 2	43
LITERATURE REVIEW.....	43
2.1 Cement manufacture CO ₂ emission.....	43
2.2 Brief History of Binders	44
2.3 Ordinary Portland Cement (OPC)	46
2.4. Supplementary Cementing Materials (SCMs).....	56
2.4.1 Blast Furnace Slag	58
2.4.2. Fly Ash.....	60
2.4.3. Silica Fume	63
2.4.4. Limestone.....	64
2.5. Calcined Clay as SCM.....	65
2.5.1 Clay Minerals.....	65
2.5.2 Kaolinite and Meta-Kaolinite	70
2.6 Clay Reactivity	71
2.6.1 Calcination of Clay	71
2.6.2 Calcination through Thermal Activation	72
2.6.2 Thermal Activation	75
2.7 Limestone Calcined Clay Cement (LC ³).....	77
2.7.2 Limestone and Metakaolin in Blended Cement.....	80
2.8 Using More Complex Clay Structure as SCM	81
CHAPTER 3	83
CALCINED CLAY CEMENT (C ³)	83
3.1. General	83
3.2 Evaluation of Raw Materials (Virgin Powders)	83
3.2.1 Chemical Phase Analysis (X-ray Diffraction and Rietveld).....	84

3.2.1.1 Bozalan Schist.....	84
3.2.1.2 Camlica Schist.....	86
3.2.1.3 Tastepe Schist.....	89
3.2.1.4 Kovukdere Schist	91
3.2.1.5 Muratbey Schist	94
3.2.1.6 Ladik Schist.....	97
3.2.1.7 Pure Kaolinite (Benchmark Sample)	99
3.2.2 Thermogravimetric Analysis (TGA)	102
3.2.2.1 Bozalan Schist.....	103
3.2.2.2 Camlica Schist.....	104
3.2.2.3 Tastep Schist	105
3.2.2.4 Kovukdere Schist	105
3.2.2.5 Muratbey Schist	106
3.2.2.6 Ladik Schist.....	107
3.2.2.7 Kaolinite.....	107
3.2.3 Electrical Conductivity Measurement (Pozzolanicity)	109
3.2.3.1 Bozalan Schist.....	115
3.2.3.2 Camlica Schist.....	116
3.2.3.3 Tastepe Schist.....	117
3.2.3.4 Kovukdere Schist	119
3.2.3.5 Muratbey Schist	120
3.2.3.6 Ladik Schist.....	121
3.2.3.7 Kaolinite.....	122
3.2.4 Microstructure and Composition Analysis (SEM-EDS)	126
3.3. Evaluation of Calcined Schists (Heat-treated and activated Powders)	142
3.3.1 Microstructure and Composition Analysis (SEM-EDS)	142
3.3.2 Pozzolanic Reactions and Heat Treatments.....	154
3.3.3 Phase Analysis, Conductivity Measurements and TGA.....	155
3.3.3.1 Kaolinite.....	156
3.3.3.2 Bozalan Schist.....	159
3.3.3.3 Tastepe Schist.....	162
3.3.3.4 Camlica Schist.....	164
3.3.3.5 Kovukdere Schist	166

3.3.3.6 Muratbey Schist	169
3.3.3.7 Ladik Schist.....	171
3.3.4 Compressive Strength Test	173
3.3.4.1 Calcined Clay Cement (C ³) by heat-treated material up to 30% of WL _T	175
3.3.4.2 Calcined Clay Cement (C ³) by heat-treated material up to 50% of WL _T	176
3.3.4.3 Calcined Clay Cement (C ³) by heat-treated material up to 80% of WL _T	177
3.5 Discussion.....	196
3.6 Conclusion.....	202
CHAPTER 4	203
LIMESTONE CALCINED CLAY and CARBONATE CEMENT (LC ⁴)	203
4.1 General	203
4.2 Experimental.....	205
4.2.1 Materials	205
4.3 Sample Preparation.....	207
4.3.1 Calcined Clay Cement (C ³) Samples	207
4.3.2 Limestone Calcined Clay and Carbonate Cement (LC ⁴) Sample	208
4.3.3 Cement Paste Sample Preparation	208
4.4 Tests and Methods	209
4.4.1 Phase Analysis	209
4.4.2 Thermal Analysis.....	210
4.4.3 Microstructure Analysis.....	210
4.4.4 Compression Test	211
4.5 Results	212
4.5.1 Virgin Materials (Before Activation)	212
4.5.1.1 Phase Distribution	212
4.5.1.1.1 M ₁ - Green	212
4.5.1.1.2 M ₂ – Brown	213
4.5.1.1.3 M ₃ – Pink.....	215
4.5.1.1.4 M ₄ – Black.....	216
4.5.1.2 Activation Process.....	218
4.5.1.2.1 M ₁ -Green	219
4.5.1.2.2 M ₂ -Brown	220
4.5.1.2.3 M ₃ -Pink.....	220

4.5.1.2.4 M ₄ -Black.....	221
4.5.1.3 Microstructure Analysis.....	223
4.5.1.3.1 M ₁ – Green	223
4.5.1.3.2 M ₂ – Brown	227
4.5.1.3.3 M ₃ – Pink.....	229
4.5.1.3.4 M ₄ – Black.....	232
4.5.2 Calcined Materials (C ³ and LC ⁴)	235
4.5.2.1 Phase Distribution and Evolution during activation process	236
4.5.2.1.1 M ₁ with and without 15% CC Addition.....	236
4.5.2.1.2 M ₂ with and without 15% CC Addition.....	238
4.5.2.1.3 M ₃ with and without 15% CC Addition.....	240
4.5.2.1.4 M ₄ with and without 15% CC Addition.....	242
4.5.2.2 Scaling up the Activation Process.....	244
4.5.2.2.1 M ₁ with and without 15% CC Addition.....	245
4.5.2.2.2 M ₂ with and without 15% CC Addition.....	246
4.5.2.2.3 M ₃ with and without 15% CC Addition.....	248
4.5.2.2.4 M ₄ with and without 15% CC Addition.....	250
4.5.2.3 Microstructure Analysis.....	252
4.5.2.3.1 M ₁ with and without 15% CC Addition.....	255
4.5.2.3.2 M ₂ with and without 15% CC Addition.....	257
4.5.2.3.3 M ₃ with and without 15% CC Addition.....	260
4.5.2.3.4 M ₄ with and without 15% CC Addition.....	262
4.5.2 Compressive Strength Measurement	266
4.6 Discussion.....	273
4.7 Conclusion.....	282
CHAPTER 5	284
CONCLUSION	284
REFERENCES	289

LIST OF FIGURES

Figure 1. 1 Schematic of the method which used for finding the proper temperatures for heat treatment.....	39
Figure 2. 1 Typical dry process of cement [16].....	47
Figure 2.2 Classification of cement based on phase composition	49
Figure 2. 3 Heat evolution of cement hydration	51
Figure 2. 4 Hydrated cement paste fracture (after 2 days), needle shaped Ettringite (e); hexagonal plates of calcium hydroxide; calcium silicate hydrate (C-S-H); Left side of image includes porosity and numerous capillary pores (up to 5 μ m); hydration cement particles.....	53
Figure 2. 5 Polished section of hydrated cement paste (after 2 years) for various w/c	54
Figure 2. 6 Slag production: fast-moving stream of water (left), and molten slag flow into the water stream and quenched (right) [54].	59
Figure 2. 7 Pelletized slag production procedure schematic [54].	59
Figure 2. 8 Powerplant station, source of fly ash [35]	61
Figure 2. 9 SEM image of fly ash particles [47].	62
Figure 2. 10 Left: Concrete particle polished section using 70 wt% OPC and 30 wt% fly ash (c: hydrated cement particles, s: silica sand, arrows: fly ash particles). The difference among fly ash particles color is associated to their chemical composition in term of iron content / Right: Concrete particle polished section using 30 wt% OPC and 70 wt% slag (circles: hydrated cement particles, s: sand mainly silica and feldspar, arrow: slag particles); the slag particle color is almost same [62].	63
Figure 2. 11 Transportation of sediments and erosion of rocks schematic [89].	66
Figure 2. 12 The clay mineral tetrahedral and octahedral sheets. Ob and Oa represent basal and apical oxygen atoms, OOct is octahedral anionic position [90]	68
Figure 2. 13 Clay mineral structural patterns [87]	68
Figure 2. 14 X-ray diffractogram of calcined clay due to flash calcination in different temperature. Grey spectrum is a virgin material [128].	74

Figure 2. 15 Kaolinite de-hydroxylation schematic that causes disorder in alumina layer [140].....	75
Figure 2. 16 The Al-NMR spectra associated to the Kaolinite, Illite and Montmorillonite, heat treated in RT, 300 and 800 °C [95]	76
Figure 2. 17 Computed phase assemblages for C ₃ A-CH system with different SO ₃ and CO ₂ amount [155].....	79
Figure 2. 18 Comparison of compressive strength among LC3-50 and PC	80
Figure 3. 1 Bozalan Schist Sample (Virgin Powder).....	84
Figure 3. 2 Bozalan Virgin Powder X-ray Diffractogram	85
Figure 3. 3 Camlica Schist Sample (Virgin Powder).....	87
Figure 3. 4 Camlica Virgin Powder X-ray Diffractogram.....	87
Figure 3. 5 The whole 2θ range x-ray diffractogram of Camlica sample.....	88
Figure 3. 6 representative picture of illite type potassium clay crystal structure with general formula of (K, H ₃ O) (Al, Mg, Fe) ₂ (Si, Al) ₄ O ₁₀ [(OH) ₂ , (H ₂ O)]	89
Figure 3. 7 Tastepe Schist Sample (Virgin Powder)	90
Figure 3. 8 Tastepe Virgin Powder X-ray Diffractogram.....	90
Figure 3. 9 Kovukdere Schist Sample (Virgin Powder)	91
Figure 3. 10 Kovukdere Virgin Powder X-ray Diffractogram	92
Figure 3. 11 X-ray diffraction of Kovukdere by focusing on 5° to 10° 2θ.....	93
Figure 3. 12 Muratbey Schist Sample (Virgin Powder)	94
Figure 3. 13 Muratbey Virgin Powder X-ray Diffractogram.....	95
Figure 3. 14 X-ray diffraction of Muratbey by focusing on 5° to 10° 2θ.....	95
Figure 3. 15 Crystal structure of Andalusite Phase	96
Figure 3. 16 Ladik Schist Sample (Virgin Powder).....	97
Figure 3. 17 Ladik Virgin Powder X-ray Diffractogram.....	98
Figure 3. 18 Kaolinite Powder Sample (Virgin Powder).....	99
Figure 3. 19 Kaolinite Virgin Powder X-ray Diffractogram	100
Figure 3. 20 Thermogravimetric Analysis of Bozalan schist (Virgin Powder).....	103
Figure 3. 21 Thermogravimetric Analysis of Camlica schist (Virgin Powder).....	104
Figure 3. 22 Thermogravimetric Analysis of Tastepe schist (Virgin Powder).....	105

Figure 3. 23 Thermogravimetric Analysis of Kovukdere schist (Virgin Powder)	106
Figure 3. 24 Thermogravimetric Analysis of Muratbey schist (Virgin Powder).....	106
Figure 3. 25 Thermogravimetric Analysis of Ladik schist (Virgin Powder).....	107
Figure 3. 26 Thermogravimetric Analysis of Kaolinite (Virgin Powder)	108
Figure 3. 27 schematic of conductivity measuring device (Pozzolanicity)	111
Figure 3. 28 Pozzolanicity measurement setup	112
Figure 3. 29 Calcium hydroxide saturated solution conductivity variation through different measurements.....	114
Figure 3. 30 Virgin Bozalan pozzolanicity measurements (two measurements are carried out for more accuracy).....	116
Figure 3. 31 Virgin Camlica pozzolanicity measurements (two measurements are carried out for more accuracy).....	117
Figure 3. 32 Virgin Tastepe pozzolanicity measurements (two measurements are carried out for more accuracy)	118
Figure 3. 33 Virgin Kovukdere pozzolanicity measurements (two measurements are carried out for more accuracy).....	119
Figure 3. 34 Virgin Muratbey pozzolanicity measurements (two measurements are carried out for more accuracy).....	120
Figure 3. 35 Virgin Ladik pozzolanicity measurements (two measurements are carried out for more accuracy)	122
Figure 3. 36 Virgin Kaolinite pozzolanicity measurements (two measurements are carried out for more accuracy).....	123
Figure 3. 37 Comparison graph of conductivity variation of all samples up to 120 seconds	124
Figure 3. 38 Variation of conductivity in solution due to calcium carbonate	125
Figure 3. 39 BSE-SEM (scanning electron microscopy-backscattered electrons mode) images of six raw materials received from mine quarries	127
Figure 3. 40 Kaolinite microstructure and elemental analysis; (a) microstructure, (b) element ratios and (c) EDS mapping (Si, Al and layered map).....	128
Figure 3. 41 Kaolinite microstructure and elemental analysis; (a) microstructure, (b) element ratios and (c) EDS mapping (Si, Al and layered map).....	129

Figure 3. 42 Kovukdere schist microstructure and elemental analysis; (a) microstructure, (b) element ratios and (c) EDS mapping (Si, Al, Ca, Fe, K and layered map).....	130
Figure 3. 43 Kovukdere schist microstructure and elemental analysis; (a) microstructure, (b) element ratios and (c) EDS mapping (Si, Al, Ca, Fe, K, Mg, Na and layered map)	131
Figure 3. 44 Muratbey schist microstructure and elemental analysis; (a) microstructure, (b) element ratios and (c) EDS mapping (Si, Al, Ca, Fe and layered map)	132
Figure 3. 45 Muratbey schist microstructure and elemental analysis; (a) microstructure, (b) element ratios and (c) EDS mapping (Si, Al, Ca, Fe, K, Mg and layered map).....	133
Figure 3. 46 Tastep clay microstructure and elemental analysis; (a) microstructure, (b) element ratios and (c) EDS mapping (Si, Al, Ca, Fe, Mg and layered map).....	134
Figure 3. 47 Tastep clay microstructure and elemental analysis; (a) microstructure, (b) element ratios and (c) EDS mapping (Si, Al, Ca, Fe, K, Mg and layered map).....	135
Figure 3. 48 Degrading clay microstructure and elemental analysis; (a) microstructure, (b) element ratios and (c) EDS mapping (Si, Al, Ca, Fe, K and layered map)	136
Figure 3. 49 Bozalan clay microstructure and elemental analysis; (a) microstructure, (b) element ratios and (c) EDS mapping (Si, Al, Ca, K, Mg and layered map).....	137
Figure 3. 50 Camlica schist microstructure and elemental analysis; (a) microstructure, (b) element ratios and (c) EDS mapping (Si, Al, Ca, Fe, K and layered map)	138
Figure 3. 51 Camlica schist microstructure and elemental analysis; (a) microstructure, (b) element ratios and (c) EDS mapping (Si, Al, Ca, Fe, K and layered map)	139
Figure 3. 52 Ladik clay microstructure and elemental analysis; (a) microstructure, (b) element ratios and (c) EDS mapping (Si, Al, Mg, Fe, K and layered map)	140
Figure 3. 53 Ladik clay microstructure and elemental analysis; (a) microstructure, (b) element ratios and (c) EDS mapping (Si, Al, Ca, Fe, K, Mg and layered map).....	141
Figure 3. 54 SEM image of Kovukdere powder, (a) not heat treated (virgin) and (b) heat treated up to temperature associated to 80% of total weight loss (500X)	143
Figure 3. 55 SEM image of Kovukdere powder, (a) not heat treated (virgin) and (b) heat treated up to temperature associated to 80% of total weight loss (1000X)	143
Figure 3. 56 Heat-treated Kovukdere schist powder up 80% of total weight loss, EDS elemental mapping.....	144

Figure 3. 57 SEM image of Tastepe powder, (a) not heat treated (virgin) and (b) heat treated up to temperature associated to 80% of total weight loss (500X)	145
Figure 3. 58 SEM image of Tastepe powder, (a) not heat treated (virgin) and (b) heat treated up to temperature associated to 80% of total weight loss (1000X)	145
Figure 3. 59 Heat-treated Tastepe schist powder up 80% of total weight loss, EDS elemental mapping	146
Figure 3. 60 SEM image of Ladik powder, (a) not heat treated (virgin) and (b) heat treated up to temperature associated to 80% of total weight loss (200X)	147
Figure 3. 61 SEM image of Ladik powder, (a) not heat treated (virgin) and (b) heat treated up to temperature associated to 80% of total weight loss (500X)	147
Figure 3. 62 Heat-treated Ladik schist powder up 80% of total weight loss, EDS elemental mapping	148
Figure 3. 63 SEM image of Muratbey powder, (a) not heat treated (virgin) and (b) heat treated up to temperature associated to 80% of total weight loss (200X)	149
Figure 3. 64 SEM image of Muratbey powder, (a) not heat treated (virgin) and (b) heat treated up to temperature associated to 80% of total weight loss (500X)	149
Figure 3. 65 Heat-treated Muratbey schist powder up 80% of total weight loss, EDS elemental mapping	150
Figure 3. 66 SEM image of Bozalan powder, (a) not heat treated (virgin) and (b) heat treated up to temperature associated to 80% of total weight loss (200X)	151
Figure 3. 67 SEM image of Bozalan powder, (a) not heat treated (virgin) and (b) heat treated up to temperature associated to 80% of total weight loss (1000X)	151
Figure 3. 68 Heat-treated Bozalan schist powder up 80% of total weight loss, EDS elemental mapping	152
Figure 3. 69 SEM image of Camlica powder, (a) not heat treated (virgin) and (b) heat treated up to temperature associated to 80% of total weight loss (1000X)	153
Figure 3. 70 Heat-treated Camlica schist powder up 80% of total weight loss, EDS elemental mapping	153
Figure 3. 71 Kaolinite x-ray diffractogram for (I) Virgin, (II) heat-treated up to 30% of WL_T , (III) heat-treated up to 50% of WL_T and (IV) heat-treated up to 80% of WL_T	158

Figure 3. 72 Thermogravimetric analysis of virgin and heat-treated Kaolinite (heat-treated up to temperature associated to 30, 50, and 80% of total weight loss).....	159
Figure 3. 73 Bozalan x-ray diffractogram for (I) Virgin, (II) heat-treated up to 30% of WL_T , (III) heat-treated up to 50% of WL_T and (IV) heat-treated up to 80% of WL_T	161
Figure 3. 74 Thermogravimetric analysis of virgin and heat-treated Bozalan (heat-treated up to temperature associated to 30, 50, and 80% of total weight loss).....	161
Figure 3. 75 Tastepe x-ray diffractogram for (I) Virgin, (II) heat-treated up to 30% of WL_T , (III) heat-treated up to 50% of WL_T and (IV) heat-treated up to 80% of WL_T	163
Figure 3. 76 Thermogravimetric analysis of virgin and heat-treated Tastepe (heat-treated up to temperature associated to 30, 50, and 80% of total weight loss).....	164
Figure 3. 77 Tastepe x-ray diffractogram for (I) Virgin, (II) heat-treated up to 30% of WL_T , (III) heat-treated up to 50% of WL_T and (IV) heat-treated up to 80% of WL_T	165
Figure 3. 78 Thermogravimetric analysis of virgin and heat-treated Camlica (heat-treated up to temperature associated to 30, 50, and 80% of total weight loss).....	166
Figure 3. 79 Kovukdere x-ray diffractogram for (I) Virgin, (II) heat-treated up to 30% of WL_T , (III) heat-treated up to 50% of WL_T and (IV) heat-treated up to 80% of WL_T	168
Figure 3. 80 Thermogravimetric analysis of virgin and heat-treated Kovukdere (heat-treated up to temperature associated to 30, 50, and 80% of total weight loss).....	168
Figure 3. 81 Muratbey x-ray diffractogram for (I) Virgin, (II) heat-treated up to 30% of WL_T , (III) heat-treated up to 50% of WL_T and (IV) heat-treated up to 80% of WL_T	170
Figure 3. 82 Thermogravimetric analysis of virgin and heat-treated Muratbey (heat-treated up to temperature associated to 30, 50, and 80% of total weight loss).....	171
Figure 3. 83 Ladik x-ray diffractogram for (I) Virgin, (II) heat-treated up to 30% of WL_T , (III) heat-treated up to 50% of WL_T and (IV) heat-treated up to 80% of WL_T	172
Figure 3. 84 Thermogravimetric analysis of virgin and heat-treated Ladik (heat-treated up to temperature associated to 30, 50, and 80% of total weight loss).....	173
Figure 3. 85 The compressive strength test results of all blended cement paste (calcination of clay up to temperature associated to the 30% of total mass loss)	175
Figure 3. 86 The compressive strength test results of all blended cement paste (calcination of clay up to temperature associated to the 50% of total mass loss)	176

Figure 3. 87 The compressive strength test results of all blended cement paste (calcination of clay up to temperature associated to the 80% of total mass loss)	178
Figure 3. 88 Effect of quartz and carbonate on composite cement paste samples [30% WL _T] (Left Quartz / Right quartz and carbonate effect).....	179
Figure 3. 89 Effect of quartz and carbonate on composite cement paste samples [50% WL _T] (Left Quartz / Right quartz and carbonate effect).....	180
Figure 3. 90 Effect of quartz and carbonate on composite cement paste samples [80% WL _T] (Left Quartz / Right quartz and carbonate effect).....	181
Figure 3. 91 Variation of the reduction in the amount of clay and carbonate by heat treatment considering the compressive strength of blended cement paste (heat treated clay up to 30% WL _T).....	182
Figure 3. 92 Variation of the reduction in the amount of clay and carbonate by heat treatment considering the compressive strength of blended cement paste (heat treated clay up to 50% WL _T).....	183
Figure 3. 93 Variation of the reduction in the amount of clay and carbonate by heat treatment considering the compressive strength of blended cement paste (heat treated clay up to 80% WL _T).....	184
Figure 3. 94 Relation of pozzolanicity with compressive strength (for 30% heat treated sample).....	185
Figure 3. 95 Relation of pozzolanicity with compressive strength (for 50% heat treated sample).....	185
Figure 3. 96 Relation of pozzolanicity with compressive strength (for 80% heat treated sample).....	186
Figure 3. 97 Compressive strength and pozzolanicity of all samples according to the reference values (calcined sample up to temperature associated to 30% of WL _T).....	187
Figure 3. 98 Compressive strength and pozzolanicity of all samples according to the reference values (calcined sample up to temperature associated to 50% of WL _T).....	188
Figure 3. 99 Compressive strength and pozzolanicity of all samples according to the reference values (calcined sample up to temperature associated to 80% of WL _T).....	188
Figure 3. 100 Comparison of compressive strength of Bozalan sample subjected to different calcination temperatures with cement and 70% of cement compressive strength.....	189

Figure 3. 101 Comparison of compressive strength of Tastepe sample subjected to different calcination temperatures with cement and 70% of cement compressive strength.....	190
Figure 3. 102 Comparison of compressive strength of Ladik sample subjected to different calcination temperatures with cement and 70% of cement compressive strength.....	191
Figure 3. 103 Comparison of compressive strength of Kovukdere sample subjected to different calcination temperatures with cement and 70% of cement compressive strength	192
Figure 3. 104 Comparison of compressive strength of Muratbey sample subjected to different calcination temperatures with cement and 70% of cement compressive strength	193
Figure 3. 105 Comparison of compressive strength of Camlica sample subjected to different calcination temperatures with cement and 70% of cement compressive strength.....	194
Figure 3. 106 Comparison of compressive strength of Kaolinite sample subjected to different calcination temperatures with cement and 70% of cement compressive strength	195
Figure 4. 1 Muratbey mine (Catalca District) – Google Earth	205
Figure 4. 2 Four different samples from Muratbey mine quarry	206
Figure 4. 3 Ground powder Muratbey schist type samples ready for calcination as (a) M ₁ -Green, (b) M ₂ -Brown, (c) M ₃ -Pink and (d) M ₄ -Black	206
Figure 4. 4 M ₁ -Green schist type sample XRD spectrum and quantification.....	212
Figure 4. 5 M ₂ -Brown schist type sample XRD spectrum and quantification	214
Figure 4. 6 M ₃ -Pink schist type sample XRD spectrum and quantification	215
Figure 4. 7 M ₄ -Black schist type sample XRD spectrum and quantification	217
Figure 4. 8 Mixture of 95 wt% calcium carbonate and 5 wt% graphite XRD diffractogram	218
Figure 4. 9 TGA of M ₁ -Green virgin powder	219
Figure 4. 10 TGA of M ₂ -Brown virgin powder.....	220
Figure 4. 11 TG of M ₃ -Pink virgin powder	221
Figure 4. 12 TGA of M ₄ -Black virgin powder	222
Figure 4. 13 M ₁ - Green schist type sample micrograph in different magnification	224

Figure 4. 14 EDS elemental analysis of M ₁ - Green Schist.....	226
Figure 4. 15 M ₂ -Brown schist type sample micrograph in different magnification.....	227
Figure 4. 16 EDS elemental analysis of M ₂ - Brown Schist.....	229
Figure 4. 17 M ₃ -Pink schist type sample micrograph in different magnification.....	230
Figure 4. 18 EDS elemental analysis of M ₃ - Pink Schist.....	232
Figure 4. 19 M ₄ -Black schist type sample micrograph in different magnification.....	233
Figure 4. 20 EDS elemental analysis of M ₄ - Black Schist	235
Figure 4. 21 X-ray spectrum of virgin vs. calcined M ₁ - Green schist powder	236
Figure 4. 22 X-ray spectrum of virgin vs. calcined M ₁ - Green with 15% (CC).....	238
Figure 4. 23 X-ray spectrum of virgin vs. calcined M ₂ - Brown schist powder	239
Figure 4. 24 X-ray spectrum of virgin vs. calcined M ₂ - Brown with 15% (CC).....	240
Figure 4. 25 X-ray spectrum of virgin vs. calcined M ₃ - Pink schist powder.....	241
Figure 4. 26 X-ray spectrum of virgin vs. calcined M ₃ - Pink with 15% (CC)	242
Figure 4. 27 X-ray spectrum of virgin vs. calcined M ₄ - Black schist powder.....	243
Figure 4. 28 X-ray spectrum of virgin vs. calcined M ₄ - Black with 15% (CC)	244
Figure 4. 29 Thermogravimetic analysis of virgin and calcined M ₁	245
Figure 4. 30 Thermogravimetic analysis of virgin and calcined M ₁ with 15% (CC)	246
Figure 4. 31 Thermogravimetic analysis of virgin and calcined M ₂	247
Figure 4. 32 Thermogravimetic analysis of virgin and calcined M ₂ with 15% (CC)	248
Figure 4. 33 Thermogravimetic analysis of virgin and calcined M ₃	249
Figure 4. 34 Thermogravimetic analysis of virgin and calcined M ₃ with 15% (CC)	250
Figure 4. 35 Thermogravimetic analysis of virgin and calcined M ₄	251
Figure 4. 36 Thermogravimetic analysis of virgin and calcined M ₄ with 15% (CC)	252
Figure 4. 37 M ₁ – Green schist powder (a) before and (b) after calcination	253
Figure 4. 38 M ₂ – Brown schist powder (a) before and (b) after calcination	253
Figure 4. 39 M ₃ – Pink schist powder (a) before and (b) after calcination.....	254
Figure 4. 40 M ₄ – Black schist powder (a) before and (b) after calcination.....	254
Figure 4. 41 M ₁ - Green schist micrographs for Virgin (Left) and Calcined (Right) Powders at the same magnification	255
Figure 4. 42 EDS elemental analysis of calcined M ₁ - Green Schist.....	257

Figure 4. 43 M ₂ - Brown schist micrographs for Virgin (Left) and Calcined (Right) Powder	258
Figure 4. 44 EDS elemental analysis of calcined M ₂ - Brown Schist	260
Figure 4. 45 M ₃ - Pink schist micrographs for Virgin (Left) and Calcined (Right) Powder	260
Figure 4. 46 EDS elemental analysis of calcined M ₃ - Pink Schist	262
Figure 4. 47 M ₄ - Black schist micrographs for Virgin (Left) and Calcined (Right) Powder	263
Figure 4. 48 EDS elemental analysis of calcined M ₄ - Black Schist	265
Figure 4. 49 M ₁ - Green schist powder (calcined) compressive strength (C ³ vs. LC ⁴)	266
Figure 4. 50 M ₂ - Brown schist powder (calcined) compressive strength (C ³ vs. LC ⁴)	268
Figure 4. 51 M ₃ - Pink schist powder (calcined) compressive strength (C ³ vs. LC ⁴)	269
Figure 4. 52 M ₄ - Black schist powder (calcined) compressive strength (C ³ vs. LC ⁴)	270
Figure 4. 53 The compressive strength test results for all samples (C ³ vs. LC ⁴ vs Cement)	272
Figure 4. 54 M ₄ -Black schist type sample XRD spectrum and quantification	274
Figure 4. 55 X-ray diffractogram of all four samples and quantification	275
Figure 5. 1 Compressive strength of Kovukdere, Muratbey and Kaolinite (28d) vs. magnitude of heat treatment (30, 50 and 80% of WL _T)	287

LIST OF TABLES

Table 1. 1 Classification of pozzolanicity of materials and var. in conductivity [20].....	41
Table 2. 1 Cement chemical composition classification (content of Cr cannot exceed 2 mg/kg).....	50
Table 2. 2 Low-lime fly ash chemical composition [57].....	61
Table 2. 3 Clay classes mineral characterization [95]	69
Table 2. 4 The amount of metakaolin content in different kaolinite sample varied in flash calcination temperature (TGA results) [128].....	73
Table 2. 5 Metakaolin content of the calcined kaolinite via different calcination method (Flash calcination is done for various temperature) [128].....	74
Table 3. 1 Phase ratios and amorphousness estimation for Bozalan virgin powder.....	85
Table 3. 2 Phase ratios and amorphousness estimation for Camlica virgin powder	88
Table 3. 3 Phase ratios and amorphousness estimation for Tastepe virgin powder	91
Table 3. 4 Phase ratios and amorphousness estimation for Kovukdere virgin powder	94
Table 3. 5 Phase ratios and amorphousness estimation for Muratbey virgin powder	96
Table 3. 6 Phase ratios and amorphousness estimation for Ladik virgin powder	98
Table 3. 7 Phase ratios and amorphousness estimation for Kaolinite virgin powder.....	100
Table 3. 8 Phase distribution of all samples	101
Table 3. 9 XRF analysis results for all schist samples.....	102
Table 3. 10 TGA results of all samples according to their mass loss (ML)	108
Table 3. 11 Pozzolanicity (conductivity variation) criteria classification [191].....	111
Table 3. 12 PH and conductivity variation of calcium hydroxide solution in the range of (23-40°C).....	113
Table 3. 13 pH / Conductivity variability of saturated calcium hydroxide solution (23-40°C)	114
Table 3. 14 Virgin Bozalan schist conductivity measurements (Pozzolanic Reactivity) ...	115
Table 3. 15 Virgin Camlica schist conductivity measurements (Pozzolanic Reactivity)...	116
Table 3. 16 Virgin Tastepe schist conductivity measurements (Pozzolanic Reactivity)....	118

Table 3. 17 Virgin Kovukdere schist conductivity measurements (Pozzolanic Reactivity)	119
Table 3. 18 Virgin Muratbey schist conductivity measurements (Pozzolanic Reactivity).	120
Table 3. 19 Virgin Ladik schist conductivity measurements (Pozzolanic Reactivity).....	121
Table 3. 20 Virgin Kaolinite conductivity measurements (Pozzolanic Reactivity)	122
Table 3. 21 Pozzolanicity measurements of all samples	123
Table 3. 22 Variation of conductivity due to calcium carbonate.....	125
Table 3. 23 Decomposition temperatures range and mass loss amounts of 30%, 50% and 80% for all samples.....	155
Table 3. 24 Pozzolanicity of virgin and heat-treated (to temperature associated to 30, 50 and 80% of total weight loss) Kaolinite powder (conductivity variation)	157
Table 3. 25 QCC amounts (% by weight) of kaolinite (virgin and heat-treated)	157
Table 3. 26 Pozzolanicity of virgin and heat-treated (to temperature associated to 30, 50 and 80% of total weight loss) Bozalan powder (conductivity variation)	159
Table 3. 27 QCC amounts (% by weight) of Bozalan (virgin and heat-treated)	160
Table 3. 28 Pozzolanicity of virgin and heat-treated (to temperature associated to 30, 50 and 80% of total weight loss) Tastepe powder (conductivity variation).....	162
Table 3. 29 QCC amounts (% by weight) of Tastepe (virgin and heat-treated).....	162
Table 3. 30 Pozzolanicity of virgin and heat-treated (to temperature associated to 30, 50 and 80% of total weight loss) Camlica powder (conductivity variation)	164
Table 3. 31 QCC amounts (% by weight) of Camlica (virgin and heat-treated)	165
Table 3. 32 Pozzolanicity of virgin and heat-treated (to temperature associated to 30, 50 and 80% of total weight loss) Kovukdere powder (conductivity variation).....	167
Table 3. 33 QCC amounts (% by weight) of Kovukdere (virgin and heat-treated).....	167
Table 3. 34 Pozzolanicity of virgin and heat-treated (to temperature associated to 30, 50 and 80% of total weight loss) Muratbey powder (conductivity variation).....	169
Table 3. 35 QCC amounts (% by weight) of Muratbey (virgin and heat-treated).....	169
Table 3. 36 Pozzolanicity of virgin and heat-treated (to temperature associated to 30, 50 and 80% of total weight loss) Ladik powder (conductivity variation)	171
Table 3. 37 QCC amounts (% by weight) of Ladik (virgin and heat-treated)	172

Table 3. 38 Compressive strength test results of samples with different hydration times (MPa) (heat treated clay up to 30% WL _T)	175
Table 3. 39 Compressive strength test results of samples with different hydration times (MPa) (heat treated clay up to 50% WL _T)	177
Table 3. 40 Compressive strength test results of samples with different hydration times (MPa) (heat treated clay up to 80% WL _T)	178
Table 3. 41 Crystalline and inert portion of clay in Kaolinite	198
Table 3. 42 Crystalline and inert portion of clay in Bozalan	199
Table 3. 43 Crystalline and inert portion of clay in Tastepe.....	199
Table 3. 44 Crystalline and inert portion of clay in Camlica.....	200
Table 3. 45 Crystalline and inert portion of clay in Kovukdere	200
Table 3. 46 Crystalline and inert portion of clay in Muratbey	201
Table 3. 47 Crystalline and inert portion of clay in Ladik.....	201
Table 3. 48 Sorting table of all sample in term of applicability of schist as possible potential for partial substitution of cement (Darker color = more potential)	202
Table 4. 1 The Phase distribution and detailed information about crystal structure and weight percentage for each chemical compound in M ₁ -Green virgin powder	213
Table 4. 2 The Phase distribution and detailed information about crystal structure and weight percentage for each chemical compound in M ₂ -Brown.....	214
Table 4. 3 The Phase distribution and detailed information about crystal structure and weight percentage for each chemical compound in M ₃ -Pink	216
Table 4. 4 The Phase distribution and detailed information about crystal structure and weight percentage for each chemical compound in M ₄ -Black	217
Table 4. 5 Decomposition temperature intervals and total weight loss for schist powders w/o carbonate additive	223
Table 4. 6 The Phase distribution and detailed information about crystal structure and weight percentage for each chemical compound in M1-Green virgin and calcined powder	237

Table 4. 7 The Phase distribution and detailed information about crystal structure and weight percentage for each chemical compound in M ₂ -Green virgin and calcined powder	239
Table 4. 8 The Phase distribution and detailed information about crystal structure and weight percentage for each chemical compound in M ₃ -Green virgin and calcined powder	241
Table 4. 9 The Phase distribution and detailed information about crystal structure and weight percentage for each chemical compound in M ₄ -Green virgin and calcined powder	243
Table 4. 10 Compressive strength of composite cement paste prepared with calcined M ₁ – Green as partial cement substitution (C ³ vs. LC ⁴)	267
Table 4. 11 Compressive strength of composite cement paste prepared with calcined M ₂ – Brown as partial cement substitution (C ³ vs. LC ⁴)	268
Table 4. 12 Compressive strength of composite cement paste prepared with calcined M ₃ – Pink as partial cement substitution (C ³ vs. LC ⁴)	269
Table 4. 13 Compressive strength of composite cement paste prepared with calcined M ₄ – Black as partial cement substitution (C ³ vs. LC ⁴)	271
Table 4. 14 Compressive strength of composite cement paste prepared with calcined schists as partial cement substitution (C ³ vs. LC ⁴)	272
Table 4. 15 The Phase distribution and detailed information about crystal structure and weight percentage for each chemical compound in M ₄ -Black	274
Table 4. 16 Phase distribution and quantifications for all 4 samples	276
Table 4. 17 Theoretical and Experimental weight loss amount of virgin M ₁ after calcination	277
Table 4. 18 Theoretical and Experimental weight loss amount of M ₁ with 15% CC after calcination	277
Table 4. 19 Theoretical and Experimental weight loss amount of M ₂ with/without 15% CC after calcination	278
Table 4. 20 Theoretical and Experimental weight loss amount of M ₃ with/without 15% CC after calcination	279

Table 4. 21 Theoretical and Experimental weight loss amount of M ₄ with/without 15%(CC) after calcination.....	279
--	-----

Glossary

Abbreviations	Definition
<hr/> Cement Notation	
C	Calcium Oxide, CaO
S	Silicon Oxide, SiO ₂
A	Aluminum Oxide, Al ₂ O ₃
F	Iron Oxide, Fe ₂ O ₃
H	Water, H ₂ O
\$	Sulfate, SO ₃
<hr/> Cement Phase	
C ₃ S	TriCalcium Silicate
C ₂ S	DiCalcium Silicate
C ₃ A	TriCalcium Aluminate
C ₄ AF	TetraCalcium Aluminoferrite
CH	Portlandite or Calcium Hydroxide
C-S-H	Calcium Silicate Hydrate
AFt	Ettringite
AFm	Monosulfo/Carboaluminate
<hr/>	
OPC or PC	Ordinary Portland Cement
SCM	Supplementary Cementitious Materials
doR	Degree of Reaction
doH	Degree of Hydration
w/c	Water-to-Cement Ratio
w/s	Water-to-Solid Ratio
<hr/> Methods	
SEM	Scanning Electron Microscope
TGA	Thermogravimetric Analysis
XRD	X Ray Diffraction
UCS	Uniaxial Compressive Strength

CHAPTER 1

INTRODUCTION

1.1 General

Cement is the binder in concrete. Its quality is important for concrete's strength and durability. The strength development is affected by the chemistry and phase distribution in cement. According to the World Business Council for Sustainable Development (WBCSD), concrete is the most widely used material on earth after water, with nearly 3 tons of annual consumption for any man, woman and child [1]. However, this industrial activity comes with a heavy environmental burden. More than 5% of world carbon dioxide emission is coming from cements industry alone. The manufacture of cement produces about 0.9 pounds of CO₂ for every pound of cement. A major raw material of cement, limestone (CaCO₃), is converted to lime (CaO) during high temperature reactions of clinker production. Another product of this calcination process is CO₂ gas. This greenhouse gas is also emitted during cement production by fossil fuel combustion [2, 5]. To mitigate the environmental impact of the cement manufacture, there are three major solutions that are proposed. First, considerable research has focused on the feasibility of using alternative fuels instead of fossil fuels. This method could reduce the overall carbon dioxide emission from cement industries by 18 to

24% in about 50 years [3]. Another solution by Lothenbach et al. is to perform efficiency measurement to reduce the requirement for fossil fuel and consequent emission up to 40% [35]. The third proposed method is to replace OPC with alternative materials such as activated clay and limestone which can further reduce the carbon dioxide emission by up to 50% [36]. Replacement of clinker by supplementary cementitious materials (SCMs) such as blast furnace slag, fly ash, silica fume, and natural pozzolans is already an industrial practice for composite cement blends. The coupled substitution of metakaolin and limestone in OPC is currently being investigated [4, 5]. Metakaolin is the heat activated form of kaolinite that is reactive in the high pH environment of hydration reactions of OPC. It is found that the metakaolin can be substituted in cement up to 35 wt%. This composite paste's 28 days strength achieved 90% of the strength of pure OPC paste [35]. A major problem with current SCMs and metakaolin is the availability and price. The existing amounts and forecast production of these alternative SCMs cannot compensate the demand from the cement manufactures around the world [5,13]. On the other hand, natural pozzolan deposits like volcanic ashes or zeolitic tuffs are results of local geology and are available only in certain regions of the world [7, 11]. The even geographical distribution and their potential pozzolanic properties focused the highlight on calcined clay as an alternative SCM [36]. They need to be properly activated under certain conditions Through thermal activation of clay minerals in the temperature range of 550 - 950°C, it is possible to obtain alumina and silica rich phases with partially disordered structures that show pozzolanic reactivity [41]. In this alternative approach, energy savings and reduced CO₂ emissions are possible due to lowered calcination temperatures that are 600-900 C lower than those required for clinkering reactions. In addition, there are no CO₂ emissions associated with the decarbonation of the virgin materials [4]. The pozzolanicity or pozzolanic activity of a candidate substitute depends on amount and the type of clayey minerals in the raw material [6]. The activation of clayey minerals for hydration reaction is possible through high temperature or mechanical treatment. Most studies about calcined clay related the type of clay minerals (mainly Kaolinite, Montmorillonite, illite) and their activation temperature to their pozzolanic activity. Those studies have shown that kaolinite has the highest pozzolanic activity and lower activation temperature followed by montmorillonite and illite [5]. Although the existence of kaolinite is common on the earth crust in many places, at the same time, the applicable and

commercially useable high-grade kaolin deposits are relatively few [10]. That puts a limitation on the availability of meta-kaolinite which is obtained by thermal decomposition of Kaolinite under controlled conditions in comparison to other SCMs. In general, clays rarely occur in nature as pure deposits but rather as mixtures of clays and non-clay minerals such as carbonates, feldspars and quartz. Therefore, a potential usage of multicomponent clay deposits as pozzolanic materials needs to be investigated. So far, low grade Kaolinitic clay deposits have been ignored as potential candidates for cement industries. Therefore, there are limited studies on thermal activation and pozzolanic reactivity of low grade kaolinitic clays [4, 11].

The use of disordered aluminosilicates as binder in constructions was practiced in the ancient history [23]. Romans have realized that the pozzolans reacted with lime in the presence of moisture to form stable cementitious hydrates. Roman cement is a volcanic ash-lime mortar that has been regarded as the principal material constituent that provides long-term durability to ancient architectural concrete. The Roman wall concrete resist micro-cracking [20]. This was believed to be due to the calcium-aluminosilicate hydrate mineral (Stratlingite) that reinforced interfacial zones in the concrete matrix [8]. Stratlingite with the chemical formula of $\text{Ca}_2\text{Al}[(\text{OH})_6\text{AlSiO}_2-3(\text{OH})_{4-3}] \cdot 2,5(\text{H}_2\text{O})$ is probably the product of reactions between (i) belite, aluminates gel, and calcium hydroxide and/or (ii) alite with aluminate gel; and/or (iii) CAH_{10} and C-S-H. Stratlingite is claimed to contribute to the early strength properties of Roman concrete [20]. Recent studies [35] revealed that Romans used free lime (CaO) in their mortars that was obtained by calcination of limestone at around 900°C. The hydration of this free lime forms calcium hydroxide with trigonal crystal structure. The core of the reactions that lead to Roman mortar is the attack of the strongly alkaline portlandite solution to the surface of the scoriaceous (highly vesicular and frothy texture) pozzolan that dissociates volcanic glass and silica mineral [36]. The alkali ions dissolved in the liquid phase together with calcium and dissolved silicate and aluminate ions formed cementitious hydrates on the scoria (vesicular) surface [35]. As such, roman concrete is a mixture of volcanic ash deposit, limestone, water and some rocks. However, since volcanic ash is not available all around the world there is a need to find alternative reactive silicate sources. Hence, the investigations on methods to generate active silicate/aluminosilicates in processes like transformation of kaolinite to meta-kaolinite by heat treatment are being conducted. During the heat-treatment,

the mineral kaolinite ($\text{Al}_2\text{O}_3 \cdot 2\text{SiO}_2 \cdot 2\text{H}_2\text{O}$) decomposes and water vapor evaporates leaving the clay structure. Carefully conducted thermal processes produce a partly amorphous and highly reactive aluminosilicate by de-hydroxylation of kaolinite, the so-called meta-kaolinite with aluminum hydroxide layers wielding unsaturated bonds. This de-hydroxylation is an endothermic reaction which occurs in the temperature range of $450^\circ\text{--}700^\circ\text{C}$ [14, 15] with concurrent weight loss. Similar reactions are expected to happen also in other types of clays.

This research study evaluates the potential of locally accessible virgin schist materials which contain a concussion of different clay types for possible activation like the one of Kaolinite for ordinary Portland cement supplement

1.2 Objectives of Study

The aim of this study is to evaluate the schist type materials as a possible potential partial substitute for ordinary Portland cement. In order to use calcined schist type materials as pozzolana, and promote the new product to the market, it should be determined how and why the new mixture could change the cement industry and provide the new generation of green composite for constructions. Hence, the following questions can be asked.

- What is the main factor that activate the calcined schist to form pozzolanic material that could react with CH?
- How is the structural alteration during the calcination process of clay type materials?
- What is the effect of heat treatment of microstructure of clay minerals?
- Why the calcined schist material could have the efficiency of metakaolin?
- How clays with more complex structures than kaolinite can be activated?
- Why the calcined limestone addition could provide further advantages?

This study includes the two phases of evaluation of the schist type material as SCMs:

- (i) Calcined Clay Cement (C^3)
- (ii) Limestone Calcined Clay and Carbonate Cement (LC^4)

In the first phase, seven different schist type was evaluated for pozzolanic reactivity and compressive strength of blended cement that is prepared by calcined form of these powders.

The second phase of study is associated to the four different sample with almost similar chemical composition and the influence of calcined carbonate on their reactivity.

1.3 Materials and Methods

1.3.1 Materials

1.3.1.1 Schist-minerals as possible supplementary cementitious materials (SCMs)

The OPC is the main known binder for concrete. But in order to make it more environmentally friendly and cost effective, people started using waste materials from different industries such as Limestone, fly ash, ground granulated blast furnace Slag, natural pozzolans and calcined clay. The most important common denominator among them is the active aluminosilicate sources. The main idea is inferred from the imperial roman concrete that is made up of burned limestone and natural lava (reactive aluminosilicate) which is mainly amorphous. Due to the limited geographical accessibility of lava, there is a need for active materials to compensate the lack of lava everywhere. Hence, in this study, I am considering schist-type materials as an alternative SCM source that contain large amounts of “activate-able” aluminosilicate phases.

1.3.1.2 Schist-type materials Studied

Schist is the medium grain size metamorphic material which mainly contains mica or talc (about 50%). It also includes some portion of clayey phases and quartz as well [3]. The metamorphism of schist rock originated from the type of initial source that are sedimentary, igneous or metamorphic. So, the schist resources could be classified according to the original rock that converted to schist type materials. For instance, the whole region occupied by intrusive junctions, chilled edges, contact alteration of porphyritic structure shows the originality of metamorphism gneiss from igneous rock. So, these type or resource could contain proper amount of aluminosilicate [4-8]. These deposits are commonly found in

mining debris. In this study, the primary investigation was performed on the samples obtained from the different mine quarries to select the proper candidate that contains sufficient sources of aluminosilicates. The active mines are currently being used to supplement the raw feeds for cement manufacture.

To prepare the schist-type materials powder, they are ground with the standard grinding procedure for ordinary Portland cement up to the average particle size of 25 μ m. These raw powder samples are going to be activated to be used as OPC substitute, perhaps modified by some addition.

1.3.1.3 Reference Kaolinite and Carbonate Source

In order to benchmark the applicability of different schist-type samples, Kaolinite was taken as a reference sample. The previous studies and literature proved that the activated form of Kaolinite (Metakaolin) was a proper supplementary material for OPC replacement. The benchmarking Kaolinite powder was provided from Sisecam manufacture as a standard sample. Moreover, calcium carbonate (calcite polymorph) is going to be partially used as an additive to our raw powders. So, the calcium carbonate was also collected from the Muratbey mine quarry that was the existing source of raw materials for cement manufacture.

1.3.1.4 Used Ordinary Portland Cement

The pure cement that was used in this study was the Ordinary Portland Cement (OPC) of ENS 197-1 CEM 42.5 R type which was provided by AkcanSA Cement Manufacturer.

1.3.2 Methods

1.3.2.1 Chemical phase composition analysis

1.3.2.1.1 X-ray powder diffraction

X-ray diffraction analyses were done on as-received (called “virgin”) and heat-treated powders using Bruker D8 Advance (Bruker AXS GmbH, Karlsruhe, Germany) diffractometer utilizing Cu-K α ($\lambda=1.54$ Å) radiation. The divergence slit size is fixed and was 0.5°. Samples were scanned on a rotating stage between 5 to 90 [$^{\circ}2\theta$] using a step size of 0.02 $^{\circ}2\theta$ and time per step of 1s. The chemical phase analysis via x-ray diffractogram were carried out at initial step to reveal the phase composition of each schist type materials in term of existence of aluminosilicate or clayey minerals. Furthermore, it will give some information about degree of crystallinity and amorphous content of raw powders. At the subsequent stage of study, x-ray diffractograms show the magnitude of decomposition of materials in term of calcination by evaluating the decrease in the peak intensities that belong to the crystalline clays and carbonate. As the clays lost their crystallinity it was preliminary assumed that they became reactive aluminosilicates (maybe similar to lava). XRD phase analyses could be the proper method to determine the amount of different types of clays and carbonate for predicting reactivity potential.

1.3.2.1.2 Quantitative Phase Analysis by Rietveld Method

Rietveld analysis was carried out on untreated and treated samples to identify the amount of potentially reactive and inert phases. After performing the phase analysis of each schist type material, the reference cards for each single chemical phase were taken from the ICSD ver.4.1 software to obtain the crystallographic information files [14]. Then the TOPAS V.5 was utilized to carry out the Rietveld phase analysis [19,22]. To find out the most accurate number of chemical phases the crystal structure of them is theoretically modified to achieve the suitable goodness of fit (GOF). The range of the GOF for this study experiment was from 1.1 to 1.3 [78].

1.3.2.2 Microstructure Evaluation

1.3.2.2.1 Imaging with secondary electrons in a scanning electron microscope (SEM)

SEM analysis of the powder samples were done with the help of JEOL JSM 6010 LV Single-Beam platform scanning electron microscope (JEOL, Akishima, Tokyo, Japan). Each sample in raw and calcined form were investigated in terms of average particle size, morphology, and distribution of the particles. The existence of clay sheets can be verified by SEM imaging. The de-hydroxylation reactions of clays through heat-treatment is assumed to modify/destroy the crystal morphology of clays, as they become amorphous. It could be like the grinding mechanism is to make the particle much smaller and finer. Hence, SEM analyses could confirm the crystal decomposition.

1.3.2.2.2 Elemental Distribution maps with Energy Dispersive Spectroscopy (EDS)

EDS elemental analysis was done by the EDS system attached to the above mentioned JEOL SEM (OXFORD X MAXN-20, High Wycombe, UK) . Virgin and heat-treated powders were coated with carbon prior to microscopy and elemental analysis. The EDS spectra illustrated the amounts of main elements in composition before and after heat treatment. There are three important parameters that can be evaluated by EDS analysis. First, it is possible to compare the elemental analysis with phase analysis to confirm the phase amounts in schist-type materials. Secondly, to correlate phase composition, minor element content, and Ca/Si ratios with morphological features. Moreover, it is applicable to evaluate changes in content, amorphization, and Ca/Si ratios after calcination.

1.3.2.3 Thermal Analysis for Determining Activation Process Parameters

Thermal analysis [TG/DTA] (NETZSCH STA 449 JUPITER, Selb, Germany) of the samples were done in a temperature range between 30° and 1000°C under Nitrogen gas. N₂ atmosphere was chosen in order to eliminate the possibility of oxygen in air reacting with

components of the samples (e.g. Sulfur). The heating rate was 10 K/min. For every run 50 mg of virgin sample was used. The thermal decomposition behavior of hydroxyl groups in the clay structure were monitored with the help of thermogravimetric analysis (TGA).

For the first phase of the study in chapter 3, the full temperature range of decomposition including the de-hydroxylation reactions of clayey components (400°C to 700°C) and decomposition of carbonate (if it existed) (700°C to 900°C) were divided into three regimes (Figure 1.1). The first range corresponded to 30% of the total weight loss due to de-hydroxylation and or calcination. Second and third ranges corresponded to 50% and 80% of the total weight loss, respectively. For the decomposition temperature regimes, the range from RT to 300 C was purposefully avoided since that range usually contains a weight loss due to absorbed moisture.

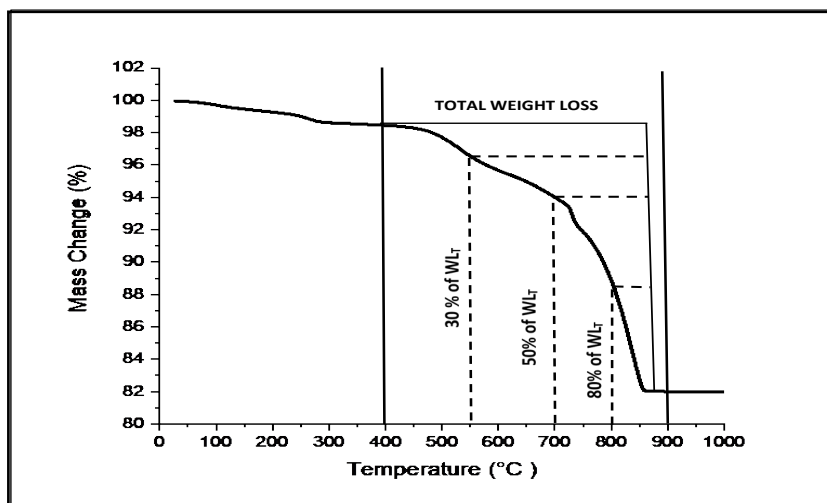


Figure 1. 1 Schematic of the method which used for finding the proper temperatures for heat treatment

Based on this parameter the amount of activated clay can be adjusted in different levels. The hypothesis is that the success of the replacement of OPC with calcined clay depends on how well the clays are activated.

1.3.2.4. Activation of schist-type SCMs by heat-treatment

1.3.2.4.1 Virgin and Carbonate-Modified SCM alternatives

For nominal OPC substitution, the 600 g by same mass of virgin schists were heat treated in high alumina crucibles. In the second phase of project, the amount of carbonate in schist powders were increased to 15 wt% and then 600 g of the mixes were heat treated.

1.3.2.5 Calcination Process

The calcination was performed to the samples, by heating the powders in a box furnace in high alumina crucibles with constant heating rate 10 °C/min up to starting point of decomposition temperature. Then an isothermal hold was scheduled for them. After this pause, the samples were heated to the temperature where the intended activation (i.e. 30, 50, or 80 wt% loss occur) was expected. The powder samples remained at this temperature isothermally for two hours. Then the most important point was to air-quench the powders on the metal desk in order to stabilize the decomposed phases.

1.3.2.6 Pozzolanicity Measurement

The evaluation of the reactivity of candidate materials can be measured through the easy and fast method, called Pozzolanicity measurement. Based on this method the variation in electrical conductivity could clarify the reactivity of powders [3] Evaluation of the pozzolanic activity is based on the measurement of compensated conductivity of a saturated calcium hydroxide “Ca (OH)₂ (CH) solution [22, 23]. Pozzolanic materials decrease the conductivity of the saturated calcium hydroxide solution as they react with the calcium and hydroxyl ions in the solution forming C-S-H and precipitating out of solution. The higher is the decrease in the conductivity, the stronger pozzolanicity does the material have. The experimental details of the method are described in the related literature [20]. Caution has been exercised with potential materials containing carbonates as they introduce additional complication in the interpretation of the pozzolanicity measurements. The details of these

complications will be discussed in the discussion section. The results of the electrical conductivity measurements were interpreted according to the criteria described in Table 1.

Table 1. 1 Classification of pozzolanicity of materials and var. in conductivity [20]

Evaluation of Pozzolanic Activity by Conductivity Measurement	
Classification of Material	Variation in Conductivity according to proposed method (mS/cm)
Non-Pozzolanic	Less than 0,4
Variable Pozzolanicity	Between 0,4 and 1,2
Good Pozzolanicity	Greater than 1,2

Since the temperature difference of the solutions can influence the electrical conductivity, the solution as well as the candidate powders were kept at 40°C before mixing. It should be assured that the solution must be saturated to have proper amount of calcium and hydroxyl ions. It is saturated whenever no more calcium hydroxide can be solved in aqueous solution. By putting the active clay, the C-S-H gel will precipitate out and by measuring the pH and conductivity for every 20 seconds, the decrease in both parameters can be observed.

1.3.2.7 Evaluation Compressive Strength of Cement Containing Schist-Type SCM Alternatives

1.3.2.7.1 Paste Preparation

The cement pastes and blended cement pastes specimens were prepared according to the ENS 197-1 standard. Based on the determined procedure, to replace the OPC up to 30 wt%, a total 1000 g of mixture was prepared by mixing 700 g OPC and 300 g SCM. The water to solid ratio was assigned to be 0.5, so the 500 ml of tap water is added to the mixture.

1.3.2.7.2 Test Specimen Preparation

Compressive strength measurements were carried out on composite cement pastes samples in the shape of 40x40x40 mm cubes. The composite cement pastes were prepared with 30 wt% cement substitution with calcined schist type materials that were mainly clay based. The paste mixture is placed in cube molds for 24 hours and then removed to cure in full moisture condition. The compressive strengths were measured on samples hydrated and cured for 2, 7, 28, 50 and 90 days in water bath at 23°C. The specimens were immersed in water bath to ensure complete hydration until strength testing. There volume of water must exceed 10 times more than total specimen volume. For each hydration duration a set of samples consisting of 3 prisms of 40 mm x 40 mm x 40mm was used according to the ENS-197-1 standard.

1.3.2.7.3 Compressive Strength Test

The compressive strength measurement is carried out by MATEST C104-04 (Console housing the servo-plus evolution, Treviolo, Italy). The three-standard specimen with 4 x 4 x 4 cm³ dimensions were tested for each setting time to optimize the variation due to the possible errors.

1.3.2.7.4 Measure Strength Data Analysis

To minimize the unexpected source of error for compressive strength test, the average strength between three specimens was considered as valid results. The error is calculated by dividing the standard deviation by the square root of number of measurements (N=3). The results were compared to the pure cement paste specimen. Moreover, the results were classified according to the calcination temperature and the obtained strength amounts were compared with the amount of activation. Since Kaolinite is chosen as reference sample, the composite cement pastes from metakaolin blended paste were also prepared to take a role as a benchmark. Besides, 70% of pure OPC paste strength was defined as minimum criteria for controlling reactivity of replaced SCM.

CHAPTER 2

LITERATURE REVIEW

2.1 Cement manufacture CO₂ emission

Concrete is widely useable construction material in whole world. The ever-increasing demand for concrete caused the increment for cement production and transportation. The more production means more energy consumption and green-house gases emission. Cement industry as a single manufacture produce approximately 7% of carbon dioxide emission [1]. The main carbon dioxide generator to the atmosphere are (i) fossil fuel consumption, (ii) deforestation and land usages, and (iii) decomposition of carbonates [2]. The carbon dioxide emission from cement production coming from the decomposition of limestone that is the main component of clinker. After World War II, the cement production increased by rapidly. This amount was about half ton per person [3]. The global cement production is increased by 3-fold after 1950 and 4-fold after 1990 and simultaneously the fuel consumption [4]. Cement industry CO₂ emission is based on the two main source. Firstly, the decomposition of main clinker component, Limestone, which provide 5% of emission and secondly fuel combustion for providing energy and heat that could add a further 60% on top of the process [6]. So, the

carbon dioxide emission in cement manufacture is coming from direct and indirect sources. Direct source is related to the fuel burning in a cement kiln and decomposition of carbonate to produce clinker. Clinker consists of heat-treated mixture of limestone, chalk and clay. It is scorched at temperature range of 1450 to 1500°C. Therefore, environmental sullyng and earth-wide temperature growing up and natural resources and characteristic energy assets will be shrunken every day. Clinker production in kiln divided to three parts: pre-heating, furnace and cooler. The produced clinker will be ground and added by gypsum to be packed for market [7]. The total delivery of cement is about 25 billion tons yearly worldwide and global production is 2.282 billion ton each year [8]. Indirect source of pollution is caused due to the usage of energies like electricity for raw material preparation, grinding, and other instruments [9]. These days, several studies are seeking for a new method to diminish the clinker production and consequently mitigation of carbon dioxide emission. Using alternative fuels which are more environmentally friendly and replacing the recycled energy sources for cement production are widely investigated in all over the world. Clinker substitution is one of the most affordable and applicable approach to reduce the energy and clinker production. Supplementary Cementitious Materials (SCMs) give off the role as a cement substitution include fly-ash, blast furnace slag, silica fume and other types of natural and manufactured pozzolanic materials. Before going more through the SCMs, it would be beneficial to find out more about history of binders and ordinary Portland cement in term of constituents and hydration process.

2.2 Brief History of Binders

During the early civilization, the construction was built by using heavy rocks and another, which friction among the stones keep them firmly beside each other. By passing the time by new binders found and utilized [10]. Egyptian have used dried clay bricks while not burned and attached with Nile slim. This construction materials are only applicable in dry and warm environment since there is no moisture durability with them. Moreover, the blocks in Sakkara (2000 years BC) were linker with clay [11, 181-183]. Plaster is also found it ancient Egypt as binder. They used the plaster to bind the limestones (calcite) since 3400 BC. Egyptians

were received the lime mortars innovation almost at 300 BC. Romans and Greeks were figured out the application of this mortar perhaps before Egyptians while had no idea about gypsum due to more efficiency in humid climate of European countries [10,11]. The lime was adopted by Greeks and Romans as a mix of lime and sand. The carefully mixed and compacted mortar has high density with no preservation of calcium hydroxide. After then, they encounter to the volcanic deposits and their reactivity while mixed with finely ground lime and sand. This time the mortar encompasses the higher strength with more durability [11]. Greeks brought their volcanic materials from the city of Santorin and Romans tuffs were provided from a district of Neapolitan gulf. Due to some experiences, it is found that the best materials were coming from Pozzuoli and it is called Pozzolana. It is believed that the pozzolana is a kind of sand which include extraordinary properties in natural state. Pozzolana were blended with lime and broken fist size rocks to build the constructions [11]. Romans are substituted natural pozzolana by porcelain, bricks and ground roofing tiles. Lea claims that the name “cement” is initially coming from the same mixture that is known as artificial pozzolans [10]. Romans also created the name “hydraulic cement” for the binders which incorporated in hydration reaction beneath the water [12]. There are some assumptions that claim, the application of artificial pozzolans were found before natural pozzolans. According to the investigations for some buildings in Cyprus, usage of hydraulic lime is begun since 1200 BC [11]. After Romans the quality of binder is decreased, and they did not contain crushed ceramic materials. Binders changed in their quality after fifteenth century. There are proofs which show the usage of pozzolanas in England, so the name “mortar” took a part in construction industries from the year 1290 [10]. There were some developments in mortars modification until 1845 that several experiments established the combination of heat-treated clay and limestone. Eventually, the Portland Cement is produced in 1872 [10]. Ordinary Portland Cement (OPC) is the main binder which is using in concrete. Concrete itself is also of great history. Lea classifies the concrete as an artificial conglomerate of gravel or broken stone with sand and lime or cement. Hence, it is possible to link the concrete with lime binder, not aggregate bind with clay [10]. The most antique concrete which is explored is based on lime and found in Israel. Research about this concrete which is used for floor surface shows the compressive strength range from 15 to 40 MPa and in one case was even 60 MPa [13]. Another old concrete was found in Serbia which dated back to 5600-year BC

and covered the floors in fishermen cabins [14]. Roman times is the epoch of vast concrete construction due to the lime mortar production technology including hydraulic lime. But still it seems that perhaps the Greeks were the prior consumer of hydraulic binder. They figured out that it would be more beneficial to use crushed tiles instead of stone pieces. Romans adopted this knowledge and used pozzolan tuff in production of hydraulic lime to build Colosseum (at 82 BC), and Pantheon (at 123 BC) [10]. After Romans, the production of good lime is happened in middle ages while the OPC entered in construction industry. Many scientists worked on cement structure during the later years to find out more about it and modify it. But in recent decades the production of clinker is become a significant problem due to the ecological footprint and greenhouse gases. Hence, reviving the Romans hydraulic binders became a drastic question these days. By considering this fact the durability of the construction which is made with Romans binder is more than the modern mortars and prepared in lower temperature than today's ordinary Portland cement.

2.3 Ordinary Portland Cement (OPC)

Cement is a hydraulic powder which forms plastic pasty mass whenever mixes with water. In European standards (EN 197-1), the quantity and type of mineral that is used for cement preparation adopted as cement classification. The basis of this classification is the (i) The strength of paste or mortar after 28 days of setting time, (ii) The rate of strength development, after 2 days for all types except 32.5 N cement which 7 days should be considered, and (iii) setting time [15]. There are rare differences in term of setting for various standards. Initial setting time is in 40 to 90 time slot and final is in 6, 8, 10 or 12 hours [16]. The main properties of cement are heat of hydration and resistance to aggressive environment. By normalizing the C_3A , it is possible to strengthening the cement in front of sulfate attack. Generally, the cement should be controlled for three main criterions. First, the volume change must be based on Le Chatelier standard. Secondly, the content of MgO may not exceed 5% and thirdly, the sulfate content should be in the range of 3.5 to 4% [16]. The MgO limitation is due to the expansion which can be caused by periclase. To know more about the cement, there should be a review about clinker phases and its production. The raw material that is used for clinker

production is already mentioned. Figure 2.1 shows the flow diagram of typical cement production.

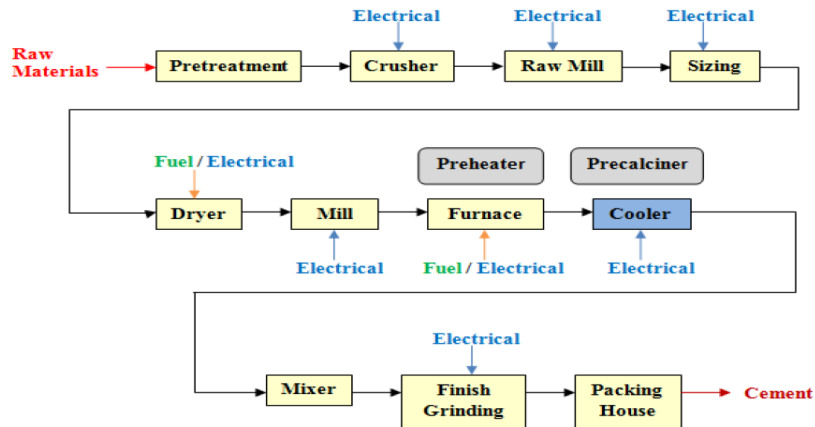


Figure 2. 1 Typical dry process of cement [16]

However, calcination of finely grounded limestone, low degree marl, clay or shale at 1450°C in rotary kiln prepare the clinker. Clinker is cooling rapidly and mixes with calcium sulfate (Gypsum) while grinding to fine powder. The composition of cement in term of average oxide constituents is CaO (60-70%), Al₂O₃ (4-6%), SiO₂ (18-22%), and Fe₂O₃ (2-4%). The clinker mainly consists of these phases (almost 95%) and the other 5% includes MgO, Na₂O, SO₃, Mn₂O₃, K₂O, and TiO₂ [10]. The four main phases of clinker are [17]:

- | | | | |
|----------------------------|--|---------------------|--------|
| • Alite | 3 CaO. SiO ₂ | (C ₃ S) | 55-65% |
| • Belite | 2 CaO.SiO ₂ | (C ₂ S) | 15-25% |
| • Aluminate (Celite) | 3 CaO.Al ₂ O ₃ | (C ₃ A) | 8-14% |
| • Ferrite (Brownmillerite) | 4 CaO.Al ₂ O ₃ .Fe ₂ O ₃ | (C ₄ AF) | 8-12% |

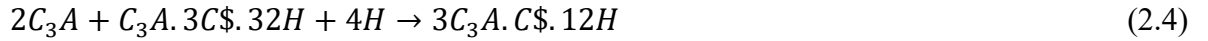
When cement powder mixes with water undergoes and changes to stiff binder. The four reactive phases of clinker enter to hydration process and provide complex compositions. Each of the phases react with water to produce different hydration product. Alite is a silicate phase which formerly enter to reaction and play the main role in paste strength during the early days (before 28 days). This reaction will produce calcium silicate hydrate (C-S-H) and calcium hydroxide (CH) [17].



Belite is the second silicate in cement composition which reacts with water. Belite is responsible for late strength development (after 28 days).



C-S-H is the principal strength provider in Portland cement. The stoichiometry of C-S-H is variable due to the different water bounding. The amount of water in C-S-H can be measured with H NMR [18]. Aluminate phase in combination with gypsum reacts with water to form Ettringite. After gypsum depletion the produced ettringite enter to the reaction with remaining aluminate to form mono-sulfoaluminate (MS) as below:



Hydration process of ferrite is resembling aluminate. The aluminum source in ettringite and mono-sulfoaluminate can be partially substitute by iron [17]. The pure ettringite and mono-sulfoaluminate provide phases which Al by Fe, and SO_4^{2-} by other ions replaced and will be named as AFm and Aft (alumina-ferric oxide, monosulfate & alumina-ferric oxide trisulfate respectively) [18]. Clinker contains alkalis that are easily soluble and together with CH phase results in high pH pore solution in hydrated paste. Considering the clinker component and cement hydration reaction, the classification of cement is shown in Figure 2.2 [19].

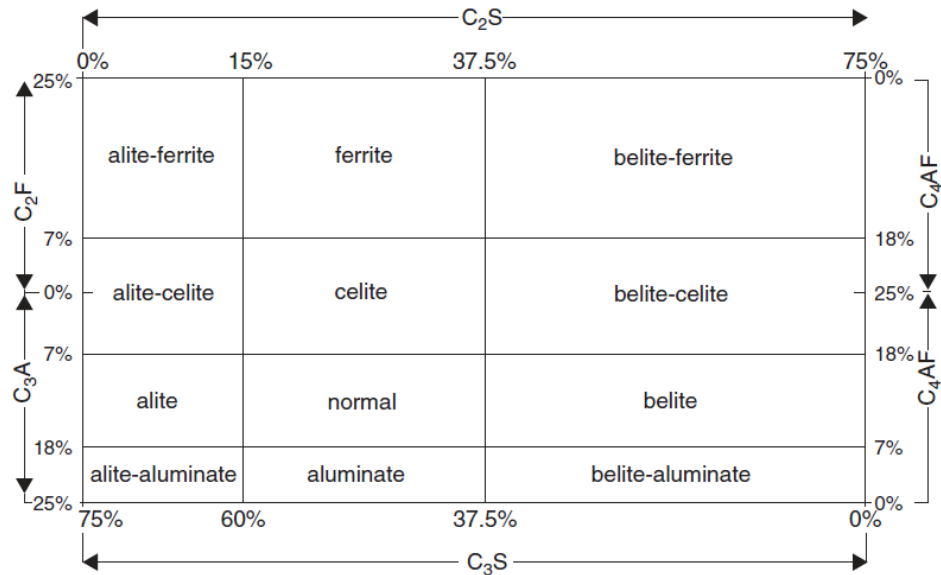


Figure 2.2 Classification of cement based on phase composition

Based on the classification diagram, it is possible to select the suitable method to define any individual component of required cement. The chemical determination of cement powder is associated to insoluble residue and loss of ignition. This relation is applied to classify the types of cement as it is shown in Table 2.1 [19]. This classification is linked to the additions. The total quantity of additive according to the EN 197-1 standard is around 1% by mass in cement composition (except for pigments), and this ratio shall not pass the 0.5% for organic additives. It should be noticed that, these additives may not cause any corrosion of reinforcement or impair the cement components [20].

Table 2. 1 Cement chemical composition classification (content of Cr cannot exceed 2 mg/kg)

1	2	3	4	5
Property	Test reference	Cement type	Strength class	Requirements ^a
Loss on ignition	EN 196-2	CEM I CEM III	all	≤ 5,0 %
Insoluble residue	EN 196-2 ^b	CEM I CEM III	all	≤ 5,0 %
Sulfate content (as SO ₃)	EN 196-2	CEM I CEM II ^c CEM IV CEM V	32,5 N 32,5 R 42,5 N	≤ 3,5 %
			42,5 R 52,5 N 52,5 R	≤ 4,0 %
		CEM III ^d	all	
Chloride content	EN 196-21	all ^e	all	≤ 0,10 % ^f
Pozzolanicity	EN 196-5	CEM IV	all	Satisfies the test
<p>^a Requirements are given as percentage by mass of the final cement. ^b Determination of residue insoluble in hydrochloric acid and sodium carbonate. ^c Cement type CEM II/B-T may contain up to 4,5 % sulfate for all strength classes. ^d Cement type CEM III/C may contain up to 4,5 % sulfate. ^e Cement type CEM III may contain more than 0,10 % chloride but in that case the maximum chloride content shall be stated on the packaging and/or the delivery note. ^f For pre-stressing applications cements may be produced according to a lower requirement. If so, the value of 0,10 % shall be replaced by this lower value which shall be stated in the delivery note.</p>				

As it is shown in Table 2.1, according to the global standards, there are five different types of cement. The general types are (i) Portland Cement, (ii) Portland-composite Cement, (iii) Blastfurnace Cement, (iv) Pozzolanic Cement, and (v) Composite cement [20]. There is also another theoretical method to calculate the cement constituent that is called as Bogue formulation [21, 22].

$$S = SiO_2 - SiO_2 \text{ (insoluble) when } M_G < 0.64 \quad (2.5)$$

$$C = CaO - CaO \text{ (free)} - 0.7 SO_3 \quad C_3S = 4.07C - 7.6S - 4.48A - 2.86F$$

$$C_3S = 4.07C - 7.6S - 1.43F - 6.72A \quad C_2S = 2.87S - 0.75C_3S$$

$$C_2S = 2.87S - 0.75C_3S \quad C_4AF = 4.77A$$

$$C_3A = 2.65A - 1.69F \quad C_2F = 1.7F - 2.6A$$

$$C_4AF = 3.04F$$

$$CaSO_4 = 1.7SO_3$$

The sensitivity of the Bogue method is enough good to make it possible to trace the wrong sets may causes by quantity of hemihydrate gypsum. Bonin investigated the stiffness of cement paste and concrete and effective reasons [22]. He mentioned the false set about alkali carbonation that react with calcium hydroxide and calcium carbonate precipitate. In this condition the in existence of moisture the ettringite formation will be changed [22].

By going beyond the cement constituent, the hydration process of cement is an important topic for many studies to find out more. As it is mentioned, when the cement powder encounter to the water, virtually all the alkali sulfate from clinker dissolves rapidly. Calcium sulfate dissolve until saturation of solution. Among the main clinker phases aluminate is the most reactive which this reactivity followed by alite, belite and ferrite. Ferrite is generally reactive phase but in hydration process it shows slow reaction [23]. Observing the heat evolution in hydration process could be the good indicator to understand cement. Hydration is an exothermic reaction and the heat rate evolves is different for first three days and so on. Figure 2.3 represent the general shape of heat evolution plot to reveals more fact about cement hydration [23].

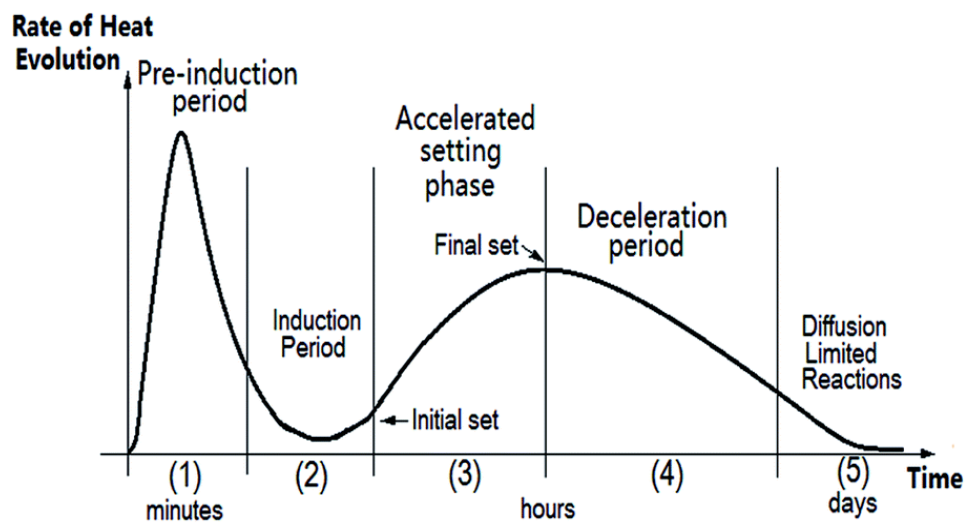


Figure 2. 3 Heat evolution of cement hydration

The graph shows the rapid exothermic reaction at the first stage when water was added to the system. The initial stage lasts few minutes and following by induction period as second stage.

Nucleation of C-S-H begins in this stage and the gel form C-S-H covers the clinker grains. The heat of hydration inclines again in third stage while the C-S-H starts to grow, and strength develops. Generally, the main characteristics of the heat evolution plot can be described as [25]:

- The initial increment in graph is due to the aluminate and alite hydration and hydration of hemi-hydrate gypsum that transfers to dihydrate form (Phase 1).
- After first stage, the hydration slows down and decreases in few minutes to deposit the hydration products on cement grains surface. During induction period, the paste is going to sets from the plastic and freely flowing condition (Phase 2).
- Third stage is the time for gradual rate up of aluminate and alite hydration and belite also begins to hydrate (Phase 3).
- During the declaration period, the total heat of evolution is going to decrease and if there is any small subsequent increase, it would be due to the ettringite formation and ferrite hydration (Phase 4).

After few days, the heat evolution rate tails off and the un-hydrated cement components become scarcer and block with hydration product. More than heat evolution of cement hydration, knowing more about the hydration products could be helpful. First, it should be noticed that the concepts of “setting” and “hardening” are different. Setting is a transition form of cement from fluid to solid state. So, the terms “initial” and “final” sets are commonly used for conventional definition of early and later set. Vicut is the usual test to describe the setting stage of cement paste and concrete. Hardening is associated to the strength of pastes. The rate of hardening is related to the increment of strength and independent from the setting rate [26]. The setting in cement paste happens whenever solid particles in the mixture connects by hydration products, mainly ettringite and C-S-H. By passing the time the connection between clinker components, hydration products and aggregates are intensified. These physical transformations can be more understandable to know more about hydration products. It is already talked about the C-S-H is the main product of cement hydration. It plays the main role in cement paste and consequently concrete strength. C-S-H or calcium silicate hydrate is a gel form or amorphous phase that is prepared from alite and belite hydration. In cement powder, the ratio of calcium to silicon is somehow variable but

commonly 2:1 [17]. The ratio of calcium to silicate is the indicator to control the cement quality in term of hydration. This ratio for belite is around 2:1 and 3:1 for alite. The excessive amount of Ca causes more production of C-S-H and calcium hydroxide. Calcium hydroxide is produced from alite and free lime hydration. It forms a hexagonal platy crystal, 1 μ m-20 μ m across. Ettringite crystals usually form a cover over the surface of aluminate phases to make a barrier for further hydration. This assumption is still controversial among the cement experts but well enough to justify the retardation of hydration products [26]. Ettringite is like acicular crystal – thin rods a micron or so in length. These crystals normally increase in size in the range of 5 μ m to 10 μ m in existence of enough water. These needle shaped hydration particles play an important role in setting of cement but not enough strong to affect on compressive strength of hydrate cement paste. Figure 2.4 shows the hydrated cement paste fracture and the products [24].

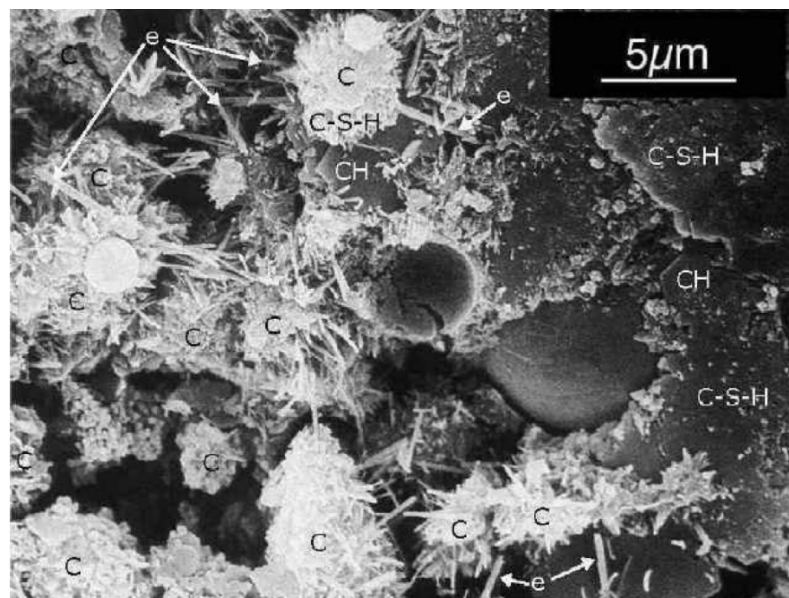


Figure 2. 4 Hydrated cement paste fracture (after 2 days), needle shaped Ettringite (e); hexagonal plates of calcium hydroxide; calcium silicate hydrate (C-S-H); Left side of image includes porosity and numerous capillary pores (up to 5 μ m); hydration cement particles

More than these products, monosulfate forms typically after 1-3 days. Monosulfate is like ettringite but structurally different. The ratio of $C_3A:CaSO_4$ is about 1:1 whereas in ettringite

1:3 [27-28]. Further consideration about cement hydration goes through the water specification. The most important factor in cement hydration is the water to cement ratios. Amount of water that is mixing with water can affect the porosity and permeability and consequently compressive strength. Most of the cement paste and concrete has w/c ratio between 0.3 to 0.7 [29]. By increasing the water to cement ratio the porosity of paste fraction will increase as well and tend to two main consequents [30].

- Weakening the paste due to the more porosity
- Interconnection of pores which makes the paste more permeable

Figure 2.5 shows the effect of changing in water to cement ratio that alters microstructure of the pastes [27].

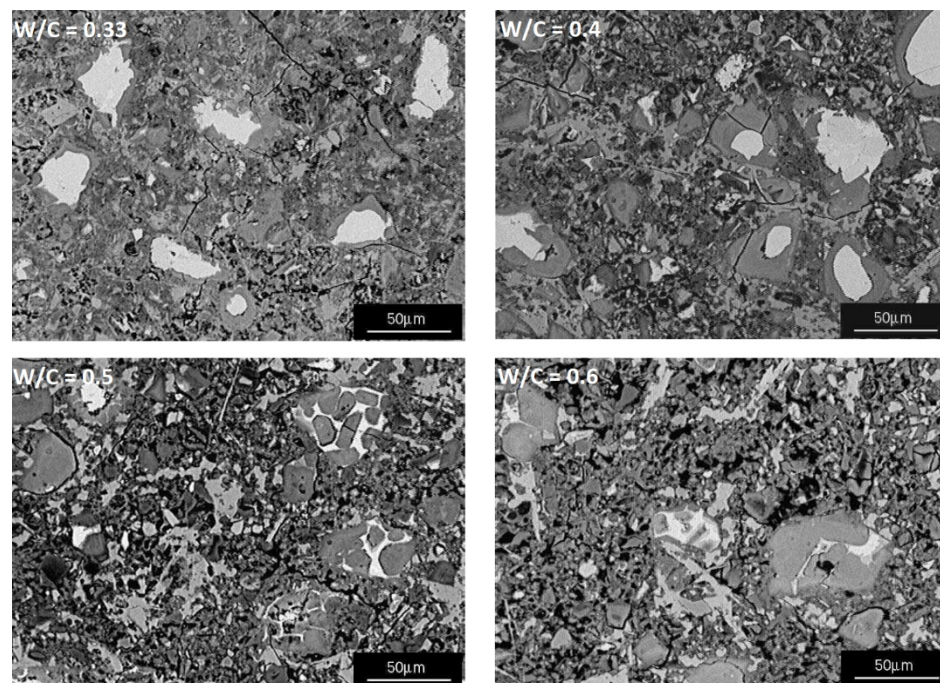


Figure 2. 5 Polished section of hydrated cement paste (after 2 years) for various w/c

In Figure 2.5 the brighter features represent the un-hydrated phases. The darker parts illustrate the capillary pores that is for instance almost less than 2-3 μm in 0.33 sample. By comparing the lower and higher water to cement ratio (w/c=0.33 vs. 0.6), two features are

rapidly emerged: higher w/c causes larger capillary pores (up to 10 μm) and so numerous and less un-hydrated particles and most of them are ferrite phase. Calcium hydroxide fills part of pores and occupied vast areas. Several regions of calcium hydroxide include 50 μm length and about 5 μm width. Based on this comparison, for middle cases the porosity and proportion of residual un-hydrated cement are intermediate. Imaging of hydrated cement paste could represent the altering of features but not enough to have any idea about the compressive strength properties. But since there is an assumption about the relation among porosity and strength, the compressive strength of 0.33 would be more than the others. Moreover, more porous sample means more permeable and less resistance to deleterious processes such as frost damage, chloride ingress or sulfate attack [31]. In summary by increasing the water to cement ratio some changing would occur as: (i) increasing the porosity of cement paste, (ii) increasing the permeability of cement paste, (iii) decrease in compressive strength, and (iv) decrease in proportion of un-hydrated cement components [32]. The testimonial facts show that the water to cement ratio has the drastic role in cement microstructure and phase distribution. By considering the whole information that is found until now, it is possible to have general description for cement hydration. Supposing there is cement paste prepared by mixing the ordinary Portland cement and water. The hydration as a function of time could be define as [33]:

- $T=0$: Instant of mixing, water and un-hydrated particles start to react
- $T=\text{a few mins or a few hours}$: High initial reaction of aluminate and alite. Sulfates from gypsum and clinker begin to dissolve and amorphous gel containing alumina, lime, sulfate and silicate start to forms. Ettringite needle shape crystals also growing up while this set followed by dormant period. This initial setting commonly takes 2 hours to happen.
- $T=6 \text{ to } 12 \text{ hours}$: C-S-H forms from the alite hydration and calcium hydroxide with large hexagonal crystal reveals. Aluminate hydration will be continued to prepare more ettringite. C-S-H dense gel coat the clinker component and delicate sheet structure bridging the water-filled gaps between the cement grains. Paste is set but still no tangible strength.
- $T=1 \text{ to } 3 \text{ days}$: almost after one day the whole sulfate phase is used while the aluminate hydration is still ongoing and that's why the change in ratio of sulfate to

aluminate happens. Hence, the altering from ettringite to mono-sulfate is taking a part in hydration process. After few days, the Al to S ratio is going to change from 2:3 to 2:1 and the platy crystal of mono-sulfate will form. Ettringite is going to decompose and substitute by mono-sulfate while the C-S-H and CH form in water-filled regions in the gap of cement grains [34]. This trend became slower through the time that means the slower formation of C-S-H. Moreover, alite phase reduces and belite begin to participate more in strength development. The Si/Ca ration in C-S-H is almost 0.5 to 0.6. After four weeks, the hydration follows ever-slowing rate and almost most of the hydration products already formed.

2.4. Supplementary Cementing Materials (SCMs)

By combination of ordinary Portland cement and another hydraulic or pozzolanic materials, composite cement will be formed. Most of these additives play a tangible role in hydration products but some admixtures such as CaCl_2 only influence on this process [35]. In general, composite cements are the blended cements including ordinary Portland cement and some other inorganic and reactive materials that could participate in forming of hydration products [36]. These materials are usually considered as extender or mineral additions which are known as supplementary cementitious materials (SCMs). They blend with the OPC during the production or on construction site. The most common SCMs are [36]:

- Blast Furnace Slag (or, granulated blast-furnace slag, pelletized slag, gbs)
- Fly Ash (Pulverized fuel ash, pfa)
- Limestone

The additional inorganic minerals commonly incorporate in cement blends for two main reasons. First, the economical saving and secondly the tangible improvement of concrete mechanical performance like strength and durability [37]. For blended cement or composite cement, to avoid the confusion, usually water to solid (w/s) is going to be used instead of water to cement (w/c) ratio which means the ratio of water to total cementing materials [38]. The application of SCMs is become profoundly significant due to the environmental benefits. Some of them like fly ash and slag are byproducts from industrial processes and give the

technical benefits to composite cement while there are some difficulties to use them [39]. These mineral additions are rarely “latently hydraulic” in some cases that means slightly reactive in water and could be more in existence of alkaline phases such as lime and cement. Slag is main representative of these kind of materials [40]. Other types of SCMs are commonly pozzolanic and would not enter to the reaction with water but react with water and lime or cement. In existence of proper amount of lime, pozzolanic material enter to the pozzolanic reaction and form calcium silicate hydrate [41]. The famous pozzolanic materials are fly ash, silica fume, metakaolin (activated Kaolinite or china clay) and volcanic glass [42]. The application of bricks and tiles that are crushed fired clay, and volcanic glass are discovered in Roman times to be used in Roman mortars. Volcanic glass (e.g. EN196-1) is the first pozzolanic material in history and then activated clay came to the construction industry [43]. SCMs could boost the concrete strength due to the consumption of calcium hydroxide and forming more C-S-H. Also, they intensify the durability of the cement and concrete by forming the C-A-S-H. The Si/Ca ratio in slag and low-lime fly ash are higher than the OPC. Silica fume and metakaolin contain almost no calcium [35,43]. Inclusion of any kind of SCM will provide the excessive source of silica and results in more formation of C-S-H comparing to the OPC. In term of porosity and permeability, literally the porosity of the blended cement is more than OPC specifically in early days, but permeability of the OPC paste is higher than the blended cement [44]. It is still somehow ambiguous that how the composite cements have more porosity and lower permeability. The feasible reason is the interconnection degree of pores in this paste. Besides, the morphology of C-S-H changes as the Si/Ca ratio increases, with the formation of isolated voids [45]. Moreover, fly ash and slag contain more aluminum than OPC. This will cause more hydrated products that containing aluminum like AFm [46]. AFm phase has contribution in strength but decrease the porosity as well. Same as pores, AFm also effects on engrossing dissolved anions, specially chloride and will cause reduction in rebar corrosion in concrete [47,48]. Generally, mineral addition provides Si/Al more than 1. The glassy fraction is usually among 2:1 and 3:1. The same ratio in low-lime fly ash is about 1.5:1 but this include alumina bound in unreactive crystals such as mullite [49].

The benefits of mineral addition can be summarized in some sentences [50]. (i) Improvement in concrete strength performance, (ii) Using the waste industrial material that causes cost

reduction, (iii) Volume reduction in materials that ease the transportation, (iv) Reduction in depletion rate of raw materials in OPC, (v) SCM production per unit volume in term of energy requirement, and (vi) carbon dioxide emission mitigation per unit volume of concrete [45,49]. Hence, one of the main concerns in cement industry is to reduce the carbon dioxide emission. The CO₂ emission is almost between 800-1000 kg ton but there are some efforts to lower it [25].

Beside the benefits of using mineral additions, some potential problems should be noted. Using of some additives may mitigate the strength development rate comparing to the OPC. Only silica fume and metakaolin could be enough reactive to partially compensate this slowing down [51]. Concrete is usually specified for 28 days compressive strength and in most cases the composite cement strength is comparing with the OPC paste in this setting time [52]. On the other hand, samples are curing in full saturated and ambient temperature (typically 20°C) that represent the strength in large pours [34, 50]. Moreover, SCMs are going to use the calcium hydroxide that is produced during the hydration reaction of cement to provide more C-S-H. This will lower the alkalinity of pore fluid as well [53].

2.4.1 Blast Furnace Slag

Blast furnace slag is by-product of iron smelting [46]. The impurities such as silica will be gathered by limestone flux and the pure iron ore is the product. By cooling the liquid which tapping off and producing latently hydraulic glass, slag will form [47]. This slag is using for concrete in large scale and will produce calcium aluminosilicate glass and some other crystalline phases like gehlenite (C₂AS) and merwinite (CMS₂). These crystalline phases are usually unreactive and if the cooling of slag occur in slower rate this fraction will be increased [47]. There are two main method for rapid cooling:

The first method for producing the slag is pouring liquid in large volume of water. The resulted cooled slag contains 90-98% of glass. Figure 2.6 shows the water manger for rapid cool down of slag.

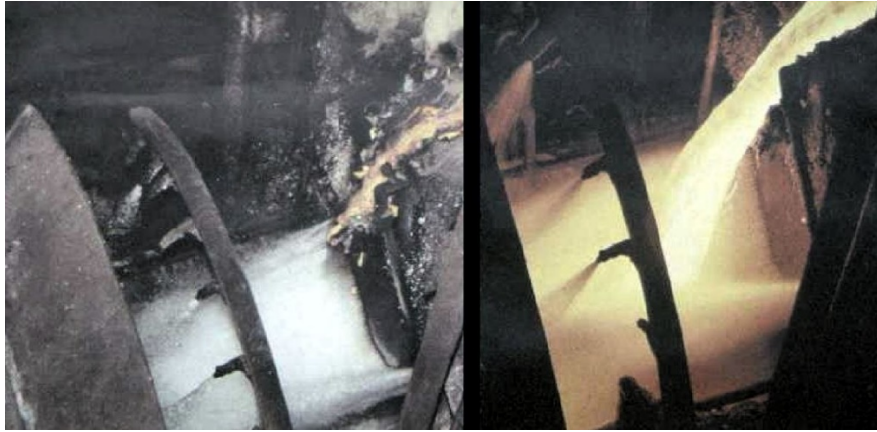


Figure 2. 6 Slag production: fast-moving stream of water (left), and molten slag flow into the water stream and quenched (right) [54].

By pouring the liquid slag into the water-cooling rotating drum, the amorphous slag will be produced. Figure 2.7 shows the procedure that slag pellets is propelled through the air in a chamber of water spray. Pelletized slag contains less glassy phases than granulated slag that is approximately 70-90% [54].

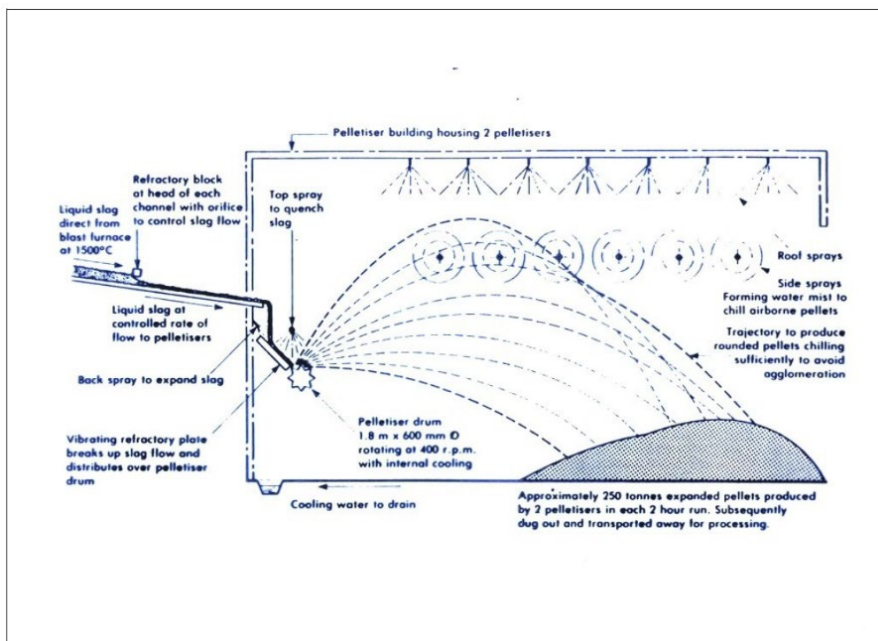


Figure 2. 7 Pelletized slag production procedure schematic [54].

The usual substitution of slag as SCM is in the range of 20-70 wt%, but in some specific applications this portion could be higher. There are several benefits of using slag as SCM that should be categorized in some main topic [54]:

- Using slag reduces raw material consumption for OPC production
- Using slag causes energy reduction for production of SCM
- Using slag reduce the total carbon dioxide emission

Focusing on application of slag in more detail, it develops the late strength more than pure OPC but reduction in early strength. It also reduces the permeability, improved durability by mitigation of alkali-silica reaction and chloride penetration. Moreover, slag will lower the heat of hydration and consequently risk of thermally-induced cracking [55]. Replacing the OPC with slag will reduce the early strength and boost the late strength. In most mature concrete, after a year almost 50-75% of slag is already entered the reaction. This amount is associated with w/s, intrinsic reactivity of slag and its fineness. The hydration product of the blended cement paste by partial slag substitution resembles OPC while the CH is going to be consumed and more C-S-H will form. This C-S-H has higher Si/Ca ratio. Besides, more accessible alumina from slag hydration, more sulfate will enter to the AFm phase causes less ettringite in system [49-55].

2.4.2. Fly Ash

Fly ash is mainly produced in powerplants (see Figure2.8) by burning pulverized coal and accordingly the chemical composition of it is related to the coal minerals.



Figure 2. 8 Powerplant station, source of fly ash [35]

According to the European standard, the fly ash composition is mainly containing high proportion of alumina and silica and glass. Table 2.2 represents the typical chemical composition of fly ash [56].

Table 2. 2 Low-lime fly ash chemical composition [57]

SiO₂	Al₂O₃	Fe₂O₃	CaO	MgO	K₂O	Na₂O	SO₃	Total
53.0	26.6	8.0	2.2	1.2	4.2	1.6	1.0	97.8
Balance is mainly carbon, with minor oxides including P ₂ O ₅ and Mn ₂ O ₃ .								

The glassy content of fly ash is almost 70-90% and the rest is allocating to crystalline phases like quartz (SiO₂) and mullite (aluminosilicate, Al₆Si₂O₁₃ or Al₆Si₃O₁₅) with the particle sizes ranging from 1μm to 50μm and in some cases up to 100μm [57]. Most of the particles in fly ash microstructure are slightly different impure aluminosilicate. Figure 2.9 shows the micrograph of the commonly known fly ash.

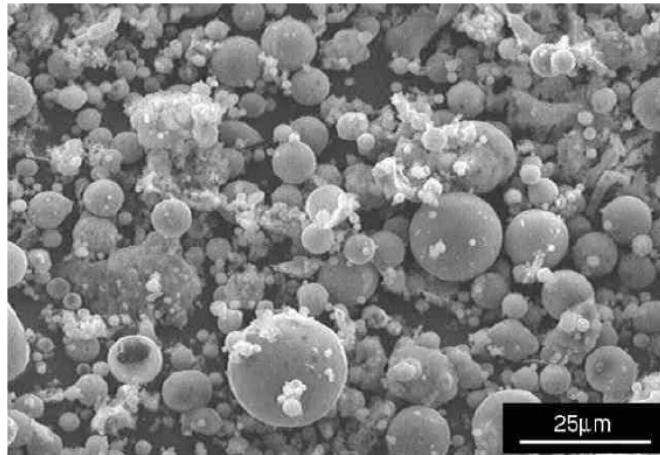


Figure 2. 9 SEM image of fly ash particles [47]

The aluminosilicate particles in fly ash are of broadly resembles each other while some are iron-rich and some other silica rich. Also, minor portion of them is rich from oxides like titanium dioxide [58].

The common substitution of OPC with fly ash is 30 wt% of the total cementitious material. The technical advantages of fly ash in blended cement is like slag [59]. Fly ash can give proper late strength in ambient temperature with less water for workability. Moreover, the intrinsic permeability decreases, perhaps due to the increment in Si/Ca of C-S-H [58]. The amount of carbon that is accommodated in fly ash can define the water demand of the mixture, so the lower carbon content can reduce the water demand. The strength development of fly ash is lower than the slag and related to the pore size, it could be somehow less than OPC [60]. The unique privilege of the fly ash is efflorescence effect of it that cause the reaching of the soluble salts to the surface (especially CH) [59].

During the hydration, the released silica from fly ash will form C-S-H while the released alumina contributes to formation of hydrogarnet (C_3AH_6) and Stratlingite (C_2ASH_8) [60]. Quartz and mullite are the inert phases of the fly ash that occasionally can be seen in SEM micrographs [61-62]. Figure 2.10 compare the composite cement paste by replacing the cement with slag and fly ash.

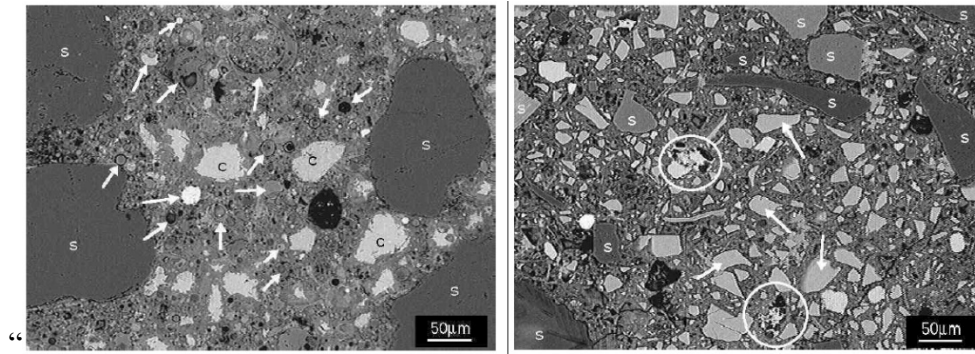


Figure 2. 10 Left: Concrete particle polished section using 70 wt% OPC and 30 wt% fly ash (c: hydrated cement particles, s: silica sand, arrows: fly ash particles). The difference among fly ash particles color is associated to their chemical composition in term of iron content / Right: Concrete particle polished section using 30 wt% OPC and 70 wt% slag (circles: hydrated cement particles, s: sand mainly silica and feldspar, arrow: slag particles); the slag particle color is almost same [62].

2.4.3. Silica Fume

Silica fume of micro-silica is by-product of silicon production that is amorphous silicon dioxide. The spheres particles with $0.1\mu\text{m}$ across introduce highly pozzolanic reactivity [63]. The surface area of silica fume is higher than the other SCMs that causes higher water demand and limits the amount of replacement [64]. The reactivity of silica fume is relatively higher than other SCMs and prepare large amount of C-S-H that reduce the porosity of concrete. Silica fume is often used for high strength mortars and high surface area mitigate the bleeding of concrete [65]. Silica fume is accessible in densified, un-densified and slurry forms and to it is important to disperse it adequately [66]. For binder replacement, densified micro-silica is more applicable [67]. The densified silica fume decreases the permeability to water and lead to better durability and chloride or sulfate resistance [68]. Furthermore, using silica fume will reduce the ASR due to the decrease in pH because of CH consumption to form C-S-H [69].

2.4.4. Limestone

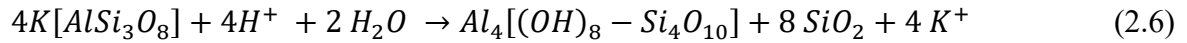
Limestone is the main raw material to produce OPC. But it is also using as a mineral addition to cement while it is not pozzolanic or latently hydraulic [70]. Generally, small addition of limestone (almost 5%) is using for the cement but as a mineral additive this portion is much higher. According to the ENS 197-1, CEM II /A-LL and CEM II/B-LL contains 6-20% and 21-35% limestone respectively [70-72]. These types of cement are commonly called as Portland Limestone Cement (PLC) [72]. The application of PLC has begun in Europe and became more widespread during the last decade and take the quarter of cement market in north Europe [73]. The main advantages of PLC are (i) Cost of production and consumption, (ii) control of shrinkage, (iii) reduction in concrete bleeding and (iv) Mitigation of carbon dioxide emission [70]. This specific type of cement may produce by inter-grinding of limestone with clinker or mixing it in the mixer. Each of these methods will result on limestone particle size and will lead to different characteristic of cement [73]. The co-grinding of clinker and limestone is typically preferable since limestone is softer than clinker and will ensure more finer cement particles [71-73]. Finer limestone has the better filler effect that fill the clinker particles gaps and is more reactive in the hydration process. For the constant w/c the 28 days strength of PLC is less than OPC, but its durability is more than cement [74]. The hydration rate of alite in PLC is increasing and giving more early strength. Besides, hemi-carbonate and mono-carbonate will be formed due to the reaction of aluminate phase with limestone. Mono and hemi carboaluminate fill the pore spaces and reduce the permeability and consequently increase the durability [75]. They may also have some contribution in paste strength [72].

Based on the lower production of slag and fly ash, undesirable transportation problems and availability of limestone PLC is highly demanded composite cement. It is also affect on lowering the clinker production.

2.5. Calcined Clay as SCM

2.5.1 Clay Minerals

There is no uniform description for clayey materials due to the different disciplines that study about clays. But as a general statement, clay is product of alteration of silicate minerals in different deposits [76]. However, there are some definition about the clay but in 1995, Association Internationale pour l'Etude des Argiles (AIPEA) and Clay Minerals Society (CMS) stated the proper definition about clayey materials. *"Clay is a naturally occurring material composed primarily of fine-grained minerals, which is generally plastic at appropriate water contents and will harden with dried or fired."* [77]. To have more sight on this definition, plasticity is the material mechanical characteristic that can shape it in any form and fineness considers the particle size less than 2 μm [78]. Nevertheless, the particle size is not uniform for any kind of clayey material. Another definition for clays is *"Clay minerals are phyllosilicates and minerals that impart plasticity to the clay, and which harden upon drying or firing."* [77]. This definition represents two different clayey material including naturals and synthetic phyllosilicates. Hence, wide range of minerals like quartz, calcite, dolomite, feldspars, iron and aluminum oxides, ilmenite, barite, zircon, rutile, iron or silica hydroxide gels may associate to clay [76,81,82]. The formation process of the clay is the trituration of the rocks due the weathering, transportation and sedimentation in an aqueous medium. By erosion of silicon and aluminum rich rock the clayey minerals form [83]. The structural difference among the clays depends on the climatic conditions, for instance illite and chlorite type clays are typically form in cold or polar condition while smectites are more observable in Mediterranean and tropical regions. Kaolinite that contains Al-Fe oxides and hydroxide mostly forms in wet tropical and equatorial zones [84]. Some other places that clayey material can be found are volcanic deposits, marine sediments, geothermal fields and low-grade metamorphic [85]. Most of the clay minerals forms by unstable silicates, but the precipitation from solution and lead to new form of clayey minerals which are different in composition [84,86]. Moreover, the acidity of the water may exchange of protons for cations. For example, Muscovite will change to illite or biotite and chlorite will transform to smectite, feldspars could destabilized and convert to Kaolinite [84].



(K-Feldspar)

(Kaolinite)

Clay minerals on the other hand can form due to the hydrothermal activity which as to relation to sedimentation [85-88]. Figure 2.11 illustrates the schematic of primary rocks weathering and erosion that will lead to clay formation.

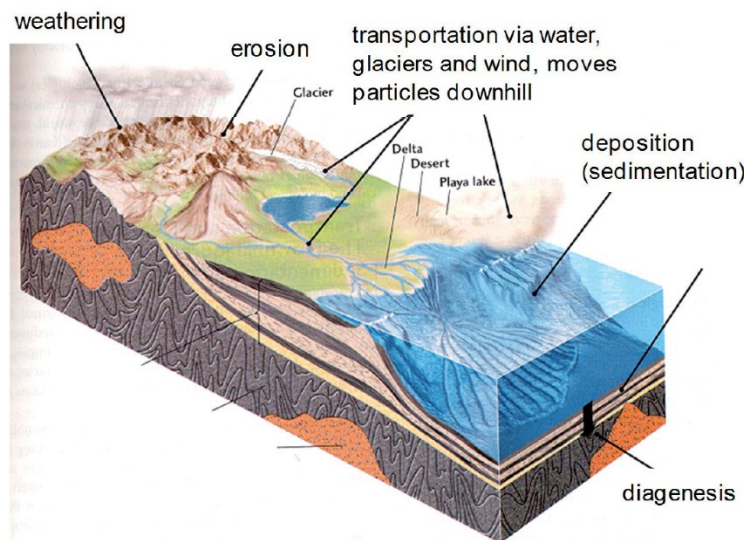


Figure 2. 11 Transportation of sediments and erosion of rocks schematic [89]

Clays can be formed due to the residual deposit of soil that will be called as primary clays or from secondary sediment source after erosion and transportation from genuine situation. The main resource of clay is the places that sedimentary rocks exist, and the erosion could transfer the rock to clay. Since water is the primary transporter of the clay, the particle distribution and mineral setting is related to the transportation procedure [88]. By continuously altering in clay, the diagenesis of unstable clay the new minerals like smectite mixed layered zeolites will be formed. Illite/Smectite mixed layer minerals represent the diagenetic evolution of sedimentary clay basin [90]. After the diagenesis (cementation) the temperature and pressure

will be launched as transformation or metamorphizing step. Clay minerals is divided to general classification including three main group [85,90]:

- Kaolin Class including Kaolinite, Dickite, Nacrite, ...
- Smectite Class including Montmorillonite, Nontronite, Beidellite, ...
- Illite Class including Illite, Glauconite, ...

The foundation of the all classes are similar but they are so different structurally and composition. The original units that define the atomic structure of all clayey type materials are the tetrahedral sheet of silica and octahedral sheet of alumina [90]. The overall clay crystal structure is composed of tetrahedras connected by sharing three corners while the not-connected corners are in same direction. The tetrahedras include Si-Al cation coordinated by four oxygen and hydroxyls [82,90]. The formation of octahedral sheet is closed-packed lattice of hexagonal oxygen and hydroxyl that are ordered around aluminum ion. The octahedras that re connecting as neighbor are sharing their edge as a pseudo-hexagonal symmetry. These layers orientation is along the a, b crystallographic directions [85]. The corners of octahedras that are not shared will be occupied by mainly hydroxyl anions or in some occasions F^- and Cl^- . These anions are located close to the pseudo-hexagonal rings center that are already formed by the tetrahedras. As it can be seen in figure 2.12 the combination of one or two tetrahedral sheet with one octahedral sheet 1:1 or 2:1 clay mineral will be formed [78,81-82,90-91].

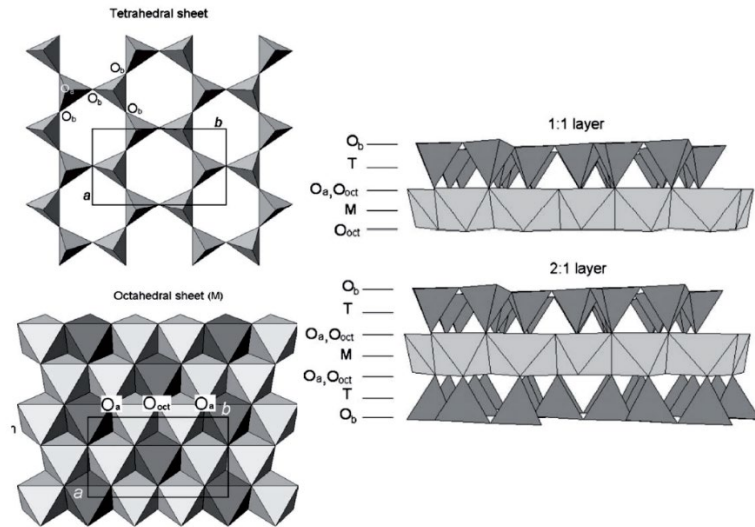


Figure 2. 12 The clay mineral tetrahedral and octahedral sheets. Ob and Oa represent basal and apical oxygen atoms, Ooct is octahedral anionic position [90]

To be clearer, all clayey type materials are introduced as layered micro structured minerals. The sandwich type crystal structure of clay consists of one layer of octahedral alumina and tetrahedral silica for simple structure clays like Kaolinite and repetitive layered for more complex structure clay like illite and smectite [92-94]. Figure 2.13 simplified the categories of clay minerals.

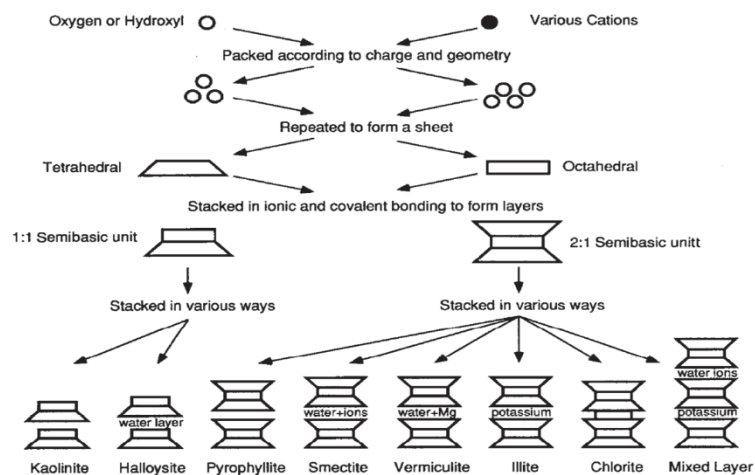


Figure 2. 13 Clay mineral structural patterns [87]

Each of the mentioned three main class of clay have their own specifications. Table 2.3 represents the different classes mineral characterization.

Table 2. 3 Clay classes mineral characterization [95]

Name	Group	Crystal system	Ideal Formula	Isomorphous substitution	Interlayer Bond	Basal spacing
Kaolinite	1:1	Triclinic	$\text{Al}_2\text{Si}_2\text{O}_5(\text{OH})_4$	Very little	O-OH, strong	7.2 Å
Illite	2:1	Monoclinic	$(\text{Si}_4)(\text{Al,Mg,Fe})_{2,3}\text{O}_{10}(\text{OH})_2 \cdot (\text{K,H}_2\text{O})$	Some Si by Al, balanced by K between layers	K ions, strong	10 Å
Montmorillonite	2:1	Monoclinic	$\text{Na}_{0.33}(\text{Al}_{1.67}\text{Mg}_{0.33})\text{Si}_4\text{O}_{10}(\text{OH})_2 \cdot n(\text{H}_2\text{O})$	Mg for Al	O-O, very weak, expanding lattice	> 9.6 Å

As it can be inferred from the given information, kaolinite is a part of 1:1-layer group and illite belongs to 2:1-layer group. On the other hand, isomorphous replacement are usual in these sheets and in some cases, cations like Mg^{2+} , Fe^{2+} , Fe^{3+} and Mn^{2+} can replace the Al^{3+} in layered structure and provide the clay diversity [95].

Considering the clay as a SCM is promoted in whole world recently. But reactivity of the clay is the main issues of several studies. Calcination of clay or in the better word activation of clay due to the heat-treatment is the main concern of the investigations about the proper activation temperature. Most of the recent studies focused on Kaolinite and the activated form of kaolinite that is so-called meta-kaolinite. Kaolinite is the simplest clay structure that could release its hydroxyl bonds through the heat-treatment. Hence, it is easy to change the kaolinite to meta form and use it as an admixture for cement substitute. However, knowing more detail about the kaolinite and destabilized form of it could lead us for further studies about activation of various class of clays.

2.5.2 Kaolinite and Meta-Kaolinite

As it is stated, Kaolinite is a 1:1 di-octahedral clay with the formula $\text{Al}_2\text{Si}_2\text{O}_5(\text{OH})_4$. Typically, 1:1 building is electrically neutral, the weak bonds among the units or Van der Waals bonds causes the significant cleavage for Kaolinite [96]. The space group of the crystals is P1-triclinic system and rare cases rhombic and trigonal structures can be seen. Kaolinite mainly forms from eroded magmatic and metamorphic rocks that contains high portion of aluminosilicates like feldspars [97].

Meta-kaolinite is the product of heat-treatment of kaolinite in temperature range of 700-900°C but usually less than 800°C. Moreover, the heating time should be aligned by the temperature regime, type of kiln and fineness of particles. More temperature (around 1000°C) can prepare “flash calcining” [96]. Based on the different experiments the best dihydroxylation temperature is around 550°C [97]. The kaolinite structure usually includes silicate layer connected to the gibbsite layer in a form that one oxygen atom from silica tetrahedron shared with gibbsite $\text{AlO}(\text{OH})_2$ tetrahedron. During the hydroxylation the alumina transforms to tetrahedral coordination [98]. This transformation can be used as proof for dihydroxylation of kaolinite. Metakaolin that is the product of partial or totally break down of crystal structure is significantly reactive in alkaline solution [99]. Hence, it can be used as a partial substitute for OPC [100]. The wide application of the composite that is made by metakaolin is for high temperature resistant concretes and hazardous wastes deposits construction [101]. Metakaolin is a great pozzolanic reactive mineral and reacts with calcium hydroxide to prepare C_4AH_{13} and hydrated gehlenite [102]. The trace of the hydrated phases from pozzolanic reaction could be detected by XRD after 3 days [103]. The more advantages of metakaolin is related to the consumption of CH and increasing the concrete resistance in front of aggressive media as well as sulphate corrosion [104]. Metakaolin is also decrease the permeability, chloride ion diffusion and protect the steel bars in term of corrosion [105]. Due to the high surface area of the metakaolin (10 to 25 m^2/kg), it could modify the rheological properties of cement and workability of concrete. Furthermore, the bleeding will be reduced, and the surface would be smoother but higher amount of metakaolin may need superplasticizer [106]. Hobbs [107] claims that the metakaolin intensify the flexural strength of concrete as well as the compressive strength after 28 days. Some studies believe that the

increment in concrete strength whenever metakaolin is used as SCM could be due to the microstructural modification in interfacial transition zone which is the cement and metakaolin zone bonding force [109, 110].

2.6 Clay Reactivity

2.6.1 Calcination of Clay

Some studies estimated the activation temperature of clayey materials and evaluated the calcined clay reactivity whenever mixed with lime and cement. Among the clayey material the class I has the highest reactivity followed by second class (e.g Ca-montmorillonite) [111]. Other calcined clays could be considered as lower pozzolanic materials even if they are activated in proper temperature [117]. Sabir [118], Siddique [119] and Fernandez [95] confirmed that the kaolin has the highest pozzolanic potential among the other clayey type materials. The other investigations showed that the optimum activation temperature is in the range of 650 – 850 °C [112-116]. This temperature range is directly associated to the impurity of clay and companion minerals [119]. According to formula 2.7, degree of dihydroxylation (α) is explained as the remaining kaolinite fraction over the primary amount of kaolinite that is measure by TGA or DTA that shows the optimum calcination [120].

$$\alpha \text{ (degree of dehydroxylation)} = \frac{\text{Remaining clay minerals fraction}}{\text{Initial amount of clays}} \quad (2.7)$$

Bich [120] investigate the reactivity of calcined clay and lime that are heat treated in nine different conditions. It is reported that the best degree of dihydroxylation is almost more than 95%. Less than this degree the results are influenced by clay crystallinity [121]. The similar studies tried various methods to observe the paste behavior in blended cement mortars when the cement is substituted by 30 wt.% and it is found that the metakaolin is the best option [122]. Besides, the NMR, TGA and X-ray diffraction results confirmed that the consumption

of CH has the higher rate when metakaolin used [123]. The other studies that are concentrated on calcined clay cement are mainly use the clayey materials with high amount of kaolinite and in most cases the metakaolin is the main reactive clay and in rare experiments the amount of kaolinite is quite low or no kaolinite in composition [122-126]. Fernandez [45] claimed that the cement pastes with 30 wt.% of calcined clay with more than 40 wt.% kaolinite showed the similar compressive strength to ordinary Portland cement in 7 and 28 days of setting time. There are two main methods for calcination that are called static and flash. Salvador [126] reported the flash calcination effect on pozzolanic reactivity that revealed that the soak calcination decreases the reactivity. Flash calcination of the sample will provide the slightly better pozzolanic reactivity of clayey type materials [127, 184-186]. The thermal reactivation and methodology will be discussed in next section.

2.6.2 Calcination through Thermal Activation

Calcination process is the main concern in thermal activation of clayey material. The proper heating rate and calcination temperature would help to obtain more reactive materials. In most investigations, kaolinite is the case study but still the exact procedure during the phase transformation is a question mark among the scientists.

According to the different studies, there are two known method for calcination of raw powders, called static and flash calcination [128]. By considering the kaolinite as a proper example, it is possible to compare the heat treatments methods. Static calcination is the method to heat treat the material by the constant heating rate (usually 10°C/min) up to the determined temperature in a formal furnace. Flash calcination is different in term of heating rate that is much higher [129-130].

In static heat treatment method, the powder will be placed half-filled in high alumina crucibles and put it in a batch furnace. The sample will be heated up to the assigned temperature and cooled on a metal tray. The temperature is monitoring through the internal sensor and in this method the typical variation is about ± 5 °C [129-131].

In flash calcination method, the temperature control is done in a flash calcination device with a single burner when the clayey material particles flow within the tube [132]. The most important parameters are the temperature profile including the heating rate, maximum temperature and cooling procedure. Flash calcination based on its intrinsic could be beneficial or detrimental. If the calcination temperature and rate of flowing could not be controllable, the imperfect de-hydroxylation or overburnt may occur [129, 132]. Overheating the clays will cause overburnt and sintering of them and phase transformation. For instance, the overheating of the kaolinite (more than 900°C) transforms the kaolinite to mullite. The mullitization of kaolinite is normally starts from 900°C and end around 1200°C [133]. The optimum calcination condition that causes the de-hydroxylation of clay is directly related to the type of clay and its mineralogy as well as the existence of impurities. More over the particle size and humidity of the powder could affect on its decomposition. Table 2.4 is an experimental data for calcined kaolinite (metakaolin) to evaluate the amount of de-hydroxylated kaolin according to the flash calcination in various temperature.

Table 2. 4 The amount of metakaolin content in different kaolinite sample varied in flash calcination temperature (TGA results) [128].

	For 100% dehydroxylation	Flash_ 630	Flash_ 660	Flash_ 690	Flash_ 725	Flash_ 750
Metakaolin content [%]	45	35	37	39	40	41

Besides, the x-ray diffraction analysis that is shown in figure 2.14 confirmed the TGA results about the de-hydroxylation of kaolinite. This data could not reflect the specification of the sintered clay in term of emerging the mullite.

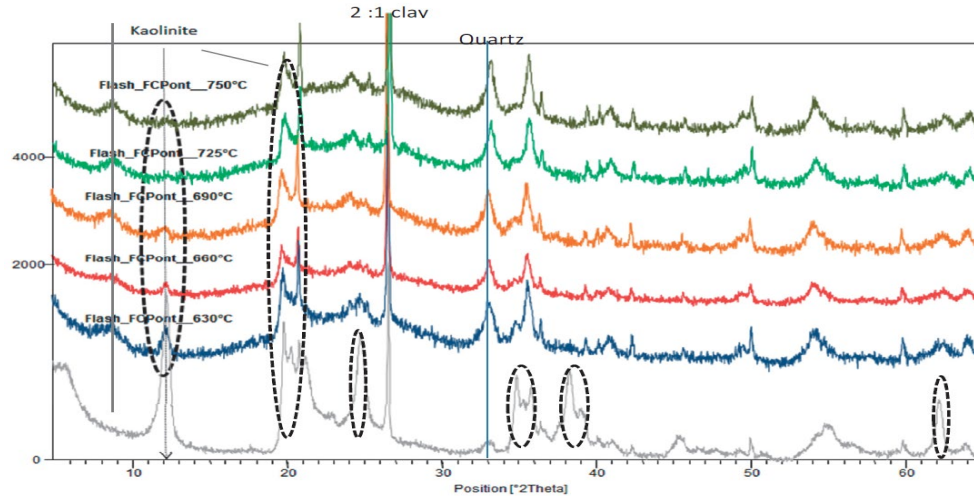


Figure 2. 14 X-ray diffractogram of calcined clay due to flash calcination in different temperature. Grey spectrum is a virgin material [128].

By comparing the static and flash calcination method which is applied in some experiments and their results, it can be inferred that the static calcination could be more applicable for most of the experimental and specifically industrial scales. The results of the two methods are shown in table 2.5. These outcomes include the flash calcination in various temperature for kaolinite de-hydroxylation in 2 batch of clay to normalize the obtained results. The percentage of the metakaolin is the indicator.

Table 2. 5 Metakaolin content of the calcined kaolinite via different calcination method (Flash calcination is done for various temperature) [128]

	Flash_2_750	Flash_2_850	Flash_2_900	Static_2
metakaolin content [%]	38	50	52	55

The illustrated results of metakaolin content is obtained from the TGA and checked twice for static calcination method. However, based on the other studies [127-133] that tried both method of calcination, there is no drastic different among the flash and static calcination while the static calcination method is more affordable for lab experiments and industrial application as well.

2.6.2 Thermal Activation

De-hydroxylation of clays in a proper temperature occur due to the structural water removal [139]. The well-known de-hydroxylated or calcinated clay is metakaolin which the decomposed form of kaolinite. Figure 2.15 shows the dihydroxylation steps of the kaolinite due to the releasing of hydroxyl bonds.

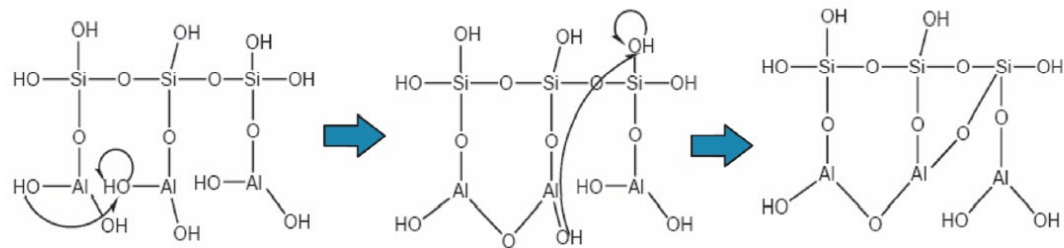


Figure 2. 15 Kaolinite de-hydroxylation schematic that causes disorder in alumina layer [140]

To quantify the atomic coordination in octahedral alumina and tetrahedral silica sheets of clay, MAS NMR test should be performed. Figure 2.16 illustrate the Al NMR spectra of kaolinite, illite and montmorillonite.

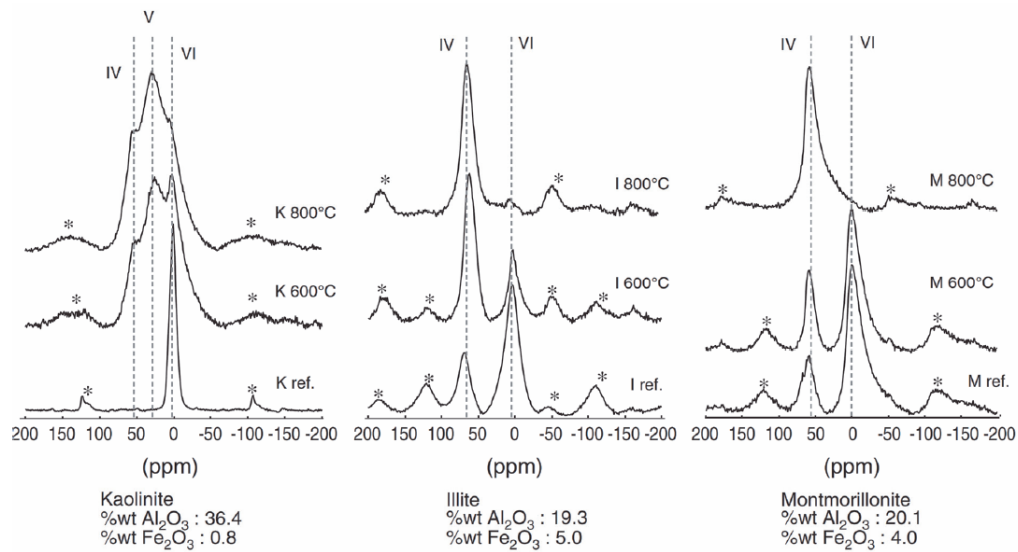


Figure 2. 16 The Al-NMR spectra associated to the Kaolinite, Illite and Montmorillonite, heat treated in RT, 300 and 800 °C [95]

The NMR spectra for Kaolinite shows Al ^[VI] while montmorillonite and illite include both Al ^[IV] and ^[VI] as well. This indicates that in kaolinite there is octahedral position for Al but in two others more than octahedral position, a substituting tetrahedral Si is also existing. Based on the related studies that utilized NMR test for characterize the calcined clay, four coordinated Al (Al ^[IV] and ^[VI]) are expensing Al ^[VI] after de-hydroxylation [113,141,142]. Montmorillonite is mainly resembling the other type of clays but Al ^[IV] is vastly dominate after heat treatment while there is no tangible trace of Al ^[VI], although it should be inferred that the broadness of the Al ^[IV] peak at the 800°C could be representative of this coordination [143]. Similarly, illite represents the gradual shift from Al ^[VI] to Al ^[IV] and clearly OH groups bound to aluminum due to de-hydroxylation. It could be beneficial to know that montmorillonite and illite are swelling clays and during the de-hydroxylation, they typically lose this specification. Hence, it is possible to consider them as a potential substitute for concrete binder [144].

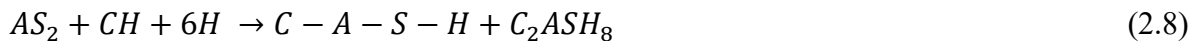
Recently, some studies [143-144] by using the density functional theory and pair distribution function analysis found that the metakaolin structure will be remained in 1:1 layering like kaolinite while the alumina sheet locally buckled. This finding is coincident to the Al NMR

test results but in 4, 5 and 7 coordinated Al, there is small percentage of three-coordinated aluminum [144, 145].

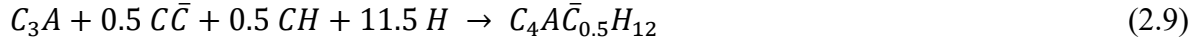
2.7 Limestone Calcined Clay Cement (LC³)

2.7.1 Calcined Clay and Limestone Effect on Hydration

The de-hydroxylated kaolinite, so called metakaolin and limestone have physical effect on cement hydration due to the providing new nucleation sites for permitting hydrate formation [35]. Besides, their substitution effects on water to cement ratio that provide more space for hydrated product. Due to the presence of the fine SCMs, shearing between the particles increases and will cause the boost in hydration. The shearing increment is mainly associated with the distance among the particles that consequently enhance the clinker hydration [28, 146]. More than physical effect, these two additives could chemically modify the hydration. It is already discussed that metakaolin as a de-hydroxylated form of kaolinite could enter to the pozzolanic reaction and consume the portlandite to form C-A-S-H and Stratlingite C₂ASH₈ [147-149, 189]. This reaction could briefly show as:



Limestone additives will help to produce aluminate phase during the hydration. In OPC without limestone additive, Ettringite (AFt) is a product of C₃A and C\$H₂ reaction and after termination of gypsum, the portion of ettringite will react with remaining C₃A to form Monosulfoaluminate or Ms [17, 192-195]. By addition of limestone to cement, it will react with C₃A and will produce carboaluminate hydrates in form of hemi- and mono- phases (Hc and Mc) [150, 151]. In addition, ettringite cannot find C₃A to convert to Ms anymore [152, 153]. The chemical reactions in term of limestone presence are as below [152, 154]:



During the hydration reactions according to the different investigations [155, 156], only 2 to 5 % of calcium carbonate enter to the reaction. The aluminate from the Celite is the determinative factor and the amount of Hc and Mc is directly related to the C₃A content [157] and primary Al/\$ ratio [151].

More detail investigations about the metakaolin and limestone addition revealed more privileges of them. Using metakaolin as SCM, could reduce the porosity and water absorption but most of them offer 10 to 20 wt% of substitution [117, 118]. Even though using calcined clay enhances the durability of blended cement, it would boost the sulfate resistant based on ASTM C1012-89 [158]. This mitigation in sulfate attack will lower the compressive strength loss [159]. Another sulfate attack involving CaCO₃ causes Thausmasite (CaSO₄-CaCO₃-15H₂O) formation. This would be detrimental in temperatures below the 15°C and in some occasion above 20°C [160]. Some experiences [161, 162] tried metakaolin to reduce the damage if thaumasite and found the significant effect compare to slag and natural pozzolans while the limestone cement shows mass loss and decay in compressive strength after two years which is due to the deterioration of C-S-H matrix. It is found that the thaumasite resistance is related to change in C-S-H composition (Al enrichment, and lofty C-S-H chain). Bellmann and Strack stated that the lower Ca/Si (1.1) ratios for C(-A)-S-H gel is more thaumasite resistant than the gels with Ca/Si = 1.7 [162].

Another claim [163] is going through the effect of CH in formation of thaumasite and stabilization of Ca/Si for C(-A)-S-H [164]. Hence, the metakaolin as SCM could be enough beneficial to increase thaumasite resistance [165, 196-197]. Although the metakaolin can make the limestone as a positive effect additive but still there is more need to know limestone. Figure 2.17 illustrates the thermodynamic modeling of carbonate effect on phase formation by assuming the excessive calcium.

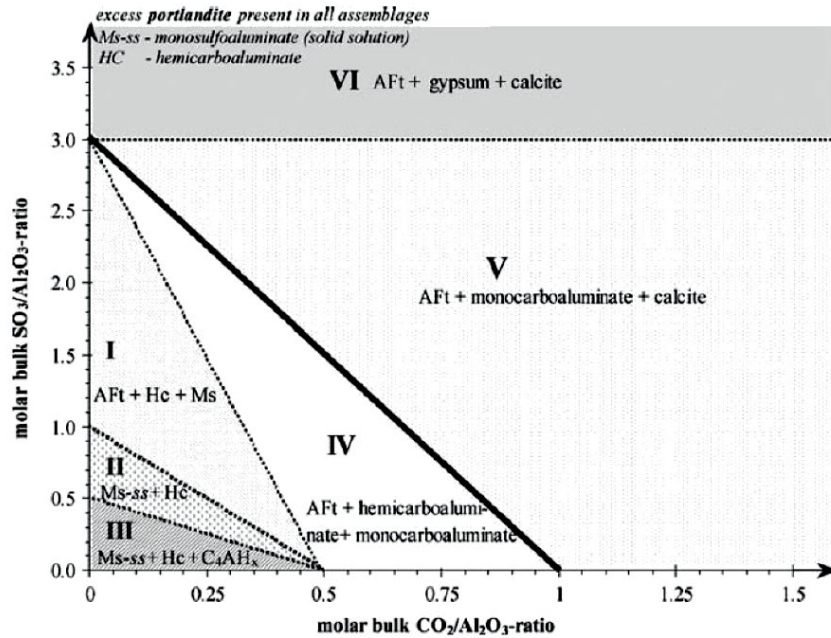
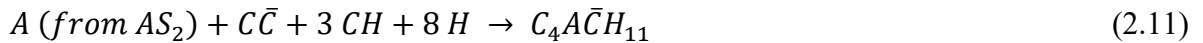


Figure 2. 17 Computed phase assemblages for C_3A -CH system with different SO_3 and CO_2 amount [155]

As it is stated before, the carbonate phase reacts with mono-sulfate to prepare Hc and then Mc while the sulphate is bound AFt. The requirement of this reaction is existence of enough source of Al and Ca and in case of supplying the Ca it would depends on ratios between Al_2O_3 , CO_2 and SO_3 . Comparing to sulfate and hydroxide AFm, the carbonate AFm is more desirable that is strongly stable and prevent ettringite decomposition after sulfate consumption and provide higher compressive strength [61]. Generally, the amount of limestone in OPC should coincide to the proper amount of Al that could overcome to carbon dioxide to form hemi-carbonate and mono-carbonate, So the excessive source of Al is needed. Besides the thermodynamic simulation to determine the proportion of limestone in mixture, kinetic and transport constraints of the real system must be evaluated. Limestone dissolution proceed more slowly than that of the clinker phases and high pH can further retard it [167, 168]. High sulfate content at the initial stage due to the fast dissolution of sulfates can be considered as retarder [169]. When the hydration process begins, some factors like low water accessibility for dissolution and more available space for ion transportation the real amount of required limestone may decrease than calculated one [72-75, 170].

2.7.2 Limestone and Metakaolin in Blended Cement

The most recent technology about blended metakaolin and limestone cement is called “Limestone Calcined Clay Cement (LC³)”. As it can be inferred from the name, the technology is a combination of calcined kaolinite as a clay and limestone in order to reduce the clinker production. Antoni claims that, more than the mentioned previous reactions, metakaolin is a proper source of excessive aluminate to reacts with limestone to provide carbo-aluminate hydrates based on equation below [171]:



As it is experienced the best compressive strength for the blended cement is for the calcined clay to limestone ratio of 2:1 [172]. According to this assumption, the mix design is defined as 45 wt% of clinker replaced by 30 wt% of metakaolin and 15 wt% of limestone. The 5 wt% of the mixture is associated to the gypsum and the rest 50 wt% refers to clinker. Figure 2.18 shows the compressive strength of the blended cement designed mix (LC³-50) comparing the ordinary Portland cement.

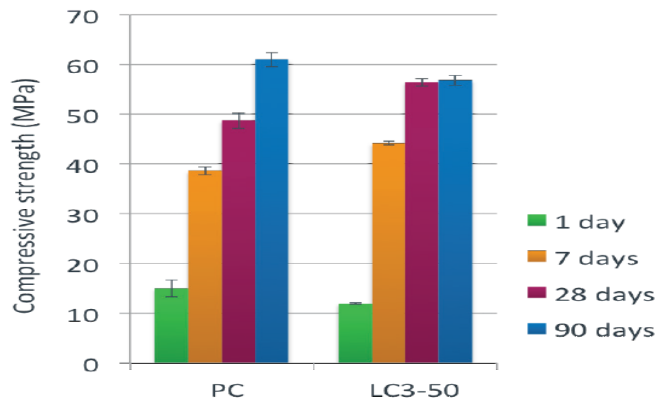


Figure 2. 18 Comparison of compressive strength among LC3-50 and PC

As it can be seen, from 7 days of setting time onward the composite cement shows the better compressive strength than PC and confirm the advantages of substitution of clinker with metakaolin and limestone. The porosity of the PC and LC3-50 is measured by Mercury Intrusion Porosimetry (MIP) that showed the higher total porosity for the composite cement as well as significant refinement of pore connectivity. The common pure metakaolin that is the calcined form of kaolinite is three times more expensive than PC [173]. Hence, it is more reliable to obtain the results from lower grade calcined kaolinitic clay that could be affordable substitute for cement [133, 147, 172, 95]. However, there is no systematic and credential study about the effect of calcined clay grade on composite cement strength yet. In next section it is tried to launch a new discussion about the lower grade clays in different classes.

2.8 Using More Complex Clay Structure as SCM

Application of low-grade clayey material for cement substitution have not been investigated in much studies. Herfort et al. [174] investigated the limestone calcined clay Portland cement by focusing on kaolinite class clays and calcite or dolomite as a carbonate source. Moreover, this study did not consider the heat treatment temperature as an important factor for reactivation of clay. Besides, like Bullerjhan [177] study, the magnesium content of dolomite has not been taken into the account. Hebert et al. [175, 176] studies are one of the rare works on different types of clayey materials. They evaluated four different clay type powders received from Lafarge cement company, with various chemical phase composition as a partial substitution of cement and in best case they reached to the 95% of cement strength. Two of the samples are with carbonate and the others without carbonate in their composition. The clayey materials include Kaolinite, illite, montmorillonite, palygorskite in combination with feldspar and mica. The calcination is performed for five hours in a temperature range of 20 to 900°C. This study confirms that more than kaolinite other class of clays could be thermally activated to replace the Portland cement. Dupuis [178] claimed the calcining a mineral load containing carbonate in order to produce a hydraulic binder. This study is concentrated on a new method of calcination setup and did not investigate the significant clay type materials. The similar patent work by Meynardi [179] is carried out to find more optimal

process for hydraulic binder production containing limestone and clay (silica, aluminium and iron oxide). The calcination temperature is in a range of 700 to 900°C. Another studies [176, 180] are concentrated on specific type of clay like palygorskite to characterize them for possible potential of reactivity [188-191].

This dissertation is going through the mine overburden schist type materials to evaluate them as a possible cement substitution.

CHAPTER 3

CALCINED CLAY CEMENT (C³)

3.1. General

In this section, the six different schist type powder with the average particle size of 40 μm are evaluated. The raw materials seem to contain proper portion of clayey phases companion with some other chemical compound. In following part, the characterization of the sample was investigated, and these initial experiments will be pursued by controlling the pozzolanic reaction of the treated powders. Furthermore, the results of compressive strength behavior of the blended cement paste are represented.

3.2 Evaluation of Raw Materials (Virgin Powders)

In this section the results of the raw material characterization are clarified. The main aim of this study is to evaluate the raw schist type powders as a possible pozzolanic reactivity and proper candidate for using as a SCM for partial cement substitution. Hence, each of the

characterization method results are shown in different parts for all the received samples to be more comparable.

3.2.1 Chemical Phase Analysis (X-ray Diffraction and Rietveld)

As it is stated before the X-ray diffraction experiments were performed by “Bruker D8 Advance” device and associated TOPAS software is used for Rietveld refinement analysis. It should be mentioned that for avoiding the texture direction dependency the samples were rotated at 15 rpm to reduce this source of error during measurements.

3.2.1.1 Bozalan Schist

The first powder is schist type material that is called Bozalan according to the region the mine located. Figure 3.1 is the received powder color.



Figure 3. 1 Bozalan Schist Sample (Virgin Powder)

Figure 3.2 shows the x-ray diffractogram of the Bozalan sample. The first glance is taking the attention to the biggest peak that is associated to the quartz. In addition, based on the phase analysis, calcium aluminosilicate “anorthite” ($\text{NaAl}_3\text{Si}_3\text{O}_{11}$) and sodium aluminosilicate ($\text{NaAl}_3\text{Si}_3\text{O}_{11}$) with base-centered monoclinic structure.

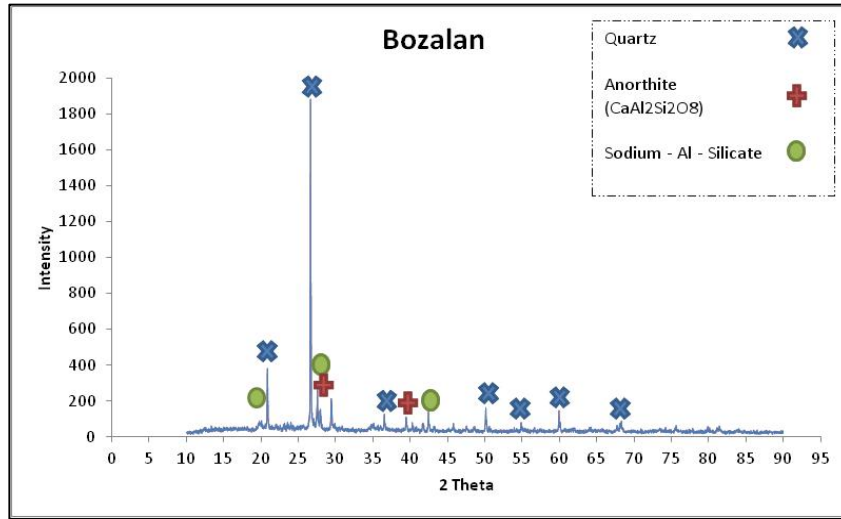


Figure 3. 2 Bozalan Virgin Powder X-ray Diffractogram

The proportions of the phases present in the sample are given in the table 3.1. These ratios were calculated from the XRD results so that the sum of the crystal phases is 100%.

Table 3. 1 Phase ratios and amorphousness estimation for Bozalan virgin powder

Sample	Chemical Phase	Phase Ratio (wt%)	Quartz / Noise	Amorphous / Noise
Bozalan	Quartz	52	57.5	1.25
	Clay	40	—	—
	Carbonate	8	—	—
	Others	—	—	—

As it can be seen in the table, quartz ratio (quartz / noise), quartz particle size, and amorphous / noise (electronic noise) ratios in the sample were also calculated in order to better predict whether the sample is stable in high pH cement hydration reactions or not. Amorphous silica and aluminate ratios, which do not emerge especially in XRD measurements, may be important for the reactivity of the raw material. Table 3.1 also shows these ratios for Bozalan

sample. A high amorphous / noise level ratio can be considered as an indication of the presence of unstable amorphous silicate in the sample. However, this assumption must also be confirmed by the results of thermogravimetric analysis (TGA). The results of this experiment are discussed in the section where the results are evaluated together. The broadness or thinness of the quartz peak contains information about the crystal size of the quartz phase and hence the possible stability in the cement reactions. Typically, particles in nanoscale become more reactive and consequently the sample with lower particle size is more reactive. It has been claimed in the literature that quartz reacts with other phases of cement, albeit slowly, over time. The crystal size of the quartz phase was calculated with the Scherrer formula ($\frac{0.97 \lambda}{\beta_{1/2} \cos \theta}$). In this formula, the length λ is the angular half width full maximum level of the $\beta_{1/2}$ peak, and from the 2θ peak angular value of θ can be defined. The quartz crystal size calculated by this method is 134 nm for the Bozalan sample. These calculations do not give a reliable result for crystal sizes greater than 150 nm due to the mechanical tolerances of the devices used in this study. Furthermore, the large quartz / noise ratio indicates that the size of these crystals may be even greater. The Scherrer formula is not applicable for over 150 nm particles and XRD device loses its accuracy. The values above 150 nm should be regarded as macroscopic (mass) values. Thus, quartz mineral with large amounts of coarse grains may indicate that this sample is not the ideal sample for pozzolanic reactions. Moreover, the amorphous / noise ratio is relatively high in the Bozalan sample. This value is suspected of having a reactive amorphous matrix, for example volcanic pozzolans. Therefore, it will not be reliable for some samples to determine whether the raw materials are suitable for pozzolan reactions by just looking at the XRD results. These results should be examined together with TGA results.

So, table 3.1 shows the distribution of the crystal phases in this sample. The table represent only the crystal phases. Possible amorphous phases are not present in this sum.

3.2.1.2 Camlica Schist

The second schist type material is called Camlica received from the west of Turkey. Figure 3.3 illustrate the virgin powder color.



Figure 3. 3 Camlica Schist Sample (Virgin Powder)

XRD measurements is carried out in 2θ range from 10° to 90° for schist samples taken from Camlica is given in Figure 3.4. As can be seen, the most dominant phase still is the quartz phase. Besides quartz, calcite (CaCO_3), non-clay orthorhombic aluminum silicate ($\text{Al}_2(\text{SiO}_4)\text{O}$; probably Silimanite), monoclinic sodium-alumino sulfide ($\text{Na}_6\text{Al}_2\text{S}_6$) and small amount of orthorhombic copper-magnesium oxide (Cu_2MgO_3) phase have been identified.

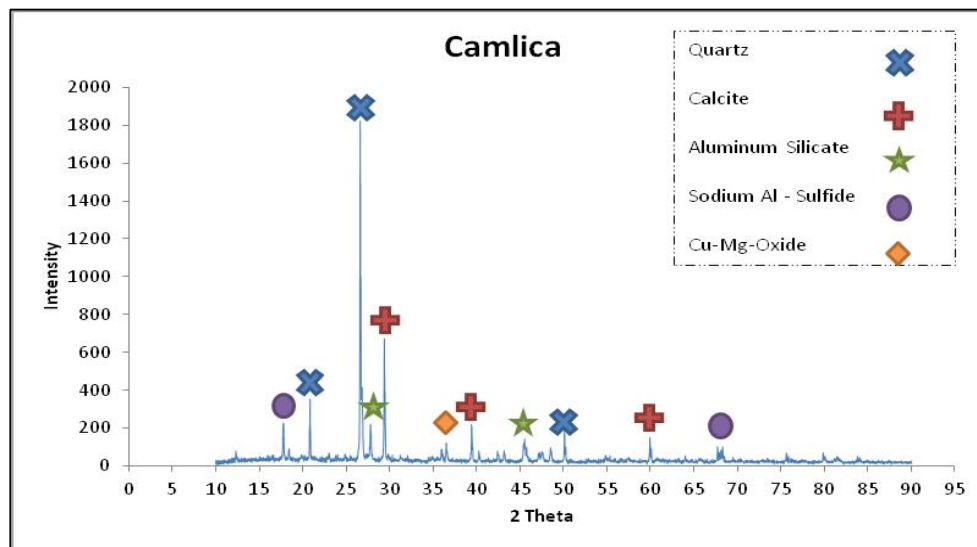


Figure 3. 4 Camlica Virgin Powder X-ray Diffractogram

The distances of the atomic planes of the clay-based phases, especially in the c-crystal direction, are large and these large distances occur at low 2θ values in XRD measurements. Therefore, $5^\circ - 90^\circ 2\theta$ measurements of each sample were also made. Figure 3.5 is the XRD spectrum in this range for the Camlica sample. As it can be seen, a peak of typical potassium illite clay is present below $10^\circ 2\theta$.

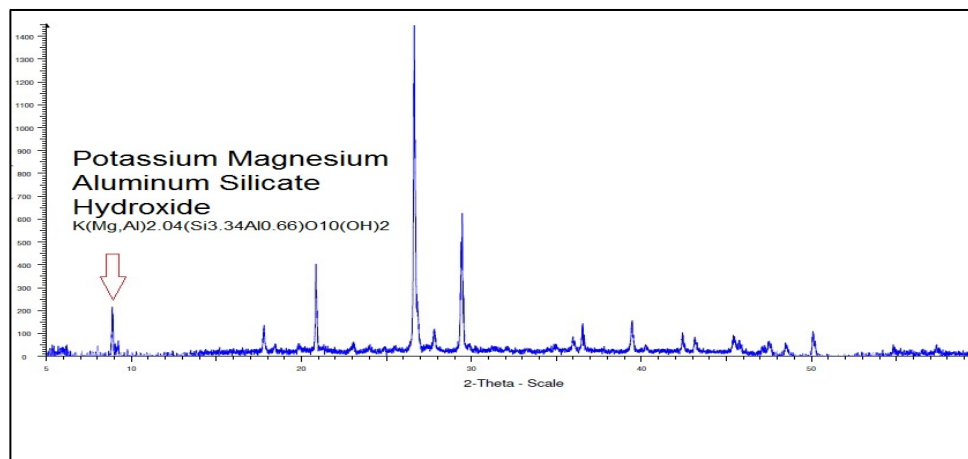


Figure 3. 5 The whole 2θ range x-ray diffractogram of Camlica sample

Although there is still a very high portion of quartz in Camlica schist, quartz / noise ratio is lower than Bozalan. In addition, there is illite type clay containing silica / alumina at a ratio of 2: 1 in Camlica. Since the hydroxide ratios of illitic clays are low, they do not swell a lot. Based on the phase distribution in the XRD results, their activation seems to have limited capacity. Table 3.2 represent the phase distribution ratios and estimation of amorphousness.

Table 3. 2 Phase ratios and amorphousness estimation for Camlica virgin powder

Sample	Chemical Phase	Phase Ratio (wt%)	Quartz / Noise	Amorphous / Noise
Camlica	Quartz	40	48.3	1
	Clay	15	—	—
	Carbonate	14	—	—
	Others	31	—	—

Since quartz / noise ratio is low, and according to Scherrer's formula, quartz crystals are smaller in this sample (110 nm). It is a more reactive quartz than the previous sample. However, the amorphous matrix ratio in this sample is quite low. The calcite ratio in Camlica sample is determined as 14 wt%. The crystal cell structure of illite type clay is given in Figure 3.6.

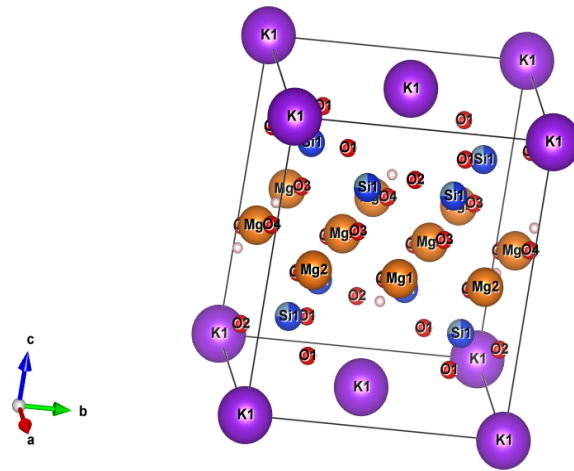


Figure 3. 6 representative picture of illite type potassium clay crystal structure with general formula of $(K, H_3O)(Al, Mg, Fe)_2(Si, Al)_4O_{10}[(OH)_2, (H_2O)]$

The two layers of silica seem to be filled with alumino ferrite layer and these three layers are filled with potassium ions.

3.2.1.3 Tastepe Schist

Tastepe mine is located within the borders of western part of Turkey. Tastepe sample was described as clayey schist that is shown in Figure 3.7.



Figure 3. 7 Tastepe Schist Sample (Virgin Powder)

The XRD diffractogram of the Tastepe sample is given in Figure 3.8 below.

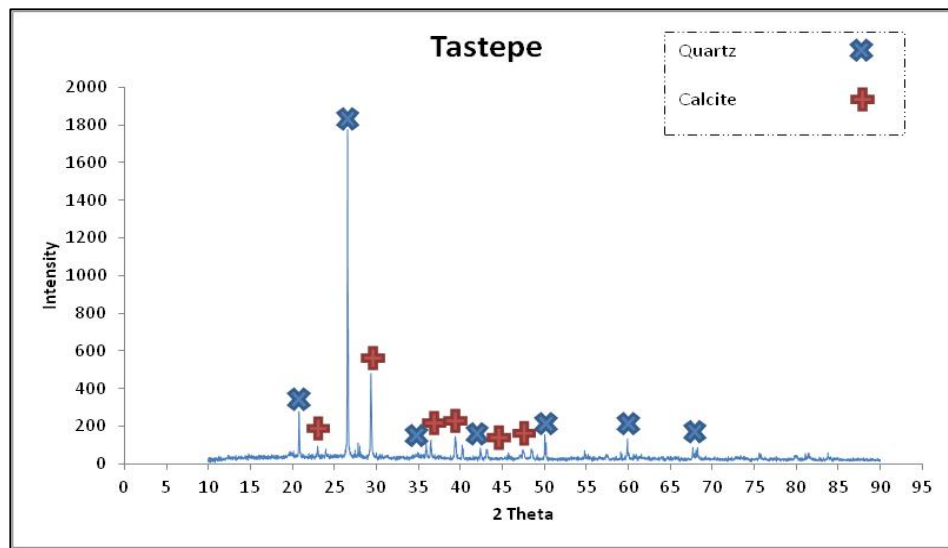


Figure 3. 8 Tastepe Virgin Powder X-ray Diffractogram

In Tastepe schist, two main phases are significant peaks among other peaks in diffractogram. These two are quartz and calcite. Quartz content is as high as 60 wt%. The quartz / noise ratio is very high, indicating that the quartz phase is coarse grained. The calculated quartz crystal size is 152 nm and is macroscopic. These quartz grains are not believed to be reactive. Furthermore, the amorphous matrix ratio in these powders is very low. At first glance,

Tastepe does not appear to be a suitable sample in term of reactivation. Calcium aluminosilicate (anorthite) crystal phase is present in small amounts. Table 3.3 represents the chemical phase distribution and amorphousness of Tastepe powder.

Table 3. 3 Phase ratios and amorphousness estimation for Tastepe virgin powder

Sample	Chemical Phase	Phase Ratio (wt%)	Quartz / Noise	Amorphous / Noise
Tastepe	Quartz	60	65	1
	Clay	–	–	–
	Carbonate	32	–	–
	Others	8	–	–

At first glance, due to the lack of clayey type materials it does not look like a sample that can be activated. Confirmation of the results with TGA results is required.

3.2.1.4 Kovukdere Schist

Kovukdere schist mine is within the boundaries of Istanbul and is named as a high schist clay content. Figure 3.9 shows the color of the virgin schist powder.



Figure 3. 9 Kovukdere Schist Sample (Virgin Powder)

As it can be seen in Figure 3.5, Kovukdere clay contains quartz and calcite, as well as kaolinitic class clays (e.g. nacrite), osumilite, rutile and orthosilicates. It is rare to have such a high amount of osumilite as in this sample. The spectrum of Kovukdere dust from 5 ° to 90 ° 2 θ is shown in Figure 3.10.

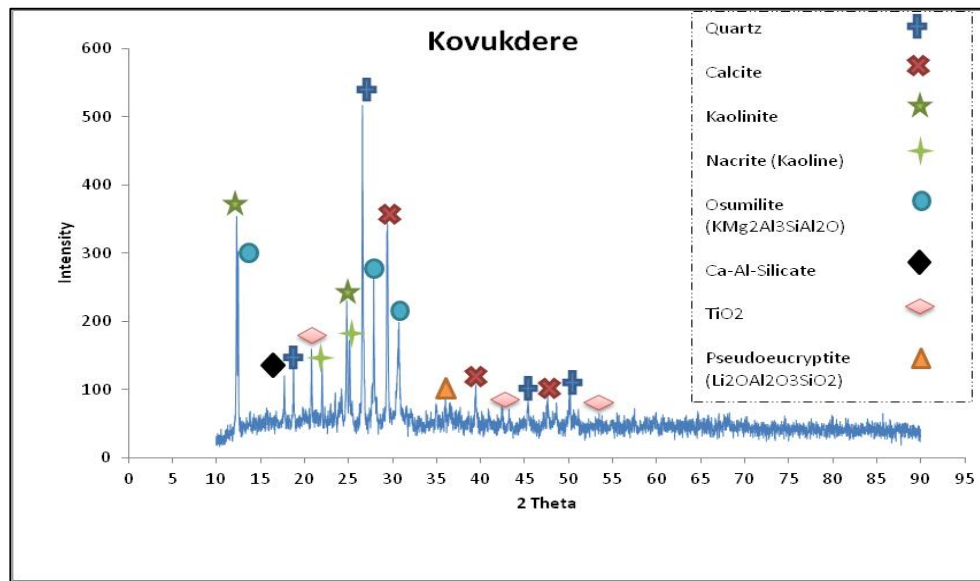


Figure 3. 10 Kovukdere Virgin Powder X-ray Diffractogram

Considering the x-ray diffraction of Kovukdere schist in range of 5° to 10° 2 θ in Figure 3.11, there are peaks besides kaolinite like muscovite and clinocllore type clayey structures are present.

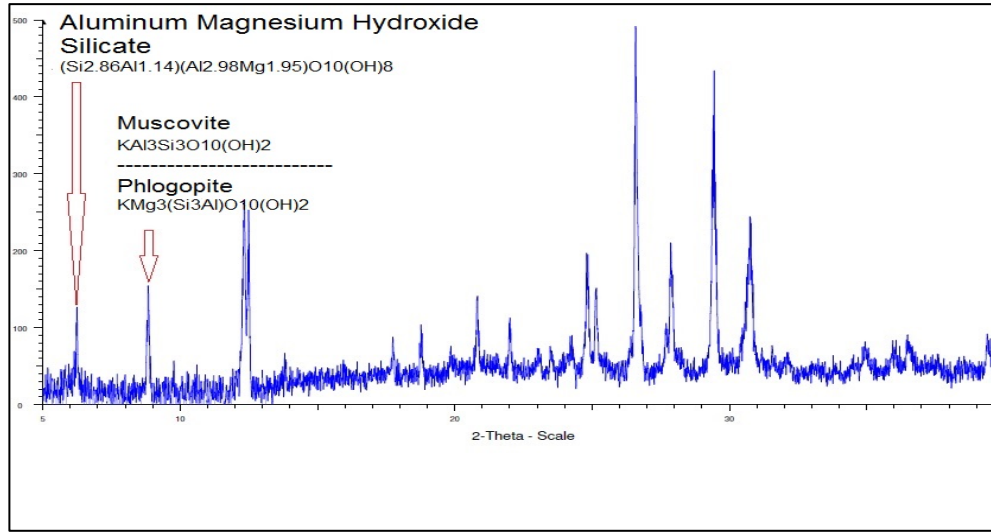


Figure 3. 11 X-ray diffraction of Kovukdere by focusing on 5° to 10° 2θ

Among the samples, Kovukdere seems to be the most proper sample for activation. In the schist sample, the phases with or without the potential for pozzolanic reactions such as quartz (33%), calcite (33%), kaolinite, muscovite, mica, phlogopite, and osumilite were uniformly distributed. Among these, osumilite with hexagonal structure ($KMg_2Al_3(Si_{10}Al_2)O_{30}$) does not seem to be activated easily. Similarly, the calcium aluminosilicate ($Ca_3Al_6Si_2O_{16}$) phase with hexagonal structure may not be activated since it is an orthosilicate. The hydrated state of this phase is montmorillonite type clay, but the montmorillonite 2:1 type is relatively difficult to activate. Rutile crystals are another minor phase in Kovukdere schist. Especially in microscopic examinations, thin rutile needles are immediately noticeable.

Table 3.4 represents the phase distribution ratios and estimation about the amorphousness of Kovukdere sample.

Table 3. 4 Phase ratios and amorphousness estimation for Kovukdere virgin powder

Sample	Chemical Phase	Phase Ratio (wt%)	Quartz / Noise	Amorphous / Noise
Kovukdere	Quartz	26	24	1.5
	Clay	54	–	–
	Carbonate	16	–	–
	Others	4	–	–

The size of quartz crystals in Kovukdere schist is below 100 nm and they have potential to be reactive. In addition, the amorphous / noise ratio is the highest schist sample. That is, the amorphous matrix of schist can also be reactive in a natural lava-like behavior.

3.2.1.5 Muratbey Schist

The Muratbey schist is a powder extracted from a region close to Kovukdere mine, but from a different layer. Looking at the color in Figure 3.12, it can be said that there is a tangible amount of iron minerals in this material.

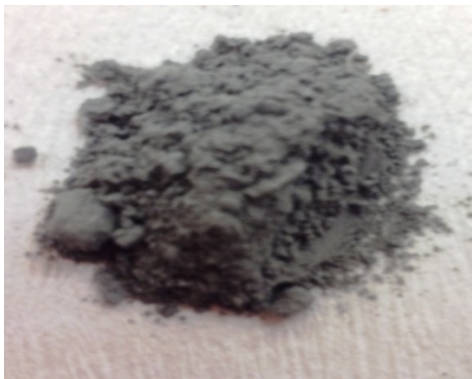


Figure 3. 12 Muratbey Schist Sample (Virgin Powder)

The XRD spectrum of the Muratbey schist sample is given in Figure 3.13. Muratbey schist is like Kovukdere sample as phase distribution. Since it contains the phases with higher sodium content, it is possible to come from a slightly higher position than Kovukdere.

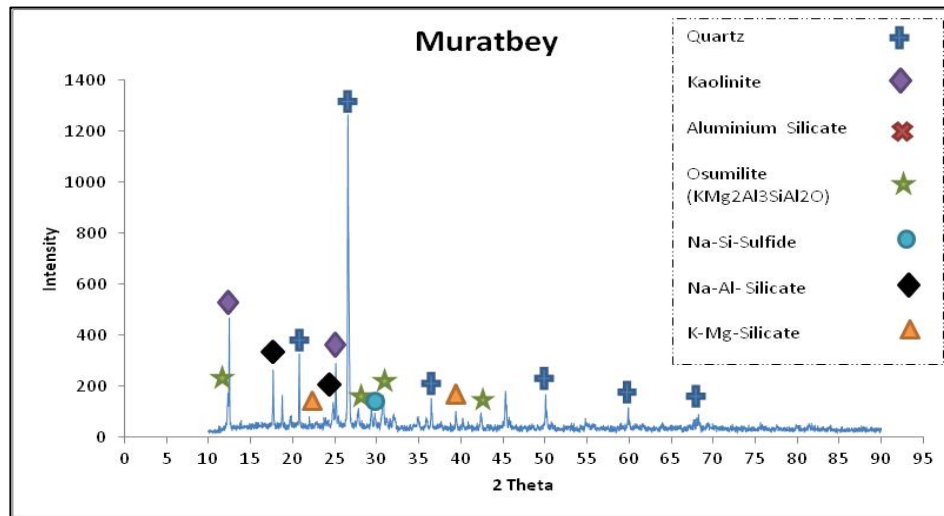


Figure 3. 13 Muratbey Virgin Powder X-ray Diffractogram

As it can be seen from the XRD spectrum in Figure 3.14 that focused on 5° to 10° 2θ , Muratbey contains kaolinite and phlogopite (potassium magnesium mica) clay as well as sodium bentonite (montmorillonite class).

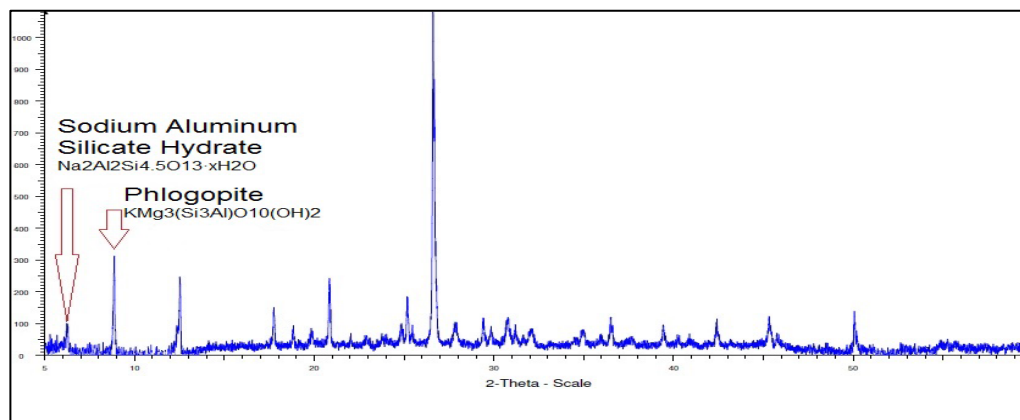


Figure 3. 14 X-ray diffraction of Muratbey by focusing on 5° to 10° 2θ

It should be noticed that Alumino silicates ($(Al_2 (SiO_4) O)$, Andalusite) are also present in small amounts. The crystal structure of Andalusite is shown in Figure 3.15 below.

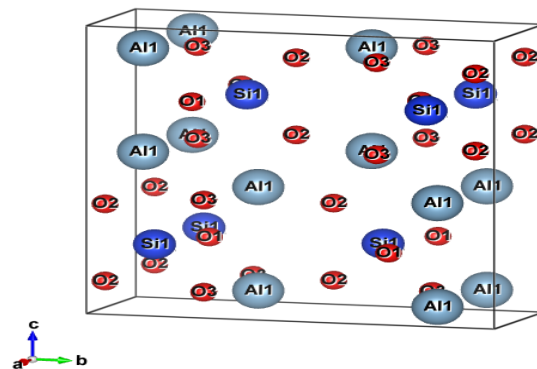


Figure 3. 15 Crystal structure of Andalusite Phase

In addition, osumillite ($KMg_2Al_3 (Si_{10}Al_2) O_{30}$), sodium-alumino silicate ($Na_6Al_6Si_{10}O_{32}$) are water-insoluble minerals with cubic structure. Hexagonal ($K_2Mg_5Si_{12}O_{30}$) combines with water to form phlogophite and thus becomes clayey material. The ($Na_4Si_4S_{10}$) phase may indicate a rapid cooling process. Looking at the amorphous / noise ratios in the table 3.5, it is concluded that the matrix may be amorphous.

Table 3. 5 Phase ratios and amorphousness estimation for Muratbey virgin powder

Sample	Chemical Phase	Phase Ratio (wt%)	Quartz / Noise	Amorphous / Noise
Muratbey	Quartz	51	43.3	1.6
	Clay	42	—	—
	Carbonate	—	—	—
	Others	7	—	—

Quartz crystals are around 100 nm and can have high reactivity with amorphous phase. There is also a large amount of clay in the Muratbey sample.

3.2.1.6 Ladik Schist

Our powder sample from north-east of Turkey is the mine extracted schist type material from Ladik region. The sample provider claimed Ladik as clayey schist. Figure 3.16 shows the virgin Ladik powder appearance.



Figure 3. 16 Ladik Schist Sample (Virgin Powder)

Figure 3.17 illustrate the X-ray diffraction of the Ladik virgin powder to identify the phase distribution.

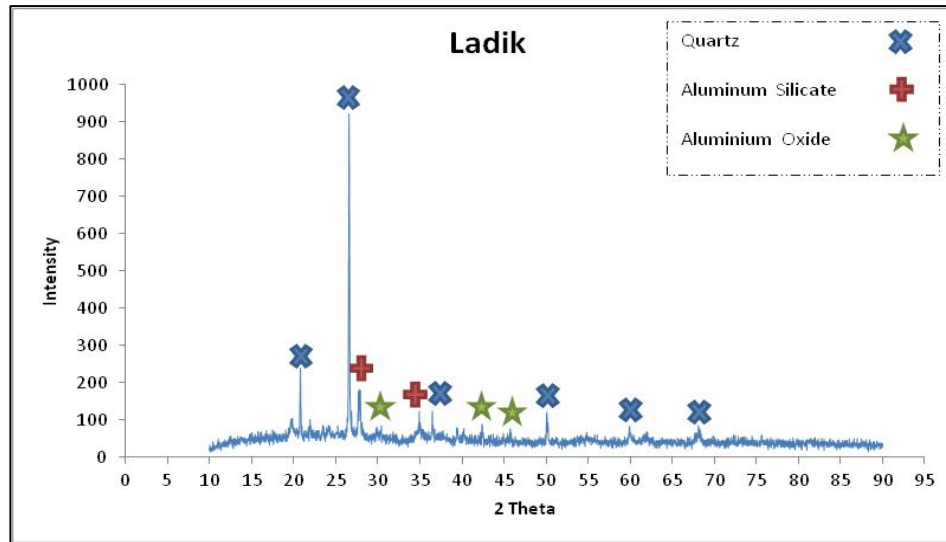


Figure 3. 17 Ladik Virgin Powder X-ray Diffractogram

The first striking point is the amorphous elevation near the quartz peak. The amount of amorphous matrix appears to be low. However, it is a sample with the possibility of glassy phase. The main phases are quartz, alumina and andalusite. Based on table 3.6, a low quartz / noise ratio versus a high quartz ratio indicates that quartz crystals may be thin in size (around 110 nm). Table 3.6 shows the phase distribution and amorphousness of Ladik schist.

Table 3. 6 Phase ratios and amorphousness estimation for Ladik virgin powder

Sample	Chemical Phase	Phase Ratio (wt%)	Quartz / Noise	Amorphous / Noise
Ladik	Quartz	52	22.9	1.1
	Clay	26	—	—
	Carbonate	—	—	—
	Others	22	—	—

3.2.1.7 Pure Kaolinite (Benchmark Sample)

The raw material samples containing 6 schist type powder are received from mine quarries inside the Turkey and the kaolinite powder obtained from “Siscam Maden” were evaluated for phase distributions, microstructures and similar behaviors to hydraulic cement without any treatment. It is known that the powder sample sent by Sisecam contains only kaolinite type clay and quartz as its chemical composition. Kaolinite is a benchmark sample in this study. According to the literatures, it is known that kaolinite is used as supplementary cementitious materials (SCM) after some heat treatments and thus provide the advantages of pozzolanic reactions to cement blends. Figure 3.18 shows the kaolinite powder that is received as standard kaolinite from Sisecam.



Figure 3. 18 Kaolinite Powder Sample (Virgin Powder)

The x-ray diffractogram of the kaolinite powder sent by Şişecam and used as control samples are shown in Figure 3.19. As it can be seen, it consists of kaolinite phase and quartz.

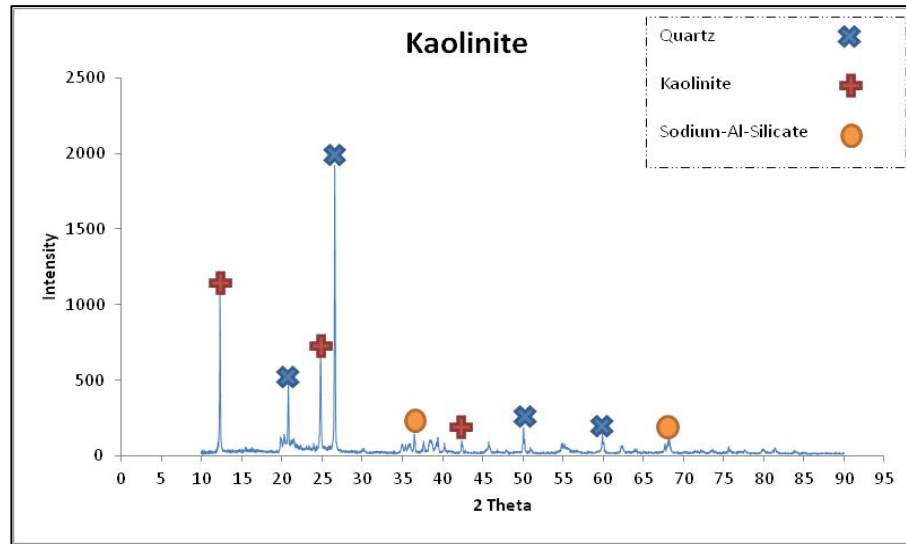


Figure 3. 19 Kaolinite Virgin Powder X-ray Diffractogram

More than quartz and kaolinite, a small amount of sodium alumino-silicate phase (Carnegieite) may also be present. The phase distribution and amorphous ratio represented in Table 3.7.

Table 3. 7 Phase ratios and amorphousness estimation for Kaolinite virgin powder

Sample	Chemical Phase	Phase Ratio (wt%)	Quartz / Noise	Amorphous / Noise
Kaolinite	Quartz	44	—	—
	Clay	56	—	—
	Carbonate	—	—	—
	Others	—	—	—

Phase distribution measurements of all schist samples based on the x-ray results are given in Table 3.8. Again, looking only at this data, the Kovukdere, Camlica and Muratbey schists seem to be more promising. However, these results should be supported by TGA and conductivity measurements.

Table 3. 8 Phase distribution of all samples

Schist (Clay) Sample Name	Chemical Phase Distribution
Kaolinite	Quartz (SiO_2) Kaolinite ($\text{Al}_2\text{Si}_2\text{O}_5(\text{OH})_4$) Sodium Alumino-silicate (Carnegieite) (NaAlSiO_4)
Bozalan	Quartz (SiO_2) Anorthite ($\text{CaAl}_2\text{Si}_2\text{O}_8$) Sodium Alumino-silicate
Camlica	Quartz (SiO_2) Calcite (CaCO_3) Alumino-Silicate (Silimanite)($\text{Al}_2(\text{SiO})_4\text{O}$) Sodium Alumino-Sulfide ($\text{Na}_6\text{Al}_2\text{S}_6$) K-Al-Mg Silicate Hydroxide [$\text{K}(\text{Mg}, \text{Al})_{2.04}(\text{Si}_{3.34}\text{Al}_{0.66})\text{O}_{10}(\text{OH})_2$]
Kovukdere	Quartz (SiO_2) Calcite (CaCO_3) Kaolinite ($\text{Al}_2\text{Si}_2\text{O}_5(\text{OH})_4$) Nacrite ($\text{Al}_2\text{Si}_2\text{O}_5(\text{OH})_4$) Rutile (TiO_2) Phlogopite [$\text{K Mg}_3(\text{Si}_3\text{Al})\text{O}_{10}(\text{OH})_2$] Al-Mg Silicate Hydrate [$(\text{Si}_{2.86}\text{Al}_{1.14})(\text{Al}_{2.98}\text{Mg}_{1.95})\text{O}_{10}(\text{OH})_8$] Muscovite [$\text{KAl}_3\text{Si}_3\text{O}_{10}(\text{OH})_2$]
Muratbey	Quartz (SiO_2) Kaolinite ($\text{Al}_2\text{Si}_2\text{O}_5(\text{OH})_4$) Alumino-Silicate (Silimanite)($\text{Al}_2(\text{SiO})_4\text{O}$) Phlogopite [$\text{KMg}_3(\text{Si}_3\text{Al})\text{O}_{10}(\text{OH})_2$] Osumilite [$\text{KMg}_2\text{Al}_3(\text{Si}_{10}\text{Al}_2)\text{O}_{30}$] Na-Al-Silicate Hydrate [$\text{Na}_6\text{Al}_6\text{Si}_{10}\text{O}_3(\text{OH})_2$]
Tastepe	Quartz (SiO_2) Calcite (CaCO_3)
Ladik	Quartz (SiO_2) Aluminium Silicate (Al_2SiO_5) Aluminum Oxide (Al_2O_3)

The chemical compositions measured by XRF (X-ray Fluorescence) for the six samples are given in Table 3.9. As it can be seen from the table, the samples are schist type materials. Especially in Kovukdere, Tastepe and Camlica samples, there is a large amount of calcium. This is a preliminary notification that the powders will certainly contain calcium-containing minerals as well as clay. Since the expected silica / aluminum ratio in clay minerals is 1-2.2, the amount of silica above it may also indicate quartz. In this way, only Kovukdere stands out. However, other analyzes will be useful to reveal the potential in other samples.

Table 3. 9 XRF analysis results for all schist samples

Sample Name	SiO ₂ (%)	Al ₂ O ₃ (%)	Fe ₂ O ₃ (%)	CaO (%)	MgO (%)	SO ₃ (%)	Cl (%)	Na ₂ O (%)	K ₂ O (%)	AZ (975C)	Total (%)
Muratbey	52.77	14.5	6.68	6.67	2.49	1.44	0.0409	0.69	2.66	11.13	99.34
Kovukdere	34.65	12.8	10.58	15.41	3.53	0.62	0.0301	1.85	1.03	18.43	98.93
Tastepe	56.7	7.08	4.43	14.34	1.93	0.86	0.0177	0.54	0.98	13.11	99.99
Bozalan	64.1	11.13	4.37	6.83	1.79	0.21	0.0285	1	2.36	8.16	99.98
Camlica	56.2	9.93	4.36	13.12	0.56	0.34	0.0285	0.6	1.83	12.13	99.1
Ladik	6.94	15.72	7.13	1.41	3.05	0.79	0.319	1.6	2.18	6.83	99.86

A series of further tests have been planned to determine the suitability of the raw material samples for pozzolanic reactions. The first of these is the mass loss due to heating. According to XRD results, the phases to be lost in the samples are clay origin and carbonate origin phases. The phases of clay origin lose hydroxyl groups and water on them. Carbonates decompose and lose carbon dioxide. Calcite-derived carbonates start to decompose above about 700-800 ° C. Clays lose hydroxyl ions by decomposition between 450 ° C and 800 ° C. Thermogravimetric measurements and mass losses below 800 ° C will give us preliminary information about the activation potential in our soil samples. Analysis of the carbonate phases decomposed at higher temperatures will also make the information already available for further work on the study.

The second planned test is to measure the resistivity of schist type materials in saturated calcium hydroxide solution. Materials reacting with calcium hydroxide reduce the conductivity of the saturated calcium hydroxide solution.

3.2.2 Thermogravimetric Analysis (TGA)

DTA / TG thermal analyzes of raw material powders were carried out by heating samples up to 1000 ° C under nitrogen gas at 10 ° C / min. According to the reviews in the literature, kaolinite will change to metakaolin under a suitable heat treatment. Activated kaolinite also

reacts as pozzolanic material during cement hydration and triggers the formation of CSH and CASH. The conversion of kaolinite to metakaolin takes place by the separation of hydroxyl ions in the crystal structure. In the meantime, the Al-O bonds are loosened, causing the metakaolin to react more easily.

While leaving the crystal structure, hydroxyl ions should not be exposed to excess heat. Therefore, the heat treatment temperatures and times are critical. Hence, mass losses between 450 ° - 850 ° C contain important clues. It was tested with the help of six samples and control samples in this study. Approximately 50-60 mg of each sample was subjected to thermogravimetric analysis.

Below are the results of these experiments. The results were then used to determine the temperature ranges at which activation procedure will be done. In the case of mass losses, the evaporation of the adsorbed water at the first 200°C was not considered.

3.2.2.1 Bozalan Schist

The thermal analysis spectrum of Bozalan schist in term of decomposition temperature range and mass loss is given in Figure 3.20.

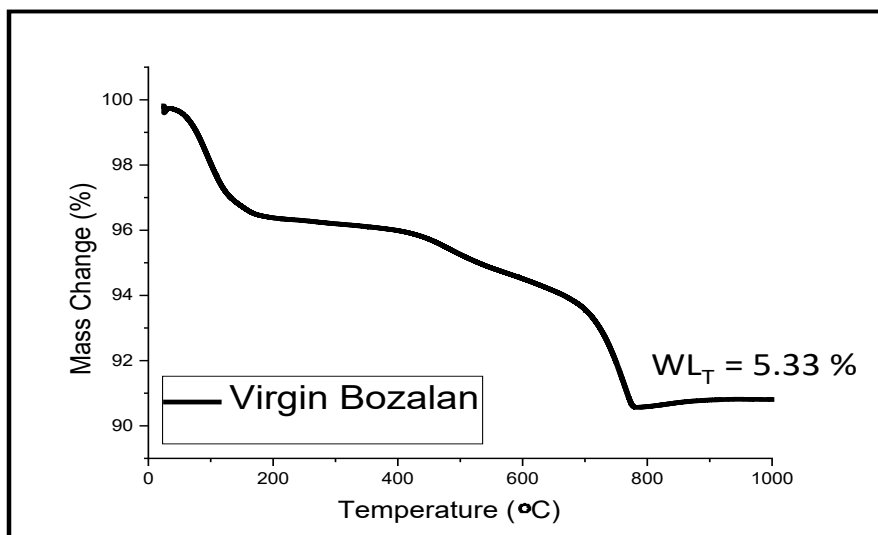


Figure 3. 20 Thermogravimetric Analysis of Bozalan schist (Virgin Powder)

Decomposition in the Bozalan schist starts at 400°C and ends at around 775°C. A total mass loss of 5.33% was observed in this temperature range. When looking at the XRD spectrum, there is no decomposition phase at low temperatures in the Bozalan sample. The Bozalan sample does not give the impression of a very promising sample.

3.2.2.2 Camlica Schist

The thermogravimetric measurement result of 50 mg Camlica sample is given in Figure 3.21. The total mass loss in the temperature range 600 °C - 820 °C is about 10.2%. This sample shows more signs of decomposition at lower temperatures than the Bozalan sample.

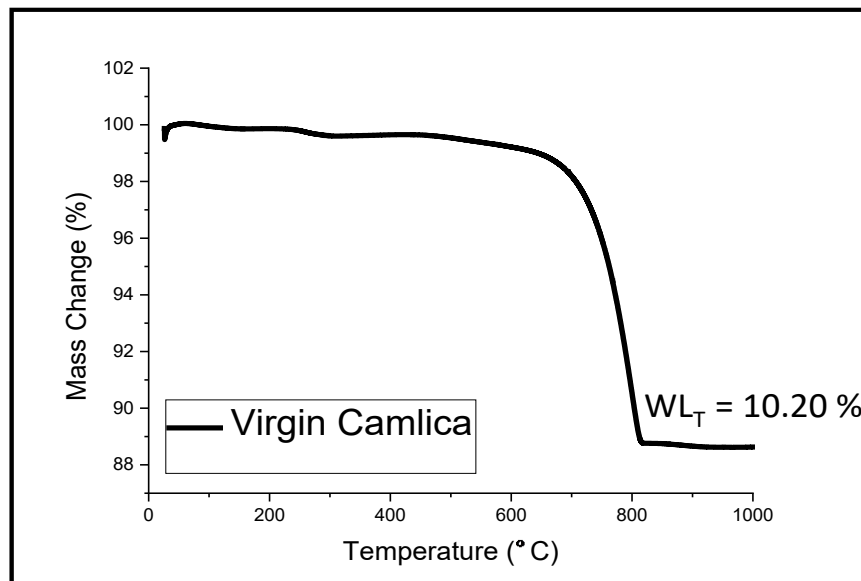


Figure 3. 21 Thermogravimetric Analysis of Camlica schist (Virgin Powder)

XRD results showed that there was some clayey phase (e.g. K-illite / muscovite) in Camlica schist. Since the decomposition temperature starts around 600°C, Camlica could be a potential powder in term of reactivity. Alumino silicate phases in Camlica schist may also be useful for pozzolanic reactions. The actual results will be confirmed by the compressive strengths of blended cement paste.

3.2.2.3 Tasted Schist

Thermal analysis results of Tasted sample are given in Figure 3.22. There is a mass loss starting at 450°C and ending at around 875°C. Calcite-like mass loss rate is about 11.25%. According to XRD results, there is no crystallized clayey phase in Tasted sample which causes 10% mass loss at such low temperatures.

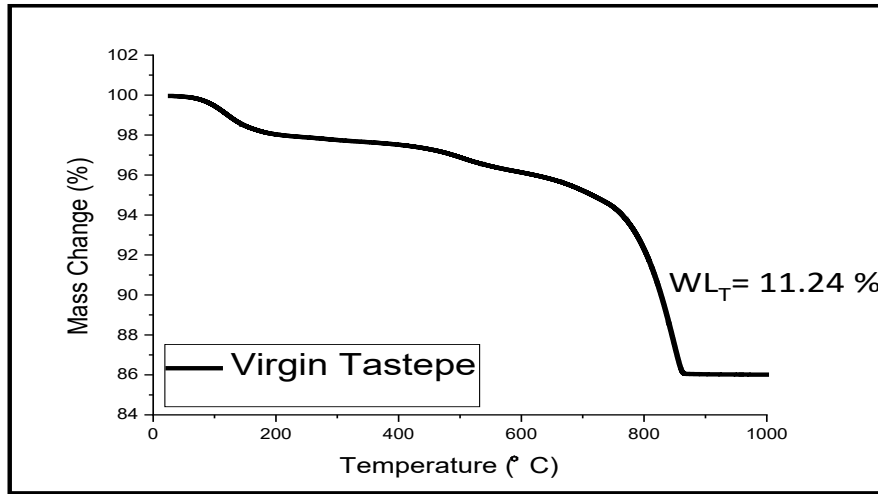


Figure 3. 22 Thermogravimetric Analysis of Tasted schist (Virgin Powder)

The only phase to be decomposed in the Tasted sample is calcite. Calcite loses 44% of its mass to CO₂ with thermal decomposition. The original Tasted powder contains about 30% calcite. In this case, a mass loss of approximately 12% can be expected during decomposition. Decay in this phase is expected above 840 °C. Calcite's decomposability at such low temperatures is also an important finding.

3.2.2.4 Kovukdere Schist

Thermal analysis results of Kovukdere powder, the most promising powder sample, are given in Figure 3.23.

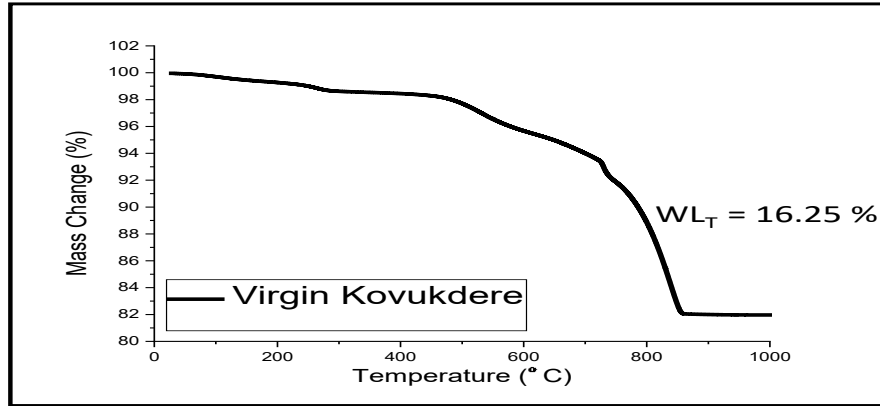


Figure 3. 23 Thermogravimetric Analysis of Kovukdere schist (Virgin Powder)

Kovukdere schist is decomposed between 450°C and 870°C. Looking at the results of Tastepe, it can be assumed that some of this decomposition is due to calcite. Total mass loss is around 16.25%. XRD and TGA results still suggest that Kovukdere is the most promising sample.

3.2.2.5 Muratbey Schist

TGA results of Muratbey sample are given in Figure 3.24.

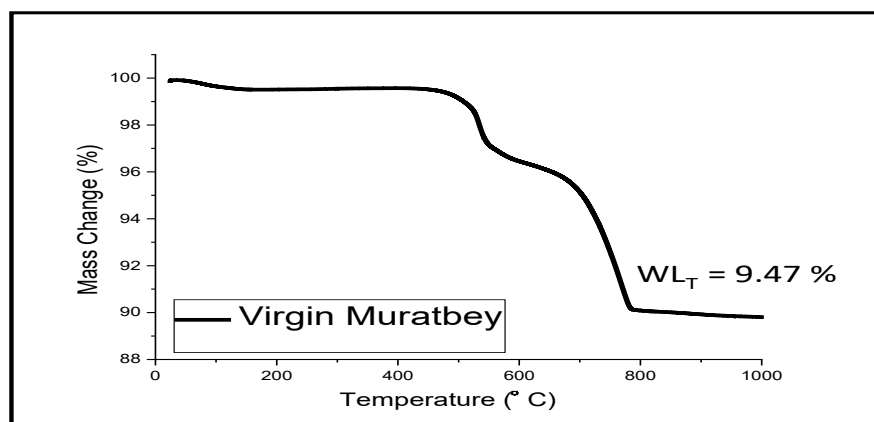


Figure 3. 24 Thermogravimetric Analysis of Muratbey schist (Virgin Powder)

Muratbey schist, which is structurally like the Kovukdere in term of phase distribution, starts to decompose earlier than Kovukdere sample. Decomposition temperature range is between 450°C- 800-C. The difference of Muratbey powder was the presence of sodium-based clay structures according to XRD results. Muratbey shows a mass loss of approximately 9.43%. All this mass loss can be assumed to come from clay-based materials. XRD results for Muratbey schist did not detect calcite phase. However, a small amount of calcium-rich phase is present in the SEM results.

3.2.2.6 Ladik Schist

One of the samples with the least mass loss is Ladik. TGA results of Ladik powder are given in Figure 3.25. As it can be seen, the total mass loss is only 2.63%. This mass loss occurs in the temperature range of 400°C to 700°C. Ladik stands out at first glance as a difficult to activate sample.

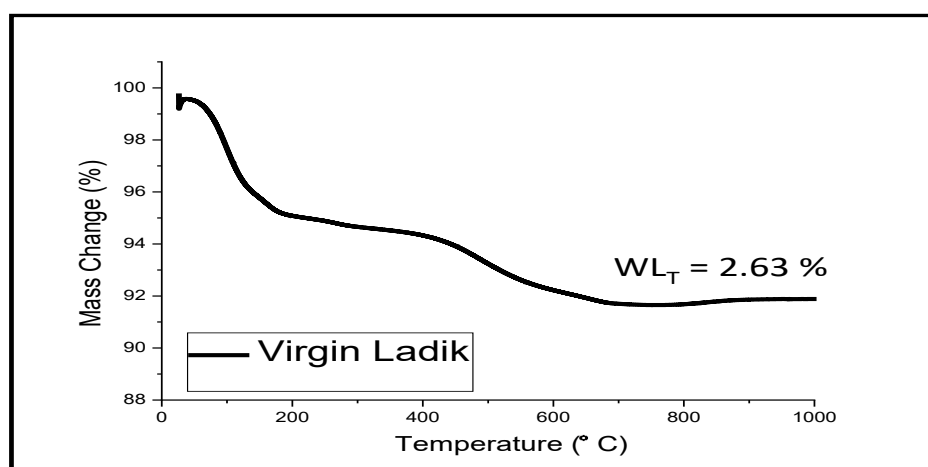


Figure 3. 25 Thermogravimetric Analysis of Ladik schist (Virgin Powder)

3.2.2.7 Kaolinite

The mass loss curve of our control sample kaolin is shown in Figure 3.26.

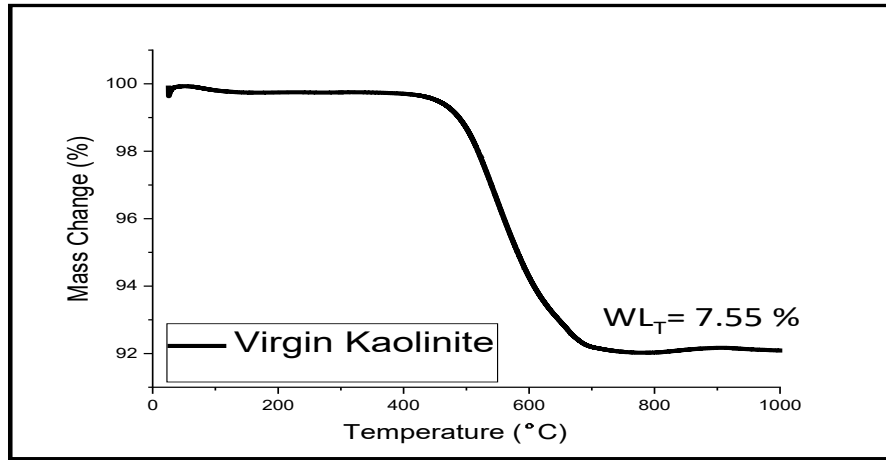


Figure 3. 26 Thermogravimetric Analysis of Kaolinite (Virgin Powder)

In this sample, only the kaolinite and quartz phases are present in high amounts and it can be assumed that the mass loss belongs to the hydroxyl ions released during the de-hydroxylation of the kaolinite. The total mass loss is 7.55% and is between 400°C and 700°C.

The mass loss measurements obtained from all samples are summarized in Table 3.10. By observing the results, it could be inferred that the most promising sample seems to be Kovukdere schist.

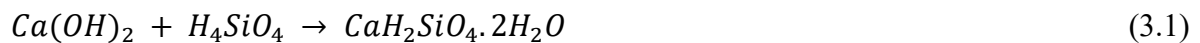
Table 3. 10 TGA results of all samples according to their mass loss (ML)

Sample Name	MS Starting Temperature (°C)	MS Ending Temperature (°C)	Mass Loss (%)
Bozalan	400	775	5.33
Camlica	600	820	10.2
Tastepe	450	875	11.25
Kovukdere	450	870	16.25
Muratbey	450	800	9.43
Ladik	400	700	2.63
Kaolinite	400	710	7.55

In general, Kovukdere, Camlica, Muratbey and Tastepe samples showed significant mass losses. Among these samples, the mass loss of Tastepe is thought to be of calcite origin. In the sections where the results are evaluated, more detailed information about this mass loss will be given.

3.2.3 Electrical Conductivity Measurement (Pozzolanicity)

The desire to incorporate activated silica sources into cement hydration reactions has graced the dreams of engineers working on this issue since the Romans [190-195]. In pozzolanic reaction, silicic acid reacts with calcium hydroxide to form the calcium silicate hydrate (CSH) phase, the main strength provider hydrated phase of cement.



Thus, a quick way to measure the pozzolanic reactivity of the silica phase is to measure the electrical conductivity in the saturated calcium hydroxide solution. Since pozzolanic reactions bind dissolved calcium hydroxide $Ca(OH)_2$ ions, the conductivity of the solution decreases with the reaction time [142]. Thus, by measuring the electrical conductivity of the solution, it is possible to obtain information about the reactivity of the silica source thrown into the solution.

The method is as follows in the literature [191]:

The following are needed with $Ca(OH)_2$ saturated solution.

- 300- or 400-mL Polyethylene bottle
- Multi-meter
- 200 mL of saturated $Ca(OH)_2$ solution at $40 \pm 1^\circ C$
- 5.00 gr dry sample (oven-dried at $105 \pm 1^\circ C$).

- pH meter
- Heater
- 2 gold electrodes

Saturated calcium hydroxide solution preparation has been described in the literature [191]. To prepare 200 mL $\text{Ca}(\text{OH})_2$ saturated solution (Lime-Water Solution):

- Place 0.35 g of calcium hydroxide in a clean 300 ml beaker (“Limewater is a saturated solution. This means there will be some insoluble extra chemical (eg $\text{Ca}(\text{OH})_2$). If the teaspoon, gallon jar or a smaller container is used, it will result in a fully saturated solution.”)
- Fill the beaker with DI water.
- Shake well for 1-2 minutes, and then leave in a quiet place to settle for 24 hours.
- strain the clear liquid from the beaker without rinsing with filter paper or coffee filter.
- repeat the filtration process until you obtain a clear liquid and store it in a cool place.

The beaker lid should be closed. If carbon dioxide is dissolved in lime, calcium carbonate forms as a white fine precipitate and blurs the liquid. Then this solution is useless. Figure 3.27 schematically describes conductivity and pH measurements.

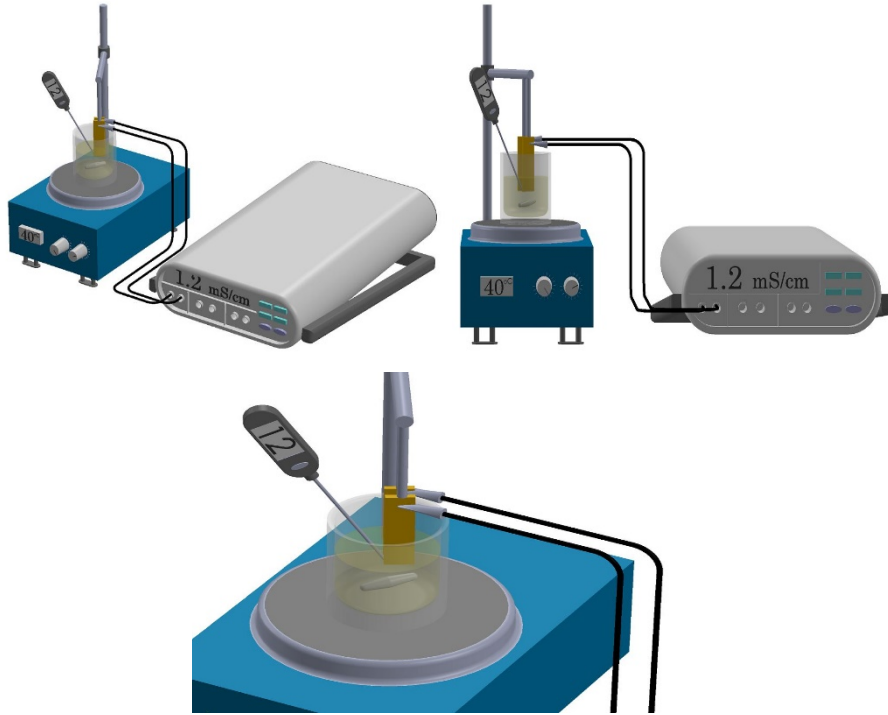


Figure 3. 27 schematic of conductivity measuring device (Pozzolanicity)

In this method, the change in conductivity is proportional to the reactivity of the material. The lower the conductivity, the more reactive the material. Luxan [191] used the following table 3.11 as a key for pozzolanic activity criteria. That is, if the conductivity variation is less than 0.4 mS / cm in the first 120 seconds after mixing the product with saturated calcium hydroxide solution, the product is not pozzolanic. If it is in the range of 0.4 to 1.2 mS / cm, then classified as variable pozzolanic. If the conductivity variation be more than 1.2 mS / cm, the product is a material that undergoes strong pozzolanic reactions in the first 120 seconds.

Table 3. 11 Pozzolanicity (conductivity variation) criteria classification [191].

Classification of Material	Variation in Conductivity according to proposed method (mS/cm)
Non Pozzolanic	Less than 0.4
Variable Pozzolanicity	Between 0.4 and 1.2
Good Pozzolanicity	Greater than 1.2

Based on the method described above, seven samples were first tested without any treatment in virgin form. The powder samples were heated in the oven at 40 ° C before being added to the saturated calcium hydroxide solution and then added to the solution at 40 ° C. In this way, variation in conductivity that may result from temperature changes are minimized. The experimental design in our laboratory is as shown in Figure 3.28. The temperature of the solution was checked regularly and kept at 40°C.

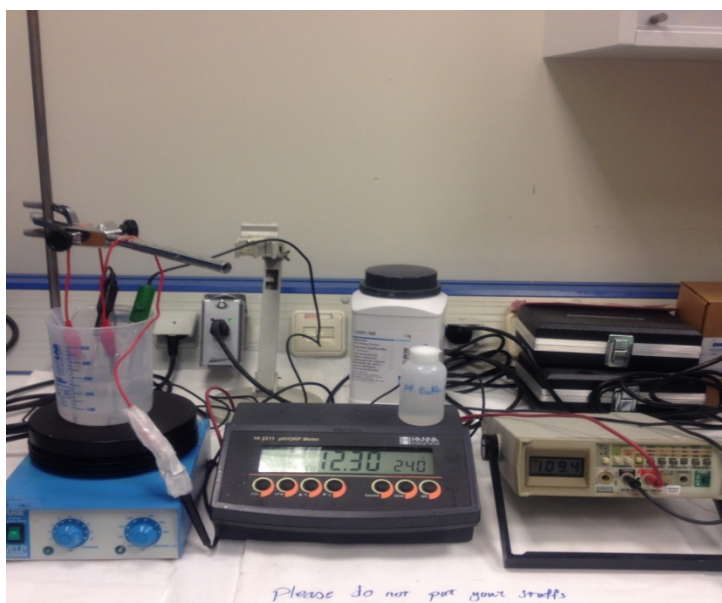


Figure 3. 28 Pozzolanicity measurement setup

In order to calculate the errors caused by the change of the temperature of the calcium hydroxide solution, it is examined that how the temperature change from room temperature to 40 ° C affects the conductivity of the calcium hydroxide solution. These measurements were repeated six times, and the results are shown in Table 3.12. Between 23°C and 40°C, the conductivity variation increases by 0.58 mS / cm. Table 3.13 also shows the pH and conductivity variations. As it can be seen, keeping the temperature under control is important for the accuracy of the measurements.

Table 3. 12 PH and conductivity variation of calcium hydroxide solution in the range of (23-40°C)

M1			
Time (min)	pH	Temp (°C)	Conductivity (mS/cm)
0	12.36	23	4.47
5	12.23	25	4.74
10	12.19	28	4.81
15	12.12	30	4.89
20	11.91	33	4.92
25	11.73	35	4.97
30	11.31	38	4.98
35	11.14	40	4.99
			Variation (M1) 0,52 mS/cm
M2			
Time (min)	pH	Temp (°C)	Conductivity (mS/cm)
0	12.22	23	4.4
5	12.06	25	4.64
10	11.76	28	4.69
15	11.57	30	4.85
20	11.41	33	4.91
25	11.28	35	4.96
30	11.14	38	4.98
35	11.06	40	5.01
			Variation (M2) 0,61 mS/cm
M3			
Time (min)	pH	Temp (°C)	Conductivity (mS/cm)
0	12.3	23	4.51
5	12.04	25	4.63
10	11.94	28	4.79
15	11.73	30	4.85
20	11.31	33	4.9
25	11.22	35	4.93
30	11.19	38	4.99
35	11.16	40	5.04
			Variation (M3) 0,53 mS/cm
M4			
Time (min)	pH	Temp (°C)	Conductivity (mS/cm)
0	12.21	23	4.39
5	12.15	25	4.48
10	11.98	28	4.54
15	11.85	30	4.68
20	11.61	33	4.76
25	11.46	35	4.89
30	11.22	38	4.96
35	11.12	40	4.99
			Variation (M4) 0,6 mS/cm
M5			
Time (min)	pH	Temp (°C)	Conductivity (mS/cm)
0	12.31	23	4.52
5	12.18	25	4.59
10	11.89	28	4.67
15	11.76	30	4.73
20	11.53	33	4.81
25	11.41	35	4.89
30	11.34	38	4.92
35	11.17	40	5.08
			Variation (M5) 0,56 mS/cm
M6			
Time (min)	pH	Temp (°C)	Conductivity (mS/cm)
0	12.26	23	4.42
5	12.1	25	4.51
10	11.81	28	4.6
15	11.62	30	4.67
20	11.47	33	4.76
25	11.31	35	4.85
30	11.1	38	4.91
35	10.93	40	4.96
			Variation (M6) 0,54 mS/cm

Table 3. 13 pH / Conductivity variability of saturated calcium hydroxide solution (23-40°C)

Measurment	Var in Conductivity (mS/cm)	Var in pH
M1	0.52	1.22
M2	0.61	1.16
M3	0.53	1.14
M4	0.6	1.09
M5	0.56	1.14
M6	0.54	1.33

These values are plotted in Figure 3.29 to evaluate the medium amount of solution conductivity.

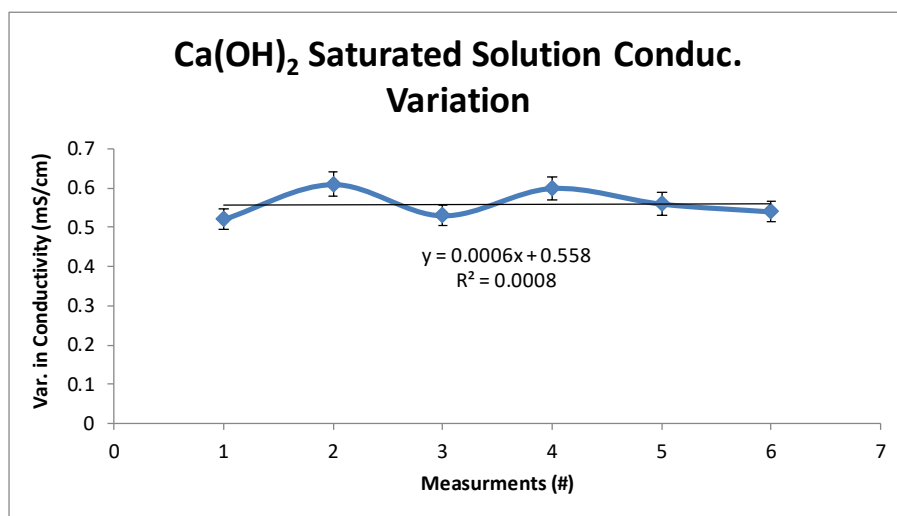


Figure 3. 29 Calcium hydroxide saturated solution conductivity variation through different measurements

The following results represent the conductivity measurements of seven different samples to measure their reactivity before any thermal treatment.

3.2.3.1 Bozalan Schist

The following are the conductivity variation values of the solution in 120 seconds by addition of 5 g of powder into the saturated calcium hydroxide solution after heating in an oven at 40°C. At this time the solution was maintained at 40°C and stirred continuously. Measurements were taken twice. Table 3.14 shows the variation in conductivity and the mass losses obtained from TGA. As it can be seen, the conductivity variation remained at 0.56 mS / cm for Bozalan sample. This result is proportional to the limited (3.5%) mass loss of the Bozalan sample and shows low pozzolanic reactivity. These samples have not yet been activated. Therefore, the reasons for the change in conductivity should be sought in other sources, not in the activation of clays. These values are important as a basis.

Table 3. 14 Virgin Bozalan schist conductivity measurements (Pozzolanic Reactivity)

BOZALAN				
Time (s)	Temperature (°C)	pH	Resistance (Ω)	Conductivity (mS/cm)
0	40	11.83	108.53	5.11
20	40	11.71	112.46	4.94
40	40	11.63	115.02	4.83
60	40	11.59	116.95	4.75
80	40	11.53	118.46	4.69
100	40	11.47	120.29	4.62
120	40	11.42	121.83	4.56
				VAR: 0.55
Time (s)	Temperature (°C)	pH	Resistance (Ω)	Conductivity (mS/cm)
0	40	11.9	108.94	5.09
20	40	11.78	112.23	4.95
40	40	11.64	116.46	4.77
60	40	11.57	119.99	4.63
80	40	11.51	121.03	4.59
100	40	11.49	122.21	4.54
120	40	11.45	123.18	4.51
				VAR: 0.58
Material	Temp. Range (°C)	WL Start Point Temp. (°C)	WL End Point Temp. (°C)	WL (%)
BOZALAN	25 to 1000	600.23	800.84	3.42

Figure 3.30 illustrate the conductivity variation for Bozalan due to the two measurements for more accuracy.

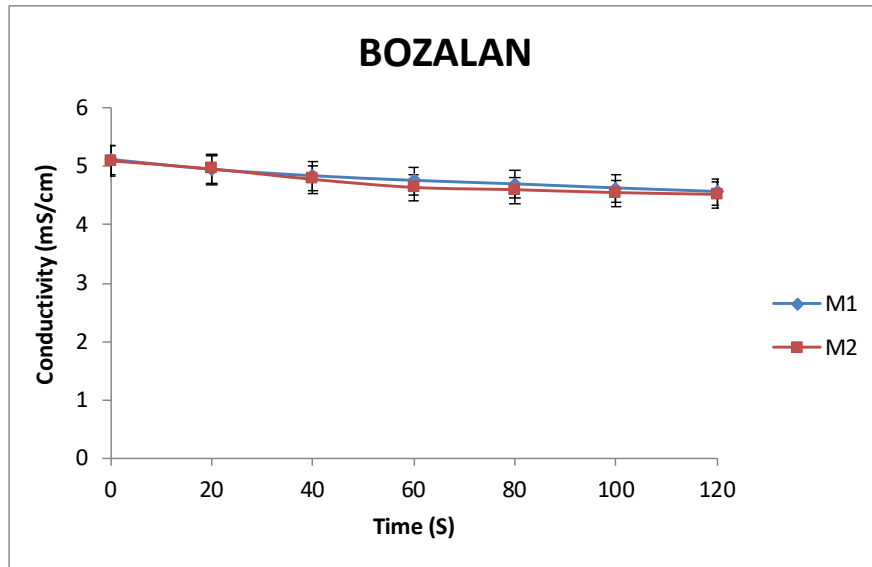


Figure 3. 30 Virgin Bozalan pozzolanicity measurements (two measurements are carried out for more accuracy)

3.2.3.2 Camlica Schist

Measurements and mass loss for the Camlica sample are shown in Table 3.15.

Table 3. 15 Virgin Camlica schist conductivity measurements (Pozzolanic Reactivity)

CAMLICA				
Time (s)	Temperature (°C)	pH	Resistance (Ω)	Conductivity (mS/cm)
0	40	11.87	108.46	5.12
20	40	11.45	121.03	4.59
40	40	11.19	127.12	4.37
60	40	11.01	132.9	4.18
80	40	10.88	138.19	4.02
100	40	10.71	140.64	3.95
120	40	10.68	142.81	3.89
				VAR: 1.23
Time (s)	Temperature (°C)	pH	Resistance (Ω)	Conductivity (mS/cm)
0	40	11.9	108.73	5.11
20	40	11.54	119.21	4.66
40	40	11.26	126.26	4.4
60	40	11.05	131.96	4.21
80	40	10.93	134.84	4.12
100	40	10.81	135.83	4.09
120	40	10.69	136.83	4.06
				VAR: 1.05
Material	Temp. Range (°C)	WL Start Point Temp. (°C)	WL End Point Temp. (°C)	WL (%)
Camlica	25 to 1000	599.75	749.33	9.85

The results of TGA showed good potential for activation with a total weight loss of 10% for the Camlica sample. Now, by considering the variation in conductivity, it shows moderate to high pozzolanic reactivity with an average value of 1.14. However, this sample shows better pozzolanicity than Bozalan and maybe the other samples. These powders have not been activated yet and the reasons for these conductivity variations should be sought elsewhere. Figure 3.31 shows the diagrams for two measurements for Camlica pozzolanicity.

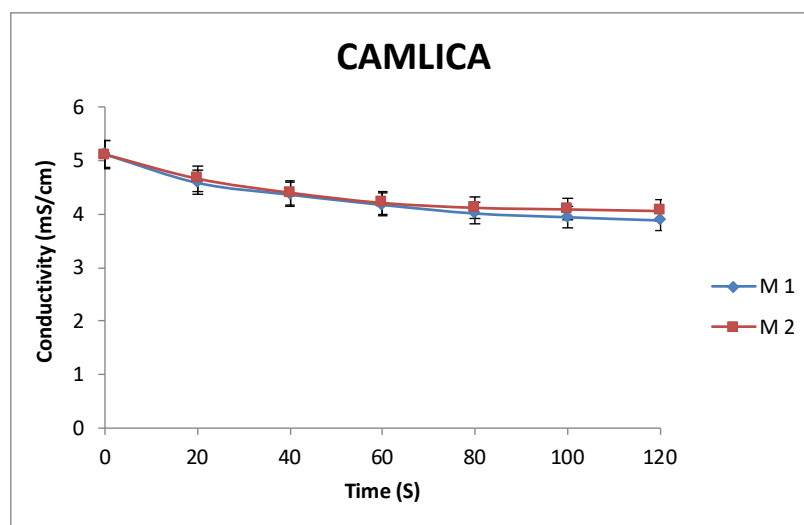


Figure 3. 31 Virgin Camlica pozzolanicity measurements (two measurements are carried out for more accuracy)

3.2.3.3 Tastepe Schist

The results of Tastepe are given in Table 3.16 and Figure 3.32. The conductivity variation is at the mid-upper level with 1.05 mS / cm. However, in the Tastepe sample, only quartz and calcite were found in XRD. It is interpreted that it is of calcite origin, albeit with very high mass loss. At this stage two idea come to mind: calcite also affects the same activated clay-like conductivity; or amorphous or very small crystalline clay-like materials that XRD cannot detect are present in this schist sample. No literature information has been found on the effect of calcite on conductivity without any treatment.

Table 3. 16 Virgin Tastepe schist conductivity measurements (Pozzolanic Reactivity)

TASTEPE				
Time (s)	Temperature (°C)	pH	Resistance (Ω)	Conductivity (mS/cm)
0	40	11.88	108.78	5.11
20	40	11.59	117.21	4.74
40	40	11.38	121.03	4.59
60	40	11.26	124.56	4.46
80	40	11.09	129.48	4.29
100	40	10.98	132.92	4.18
120	40	10.93	134.84	4.12
				VAR: 0,99
Time (s)	Temperature (°C)	pH	Resistance (Ω)	Conductivity (mS/cm)
0	40	11.64	108.52	5.12
20	40	11.48	116.71	4.76
40	40	11.29	120.25	4.62
60	40	11.12	127.67	4.35
80	40	10.97	132.84	4.19
100	40	10.85	135.17	4.11
120	40	10.76	138.54	4.01
				VAR: 1,11
Material	Temp. Range (°C)	WL Start Point Temp. (°C)	WL End Point Temp. (°C)	WL (%)
TASTEPE	25 to 1000	599.26	799.8	9.54

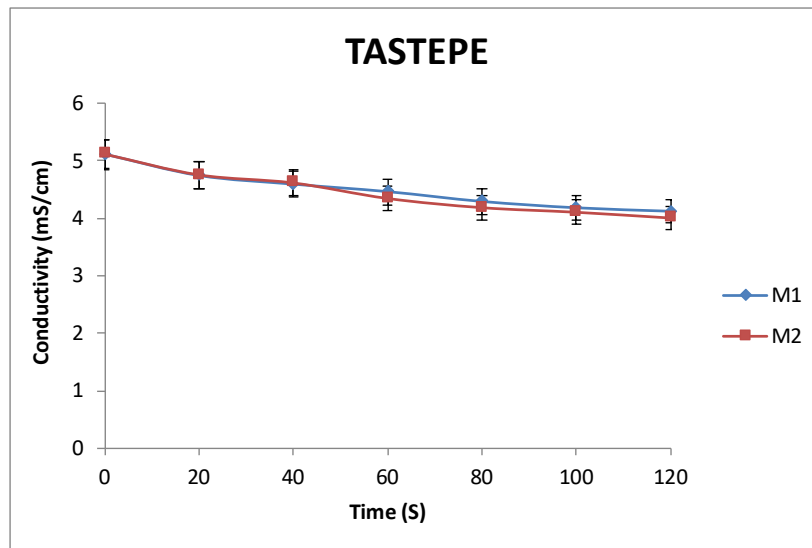


Figure 3. 32 Virgin Tastepe pozzolanicity measurements (two measurements are carried out for more accuracy)

3.2.3.4 Kovukdere Schist

Measured values of the most promising sample of Kovukdere schist are given in Table 3.17 and Figure 3.33. Kovukdere is still the most important candidate in terms of both conductivity change (1.53 mS / cm) and mass loss (16.7%).

Table 3. 17 Virgin Kovukdere schist conductivity measurements (Pozzolanic Reactivity)

KOVUKDERE				
Time (s)	Temperature (°C)	pH	Resistance (Ω)	Conductivity (mS/cm)
0	40	11.92	109.12	5.09
20	40	11.08	134.84	4.12
40	40	10.94	141.36	3.93
60	40	10.63	146.19	3.8
80	40	10.47	150.96	3.68
100	40	10.28	150.55	3.59
120	40	10.12	158.27	3.51
				VAR: 1,58
Time (s)	Temperature (°C)	pH	Resistance (Ω)	Conductivity (mS/cm)
0	40	11.81	108.95	5.08
20	40	11.29	130.71	4.25
40	40	11.11	138.54	4.01
60	40	10.9	142.26	3.94
80	40	10.78	143.55	3.87
100	40	10.62	148.14	3.75
120	40	10.52	153.89	3.61
				VAR: 1,48
Material	Temp. Range (°C)	WL Start Point Temp. (°C)	WL End Point Temp. (°C)	WL (%)
Kovukdere	25 to 1000	501.22	801.17	16.68

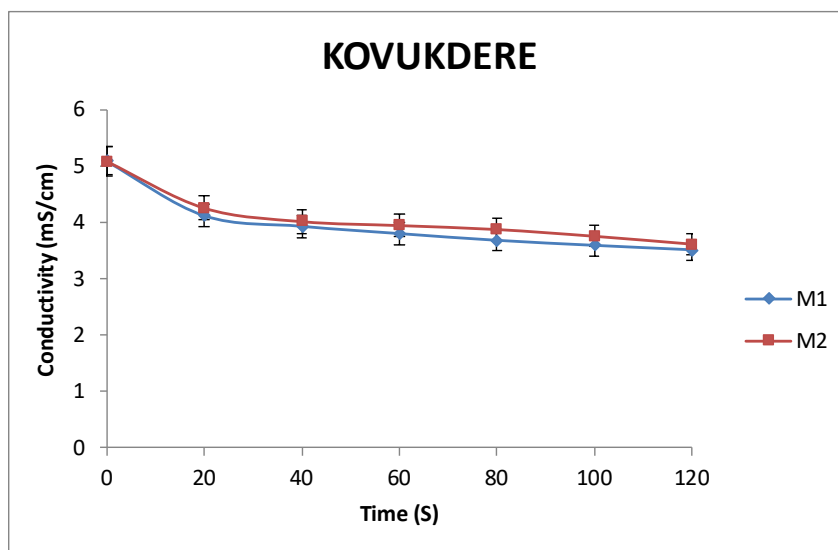


Figure 3. 33 Virgin Kovukdere pozzolanicity measurements (two measurements are carried out for more accuracy)

The obtained values for Kovukdere shows the high reactivity of this schist material. It would be the reliable sign of amorphous portion existence.

3.2.3.5 Muratbey Schist

Table 3.18 and Figure 3.34 represent the Muratbey schist pozzolanicity measurements. Muratbey has already identified as similar schist to Kovukdere but without any calcite phase.

Table 3. 18 Virgin Muratbey schist conductivity measurements (Pozzolanic Reactivity)

MURATBEY				
Time (s)	Temperature (°C)	pH	Resistance (Ω)	Conductivity (mS/cm)
0	40	11.92	109.45	5.07
20	40	11.64	121.59	4.58
40	40	11.35	131.33	4.23
60	40	11.11	135.5	4.1
80	40	10.91	138.54	4.01
100	40	10.78	140.63	3.95
120	40	10.64	143.18	3.88
				VAR: 1,19
Time (s)	Temperature (°C)	pH	Resistance (Ω)	Conductivity (mS/cm)
0	40	11.88	109.13	5.09
20	40	11.35	122.1	4.55
40	40	11.21	128.89	4.31
60	40	11.03	133.86	4.15
80	40	10.9	137.17	4.05
100	40	10.78	140.29	3.96
120	40	10.64	144.67	3.84
				VAR: 1,25
Material	Temp. Range (°C)	WL Start Point Temp. (°C)	WL End Point Temp. (°C)	WL (%)
Muratbey	25 to 1000	399.62	799.79	9.64

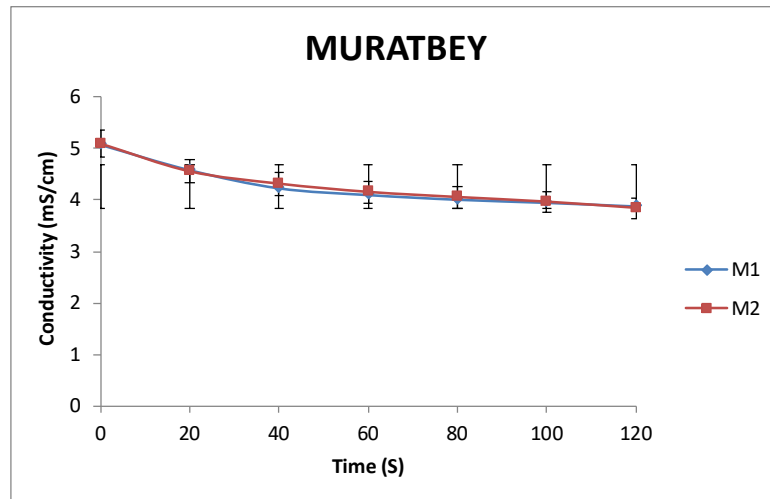


Figure 3. 34 Virgin Muratbey pozzolanicity measurements (two measurements are carried out for more accuracy)

It already showed good pozzolanic reactivity with a very strong (1.22 mS / cm) conductivity variation. No calcite phase was found in Muratbey sample. Therefore, the change in conductivity cannot be explained by the calcite effect. This powder contains very abundant clay-based phases in its content. Hence, it is one of the samples with high hope of activation.

3.2.3.6 Ladik Schist

Ladik schist is the most desperate sample but the variation in conductivity measurements was still better than the Bozalan sample. There is no calcite in Ladik. However, as it can be seen, it has a reactive phase that can affect conductivity. This result may indicate the importance of undetectable (perhaps amorphous) phases in the XRD. Table 3.19 shows the variation in conductivity for this sample and Figure 3.35 also illustrates the conductivity drop.

Table 3. 19 Virgin Ladik schist conductivity measurements (Pozzolanic Reactivity)

LADIK				
Time (s)	Temperature (°C)	pH	Resistance (Ω)	Conductivity (mS/cm)
0	40	11.85	108.28	5.13
20	40	11.72	115.98	4.79
40	40	11.59	119.21	4.66
60	40	11.46	121.59	4.57
80	40	11.37	123.45	4.5
100	40	11.32	124.77	4.46
120	40	11.29	126.52	4.39
				VAR: 0,74
Time (s)	Temperature (°C)	pH	Resistance (Ω)	Conductivity (mS/cm)
0	40	11.97	109.01	5.09
20	40	11.78	115.52	4.81
40	40	11.63	118.46	4.69
60	40	11.46	120.73	4.6
80	40	11.41	122.1	4.55
100	40	11.38	123.09	4.52
120	40	11.3	123.73	4.49
				VAR: 0,6
Material	Temp. Range (°C)	WL Start Point Temp. (°C)	WL End Point Temp. (°C)	WL (%)
Ladik	25 to 1000	401.6	700.5	2.47

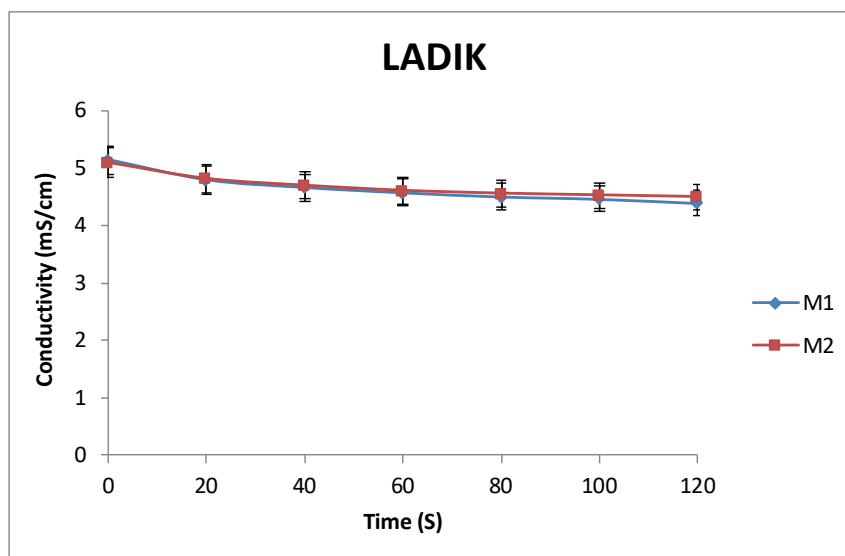


Figure 3. 35 Virgin Ladik pozzolanicity measurements (two measurements are carried out for more accuracy)

3.2.3.7 Kaolinite

The pozzolanicity of benchmark sample, Kaolinite is measured and represented in Table 3.20 and Figure 3.36.

Table 3. 20 Virgin Kaolinite conductivity measurements (Pozzolanic Reactivity)

KAOLINITE				
Time (s)	Temperature (°C)	pH	Resistance (Ω)	Conductivity (mS/cm)
0	40	11.84	108.25	5.13
20	40	11.45	121.03	4.59
40	40	11.23	125.97	4.41
60	40	11.14	128.01	4.34
80	40	11.09	130.71	4.25
100	40	10.96	134.84	4.12
120	40	10.86	139.58	3.98
				VAR: 1,15
Time (s)	Temperature (°C)	pH	Resistance (Ω)	Conductivity (mS/cm)
0	40	11.97	108.84	5.1
20	40	11.39	124.01	4.48
40	40	11.2	129.19	4.3
60	40	11.13	130.71	4.25
80	40	11.01	133.22	4.17
100	40	10.95	136.83	4.06
120	40	10.82	139.23	3.99
				VAR: 1,11
Material	Temp. Range (°C)	WL Start Point Temp. (°C)	WL End Point Temp. (°C)	WL (%)
KAOLINITE	25 to 1000	399.46	698.22	7.4

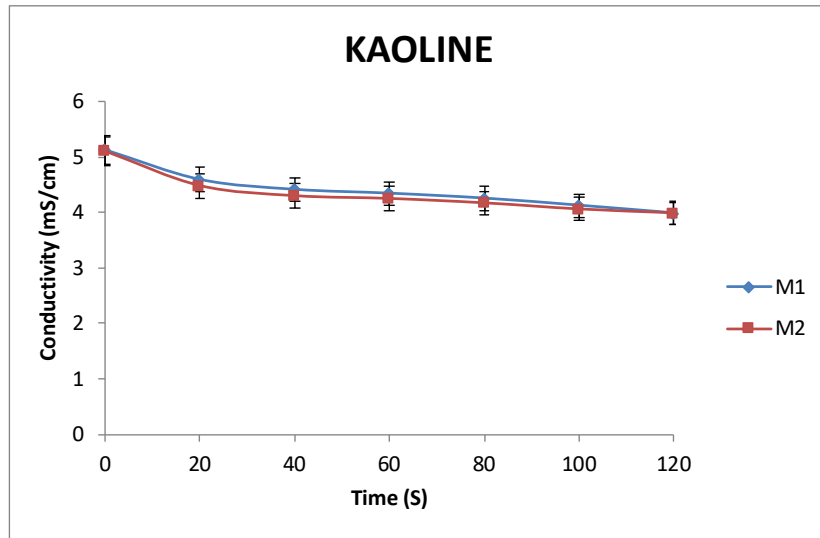


Figure 3. 36 Virgin Kaolinite pozzolanicity measurements (two measurements are carried out for more accuracy)

Kaolinite also showed the highest conductivity variation with Kovukdere and Muratbey samples. Kaolinite is known to be activatable and has been shown to be used as cement substitution up to 30%. So far, Kovukdere and Muratbey samples can be monitored as possible potential.

In general, the comparison results from the pozzolanicity measurements is given in Table 3.21. The most promising example is Kovukdere. The following table shows the activation potential by top-down color code.

Table 3. 21 Pozzolanicity measurements of all samples

Sample	Time (S)	Var. in Conductivity (mS/cm)
BOZALAN	120	0.55
	120	0.58
CAMLICA	120	1.23
	120	1.05
TASTEPE	120	0.99
	120	1.11
KOVUKDERE	120	1.58
	120	1.48
MURATBEY	120	1.19
	120	1.25
LADIK	120	0.74
	120	0.6
KAOLINITE	120	1.15
	120	1.11

This ranking is shown in Figure 3.37 to compare the conductivity variation among the all samples.

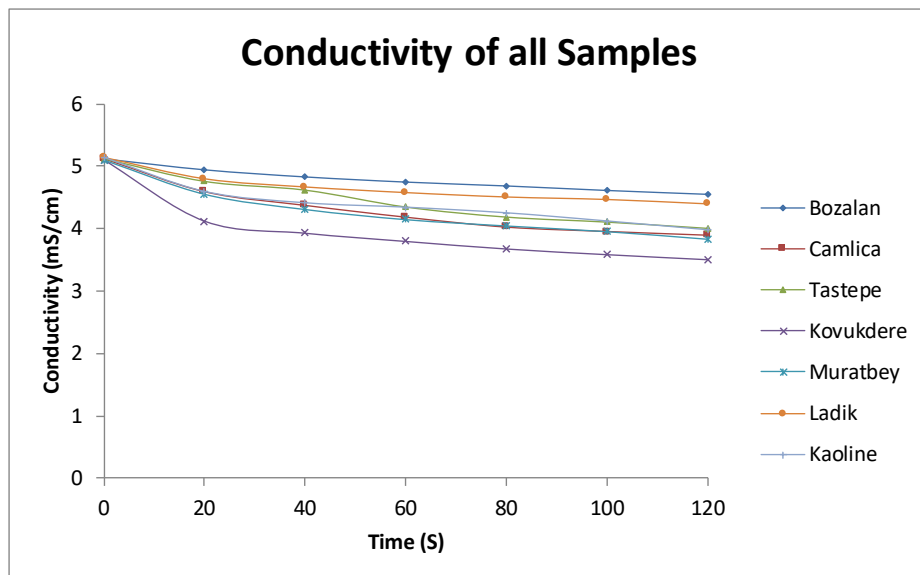


Figure 3. 37 Comparison graph of conductivity variation of all samples up to 120 seconds

XRD measurements showed calcite in many of raw materials. In order to determine the effect of calcite on calcium hydroxide solution, 5 g calcite powder was thrown into the same calcium hydroxide solution at 40°C. Table 3.22 and Figure 3.38 show the variation in conductivity caused by calcite. Accordingly, some of the conductivity variation in calcite-containing samples come from the reaction of calcite with calcium hydroxide solution.

Table 3. 22 Variation of conductivity due to calcium carbonate

CALCIUM CARBONATE				
Time (s)	Temperature (°C)	pH	Resistance (Ω)	Conductivity (mS/cm)
0	40	11.21	95.31	5.83
20	40	11.16	100.31	5.53
40	40	11.14	102.68	5.41
60	40	11.08	104.01	5.34
80	40	11.05	105.18	5.28
100	40	11.01	106.25	5.22
120	40	10.98	107.56	5.16
				VAR: 0,67
Time (s)	Temperature (°C)	pH	Resistance (Ω)	Conductivity (mS/cm)
0	40	11.28	96.45	5.76
20	40	11.22	103.67	5.35
40	40	11.17	105.06	5.28
60	40	11.13	106.82	5.2
80	40	11.1	108.11	5.14
100	40	11.09	108.95	5.09
120	40	11.06	109.35	5.07
				VAR: 0,69

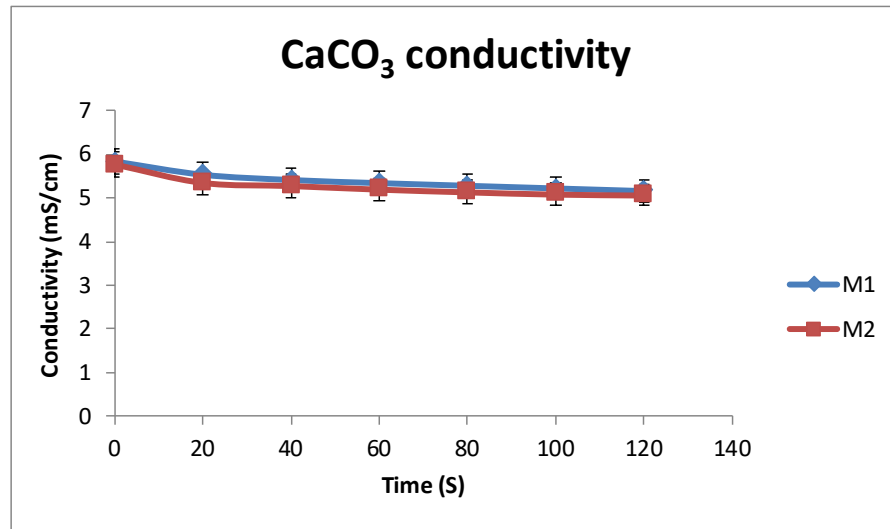


Figure 3. 38 Variation of conductivity in solution due to calcium carbonate

The electrical conductivity of as it is called “pozzolanicity” is a shortcut method to evaluation the pozzolanic reactivity of materials. Even though this method is not proper for the powders with carbonate content, it is applicable for the clayey type materials to estimate the pozzolanic behavior and portion of amorphous aluminosilicates.

3.2.4 Microstructure and Composition Analysis (SEM-EDS)

The received raw powders were evaluated by SEM (scanning electron microscope) for microstructure and mineral distribution for possible cement substitution. The aim is to predict whether the phases that will be prominent in the microstructure are activated or could be reactivated for pozzolanic reactions or not. According to the literatures [193-197], kaolinite type clays can be activated. Activated form of this clay, called metakaolin, reacts with calcium and water in high pH cement paste environments due to the degradation of the bonds in its structure and shows cement-like binder. In this section, the original microstructures of the samples are displayed in powder samples. The morphologies of the same powder samples after heat treatment are shown in the following sections. The morphology of the phases that can be activated and whether they have changed or not, express the indications of their suitability for pozzolanic reactions. Figure 3.39 shows the BSE-SEM (back-scattered electrons mode) images of the six raw materials. The samples appear to have different microstructures. In the Kovukdere, Muratbey and Camlica samples, the crystalline phases appear more prominent. Tastepe and Bozalan samples also show some portion of amorphous structure. These amorphous structures may explain why these samples give a change in conductivity indicating high pozzolanic activity, although there are no crystalline clay samples in the XRD results. Clay layers are visible in Kovukdere sample and leaf-shaped bentonite-like crystals are found in Muratbey sample. Although crystallized layers appear in the Bozalan sample, the amorphous phase is more dominant in Tastepe sample. In the Camlica sample, both leaf crystals and amorphous structure can be seen. The Ladik specimen has a completely different structure and the clay type structure is observed.

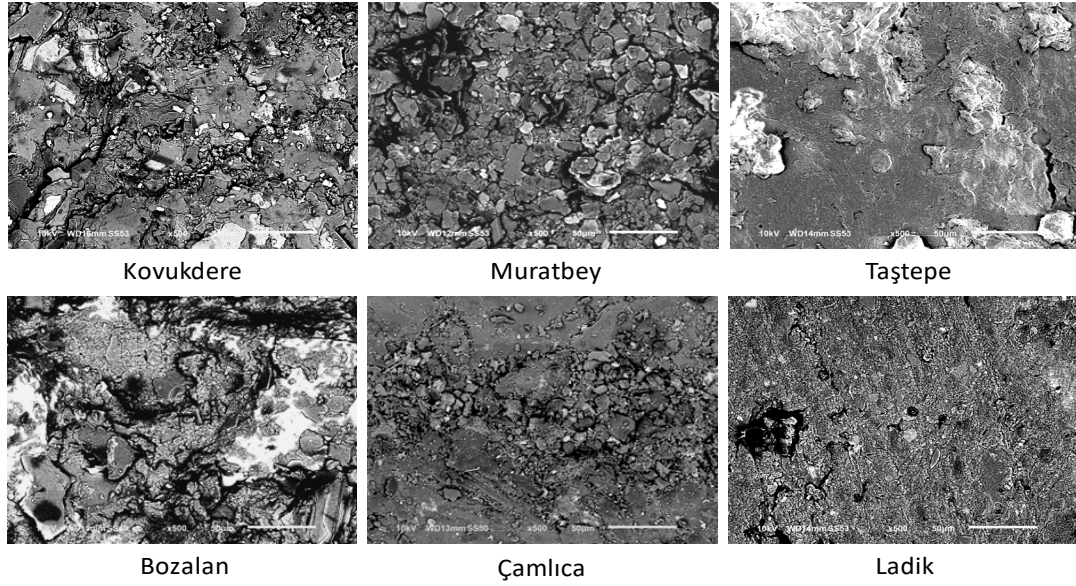


Figure 3. 39 BSE-SEM (scanning electron microscopy-backscattered electrons mode) images of six raw materials received from mine quarries

In order to evaluate the chemical and phase structure of mineral samples, EDS (Energy dispersive spectroscopy) chemical analysis was employed. Figure 3.40 shows the (a) microstructure and (b) elemental ratios and (c) EDS analysis of the kaolinite mineral. This sample is considered as a standard sample. As it is shown in Figure 3.40b, Si and Al are dominant elements in the sample. The Si / Al ratio is about 2.5, and since the formula of the kaolinite is $\text{Al}_2\text{Si}_2\text{O}_5(\text{OH})_4$, the excess Si can show the amount of quartz. Figure 3.40c shows the EDS elemental maps. It is possible to see a layered map of Si, Al and two elements. The more prominent regions of Si are the quartz phase. The overlay map shows regular distribution of clay and quartz.

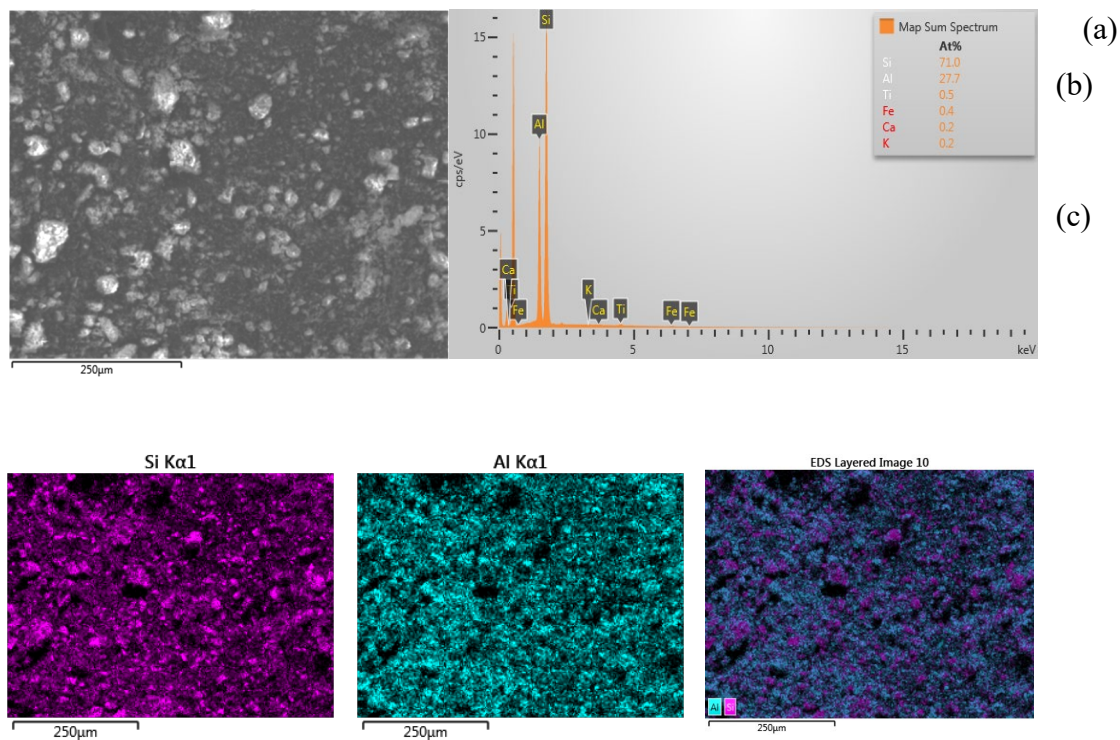
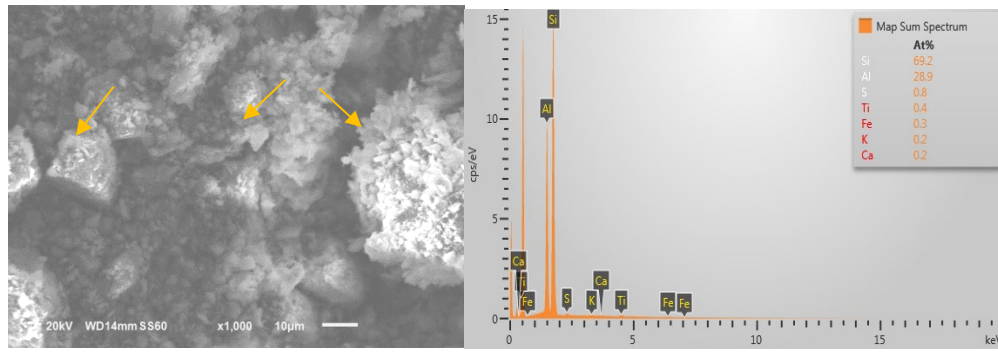


Figure 3. 40 Kaolinite microstructure and elemental analysis; (a) microstructure, (b) element ratios and (c) EDS mapping (Si, Al and layered map)

In order to discuss the microstructure and chemical structure in more detail, the analysis was applied at higher magnifications. Figure. 3.37a shows the kaolinite microstructure at higher magnification. Arrows point to layered structure. Chemical analysis (Figure 3.41b) shows trace amounts of S, Ti and Fe in the sample. The Si dominant regions (red rings) appearing on the elemental map (Figure 3.41c) show the quartz phase. In the integrated image, the pink areas represent quartz.



(a)

(b)

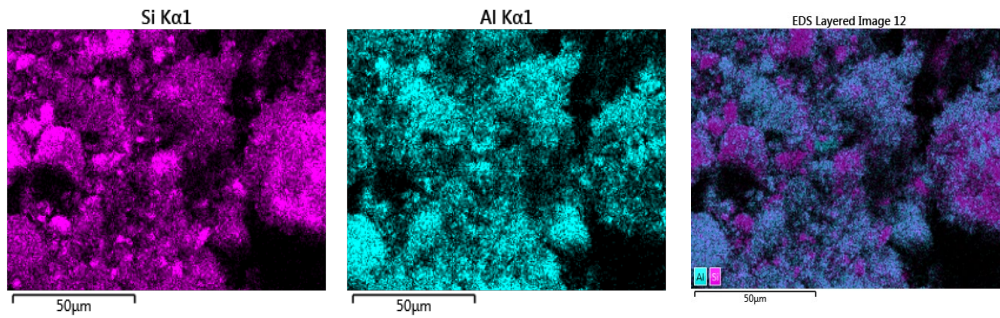
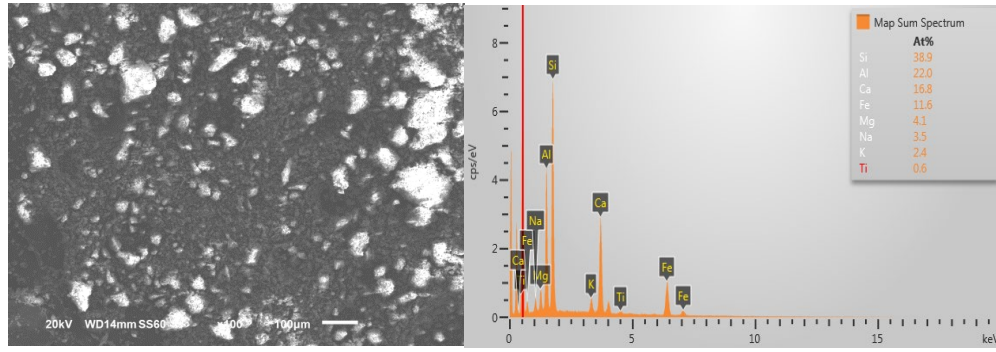


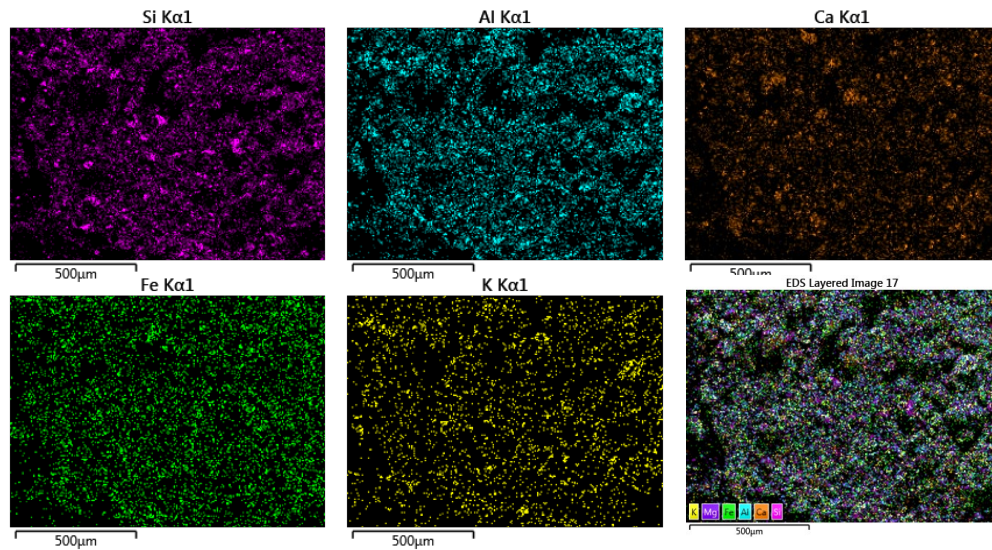
Figure 3. 41 Kaolinite microstructure and elemental analysis; (a) microstructure, (b) element ratios and (c) EDS mapping (Si, Al and layered map)

Figure 3.42 shows the microstructure and chemical analysis of Kovukdere mineral powder. Figure 3.42b shows that the Si / Al ratio is 1.8. Ca ratio is 16% and Fe ratio is 11%. There are also Mg, Na, K and trace amounts of Ti. In elemental maps, the Si and Al distributions generally overlap, but in some regions the Si or Al ratio appears to be higher. The overlapping portions represent kaolinite and K-ilite mica clays. The dominant portions Si and Al may indicate quartz and / or silimanite, respectively.



(a)

(b)



(c)

Figure 3. 42 Kovukdere schist microstructure and elemental analysis; (a) microstructure, (b) element ratios and (c) EDS mapping (Si, Al, Ca, Fe, K and layered map)

In Figure 3.43, a sample of the Kovukdere powder is shown at higher magnification. It is possible to see that the microstructure in the form of clay layers. The orange arrows show the layers in Figure 3.43a. Figure 3.43c shows the element maps. Al and Si (sometimes K and Na) overlapping parts represent clay, and red rings show quartz phase. In addition, the blue rings are Ca-dominant regions and show the calcite mineral. Green circles indicate areas where Ca and Mg overlap and other elements are absent and therefore Dolomite. The purple rings show the Iron oxide phase. Iron oxides and illites and smectites can also settle for 5-

8% Al and the overlapping parts may belong to these minerals. It is also possible to see the distribution of the different phases more clearly in the layered image.

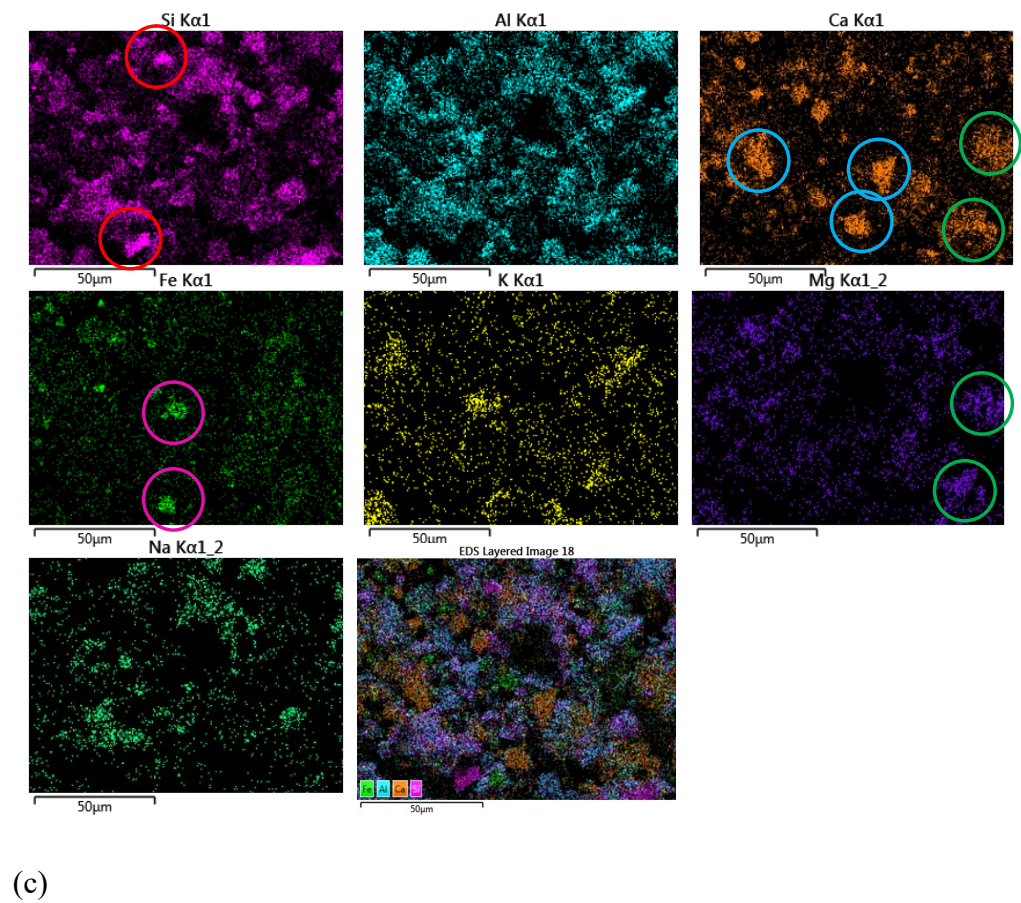
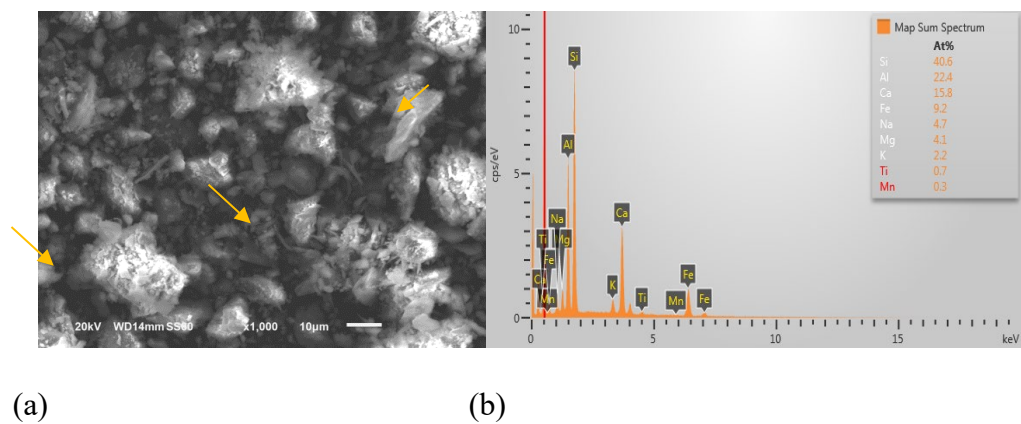


Figure 3. 43 Kovukdere schist microstructure and elemental analysis; (a) microstructure, (b) element ratios and (c) EDS mapping (Si, Al, Ca, Fe, K, Mg, Na and layered map)

Figure 3.44 shows the microstructure and chemical analysis of the Muratbey schist. Si / Al ratio is around 2.5. In addition, K, Ca, Mg, Na and Ti elements are also available. Ca and Fe ratio is lower compared to Kovukdere sample. In the maps, Si, Al, K and Fe are scattered everywhere and Ca does not appear alone.

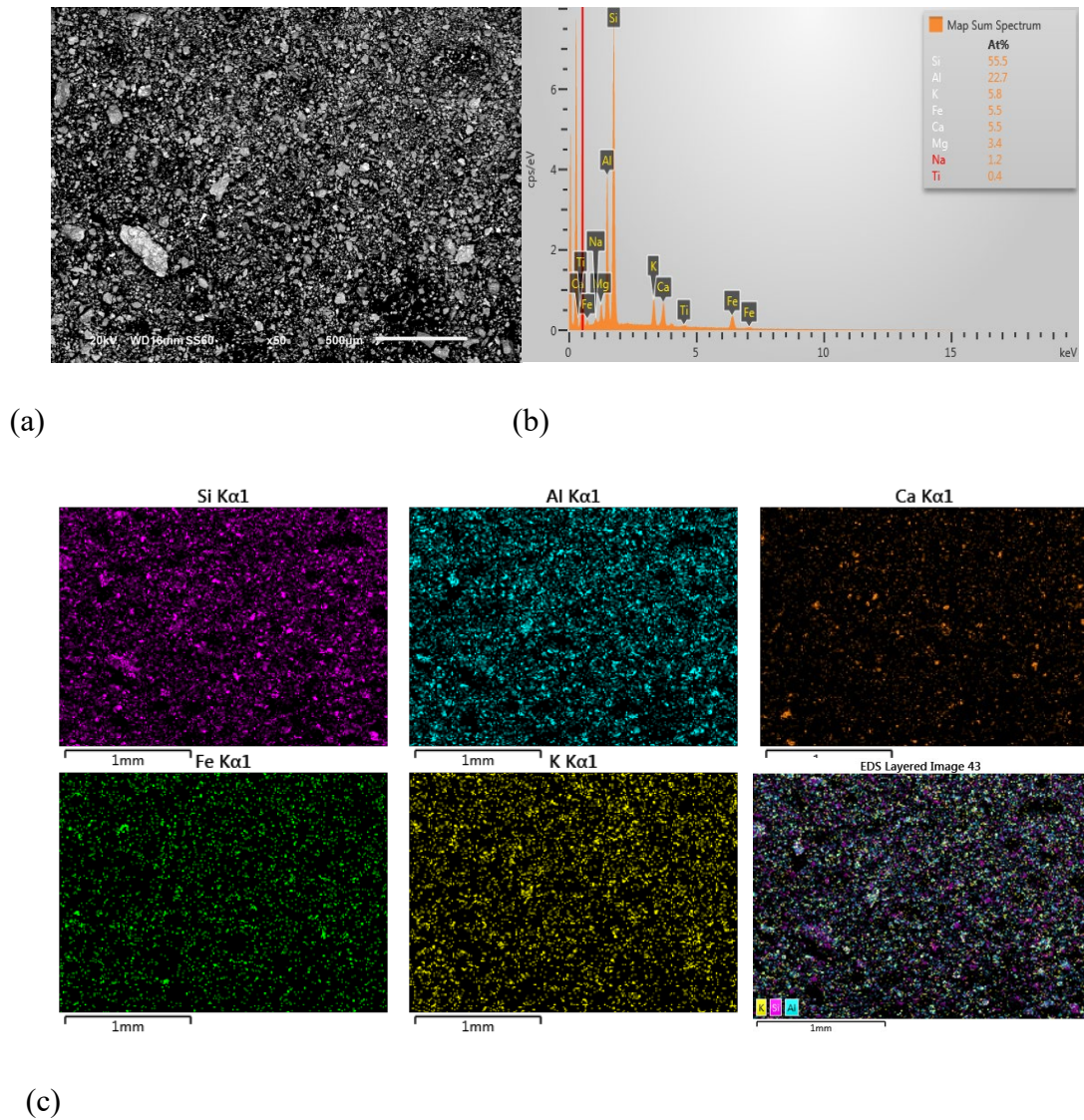
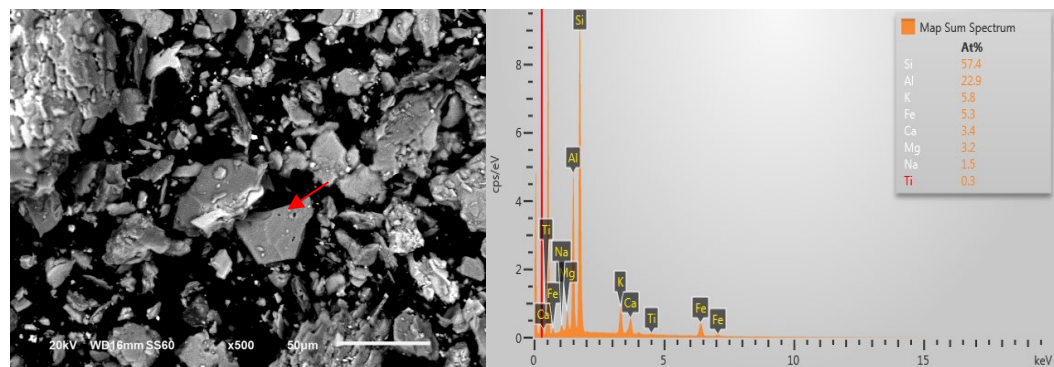


Figure 3. 44 Muratbey schist microstructure and elemental analysis; (a) microstructure, (b) element ratios and (c) EDS mapping (Si, Al, Ca, Fe and layered map)

Figure 3.45 shows the Muratbey schist at higher magnification. A large proportion of the sample is composed of layers and leaf-shaped particles. The region indicated by the red arrow may belong to the quartz phase due to the crystalline angle. When we look at elemental maps, we see a higher Si ratio in that area (red rings). The orange rings on the maps indicate the areas where Al, Mg and Fe overlap and therefore probably belong to the smectite or illite type clay phase. The blue, green and purple rings show the calcite, dolomite and iron oxide phases, respectively. The K-aluminosilicate phases may be clay or feldspar.



(a)

(b)

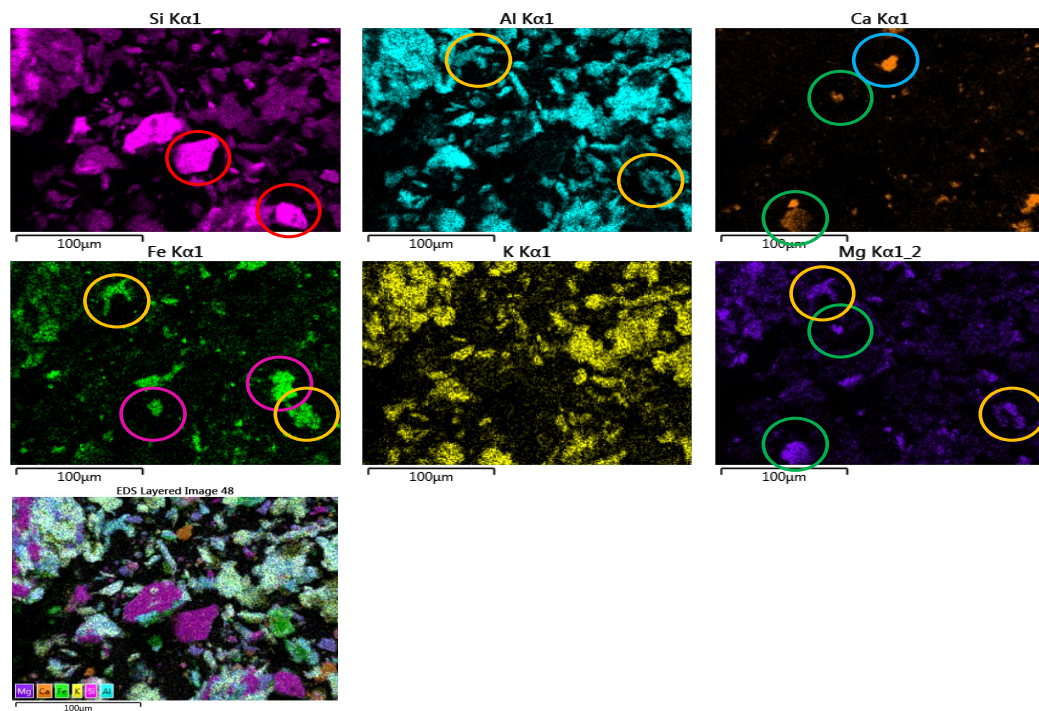


Figure 3. 45 Muratbey schist microstructure and elemental analysis; (a) microstructure, (b) element ratios and (c) EDS mapping (Si, Al, Ca, Fe, K, Mg and layered map)

Figure 3.46 shows the microstructure and elemental analysis results of the sample of Tastepe region. Figure 3.42b shows that the Si / Al ratio is ~ 4 . The chemical structure also contains high amounts of Ca (26%) and less Fe, Mg and K. Na is not available. In the element maps (Figure 3.46c), Ca, Fe and Mg are scattered all over. Where Ca, Al and Si overlap may belong to amorphous aluminocalcium-silicate phases.

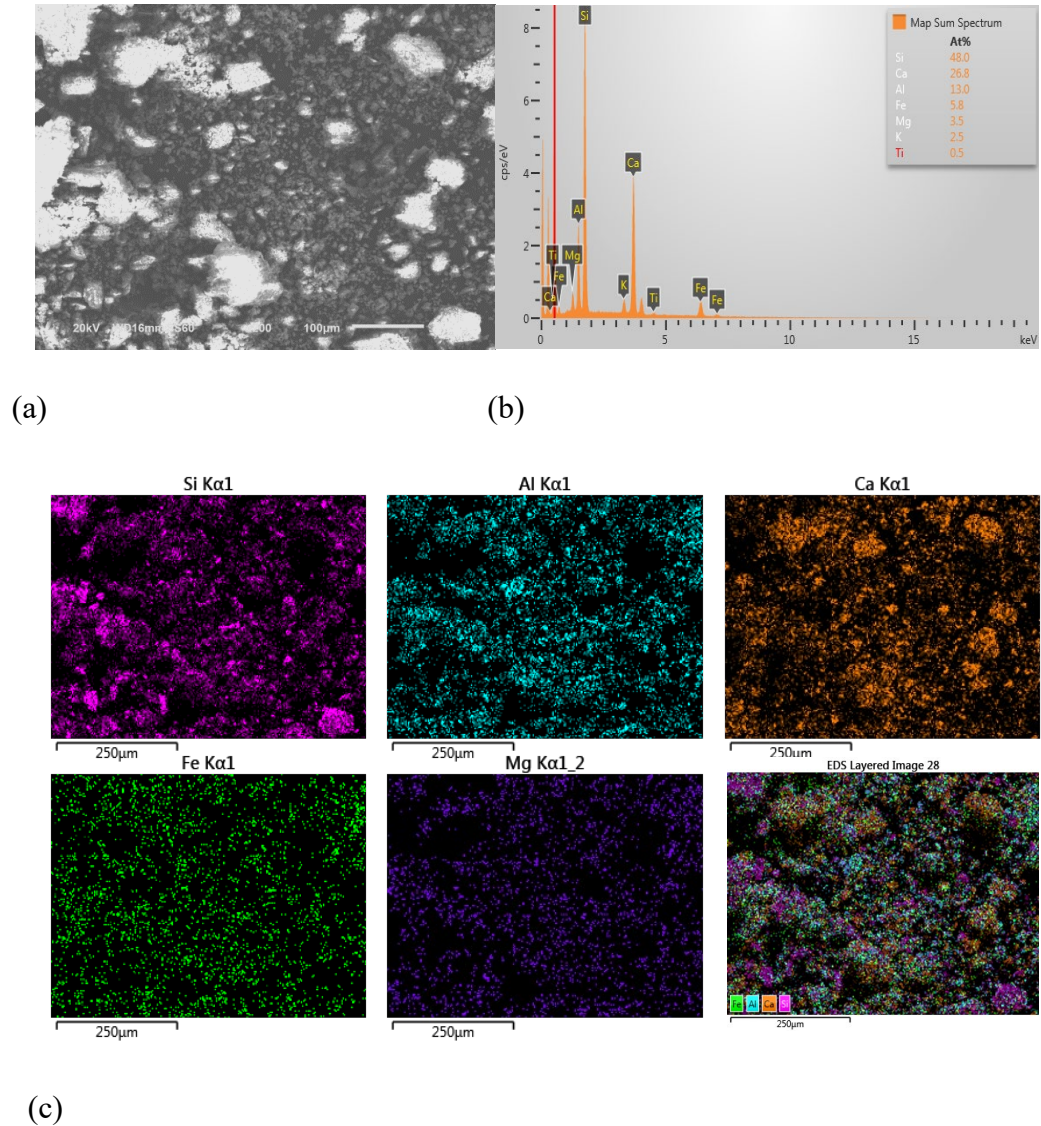
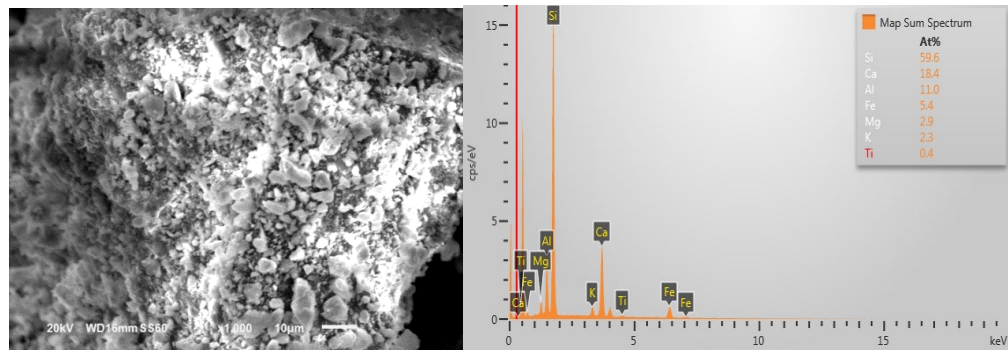


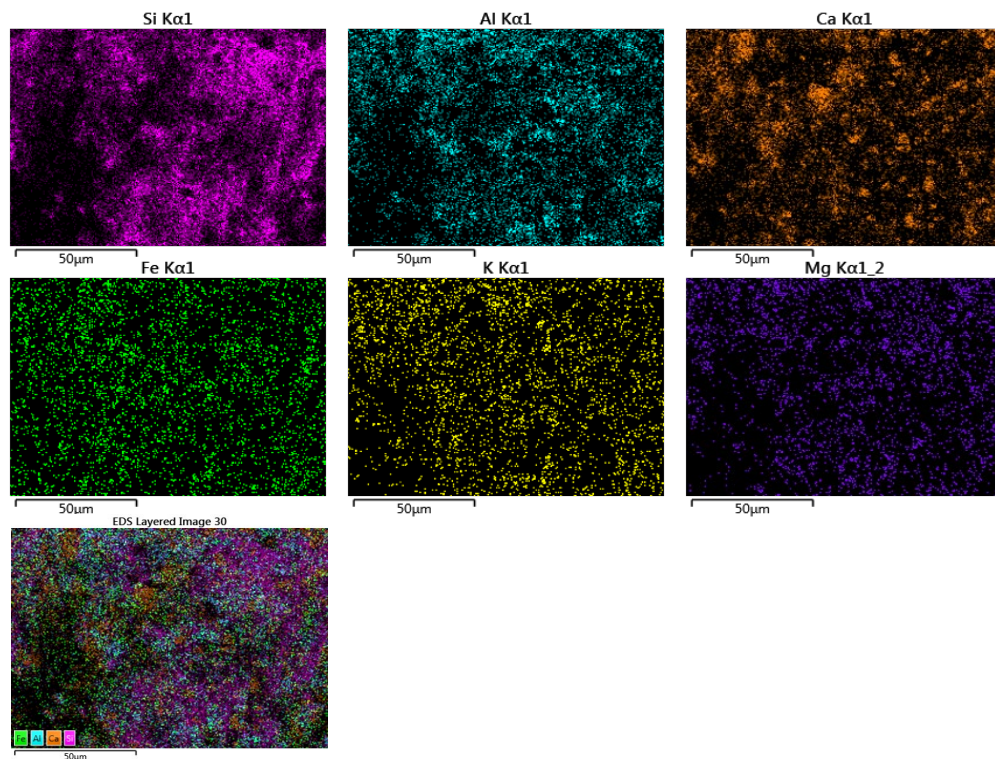
Figure 3. 46 Tastepe clay microstructure and elemental analysis; (a) microstructure, (b) element ratios and (c) EDS mapping (Si, Al, Ca, Fe, Mg and layered map)

Figure 3.47 shows the microstructure of the Tastepe sample at higher magnification. The microstructure and element distribution differ greatly from the previous samples. Calcium content in the sample is very high, indicating a high amount of calcite minerals. Si is more pronounced in some areas, but other elements seem to be scattered everywhere. Si ratio is very high and shows a high amorphous structure.



(a)

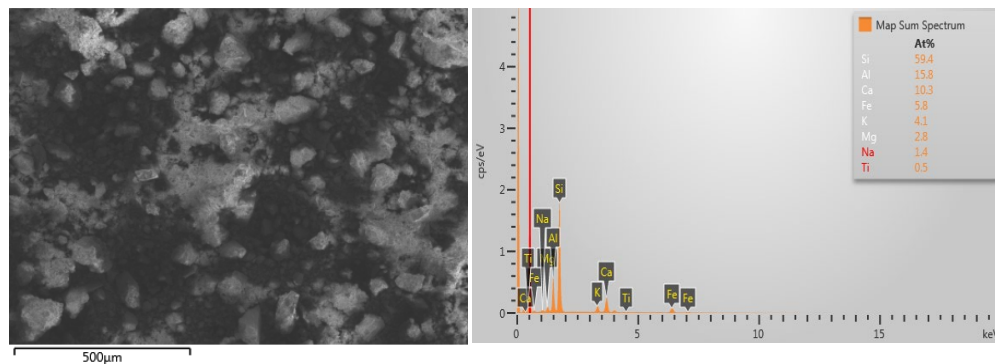
(b)



(c)

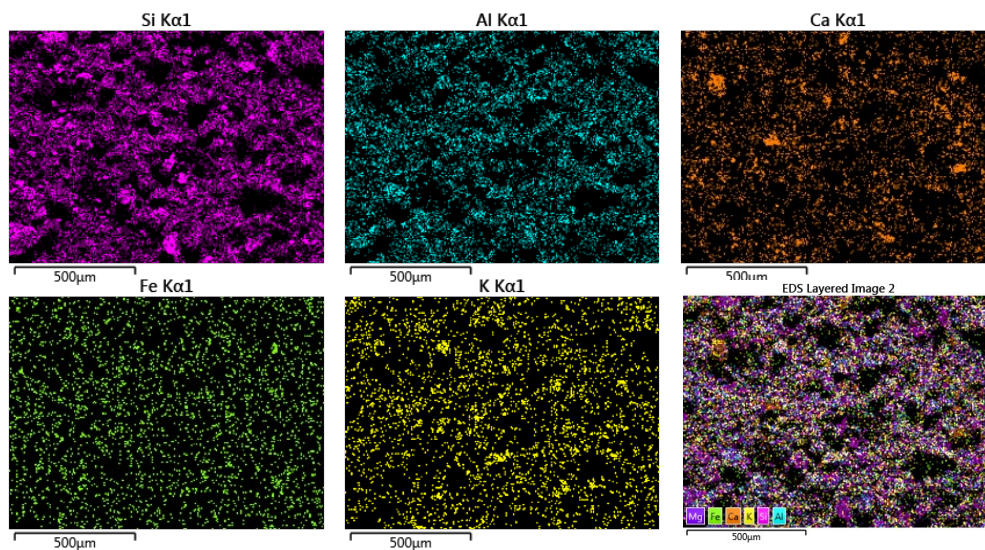
Figure 3. 47 Tastepe clay microstructure and elemental analysis; (a) microstructure, (b) element ratios and (c) EDS mapping (Si, Al, Ca, Fe, K, Mg and layered map)

Figure 3.48 shows the microstructure and chemical analysis of the Bozalan mineral. Si / Al ratio is very high as in the case of Tastepe is approximately 4. In addition, Ca, Fe, K, Mg, Na and trace amounts of Ti are also present. Other elements except Si and Ca show an even distribution on all sides (Figure 3.48c).



(a)

(b)



(c)

Figure 3. 48 Degrading clay microstructure and elemental analysis; (a) microstructure, (b) element ratios and (c) EDS mapping (Si, Al, Ca, Fe, K and layered map)

Figure 3.49 shows the Bozalan sample at higher magnification and in more detail. Although the microstructure has layered crystals, heap-shaped crystals are also present and possibly belong to feldspar. By looking at element maps, the distribution of K, Al and Si overlaps in these regions that may belong to K-feldspar. The red arrows on Si indicate the quartz. The blue and green rings show the calcite and dolomite minerals respectively. In the layered picture, the decomposition of calcite and aluminosilicates is clearly shown.

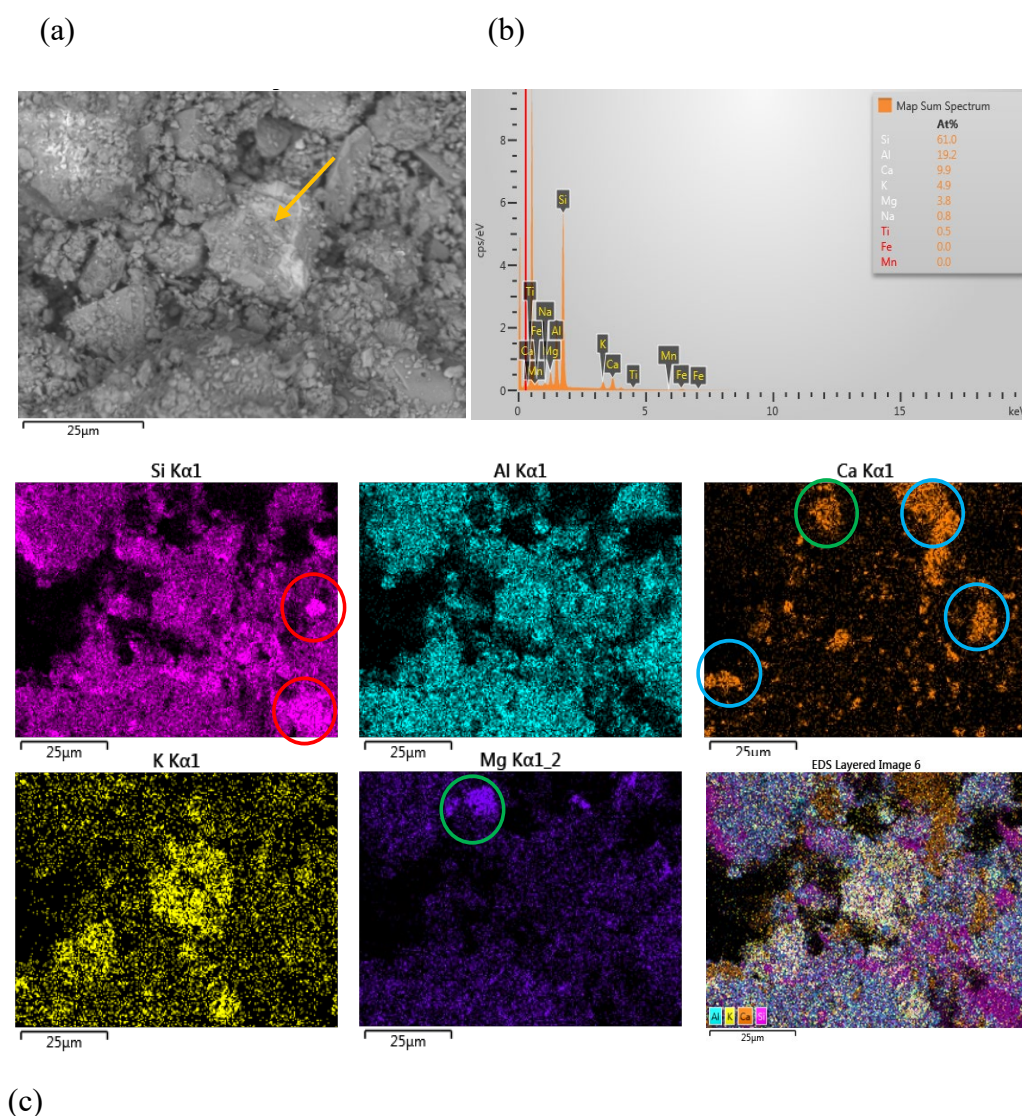


Figure 3. 49 Bozalan clay microstructure and elemental analysis; (a) microstructure, (b) element ratios and (c) EDS mapping (Si, Al, Ca, K, Mg and layered map)

Figure 3.50 shows the microstructure and chemical analysis of the Camlica schist sample. The microstructure shows both layers and heap-shaped crystals. Figure 3.50b shows that the Si / Al ratio is 3 and there is a high amount of Ca. There are also Fe, K, Na and Mg structures.

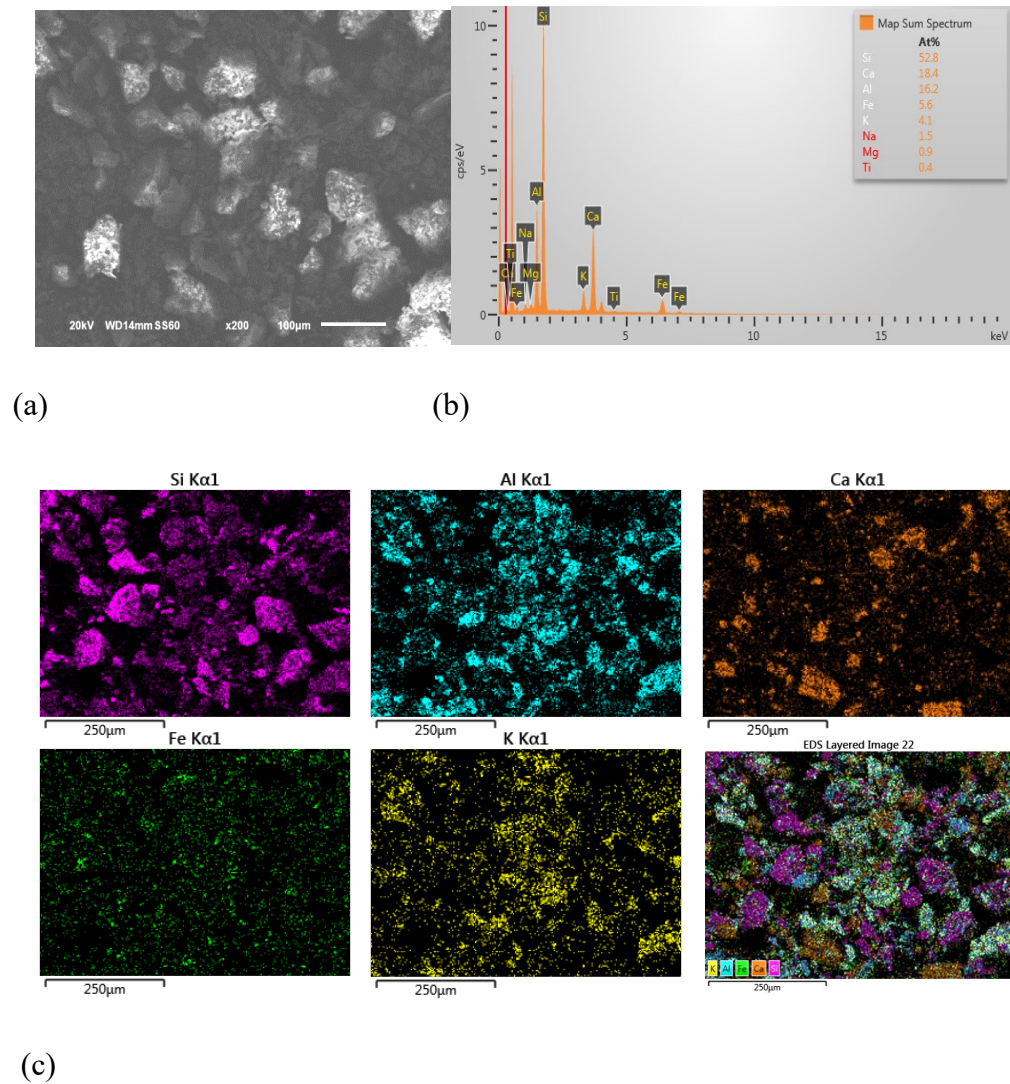


Figure 3. 50 Camlica schist microstructure and elemental analysis; (a) microstructure, (b) element ratios and (c) EDS mapping (Si, Al, Ca, Fe, K and layered map)

Figure 3.51 shows the Camlica sample at higher magnification. Element maps are shown in Figure 3.51c. The red rings on the Si map belong to the quartz phase. Blue and purple rings

show calcite and iron oxide respectively. The overlapping parts of K-Al-Si show the clay layers. Minerals are also clearly visible in the layered image.

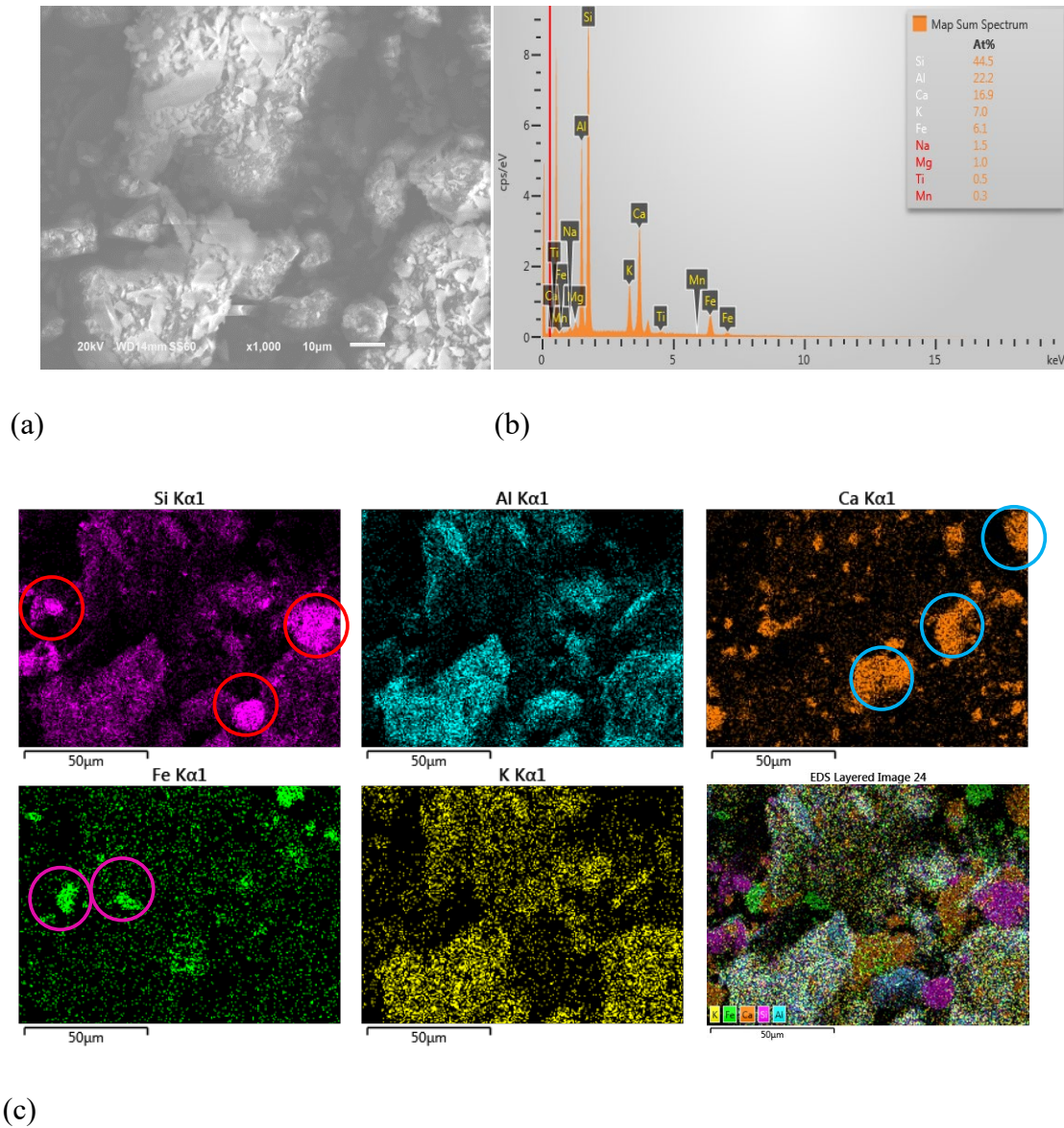


Figure 3. 51 Camlica schist microstructure and elemental analysis; (a) microstructure, (b) element ratios and (c) EDS mapping (Si, Al, Ca, Fe, K and layered map)

Figure 3.52 shows the microstructure and chemical analysis of the Ladik clay. In this sample, the Si / Al ratio is ~ 3 . Fe, K, Mg and Na are also available. The Ca ratio is only $\sim 2\%$ and is

very low compared to other samples (Figure 3.52b). Element maps show Si, Al, Mg, Fe and K maps. All elements are located at almost the same points. The same distribution can be seen in the layered image.

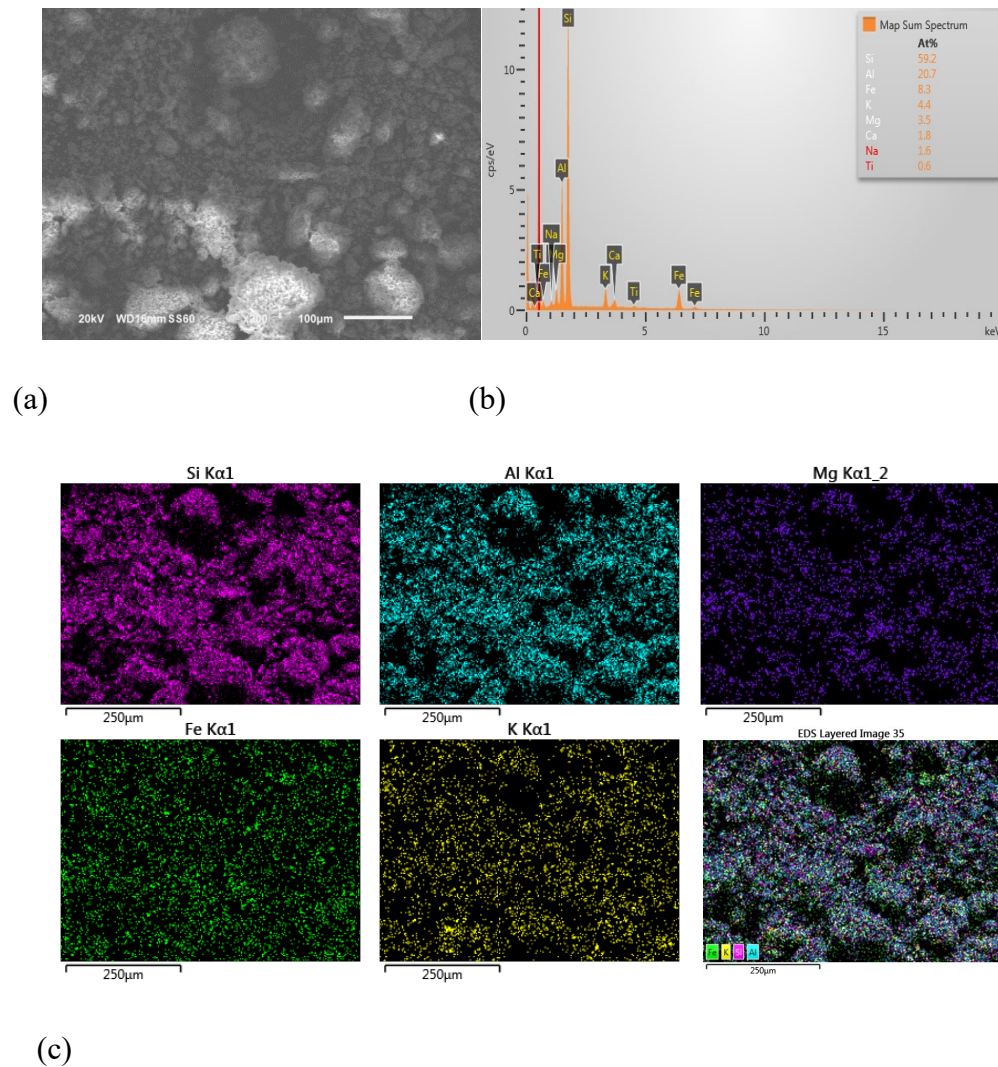
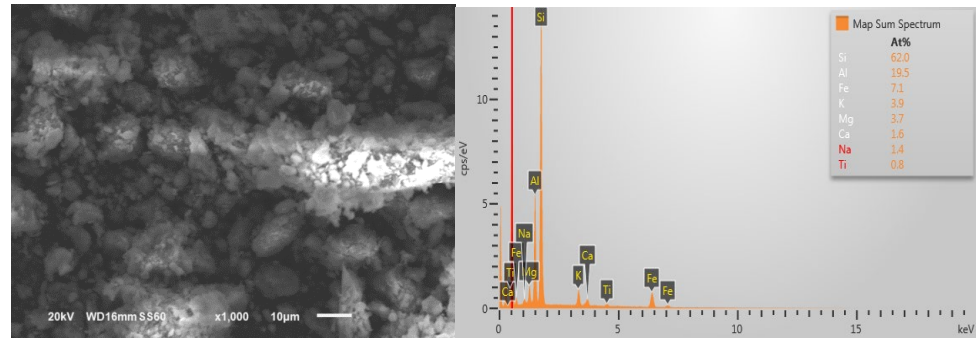


Figure 3. 52 Ladik clay microstructure and elemental analysis; (a) microstructure, (b) element ratios and (c) EDS mapping (Si, Al, Mg, Fe, K and layered map)

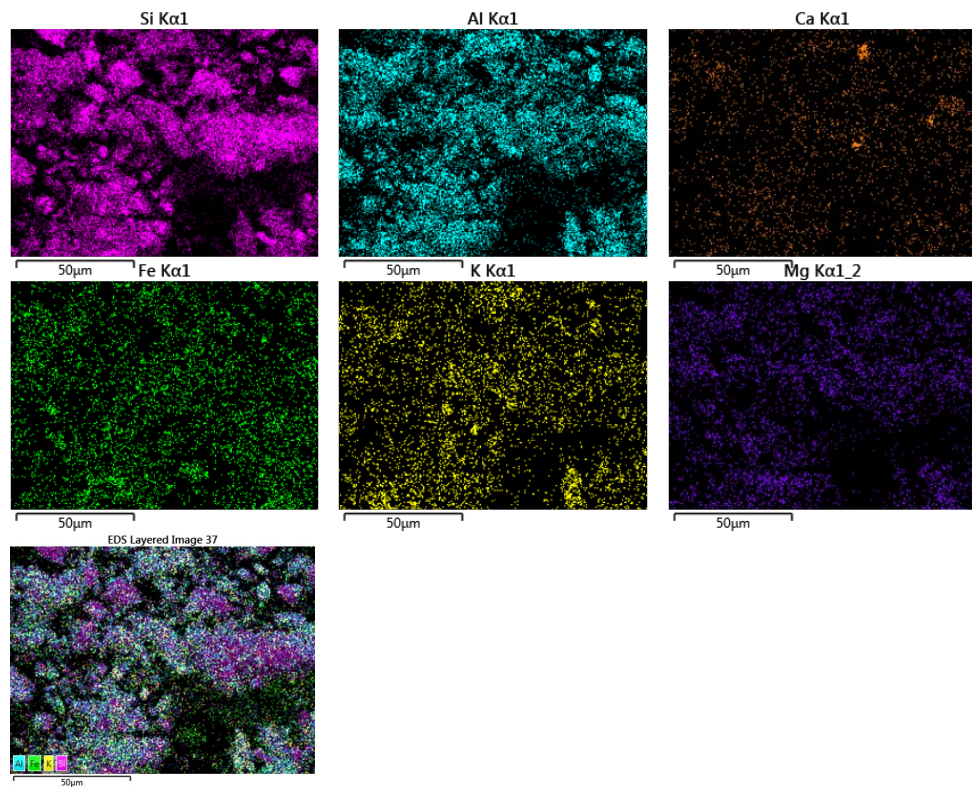
Figure 3.53 shows the Ladik sample at higher magnification. Although the microstructure shows layers at some points, the amorphous phase is also present. By evaluation of the elemental maps, it shows that the elements of Al and Si generally overlap, but Si stands alone

in some regions. As it is understood from the Ca map, calcite is present in very small amounts. It is seen that the element distribution in the layered map is balanced.



(a)

(b)



(c)

Figure 3. 53 Ladik clay microstructure and elemental analysis; (a) microstructure, (b) element ratios and (c) EDS mapping (Si, Al, Ca, Fe, K, Mg and layered map)

3.3. Evaluation of Calcined Schists (Heat-treated and activated Powders)

In this section, thermal activation and the composite pozzolanic cement paste compressive strength and behavior were evaluated and the results were shared. In the following parts, microstructure and phase alteration of heat-treated samples were studied. The results of thermal and conductivity tests were also shared. In the composite cement paste samples, hydration and pozzolanic reactions prepare the strength providing product and the compressive strength was measured and reported.

3.3.1 Microstructure and Composition Analysis (SEM-EDS)

The clay and schist powders samples were subjected to heat treatment in order to activate. Considering the mass loss calculated from TGA analysis and based on the method that is described in chapter 1, 30%, 50% and 80% of total mass loss temperatures were found and heat treatment was applied at these associated temperatures. In this section, the microstructures of 80% heat treated powder samples are compared with untreated powder samples. In this way, the changes in the microstructure and level of activation were observed.

In Figure 3.54 and Figure 3.55, the Kovukdere powder sample microstructure is shown in two different condition, (a) before heat treatment and (b) after heat treatment in various magnifications. By comparing the micrographs, changes resulting from heat treatment can be observed. The morphology of the samples resulted in changes in heating, resulting in rougher and lacy phases. Some of these structures are marked with yellow arrows in micrographs. The small size of the foliar clay particles in the background has been reduced in size in jagged form. The comparison of the shapes of the heat treated and untreated samples confirms the activation in the Kovukdere sample.

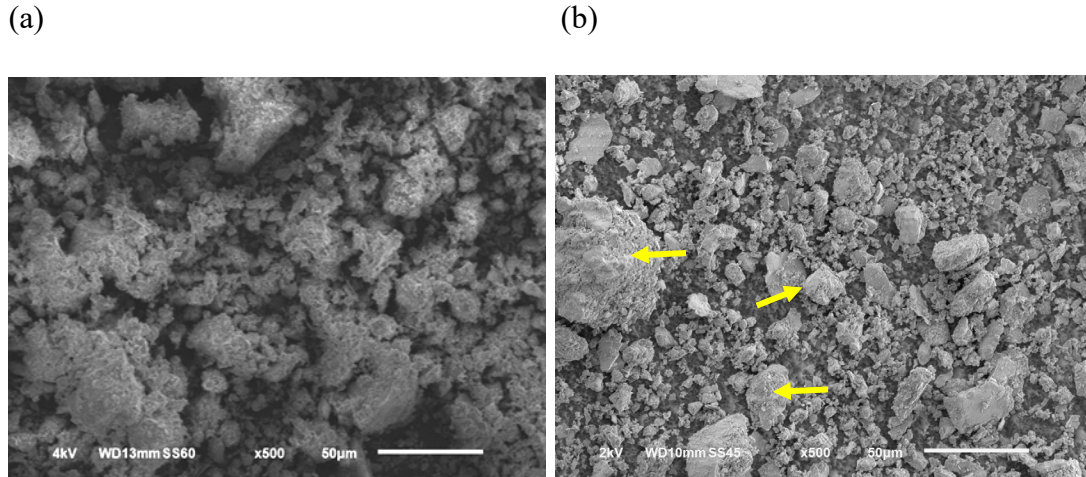


Figure 3. 54 SEM image of Kovukdere powder, (a) not heat treated (virgin) and (b) heat treated up to temperature associated to 80% of total weight loss (500X)

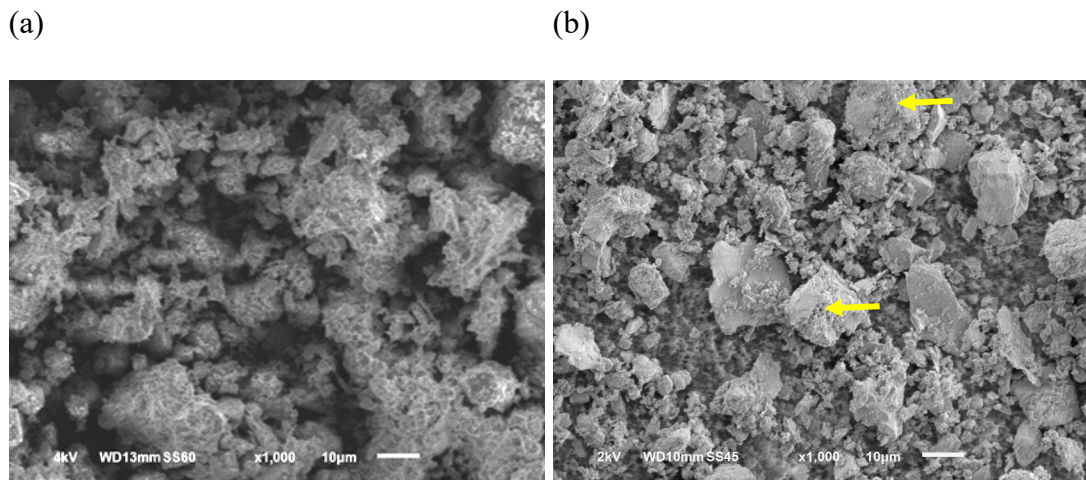


Figure 3. 55 SEM image of Kovukdere powder, (a) not heat treated (virgin) and (b) heat treated up to temperature associated to 80% of total weight loss (1000X)

Figure 3.56 shows the chemical elemental mapping of 80% heat treated Kovukdere powder sample due to the EDS analysis. In the lower part, each of the different elements is shown separately, and in the upper right, the map of the elements is shown on top of each other (integrated map). The silicon-only regions show the quartz phase, the silicon and aluminum co-regions show the clay type phases, and the calcium parts mainly calcite phase. Compared to the elemental analysis of the virgin samples shown in the previous section, there was little

change in the overall phase distribution. Decrease in the quantity and size of calcite particles is observed.

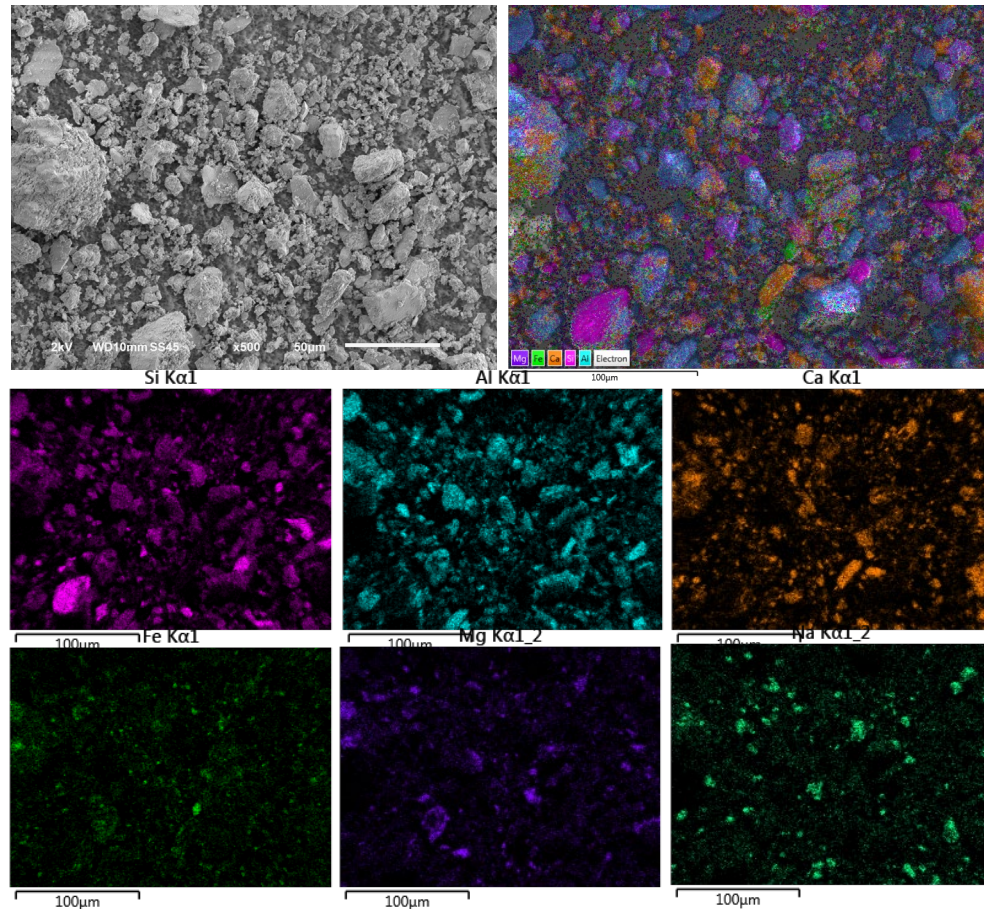
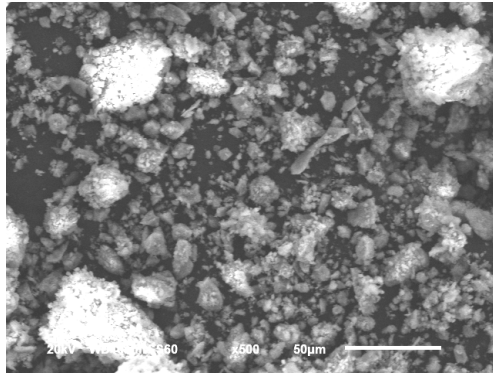


Figure 3. 56 Heat-treated Kovukdere schist powder up 80% of total weight loss, EDS elemental mapping

Figures 3.57 and 3.58 show the microstructure of Tastepe schist material (a) before heat treatment and (b) after 80% heat treatment. Although heat treatment causes decomposition, this change is not very significant. The large and solid particles have not undergone much modification as a result of heat treatment as it is appeared in microstructure. Small particles in the background give the impression of being decomposed.

(a)



(b)

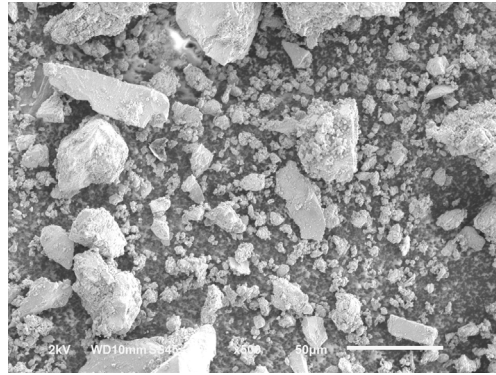
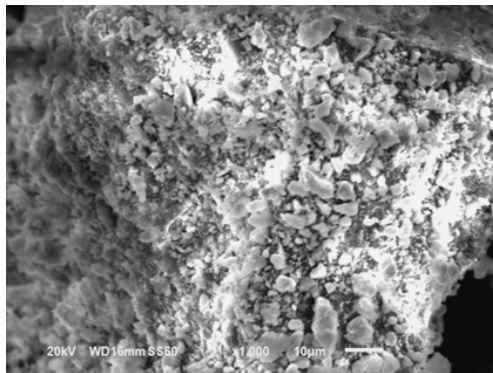


Figure 3. 57 SEM image of Tastepe powder, (a) not heat treated (virgin) and (b) heat treated up to temperature associated to 80% of total weight loss (500X)

(a)



(b)

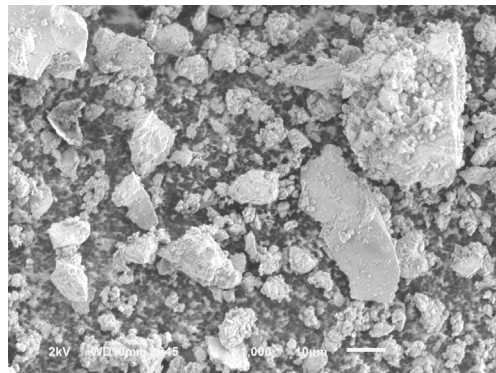


Figure 3. 58 SEM image of Tastepe powder, (a) not heat treated (virgin) and (b) heat treated up to temperature associated to 80% of total weight loss (1000X)

Elemental analysis of Tastepe sample after heat treatment is shown in Figure 3.59 as EDS mapping. The analysis shows that the calcite phase is reduced due to the decomposition. However, the decomposed calcite particles are still present in the matrix and the orange elemental map of calcium shows this. The particle identified by the yellow arrow comprises silicon, aluminum and sodium and is the sodium aluminosilicate phase. Quartz particles are clearly visible on the map with a light purple color.

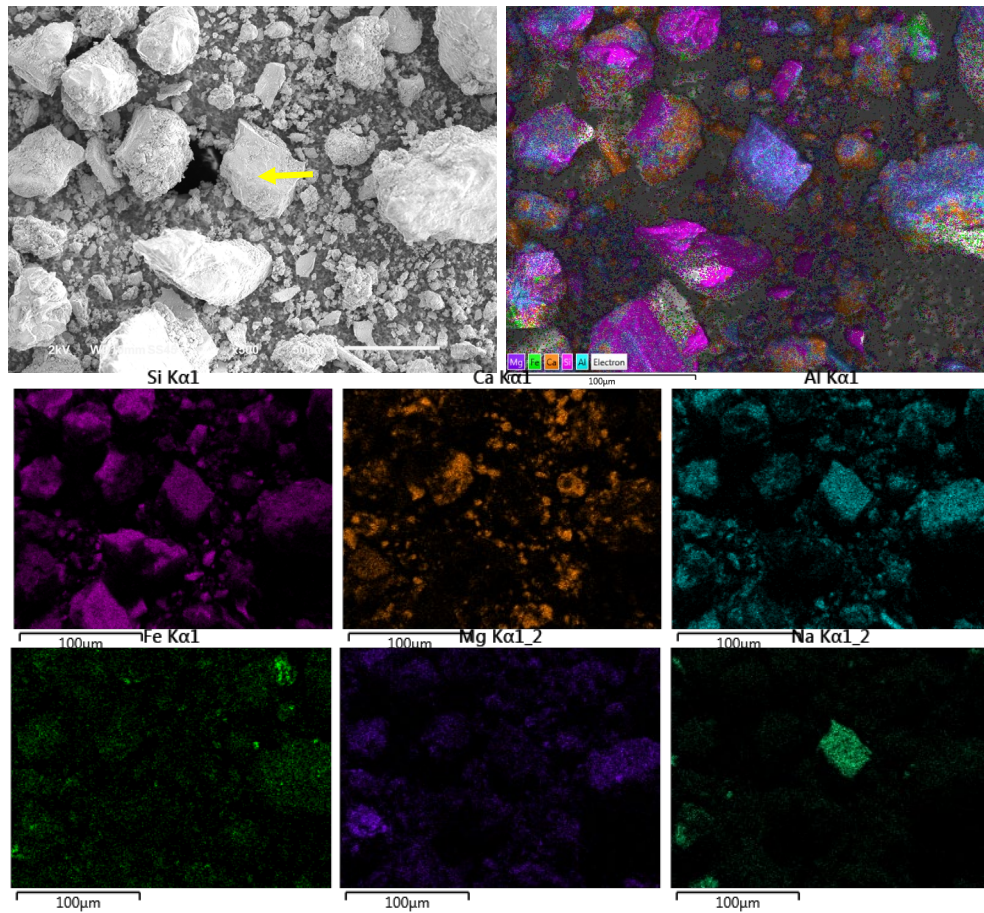
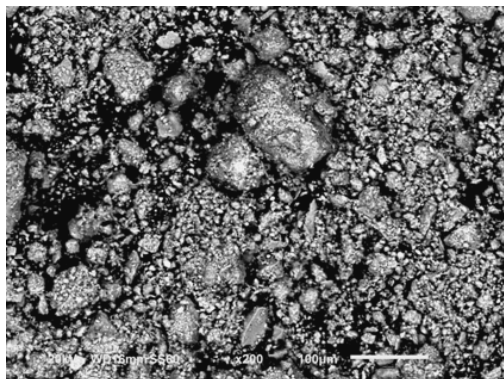


Figure 3. 59 Heat-treated Tastepe schist powder up 80% of total weight loss, EDS elemental mapping

The microstructure of ladik schist powder is illustrated in Figure 3.60 and Figure 3.61 (a) before and (b) after heat treatment. By looking at the 80% heat treated sample, it appears on the micrograph that the magnitude of decomposition is not too high. As it is shown in Figure 3.62 (elemental analysis), the distribution of the silicon and aluminum element can be seen all over the microstructure, indicating that the aluminosilicate phases are present. Although quartz particles are present, they are smaller in size than other samples. The elemental map confirms that there is no calcite in this sample. Figure 3.60 illustrate some of the amorphous particles as indicated by yellow arrows.

(a)



(b)

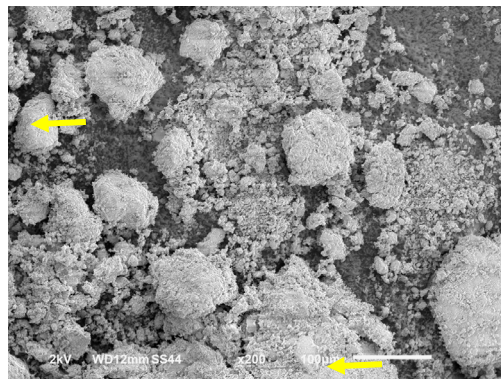
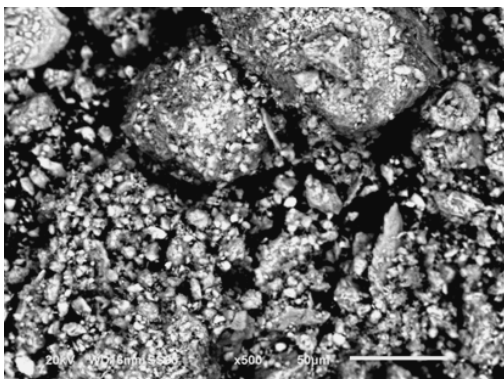


Figure 3. 60 SEM image of Ladik powder, (a) not heat treated (virgin) and (b) heat treated up to temperature associated to 80% of total weight loss (200X)

(a)



(b)

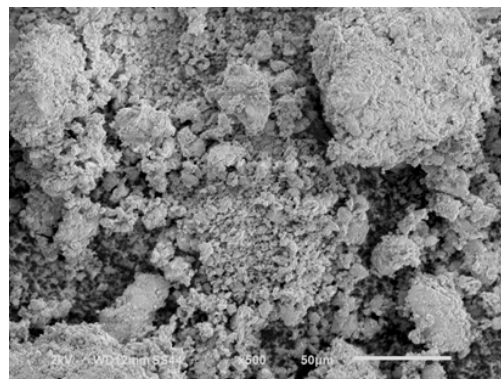


Figure 3. 61 SEM image of Ladik powder, (a) not heat treated (virgin) and (b) heat treated up to temperature associated to 80% of total weight loss (500X)

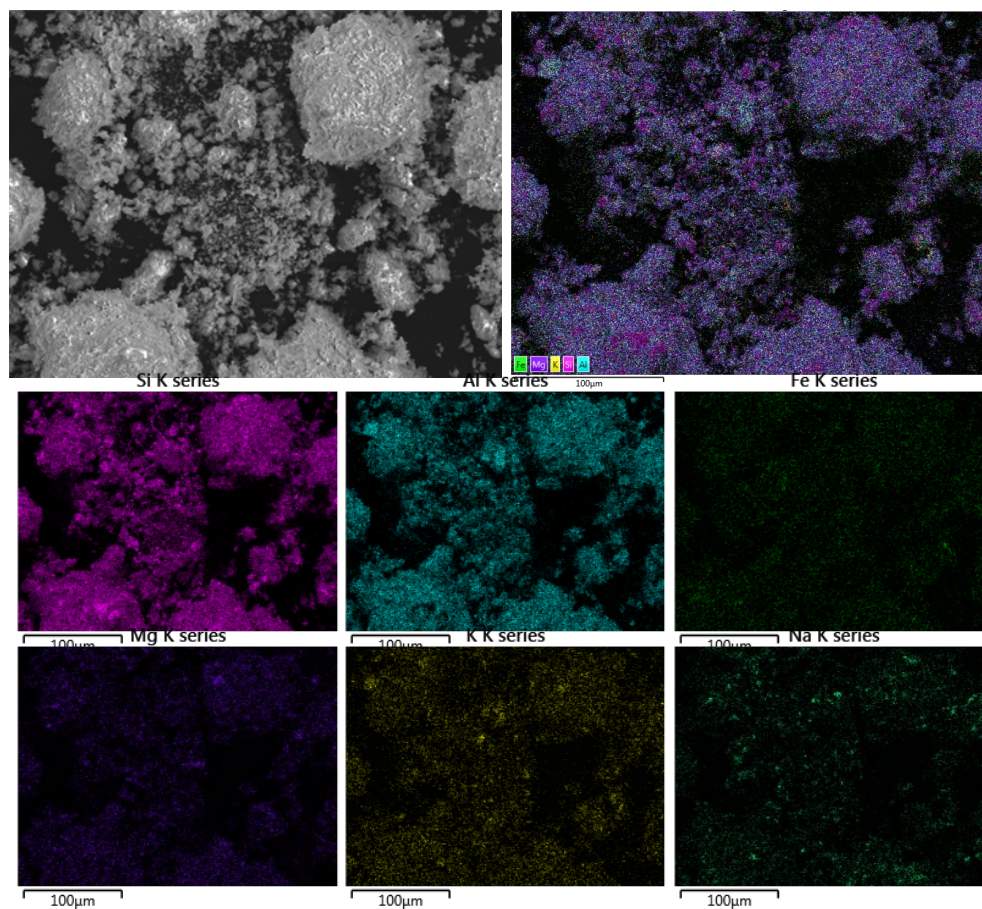
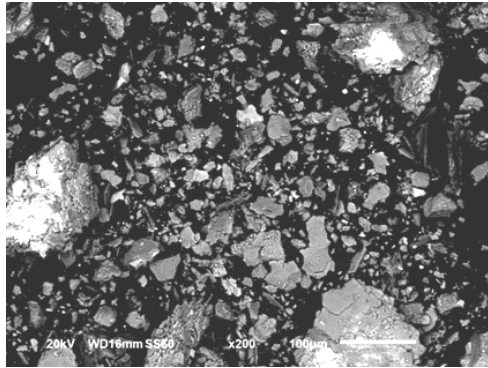


Figure 3. 62 Heat-treated Ladik schist powder up 80% of total weight loss, EDS elemental mapping

Figures 3.63 and 3.64 show the microstructure of the Muratbey sample at two different magnifications (a) before and (b) after heat treatment. By comparing two pictures, the particle size decreases after heat treatment. This change indicates that activation was effective, and decomposition occurred. In addition, the “jagged shape edges” or “ruffled edged” of the particles indicate that the heat treatment decomposed proper portion of sample.

(a)



(b)

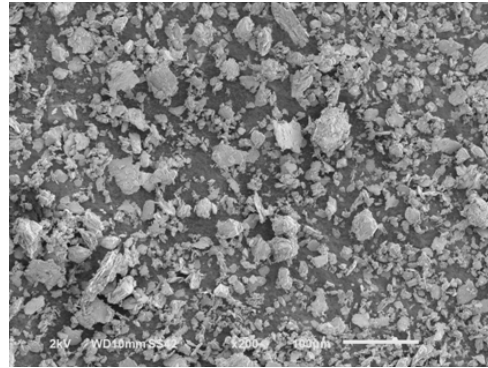
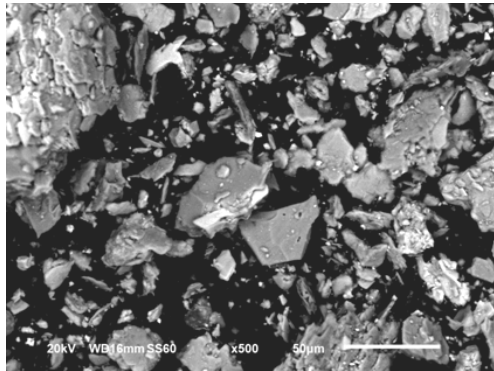


Figure 3. 63 SEM image of Muratbey powder, (a) not heat treated (virgin) and (b) heat treated up to temperature associated to 80% of total weight loss (200X)

(a)



(b)

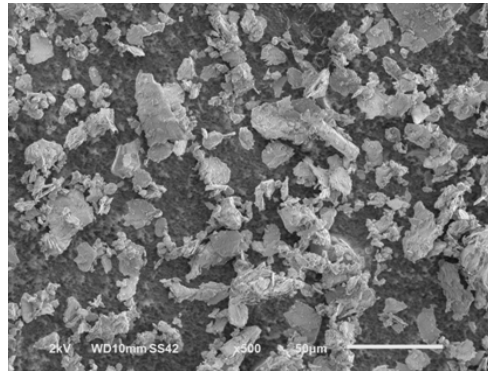


Figure 3. 64 SEM image of Muratbey powder, (a) not heat treated (virgin) and (b) heat treated up to temperature associated to 80% of total weight loss (500X)

Figure 3.65 shows the elemental maps of the Muratbey sample after heat treatment. It is possible to distinguish between quartz and aluminosilicate phases. The sample contains only trace amounts of calcium. The absence of calcite in the Muratbey sample contrasts with the Kovukdere sample.

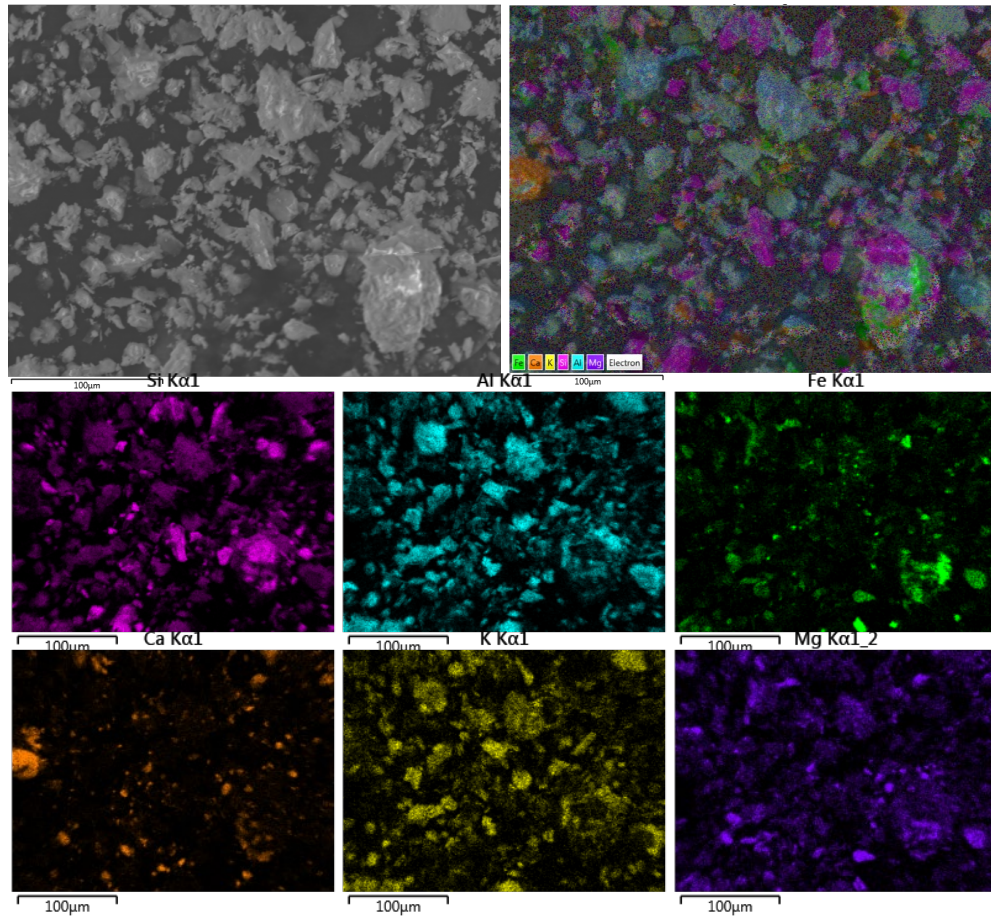


Figure 3.65 Heat-treated Muratbey schist powder up 80% of total weight loss, EDS elemental mapping

The Bozalan sample (a) before and (b) after heat treatment are visualized by SEM micrograph are shown in Figures 3.66 and 3.67. The microstructure of the heat-treated sample represents the effect on the particle size due to the heat treatment, causing smaller particles to form. Although this image indicates that Bozalan may be activatable by calcination, but there is no other evidence of decomposition in the sample. The absence of calcite in both Muratbey and Bozalan samples may cause them to be ineffective in cement hydration reactions.

(a)

(b)

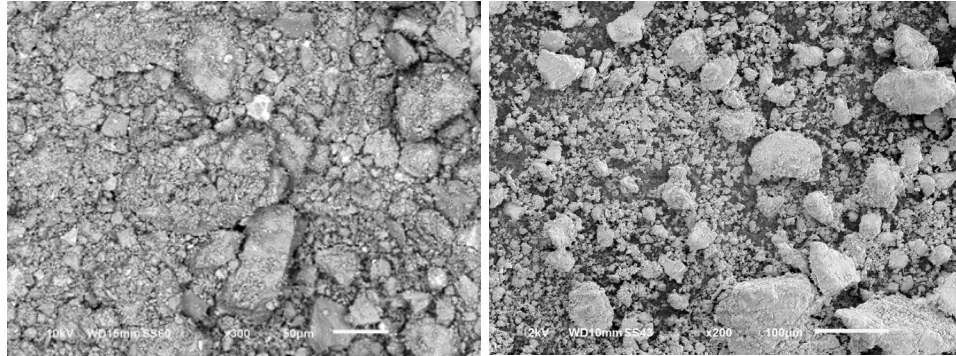


Figure 3. 66 SEM image of Bozalan powder, (a) not heat treated (virgin) and (b) heat treated up to temperature associated to 80% of total weight loss (200X)

(a)

(b)

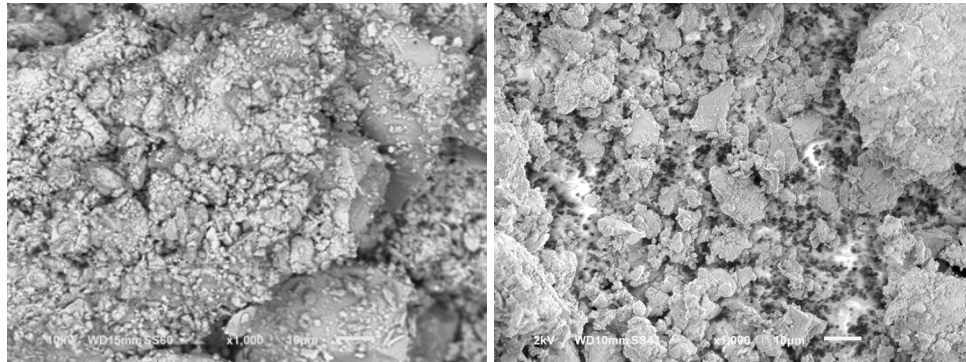


Figure 3. 67 SEM image of Bozalan powder, (a) not heat treated (virgin) and (b) heat treated up to temperature associated to 80% of total weight loss (1000X)

Figure 3.68 shows the chemical EDS mapping of the Bozalan sample after heat treatment. As it appears in the maps, the microstructure is mostly composed of quartz and aluminosilicate (crystal and amorphous) phases and trace amounts of calcite are also present.

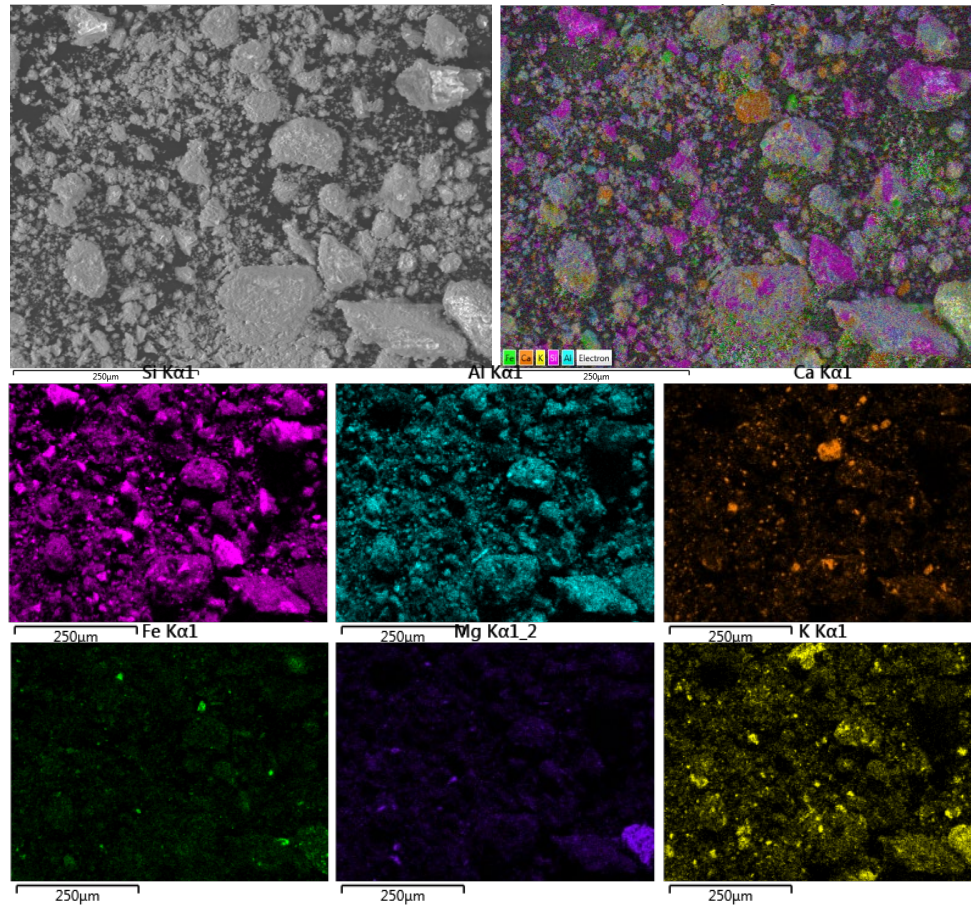


Figure 3. 68 Heat-treated Bozalan schist powder up 80% of total weight loss, EDS elemental mapping

Figure 3.69 compares the (a) untreated and (b) heat-treated microstructures of the Camlica powder sample. The particles began to decompose after heat treatment and show deformation. This difference is an indication that they have become more reactive. However, when compared with the microstructures of the other samples, the amount of decomposition in the Camlica sample seems to be less.

(a)

(b)

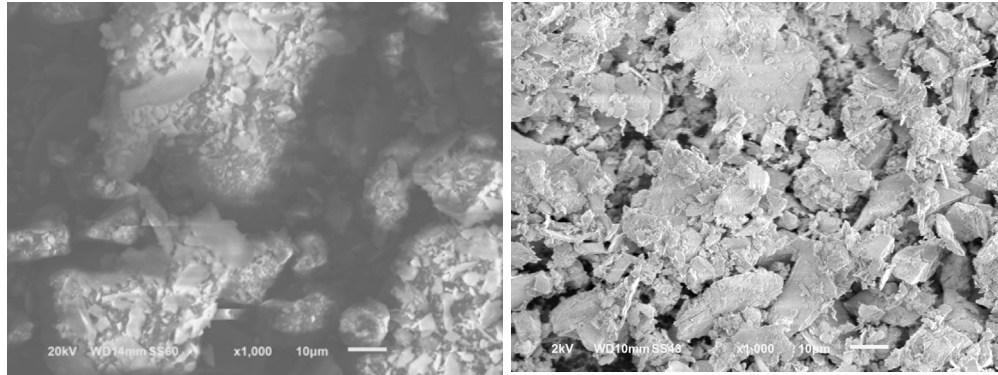


Figure 3. 69 SEM image of Camlica powder, (a) not heat treated (virgin) and (b) heat treated up to temperature associated to 80% of total weight loss (1000X)

EDS chemical maps are also shown in Figure 3.70 for Camlica sample. In addition to quartz and aluminosilicate particles, the amount of calcite (whether decomposed or not) appears to be high. Iron oxide is also present in trace amounts.

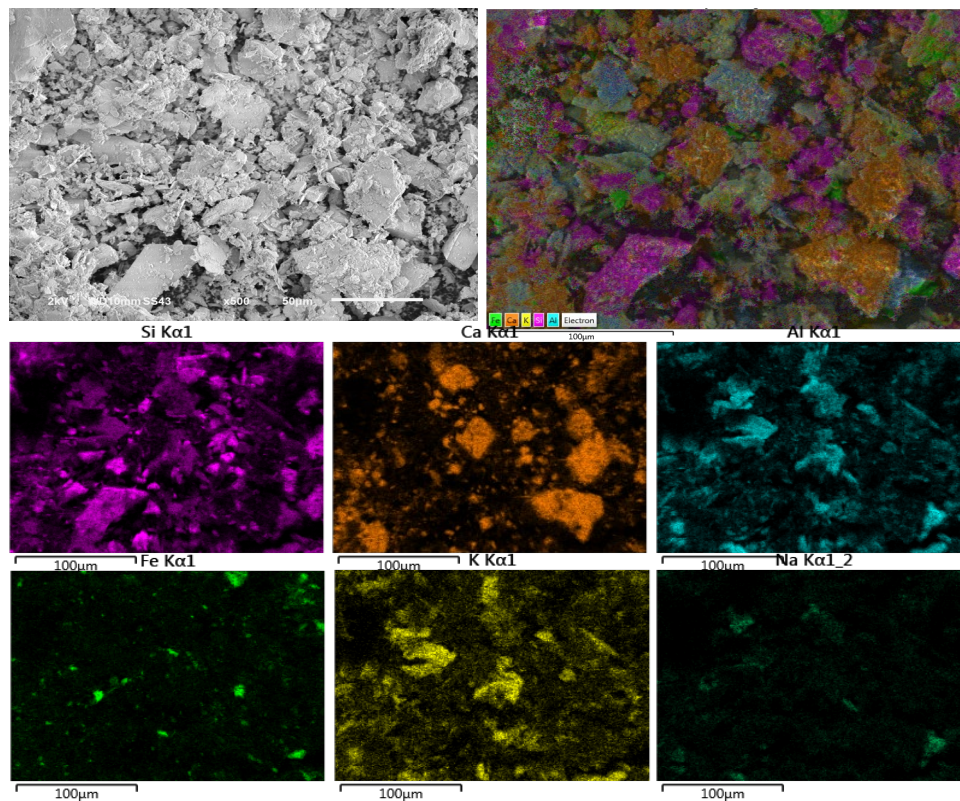
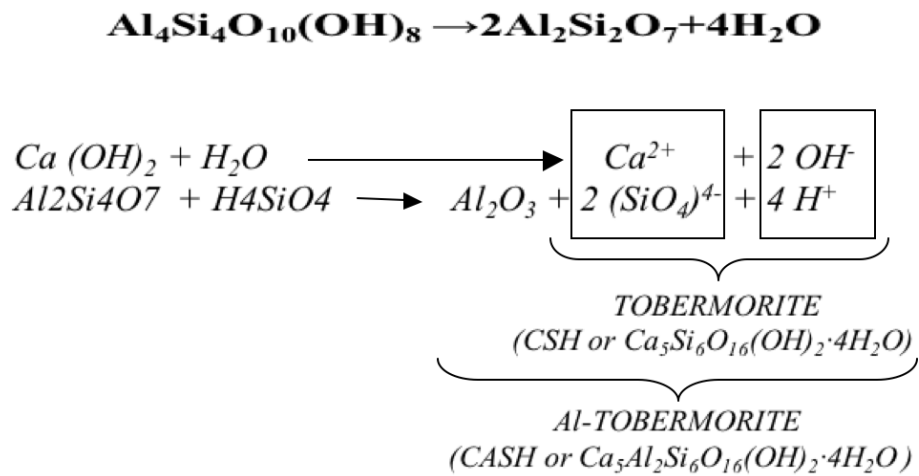


Figure 3. 70 Heat-treated Camlica schist powder up 80% of total weight loss, EDS elemental mapping

3.3.2 Pozzolanic Reactions and Heat Treatments

Different experiments were conducted to evaluate the pozzolanic reactivity of the raw materials and the possible potential of cement substitution. To remind the pozzolanic behavior of reactive minerals, chemical reactions associated with it can be reviewed. For example, in the case of Kaolinite, the main reaction is the reactions of CH with water, which were introduced during hydration of cement with meta-kaolinite. These reactions result in the binding phases of the so-called CSH and CASH.



In all schist-type raw materials, the primary evaluation of all samples reveals that some of them are reliable candidates for partial cement substitution. As it is mentioned before, specific method was used to activate the raw materials by heat treatment. Considering the decomposition temperature of each, these ranges are associated with mass loss and divided into 3 parts according to the percentage of mass loss. These temperature points are those where the mass loss is 30%, 50% and 80% of the total mass loss between 350-850°C. After defining the calcination temperature, the raw materials taken in equal amounts are heated up to these temperatures. The aim of this method is to compare the activation rate and the results of the effect of partial degradation of calcined clay behavior. Therefore, the same characterization methods have been used to evaluate the heat-treated materials. Table 3.23 shows raw material decomposition range and calculated temperatures for heat treatment of clays.

Table 3. 23 Decomposition temperatures range and mass loss amounts of 30%, 50% and 80% for all samples

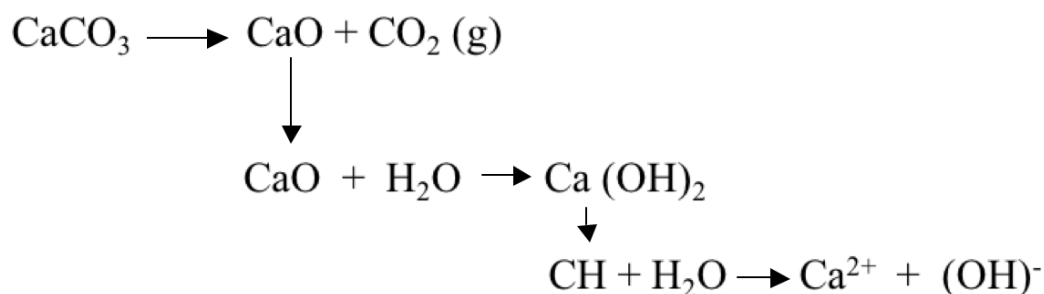
Sample	%30 WL _T Temp. (°C)	%50 WL _T Temp. (°C)	%80 WL _T Temp. (°C)	Start Temp. (°C)	End Temp.(°C)	WL _T (%)
BOZALAN	620	710	750	400	775	5.33
CAMLICA	745	770	795	600	820	10.2
TASTEPE	765	810	845	450	875	11.25
KOVUKDERE	725	785	830	450	870	16.25
MURATBEY	575	710	760	450	800	9.43
LADIK	480	520	600	400	700	2.63
KAOLINITE	530	560	620	400	710	7.55

3.3.3 Phase Analysis, Conductivity Measurements and TGA

This section includes X-ray diffraction (XRD), thermogravimetric analysis (TGA) and conductivity measurements of the activated materials. The aim of the study is to compare the compressive strength of composite cement paste specimens prepared by replacing 30% of cement with calcined schist material after 28 days of hydration time with specimens prepared with 100% cement. The blended cement paste compressive strength is acceptable with the maximum strength drop up to 10% of pure cement strength. Thus, cube samples are prepared for the compression test will demonstrate the strength of the composition. These samples were prepared with a water to solid ratio of 0.5. The blends contained 70% Cement (700 g) and 30% activated schist material (300 g). Furthermore, a 100% pure cement sample was prepared to be the basis for comparison with composite clay cement blend samples. The mechanical strength of all samples was tested after 2, 7, 28, 50 and 90 days of hydration. The substitute calcined schist was heat treated to the temperature associated to (1) 30%, (2) 50% and (3) 80% of total weight loss.

Before going through the results, two important parts should be considered. The first part is the method used for heat treatment of the samples. The appropriate amount of powder sample should be placed in the crucible and placed in the oven and heated to the specified

temperature. The furnace temperature should then remain constant for two hours to ensure that heat is transferred to all parts of the sample. The sample must then be removed from the furnace and allowed to cool in air. It should be noted that prolonged heating may cause dead-burnt of the powder. The purpose of allowing the sample to quench in air is to maintain the dissociated structures formed during calcination. Excessive heat treatment may result in sintering reactions between activated bonds and aluminosilicate layers. The second important point concerns the conductivity measurements in the clay samples taken, which is not a good indicator for most of the received samples. According to the X-ray diffraction analysis, most of the clay samples contain calcium carbonate which may affect conductivity measurements. The decrease in conductivity showed reactivity due to pozzolanic reaction, whereas the behavior in calcined calcium carbonates was reversed, as follows:



Considering all these facts, the results were discussed separately, considering all the mineral phases in the samples.

3.3.3.1 Kaolinite

Kaolinite is a simple structure clay and de-hydroxylation of kaolinite forms a transition phase called meta-kaolin, which is formed by the breakdown or partial breakdown of the crystal lattice structure. Meta-kaolin is a semi-stable phase and, as it is already used in many studies,

is the benchmark of this study. Conductivity measurement results for untreated and heat treated or activated kaolinite powder are as follows:

Table 3. 24 Pozzolanicity of virgin and heat-treated (to temperature associated to 30, 50 and 80% of total weight loss) Kaolinite powder (conductivity variation)

Pozzolanicity (Conductivity Variation)				
Sample	Virgin Powder	%30 of WL _T	%50 of WL _T	%80 of WL _T
Kaolinite	1,11 & 1,15	1,32 & 1,41	1,63 & 1,7	1,94 & 1,98

Heat treatment influenced kaolinite reactivity. Further decomposition of the kaolinite and increasing efficiency for the pozzolanic reaction by increasing the processing temperature is also shown in Table 3.24. In order to get an idea of the extent of decomposition of the phases, the weight percentages of the quartz phase (inert), clay and carbonate (QCC) phases were calculated by the Rietveld method. The results are shown in Table 3.25:

Table 3. 25 QCC amounts (% by weight) of kaolinite (virgin and heat-treated)

QCC (QUARTZ , CLAY, CARBONATE)					
Sample	Chemical Phase	Phase Amount (wt%)			
		Virgin Powder	%30 of WLT	%50 of WLT	%80 of WLT
Kaolinite	Quartz	44	70	89	92
	Clay	56	30	11	8
	Carbonate	—	—	—	—
	Others	—	—	—	—

Table 3.25 shows the amount of clay that decreases with increasing temperature. It is evident and noted here that the amount of quartz as an inert phase will not change with the increase of temperature and must remain constant. However, the TOPAS software used in this study calculates the total phase from 100%, and since there are only two phases in this powder, the other non-decomposable crystal phase appears to be increasing since the decomposition /

degradation fraction will fall from the calculations. In the case of kaolinite, the decomposition of the clay material is determined by the results of the x-ray diffraction analysis shown in Figure 3.71.

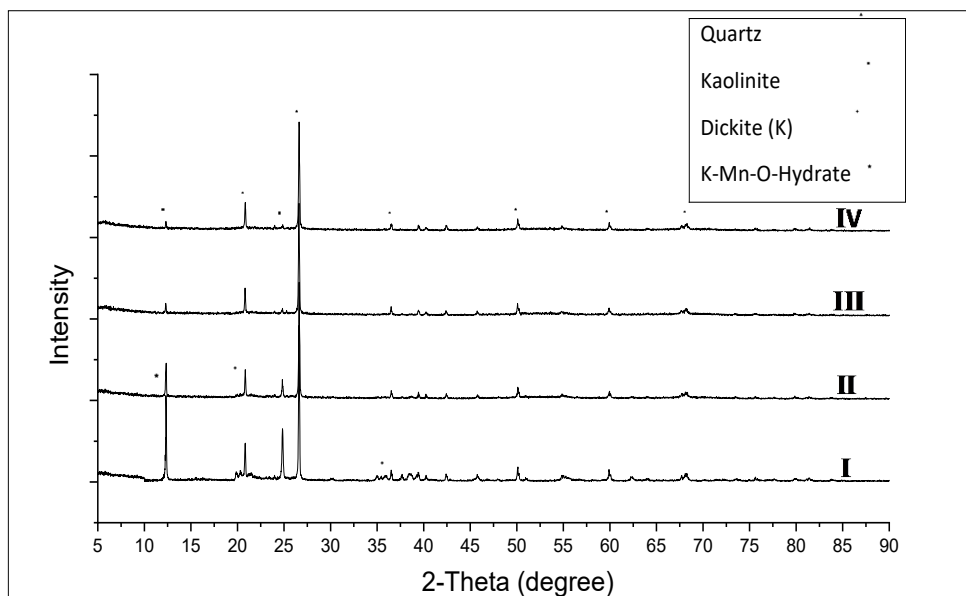


Figure 3. 71 Kaolinite x-ray diffractogram for (I) Virgin, (II) heat-treated up to 30% of WL_T, (III) heat-treated up to 50% of WL_T and (IV) heat-treated up to 80% of WL_T

XRD analysis results show the de-hydroxylation of Kaolinite, $\text{Al}_2\text{Si}_2\text{O}_5(\text{OH})_4$, and Dickite, $\text{Al}_2\text{Si}_2\text{O}_5(\text{OH})_4$ (another polymorph of Kaolinite). In addition, $\text{K}_{0.27}\text{MnO}_2(\text{H}_2\text{O})_{0.54}$ (K-Mn-O-Hydrate), another clay-type material, was investigated in partial decomposition with heat increase in each step of treatment. The TGA results include the comparison of heat-treated and untreated kaolinite powder at different temperatures according to the amount of weight loss. This TGA spectrum can be seen in Figure 3.72.

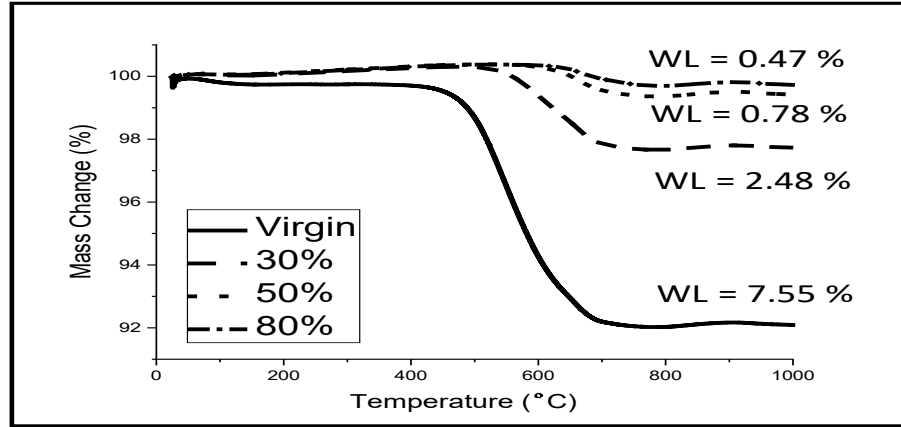


Figure 3. 72 Thermogravimetric analysis of virgin and heat-treated Kaolinite (heat-treated up to temperature associated to 30, 50, and 80% of total weight loss)

3.3.3.2 Bozalan Schist

Characterization of the decomposed material that is subjected to heat treatment and untreated, was carried out. By considering the conductivity values of Bozalan virgin schist, Bozalan's strength behavior does not meet the expectation of pozzolanic behavior estimated by electrical conductivity measurements. In this sample, the misleading effect of calcium carbonate on electrical conductivity measurements appears. Table 3.26 shows the conductivity variation due to heat treatment.

Table 3. 26 Pozzolanicity of virgin and heat-treated (to temperature associated to 30, 50 and 80% of total weight loss) Bozalan powder (conductivity variation)

Pozzolanicity (Conductivity Variation)				
Sample	Virgin Powder	%30 of WL _T	%50 of WL _T	%80 of WL _T
Bozalan	0,55 & 0,58	0,69 & 0,73	0,84 & 0,87	1,02 & 1,08

This table shows the pozzolanicity of Bozalan. The values of Bozalan sample are lower than those of some other samples. Although the increase in temperature increases the pozzolanicity of Bozalan, this feature does not show up in the measurements of electrical

conductivity due to the carbonate phase and its polymorph. However, by observing the compressive strength of the blended cement paste sample, it is revealed that Bozalan schist is a reactive sample. The QCC amounts in this sample is also shown in Table 3.27. These ratios are calculated by the Rietveld method.

Table 3. 27 QCC amounts (% by weight) of Bozalan (virgin and heat-treated)

		QCC (QUARTZ , CLAY, CARBONATE)			
Sample	Chemical Phase	Phase Amount (wt%)			
		Virgin Powder	%30 of WLT	%50 of WLT	%80 of WLT
Bozalan	Quartz	52	37	33	39
	Clay	40	3	—	—
	Carbonate	8	5	4	1
	Others	— (Anorthite)	55	63	60

Based on Figure 3.72, XRD analysis shows that sodium-zeolite component was present in Bozalan powder. This phase may decompose and forms the Anorthite phase. This reaction also increased the amount of glassy material. It should also be noted again that the amount of quartz must be constant. In addition, it was observed that the carbonate phase decomposes with the same tendency as the increase in temperature. Figure 3.73 shows the change in the results of XRD analysis of the de-hydroxylated clay-type materials and carbonates subjected to different heat treatments based on angle-intensity size.

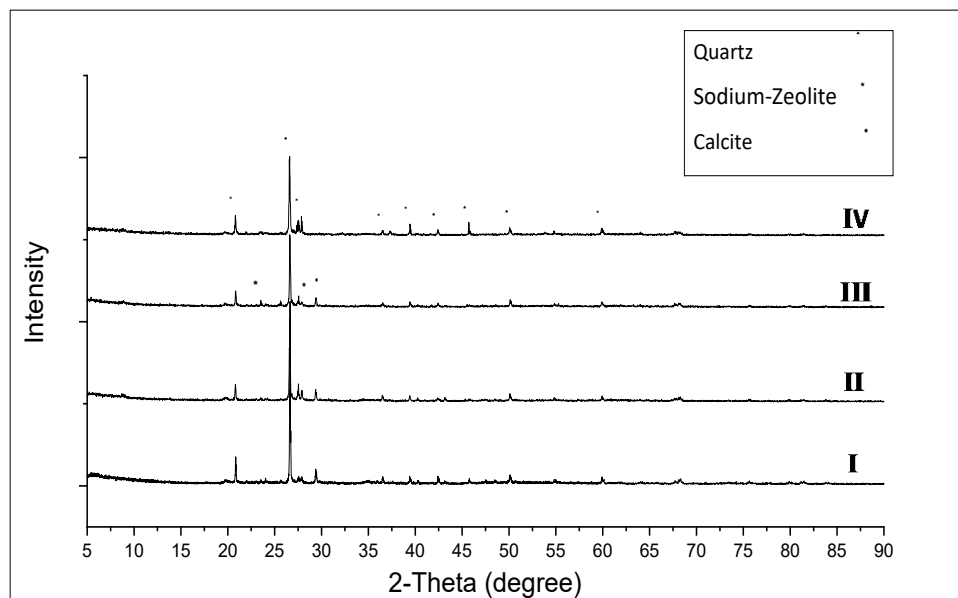


Figure 3. 73 Bozalan x-ray diffractogram for (I) Virgin, (II) heat-treated up to 30% of WL_T , (III) heat-treated up to 50% of WL_T and (IV) heat-treated up to 80% of WL_T

The Bozalan schist powders were composed of quartz, sodium-zeolite ($NaAlSi_2O_6 \cdot H_2O$) and calcite ($CaCO_3$). Zeolite and calcium carbonate have a chance to react with each other as they decompose to form anorthite. The reduction in the clay type phase can be observed in the spectrum. This dissociation is supported by the TGA results shown in Figure 3.74.

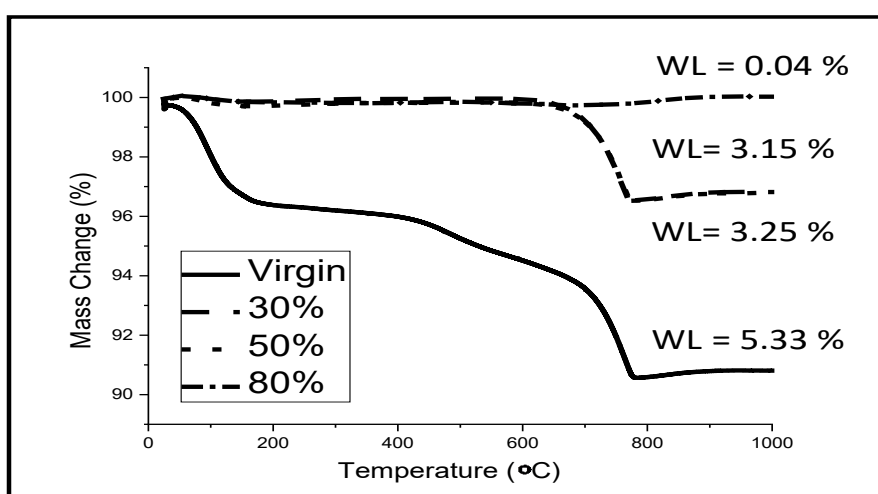


Figure 3. 74 Thermogravimetric analysis of virgin and heat-treated Bozalan (heat-treated up to temperature associated to 30, 50, and 80% of total weight loss)

3.3.3.3 Tastepe Schist

The conductivity values of Tastepe virgin powder did not show the potential of this powder sufficiently well for pozzolanic reactivity. Although, these values are much better than Ladik and Bozalan, but worse than Muratbey and Camlica. Only when looking at the pozzolanicity of the treated powders, this schist was not considered as a proper candidate. However, again in the case of Tastepe, the decrease in conductivity values (pozzolanicity) for the sample heat-treated up to 80% of mass loss shown in Table 3.28 results in the misleading effect of the carbonate phase on the conductivity measurements.

Table 3. 28 Pozzolanicity of virgin and heat-treated (to temperature associated to 30, 50 and 80% of total weight loss) Tastepe powder (conductivity variation)

Sample	Pozzolanicity (Conductivity Variation)			
	Virgin Powder	%30 of WL _T	%50 of WL _T	%80 of WL _T
Tastepe	0,99 & 1,11	1,06 & 1,08	1,1 & 1,12	0,89 & 0,97

According to the table above, pozzolanicity is reduced when heat treatment is carried out at higher temperature (80%). This is thought to be due to the decomposition of the carbonate phases because the amount of carbonate phase is known to affect pozzolanicity. The amount of QCC phases is shown in Table 3.29.

Table 3. 29 QCC amounts (% by weight) of Tastepe (virgin and heat-treated)

		QCC (QUARTZ , CLAY, CARBONATE)			
Sample	Chemical Phase	Phase Amount (%)			
		Virgin Powder	%30 of WL _T	%50 of WL _T	%80 of WL _T
Tastepe	Quartz	60	57	58	72
	Clay	–	–	–	–
	Carbonate	32	25	22	3
	Others	8 (Anorthite)	18	20	25

According to XRD results, there was almost no clay in this sample, or the amount was too small to be significant. The main phases of this sample are quartz, carbonate and anorthite, which is a glassy material as indicated. In this case, the high strength of Tastepe may be directly related to the anorthite and carbonate phases. In addition, Tastepe calcination occurs in higher temperature ranges due to the carbonate phase decomposition. The XRD spectrum shown in Figure 3.75 is intended to prove this idea.

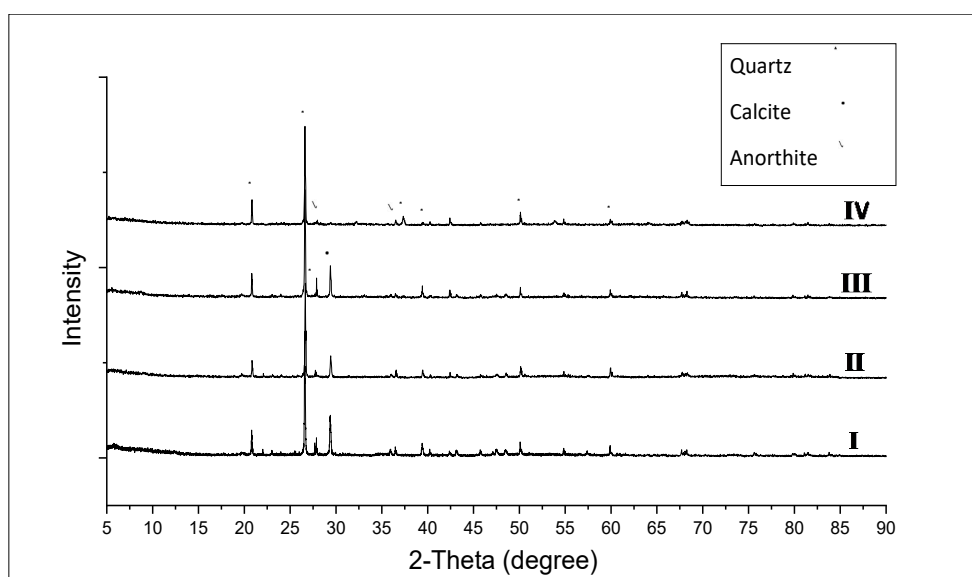


Figure 3. 75 Tastepe x-ray diffractogram for (I) Virgin, (II) heat-treated up to 30% of WL_T , (III) heat-treated up to 50% of WL_T and (IV) heat-treated up to 80% of WL_T

This spectrum shows the effect of increasing the heat treatment temperature on the carbonate phase. As it can be seen, the carbonate phase is lost when the temperature is increased. Tastepe contains calcite as carbonate phase. Another measurement in the TGA, represented the amount of decomposition of the phases in comparison with the virgin powder that is shown in Figure 3.76.

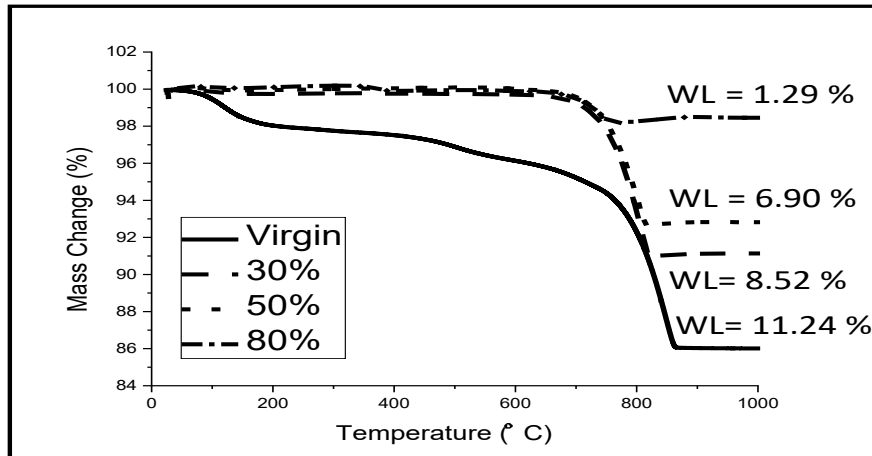


Figure 3. 76 Thermogravimetric analysis of virgin and heat-treated Tassepe (heat-treated up to temperature associated to 30, 50, and 80% of total weight loss)

3.3.3.4 Camlica Schist

Conductivity measurement results of Camlica as virgin and heat-treated material may show this material as one of the good pozzolans, but mechanical behavior of this sample did not confirm its pozzolanicity. The pozzolanicity of the raw and processed Camlica powder is shown in Table 3.30.

Table 3. 30 Pozzolanicity of virgin and heat-treated (to temperature associated to 30, 50 and 80% of total weight loss) Camlica powder (conductivity variation)

Pozzolanicity (Conductivity Variation)				
Sample	Virgin Powder	%30 of WL _T	%50 of WL _T	%80 of WL _T
Camlica	1,05 & 1,23	1,19 & 1,25	1,18 & 1,33	1,05 & 1,12

As it can be seen in Table 3.31, the virgin and heat-treated Camlica powder is thought to be in the variable pozzolanicity range. Moreover, a significant amount of carbonate phases resulted in conductivity reduction at higher temperatures. The amounts of QCC phases are also shown in Table 3.29.

Table 3. 31 QCC amounts (% by weight) of Camlica (virgin and heat-treated)

		QCC (QUARTZ , CLAY, CARBONATE)			
Sample	Chemical Phase	Phase Amount (%)			
		Virgin Powder	%30 of WL _T	%50 of WL _T	%80 of WL _T
Camlica	Quartz	40	24	23	19
	Clay	15	7	6	5
	Carbonate	14	7	6	5
	Others	31 (Kyanite)	62	65	71

The QCC table shows the reduction in clay phase and carbonate. Camlica powder contains several different phases as indicated in the XRD results in Figure 3.77. Besides, according to Table 3.31, an important portion of Camlica consists of kyanite (Al₂SiO₅).

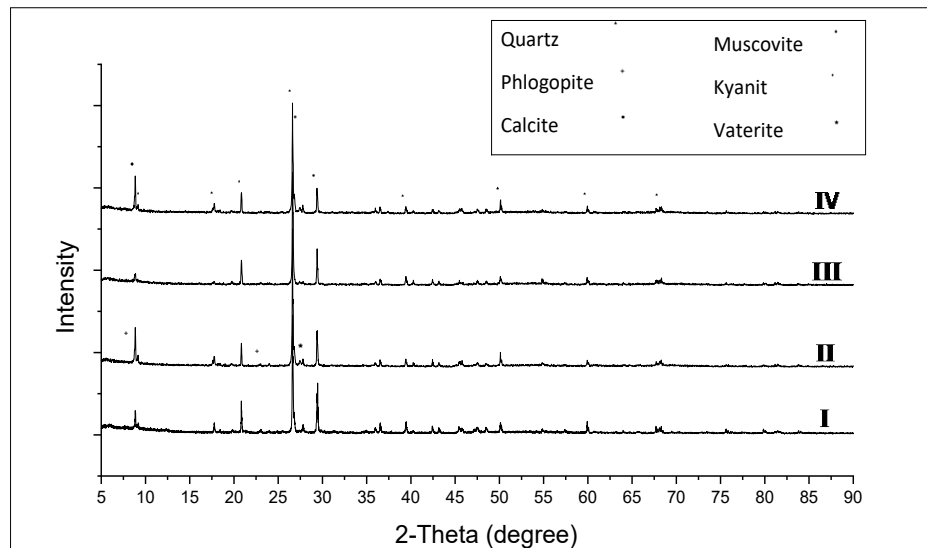


Figure 3. 77 Tastepe x-ray diffractogram for (I) Virgin, (II) heat-treated up to 30% of WL_T, (III) heat-treated up to 50% of WL_T and (IV) heat-treated up to 80% of WL_T

As it can be seen in Figure 3.77, the clay-type phases Phlogopite, $\text{KMg}_3(\text{Si}_3\text{Al})\text{O}_{10}(\text{OH})_2$, and Muscovite, $\text{KAl}_2(\text{Si}_3\text{Al})\text{O}_{10}(\text{OH}, \text{F})_2$, are present in the structure. Carbonates are in

calcite and vaterite polymorphs. Moreover, Kyanite, Al_2SiO_5 , a widely available aluminosilicate, forms portion of this powder. Camlica powder may seem remarkable in terms of reactivity, but compressive strength tests show less strength behavior than expected. This may be due to the low amount of clay and carbonate compared to the inert phases. For example, kyanite decomposition occurs at elevated temperature (1150°C). The TGA results show the decomposition of reactive phases as it can be seen in Figure 3.78.

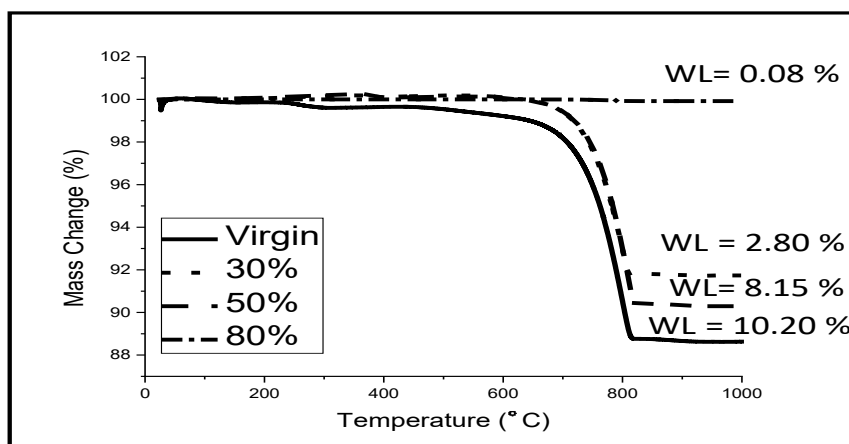


Figure 3. 78 Thermogravimetric analysis of virgin and heat-treated Camlica (heat-treated up to temperature associated to 30, 50, and 80% of total weight loss)

3.3.3.5 Kovukdere Schist

According to primary characterization tests and conductivity measurements, virgin Kovukdere is considered as the best candidate when it is looked at its reactivity. This is also evidenced by the results obtained from the treated powder. Table 3.32 shows the conductivity of Kovukdere virgin powder compared to heat-treated one.

Table 3. 32 Pozzolanicity of virgin and heat-treated (to temperature associated to 30, 50 and 80% of total weight loss) Kovukdere powder (conductivity variation)

Pozzolanicity (Conductivity Variation)				
Sample	Virgin Powder	%30 of WL _T	%50 of WL _T	%80 of WL _T
Kovukdere	1,48 & 1,58	1,49 & 1,53	1,66 & 1,72	1,34 & 1,41

As it is told, Kovukdere virgin powder can be considered as good pozzolan and this pozzolanicity increases as the processing temperature is increased. However, when the temperature is high enough to decompose almost all carbonates, it reduces the electrical conductivity by adverse effect. Table 3.33 shows the amount of QCC phases.

Table 3. 33 QCC amounts (% by weight) of Kovukdere (virgin and heat-treated)

QCC (QUARTZ , CLAY, CARBONATE)					
Sample	Chemical Phase	Phase Amount (%)			
		Virgin Powder	%30 of WL _T	%50 of WL _T	%80 of WL _T
Kovukdere	Quartz	26	36	58	65
	Clay	54	27	11	5
	Carbonate	16	21	4	1
	Others	4 (Anorthite + Rutile)	16	27	29

According to QCC phase quantities that are shown in Table 3.33, the reduction in clay and carbonate phases is remarkable. The inert quartz phase in the composition is much lower than other samples, while the clay portion is higher than the other samples. XRD analysis of this schist is shown in Figure 3.79. The (IV) spectrum contains a significant proportion of carbonates decomposed by increasing heat treatment.

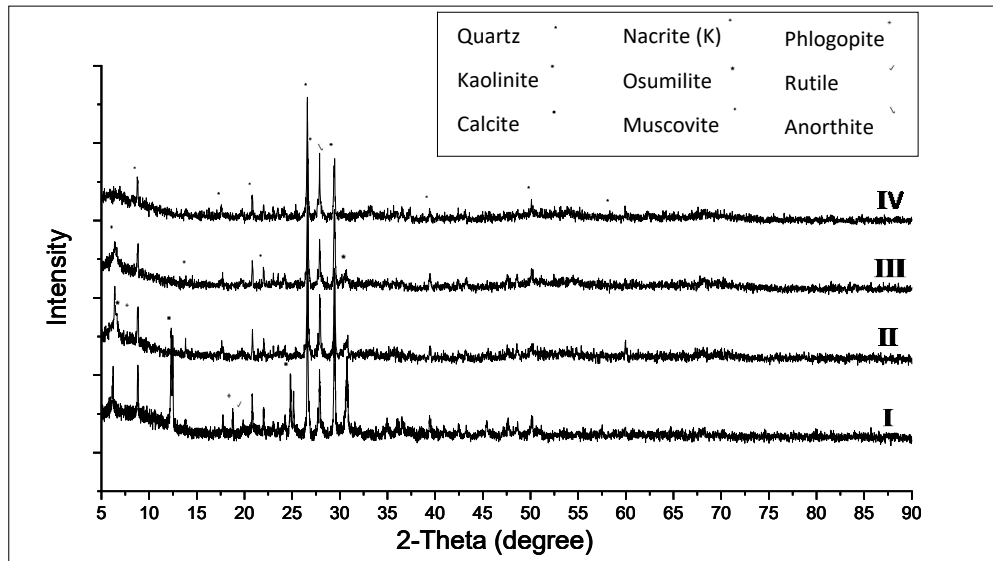


Figure 3. 79 Kovukdere x-ray diffractogram for (I) Virgin, (II) heat-treated up to 30% of WL_T , (III) heat-treated up to 50% of WL_T and (IV) heat-treated up to 80% of WL_T

Kovukdere schist content various phases such as Quartz, Calcite, Kaolinite, Nacrite (another Kaolinite polymorph $Al_2Si_2O_5(OH)_4$), Osumillite ($KMg_2Al_3SiAl_2O$), Muscovite, Phlogopite, Rutile and Anorthite. Detailed information about these phases has been given previously. However, the XRD spectrum shows that these phases are decomposed at high temperature by considering the residual clay and carbonates. Besides, TGA graphs support these results as it is shown in Figure 3.80.

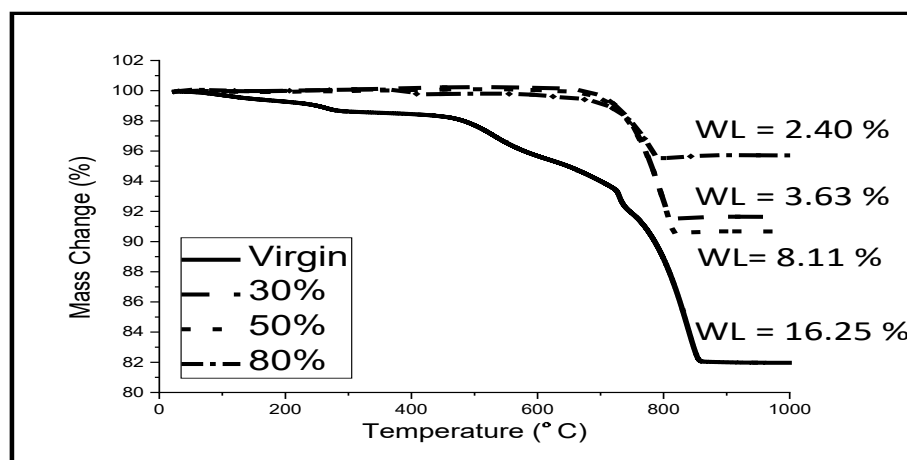


Figure 3. 80 Thermogravimetric analysis of virgin and heat-treated Kovukdere (heat-treated up to temperature associated to 30, 50, and 80% of total weight loss)

3.3.3.6 Muratbey Schist

Conductivity measurements and other characterization analysis of Muratbey virgin powder suggest that this material is one of the potential candidates for cement. The pozzolanicity of untreated and heat-treated Muratbey is shown in Table 3.34.

Table 3. 34 Pozzolanicity of virgin and heat-treated (to temperature associated to 30, 50 and 80% of total weight loss) Muratbey powder (conductivity variation)

Sample	Pozzolanicity (Conductivity Variation)			
	Virgin Powder	%30 of WL _T	%50 of WL _T	%80 of WL _T
Muratbey	1,19 & 1,25	1,22 & 1,24	1,29 & 1,35	1,42 & 1,44

By increment in heat treatment temperature, the conductivity values of Muratbey have not changed significantly. Although Muratbey virgin and heat-treated powder is in the good pozzolanicity range, it is seen that heat treatment may not activate all reactive phases. Regardless of the heat treatment of the clay phases in this sample, it could be observed that the amount of inert quartz phase is quite high, while the kyanite is excess between the other phases and the decomposition temperature of this phase is higher than the treatment temperature range. The QCC phase quantity of Muratbey is shown in Table 3.35.

Table 3. 35 QCC amounts (% by weight) of Muratbey (virgin and heat-treated)

		QCC (QUARTZ , CLAY, CARBONATE)			
Sample	Chemical Phase	Phase Amount (%)			
		Virgin Powder	%30 of WL _T	%50 of WL _T	%80 of WL _T
Muratbey	Quartz	51	43	36	33
	Clay	42	19	8	2
	Carbonate	—	—	—	—
	Others	7 (Kyanite)	38 (Kyanite + Anorthite)	56	65

The amount of clay phases decreases by the increasing the temperature, while the amount of quartz is constant. The phases in the material are indicated in Figure 3.81 in the XRD analysis results.

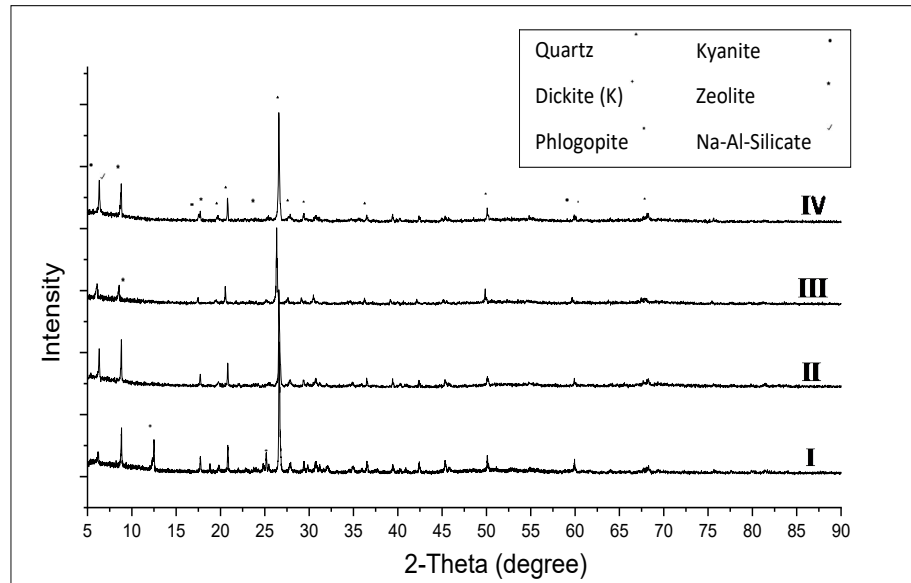


Figure 3. 81 Muratbey x-ray diffractogram for (I) Virgin, (II) heat-treated up to 30% of WL_T , (III) heat-treated up to 50% of WL_T and (IV) heat-treated up to 80% of WL_T

Based on XRD results, the primary phases of this sample are the Kaolinite species Dickite, Phlogopite, Kyanit and Zeolite. The need for high temperatures to decompose Kyanit was mentioned earlier. Besides, the zeolite is a solid and hard mineral that can affect the behavior of the material. TGA results compare the decomposition of virgin mineral and heat-treated Muratbey powder. This can be observed in Figure 3.82.

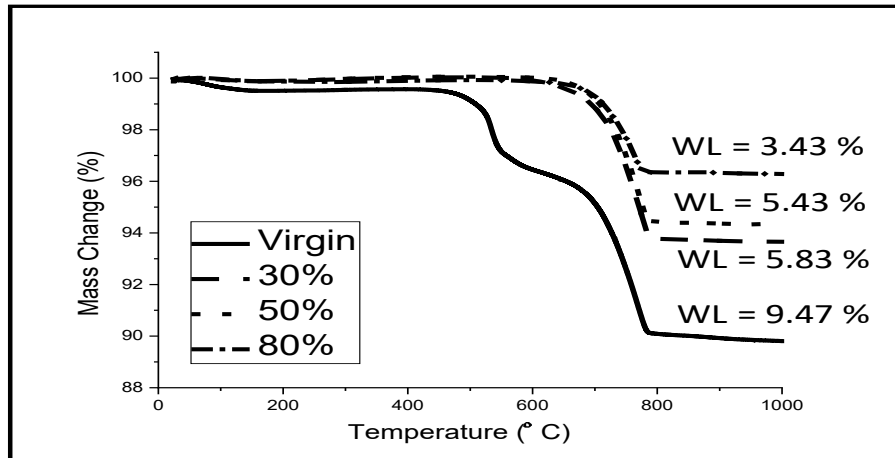


Figure 3. 82 Thermogravimetric analysis of virgin and heat-treated Muratbey (heat-treated up to temperature associated to 30, 50, and 80% of total weight loss)

3.3.3.7 Ladik Schist

Ladik virgin powder did not perform well in terms of conductivity measurements. The pozzolanicity values of the virgin and heat-treated powders are given in Table 3.36.

Table 3. 36 Pozzolanicity of virgin and heat-treated (to temperature associated to 30, 50 and 80% of total weight loss) Ladik powder (conductivity variation)

Pozzolanicity (Conductivity Variation)				
Sample	Virgin Powder	%30 of WL _T	%50 of WL _T	%80 of WL _T
Ladik	0,6 & 0,74	0,69 & 0,78	0,8 & 0,87	1,01 & 1,12

The conductivity measurement of Ladik schist powder is ranked as variable pozzolanicity for virgin and even heat-treated mineral. Table 3.37 shows the amount of QCC phases in Ladik schist.

Table 3. 37 QCC amounts (% by weight) of Ladik (virgin and heat-treated)

		QCC (QUARTZ , CLAY, CARBONATE)			
Sample	Chemical Phase	Phase Amount (%)			
		Virgin Powder	%30 of WL _T	%50 of WL _T	%80 of WL _T
Ladik	Quartz	52	39	32	23
	Clay	26	16	11	8
	Carbonate	—	—	—	—
	Others	22 (Anorthite)	45	57	69

Despite the decomposition of some of the clay in the Ladik sample, it contains almost too much quartz. Among the other phases anorthite is the main one. There is also no or almost no carbonate phase. According to XRD analysis and phase distribution results, the principal clay “halloysite” in Ladik schist is a member of the kaolin-serpentine group with crystal structure of monoclinic. On the other hand, the interlayer distance in the crystal structure of halloysite are smaller than in other kaolinite groups, thus making this structure less reactive. The XRD spectrum can be viewed in Figure 3.83.

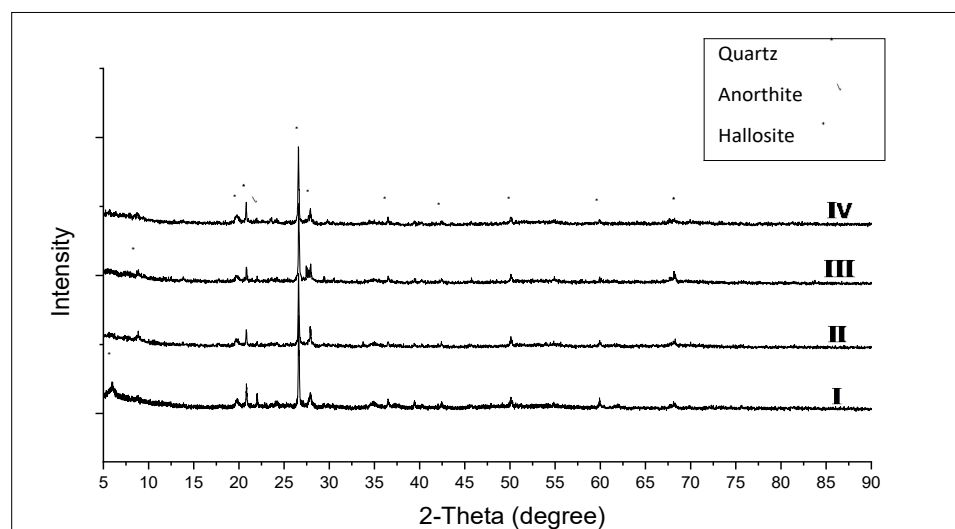


Figure 3. 83 Ladik x-ray diffractogram for (I) Virgin, (II) heat-treated up to 30% of WL_T, (III) heat-treated up to 50% of WL_T and (IV) heat-treated up to 80% of WL_T

As it can be inferred from XRD analysis, the amounts of the reactive phases are not enough to consider this powder as a proper potential substitute and the heat treatment has no significant effect on its reactivity. Based on this test, it is understood that quartz is the main phase forming the composition of Ladik mineral. Figure 3.84 shows the TGA measurements of this schist type mineral to understand the separation of phases:

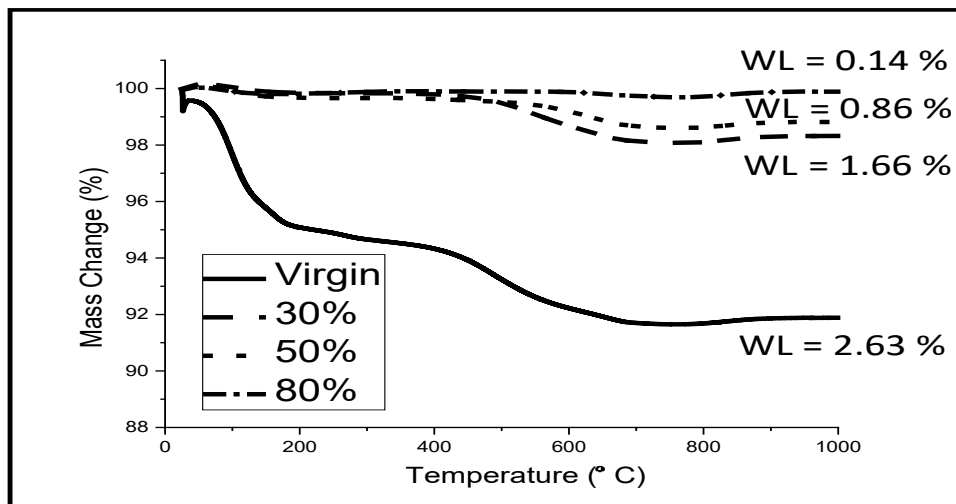


Figure 3. 84 Thermogravimetric analysis of virgin and heat-treated Ladik (heat-treated up to temperature associated to 30, 50, and 80% of total weight loss)

3.3.4 Compressive Strength Test

The aim of this study is to find a suitable schist material for cement substitution which can be activated due to the calcination procedure. Among the characterization measurements, compressive strength tests are one of the most important tests to demonstrate the success of this substitution. Among the physical properties of cement, compressive strength is the most important one. The experimental procedure is as 30 wt% of the cement content was replaced with different activated schist samples to prepare cube samples. sampling procedure was carried out by mixing 700 g cement, 300 g calcined clay in each mixture by water / solid ratio of 0.5. Samples were prepared. These samples were subjected to hydration for 2, 7, 28, 50

and 90 days. Composite cements containing calcined clay are thought to be much more durable in terms of long hydration time.

In this part, the compressive strength test results of the cubic blended cement paste sample is evaluated. The samples were prepared by the partial substitution of calcined clay that is heat-treated up to 30%, 50% and 80% of total mass loss. This replacement is 30% by weight of cement. Afterwards, the mechanical strength performance of each sample will be analyzed, considering the magnitude of heat treatment of different samples. For each sample, the compressive strength of the samples prepared with composite cement was compared with 100% pure cement and as a criterion for applicability of replacement, 70% of the compressive strength of pure cement. It is also representing the effect of inert filler in mixture.

This section firstly contains the compressive strength results to evaluate the clay samples activated by different heat treatments; that is, the results will be based on replaced clayey material heated up to 30%, 50% and 80% of total mass loss. This will determine the appropriate criterion for comparing the mechanical strength behavior of the samples in response to treatment at different temperatures applied to the raw materials. It will also provide important information on the activation rates of the reactive phases in the schist composition. Then, graphs will be shown to investigate the effect of the amount of quartz and carbonates on the mechanical strength measurements. In addition, two evaluations will be made on the charts to compare pozzolanicity and strength results and to show the suitability of the results. Column graphs were prepared to reveal the relationship between strength and pozzolanicity of composite samples. The final part will be based on the evaluation of the material strength for all samples according to all raw materials treated at different temperatures. As a result, the graph of each sample will be compared with the pure cement strength and the 70% of the pure cement strength. Based on the initial characterization, it could be claimed that some of the activated raw materials may meet the expectations of this study. The relationship between conductivity measurements and strength is mentioned. The results obtained from the kaolinite used cement samples were always shown and compared together with the candidate clay mineral samples.

3.3.4.1 Calcined Clay Cement (C³) by heat-treated material up to 30% of WL_T

This mixture contains 70% cement and 30% calcined clay. Clayey mineral was subjected to heat treatment by increasing their temperature until they 30% of total mass loss. The water / solid ratio (w / s) is 0.5. The compressive strength test results obtained for all samples are shown in Figure 3.85.

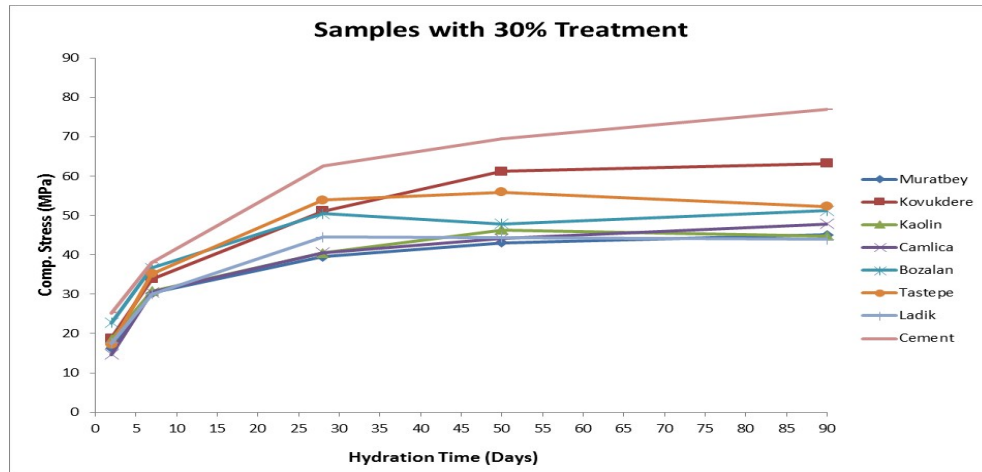


Figure 3. 85 The compressive strength test results of all blended cement paste (calcination of clay up to temperature associated to the 30% of total mass loss)

According to the strength graphs, Tastepe, Kovukdere and Bozalan performed better than other samples. Table 3.38 shows the mechanical strength values.

Table 3. 38 Compressive strength test results of samples with different hydration times (MPa) (heat treated clay up to 30% WL_T)

Day	Bozalan	Tastepe	Ladik	Kovukdere	Muratbey	Camlica	Kaolin	Cement
2	22.7	17.2	17.5	18.8	16.3	14.7	18.5	25.2
7	36.6	35.2	30	33.9	30.3	30.5	30.8	38
28	50.5	53.9	44.5	51.1	39.5	40.6	40.5	62.6
50	47.9	55.9	44.4	61.23	43.1	44.1	46.3	69.6
90	51.2	52.3	43.9	63.2	45.1	47.9	44.8	77

Compressive strength is the most informative data about the effect of calcined clay. Among the 30% activated raw materials, there is no numerically supportive sample of the study objective, which is intended to reduce the strength of the pure cement not more than 10% of the pure cement strength. However, by comparing these amounts to 70% of cement strength, the above-mentioned three samples can be considered eligible candidates. It is possible to suppose that by increasing heat treatment temperature, the decomposition of the reactive phases may increase and become more reactive. It is also interesting to note that the compressive strength of some samples is higher than that of kaolinite used composite cement. However, one of the most important issues observed during all experiments is that the raw material samples are not very homogeneous.

3.3.4.2 Calcined Clay Cement (C^3) by heat-treated material up to 50% of WL_T

The mixture ratio is same as previous part, contains 70% cement and 30% clay mineral resource. Clays were heat-treated at a temperature corresponding to 50% of total weight loss. The water / solid ratio (w / s) is specified as 0.5. The compressive strength test results for all samples are shown in Figure 3.86.

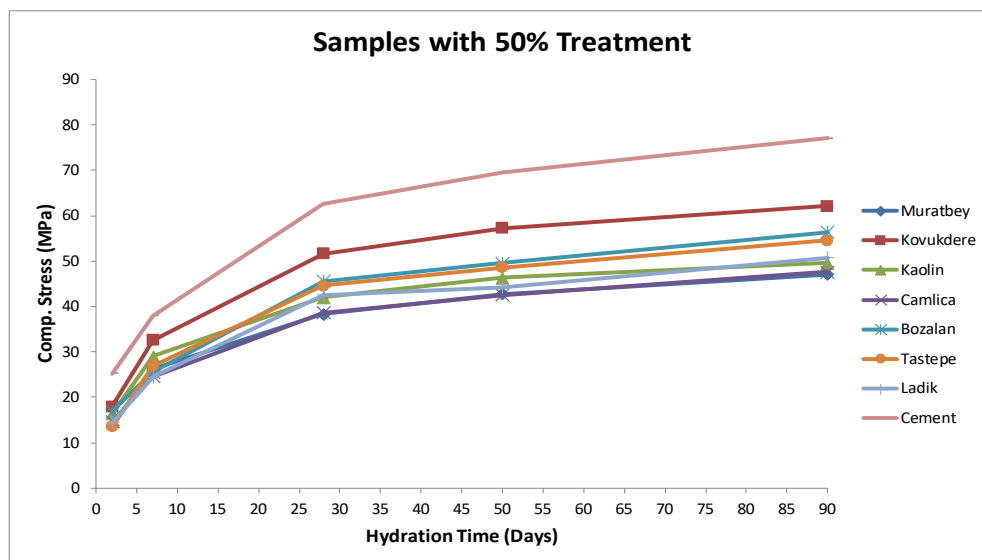


Figure 3. 86 The compressive strength test results of all blended cement paste (calcination of clay up to temperature associated to the 50% of total mass loss)

For the 50% blended cement paste, compressive strength tests were performed for all samples at specified hydration times and results were evaluated. According to the compressive strength measurement results, the strength development of 50% samples is significantly resembles the behavior of the previous part (30%). Kovukdere and Tastepe again gave better results than the others. It should be noted that the compressive strength behavior of Tastepe and Bozalan will be similar if hydration is exposed for a long time. These samples still perform better than Kaolinite. The compressive strength values for all samples are shown in Table 3.39.

Table 3. 39 Compressive strength test results of samples with different hydration times (MPa) (heat treated clay up to 50% WL_T)

Day	Bozalan	Tastepe	Ladik	Kovukdere	Muratbey	Camlica	Kaolin	Cement
2	16.9	13.5	14.4	18	13.8	14.6	16.3	25.2
7	25.6	27	24.5	32.6	26.3	24.6	29	38
28	45.6	44.6	42.5	51.6	38.3	38.6	42	62.6
50	49.6	48.6	44.3	57.3	42.7	42.5	46.3	69.6
90	56.4	54.5	50.8	62.11	47.1	47.6	49.6	77

According to the table, the compressive strength of the calcined clay cement sample was slightly affected by increment in thermal treatment. This is based on 28-day measurement results, but longer-term measurement values are more acceptable. The performance of Tastepe, Kovukere and Bozalan seem to be better by further treatment. In the next part, the results are given when more heat treatment is applied to the clay.

3.3.4.3 Calcined Clay Cement (C³) by heat-treated material up to 80% of WL_T

This mixture contains 70% cement and 30% clay mineral resource. Clayey minerals were heat treated at a temperature corresponding to 80% of total mass loss. The water / solid ratio (w / s) is 0.5. The compressive strength test results of all samples are presented in Figure 3.87.

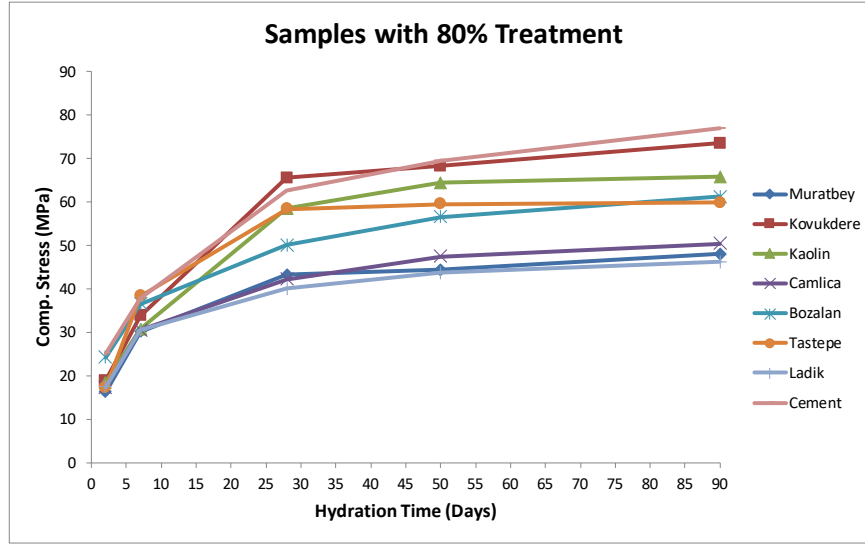


Figure 3. 87 The compressive strength test results of all blended cement paste (calcination of clay up to temperature associated to the 80% of total mass loss)

The results in Figure 3.84 differ greatly from previous ones. The performance of Tastepe is remarkable in the first days and the same behavior is observed for Kovukdere after 28 days of hydration. Kaolinite results show higher values of strength than Bozalan. Similarly, Kovukdere shows higher values than the compressive strength of pure cement sample. The compressive strength values are shown in Table 3.40.

Table 3. 40 Compressive strength test results of samples with different hydration times (MPa) (heat treated clay up to 80% WL_T)

Day	Bozalan	Tastepe	Ladik	Kovukdere	Muratbey	Camlica	Kaolin	Cement
2	24.26	17.2	17.5	18.9	16.3	17.4	18.5	25.2
7	36.6	38.4	30.5	33.9	30.2	30.5	30.8	38
28	50.1	58.4	40.1	65.6	43.3	42.3	58.5	62.6
50	56.6	59.6	43.7	68.3	44.4	47.5	64.4	69.6
90	61.3	59.9	46.2	73.5	48.1	50.5	65.8	77

According to these values, Kovukdere, Tastepe and Kaolinite have passed the criterion and can be accepted as proper substitutes. By activation of Kovukdere raw material, the

composite cement paste performance made from it seems to be better than pure cement. In addition, strength measurements in early hydration times are much better than previous samples prepared by 30 and 50% heat-treated clay. For instance, Bozalan's early strength values captured the early strength values of pure cement. Proper activation of the raw materials perhaps affects the performance of the reactive samples. Kovukdere and Tastepe samples contain carbonate phases more specifically calcite. According to recent studies on limestone and calcined clay cement, it is reported that the decomposition of carbonate phase plays a significant role in these materials [195-197]. The quartz phase is considered as inert in cement mortar. All raw materials contain quartz phase. In order to interpret the activated clay effect, some calculations were made assuming what would have been the results if the clay had been replaced by quartz. These calculations can also be used to calculate the effect of the amount of clay phase when new raw material resources are available. It is assumed that quartz and carbonates have an adverse effect on the performance of the material. While quartz is an inert filler, carbonate is assumed as reactive material. Therefore, it is important to compare the compressive strength graphs with respect to quartz and carbonate quantities. The effect of quartz and carbonates on the sample strength for the 30% sample is presented in Figure 3.88.

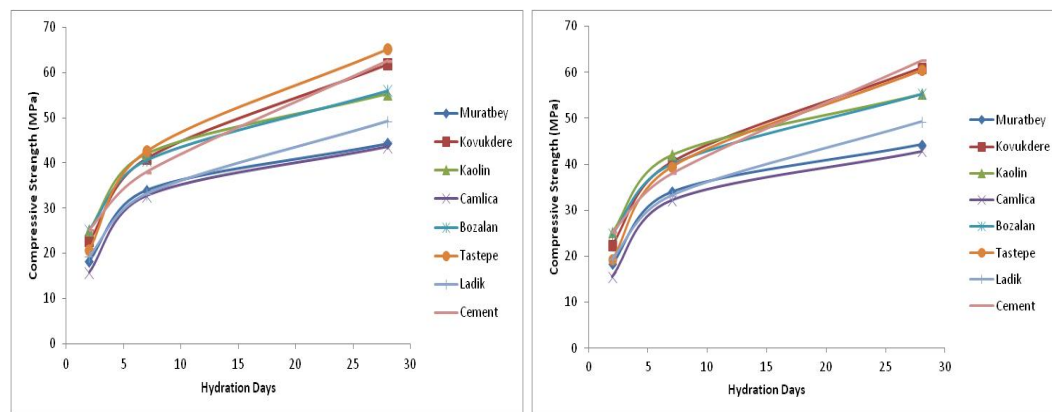


Figure 3. 88 Effect of quartz and carbonate on composite cement paste samples [30% WL_T] (Left Quartz / Right quartz and carbonate effect)

The plots if Figure 3.85 is provided by using two basic formula.

$$\sigma_2 = \frac{\sigma_1}{(1-(Q \times 0.3))} \quad (\text{for quartz content}) \quad (3.1)$$

$$\sigma_2 = \frac{\sigma_1}{(1-((Q-C) \times 0.3))} \quad (\text{for quartz and carbonate content}) \quad (3.2)$$

These calculations were used to understand the role of inert quartz and reactive carbonates on compressive strength. In this case, σ_1 is corrected by the amounts of quartz and carbonate in the samples, σ_2 is obtained and thus can be applied to evaluate the effectiveness of quartz and carbonate. In both cases, the results overlap with the expectation that a lower amount of quartz and a higher amount of reactive carbonate may affect the strength of the sample. As a result, these formulas could be a suitable technique to control the results of 50% and 80% as well. Figure 3.89 and 3.90 shows the results of this calculation with 50% sample.

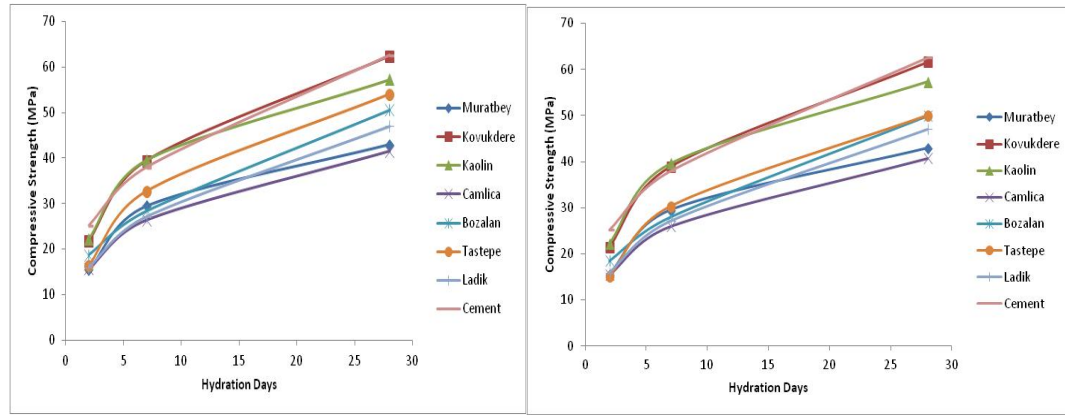


Figure 3. 89 Effect of quartz and carbonate on composite cement paste samples [50% WL_T]
(Left Quartz / Right quartz and carbonate effect)

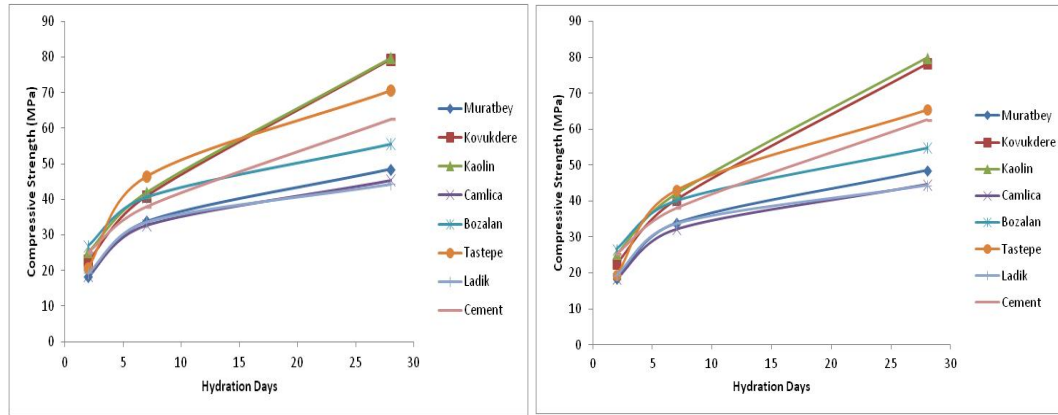


Figure 3. 90 Effect of quartz and carbonate on composite cement paste samples [80% WL_T] (Left Quartz / Right quartz and carbonate effect)

By applying the formulas to all samples, the Kaolinite values increase as expected. This is due to presence of quartz as single co-exist phase with clay in Kaolinite. Compensation of filling effect of quartz reveals the effect of pure Kaolinite. By removing the quartz effect from Kovukdere, it reached up to high values again. The amount of clay in these two samples was much more than quartz. On the other hand, Kovukdere contains significant amount of carbonate phase compared to other samples. Another premise of pozzolanic activity may be the reduction of clay and carbonate amounts as a result of heat treatment. More information is needed to understand the durability of the mixed samples and the relationship between the decomposition of reactive phases (clay and carbonate phases). The decomposition of both clay and carbonates is important because these two phases are reactive phases in the composite cement composition. The pozzolanicity of calcined powder depends on the degree of decomposition of these phases. Figure 3.91 shows graphs of time-dependent strength and reduction in clay-carbonate quantities as a result of heat treatment (e.g. decomposition rates) for the 30% activated sample. By reading these graphs together, it gives information about the effectiveness of clay and carbonates on decomposition rates and compressive strength.

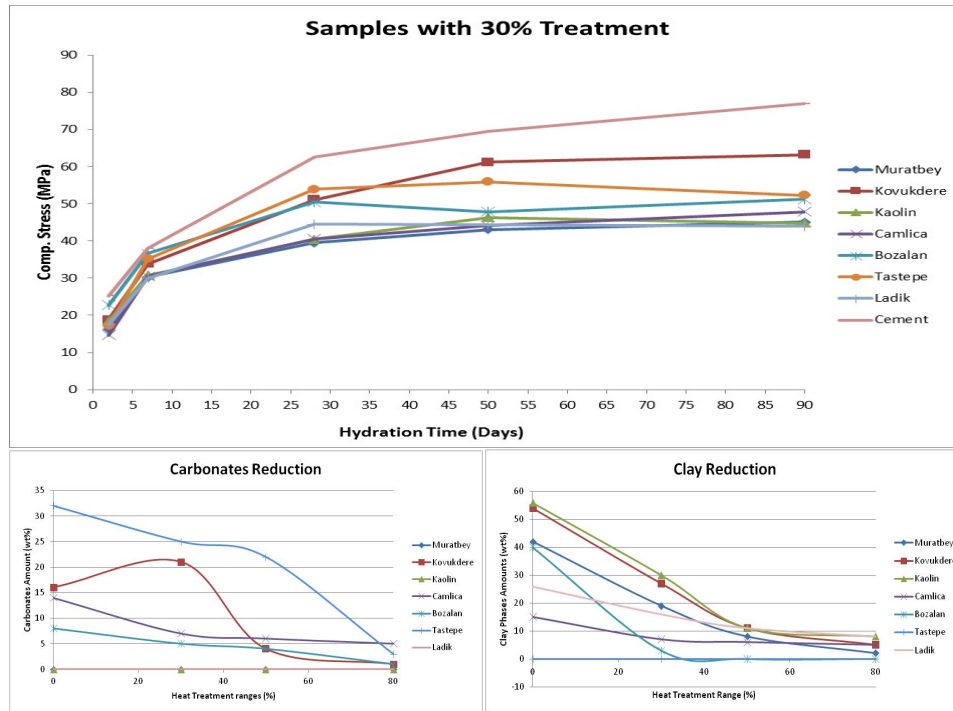


Figure 3.91 Variation of the reduction in the amount of clay and carbonate by heat treatment considering the compressive strength of blended cement paste (heat treated clay up to 30% WL_T)

In general, carbonate decomposition in carbonate-containing samples started at the temperature correspond to 80% mass loss rates. Proper substitutes such as Kovukdere, Kaolen and Tastepe can be an important indicator of the role of carbonates between 50% and 80% associated temperature range. On the other hand, this situation is not the same for Camlica or Muratbey samples. It is important to note that the carbonates are decomposed at elevated temperatures. Based on the phase ratios calculated by Rietveld method, since the carbonate phase has not yet decomposed at low temperatures, the carbonate phase may appear to increase relatively when the clay phase de-hydroxylated (e.g. Kovukdere example). However, this should not be perceived as an increase in the amount of carbonate phase. Figure 3.92 contains the strength plot of the heat-treated samples of 50% compare the reduction rates. It is already known that 30% and 50% activated samples are similar. This similarity is due to the constant decomposition of the reactive phases. The strength values of heat-treated powders at high temperatures vary and should be associated with carbonate decomposition.

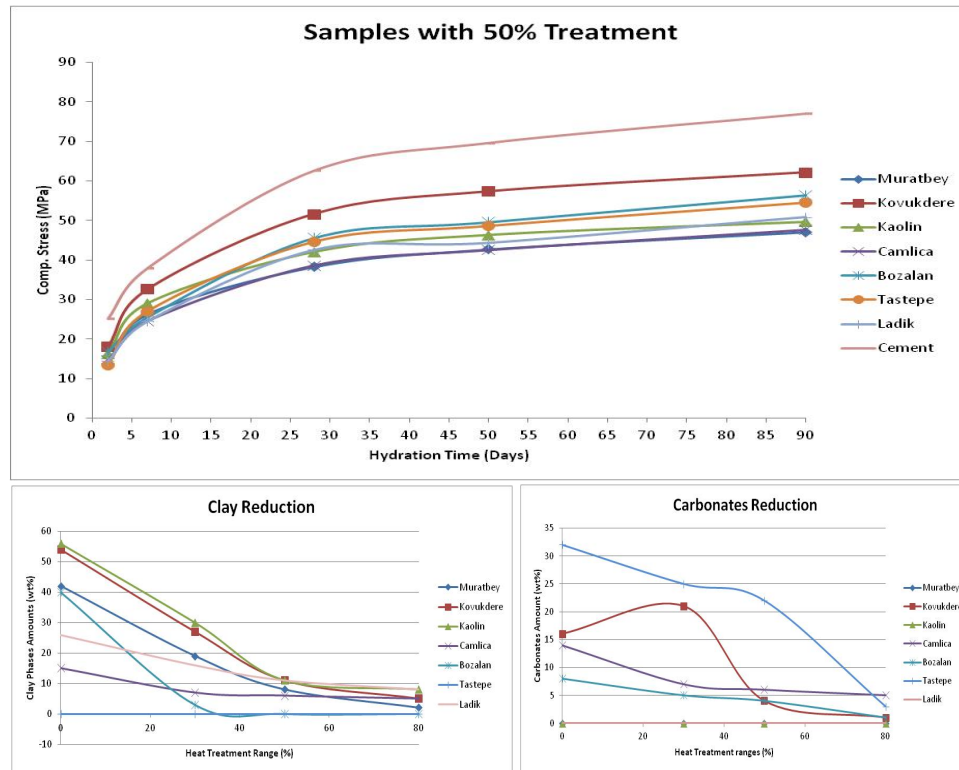


Figure 3.92 Variation of the reduction in the amount of clay and carbonate by heat treatment considering the compressive strength of blended cement paste (heat treated clay up to 50% WL_T)

The relationship between the compressive strength of the 50% sample and the reduction in the amount of clay and carbonate crystal phases (e.g. the rate of decomposition) shows a behavior like that of the 30% sample. This result indicates that 30% and 50% calcined samples are similar, and the basis is due to the decomposition of certain phases in the clay structure. Figure 3.93 shows the data of 80% samples.

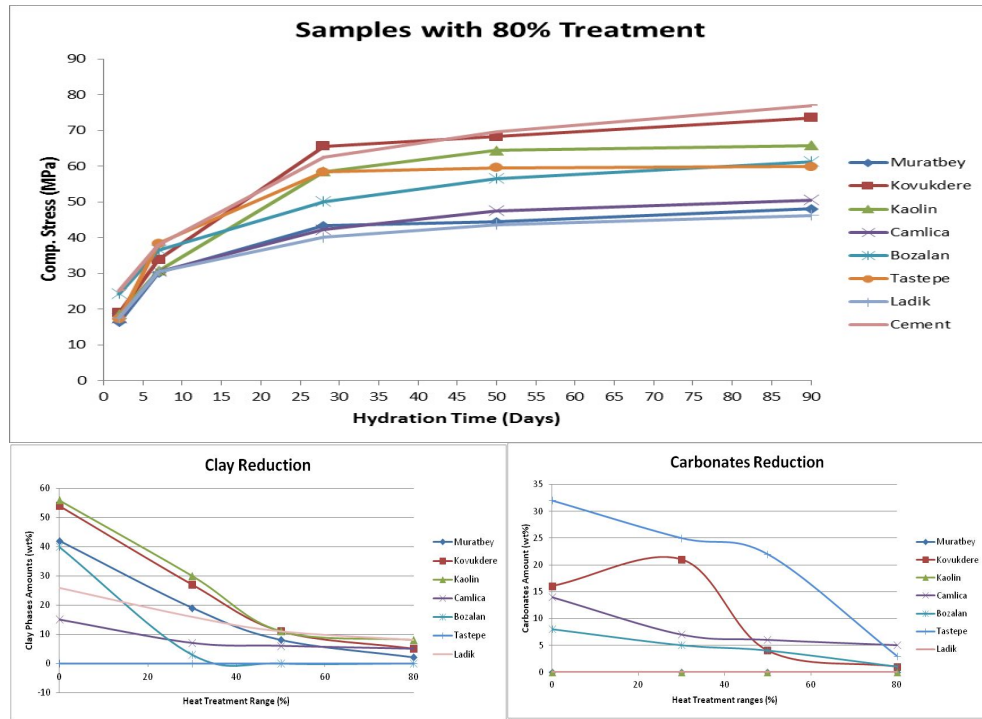


Figure 3.93 Variation of the reduction in the amount of clay and carbonate by heat treatment considering the compressive strength of blended cement paste (heat treated clay up to 80% WL_T)

By considering these two plots at the same time, it is possible to interpret the relationship between decomposition and compressive strength of different heat-treated materials. It is seen that the samples with high strength values start to decompose in clay and carbonates at a low temperature but the decomposition with a steep slope at high temperature is observed. Other samples were found to exhibit an inverse behavior, i.e., decomposition at low rate and low reactivity. It should be noted that the amount of clay and carbonates is an important factor in this interpretation. The carbonate phase is not present in the kaolinite. Therefore, the mass loss due to all decomposition comes from clay materials. Therefore, the effect of the increase in strength directly comes from the de-hydroxylated clay. This shows the maximum strength gain that can be obtained from the active material calculated by the available data.

At this stage, it would be useful to check the pozzolanicity measurements and their level of reliability by comparing them with the strength values obtained from the same samples.

Figure 3.94 shows the pozzolanicity of virgin and heat-treated materials having calcined clay cement strengths with treating temperatures up to 30% of total mass loss.

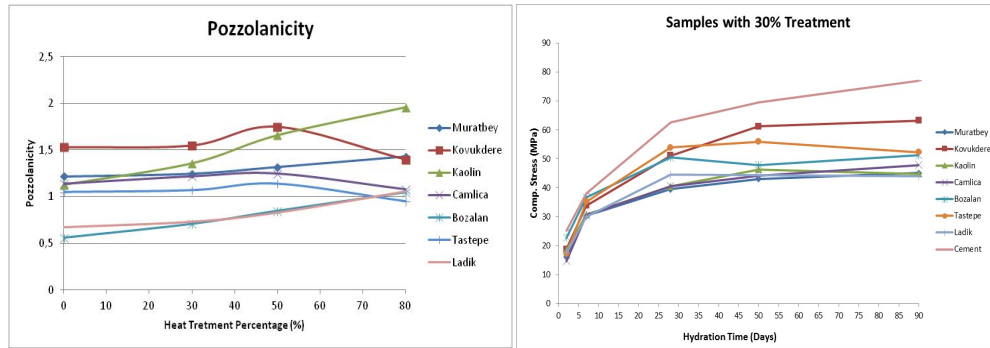


Figure 3. 94 Relation of pozzolanicity with compressive strength (for 30% heat treated sample)

The pozzolanic property (determined by conductivity measurements) was increased for all samples from virgin (untreated) powder to 30% heat treated powders. However, some samples such as Kovukdere, Kaolinite, Muratbey and Camlica have higher pozzolanicities. Through the temperature range up to 30%, some clays are partially de-hydroxylated (activated) and the trend is normal. Figure 3.95 shows the pozzolanicity and compressive strength behavior of the sample of 50%.

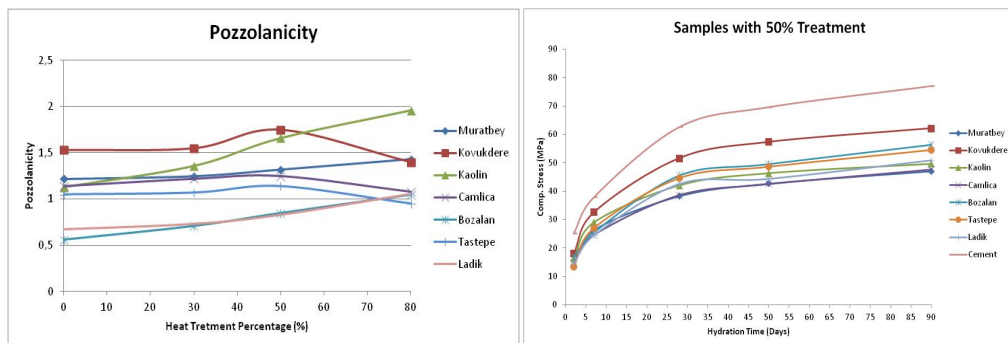


Figure 3. 95 Relation of pozzolanicity with compressive strength (for 50% heat treated sample)

From 30% to 50% the trend of the samples in term of pozzolanicity (i.e. the activation indicator obtained from the electrical conductivity) proceeds as expected. However, only the samples mentioned above are in the good pozzolanicity range, while others are in the variable or low pozzolanicity range. By increasing the treatment temperature to 700 ° C and above, it was found that the results did not fully coincide with the strength measurements. According to conductivity measurements, Kovukdere, Kaolinite, Camlica and Muratbey were expected to be more reactive and effective. However, as it can be seen in the graph on the right in Figure 3.93, Kovukdere, Kaolinite and Tastepe were found to have optimum properties. Consequently, it was confirmed that the carbonates had an adverse effect on the pozzolanic properties. In most cases, since the decomposition temperature of the carbonates is more than 650 ° - 700 ° C, 80% heat treatment may help to better understand the situation. Figure 3.96 is given to compare pozzolanicity measurements and strengths of samples prepared with heat treated clay to mass loss of 80%.

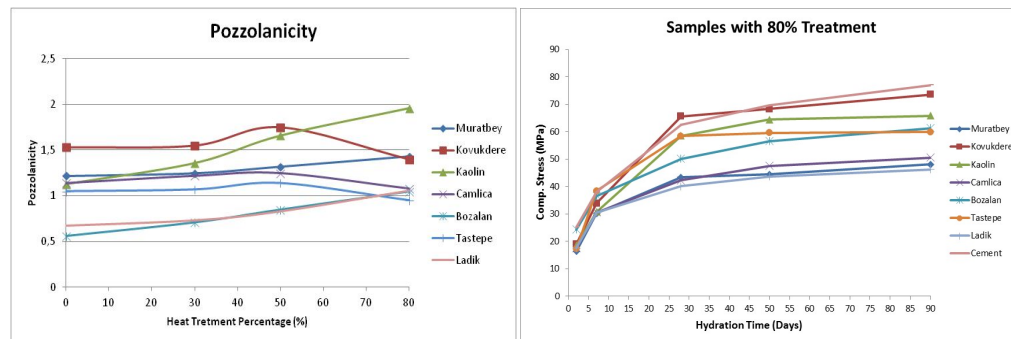


Figure 3. 96 Relation of pozzolanicity with compressive strength (for 80% heat treated sample)

Regardless of Kaolinite, comparison of plots shows that the expectations from pozzolanicity measurement and compressive strength are not adjusted correctly. For example, Kovukdere's pozzolanicity is further reduced than the original virgin powder. This occurs in high temperature heat treatment due to the decomposition of carbonates based on the reaction indicated. It can be considered to have an adverse effect on electrical conductivity. Thus, in the case of carbonate-containing materials, it is possible to consider the role of carbonates and the inefficiency of the electrical conductivity measurement results. However, it is

necessary to evaluate the pozzolanicity and strength of the samples in terms of meeting this study expectations. The following graphs are provided as a step in obtaining these results appropriately. Figure 3.97 is a comparison of the pozzolanicity of the 30% sample (after 28 days) with the reference amount of 1.2 and the ratio of the calcined clay cement sample to the pure cement strength (0.7 as a reference).

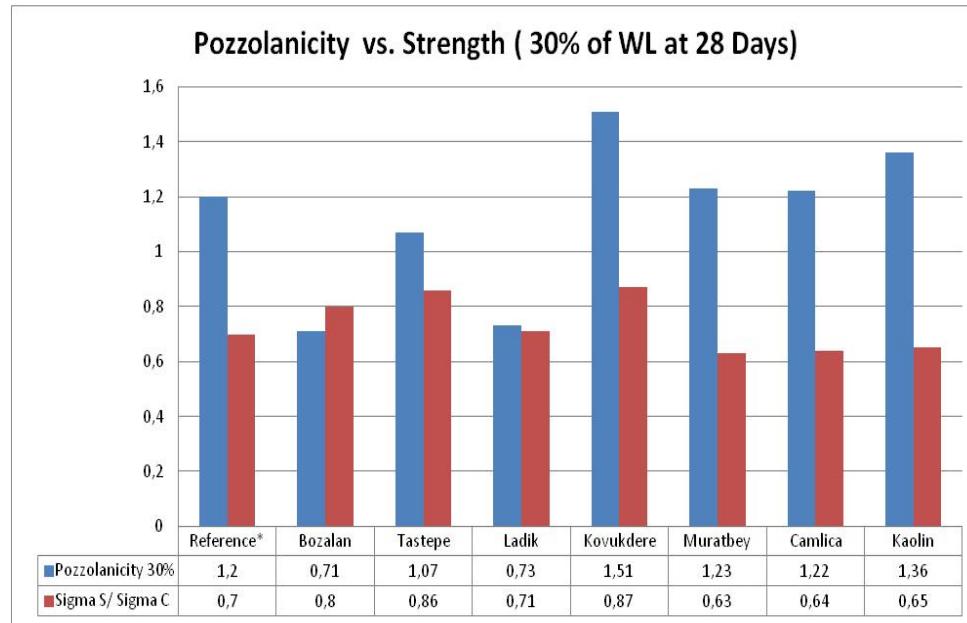


Figure 3. 97 Compressive strength and pozzolanicity of all samples according to the reference values (calcined sample up to temperature associated to 30% of WL_T)

At this temperature, the pozzolancity of Kovukdere, Kaolinite, Camlica and Muratbey, as well as the mechanical strengths of Kovukdere, Tastepe and Bozalan, were higher than the reference value. Even the Ladik sample appears to be at the border. Factors affecting pozzolanicity is mentioned, and the difference between the two experiments clearly demonstrates this. Figure 3.98 represents 50% heat treated samples and their comparison with the specified reference values.

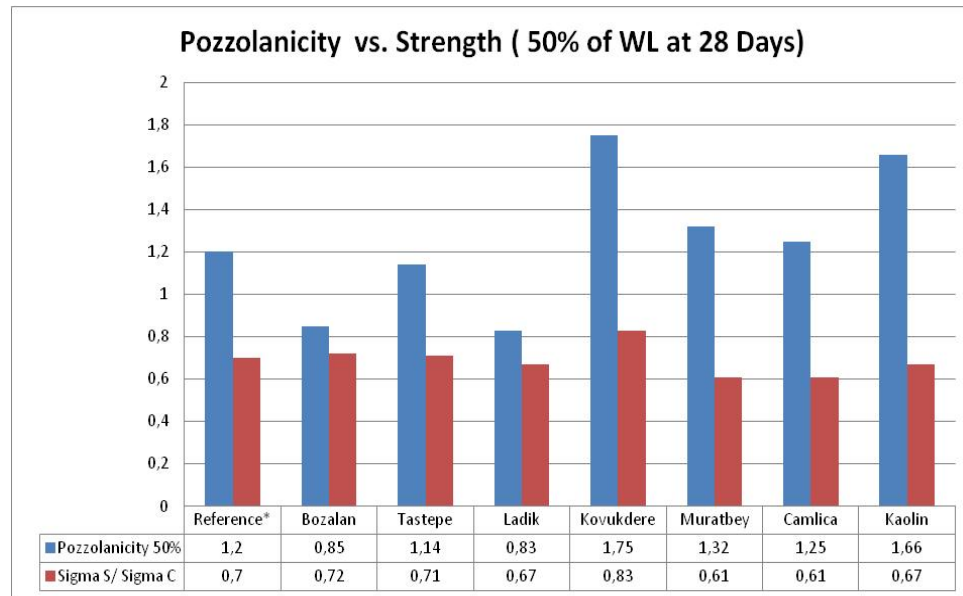


Figure 3. 98 Compressive strength and pozzolanicity of all samples according to the reference values (calcined sample up to temperature associated to 50% of WL_T)

For this temperature value, the pozzolanicity of Kovukdere, Camlica, Kaolinite and Muratbey is above the reference point like the 30% treated material. There are three candidates in strength tests, Kovukdere, Tastepe and Kaolinite have a higher value than reference. Figure 3.99 shows the column graph of 80% samples.

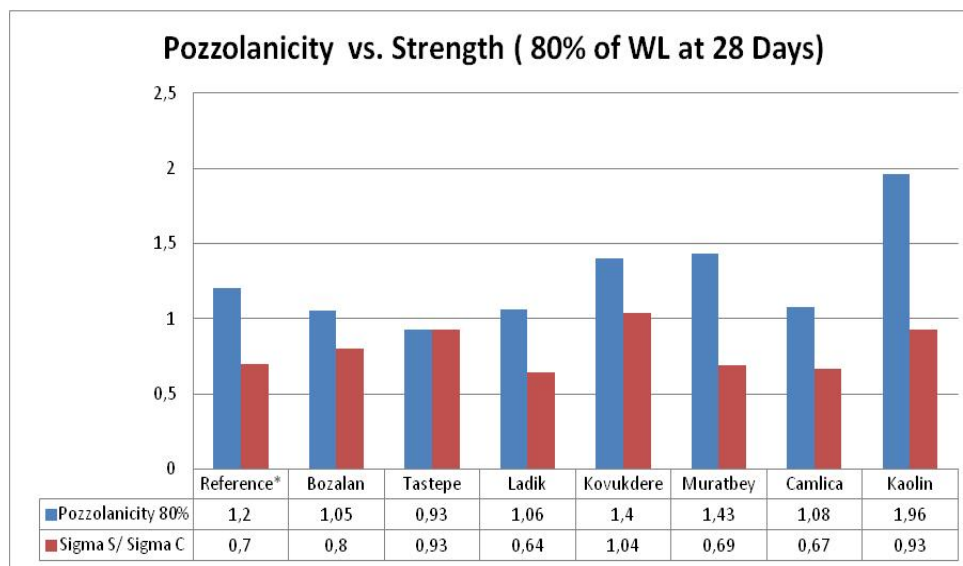


Figure 3. 99 Compressive strength and pozzolanicity of all samples according to the reference values (calcined sample up to temperature associated to 80% of WL_T)

Up to this point, all experiments are interpreted, and important information is obtained. Kaolinite was chosen as a touchstone sample. Besides, it was found that their behavior was coincided with the expected behavior. Kovukdere and Tastepe clay materials also show the potential of cement substitution. To make the final evaluation of the samples, it is useful to consider each sample separately and compare the compressive strength of the each with pure cement. Figure 3.100 shows the values of compressive strength in different calcination temperatures in the Bozalan sample.

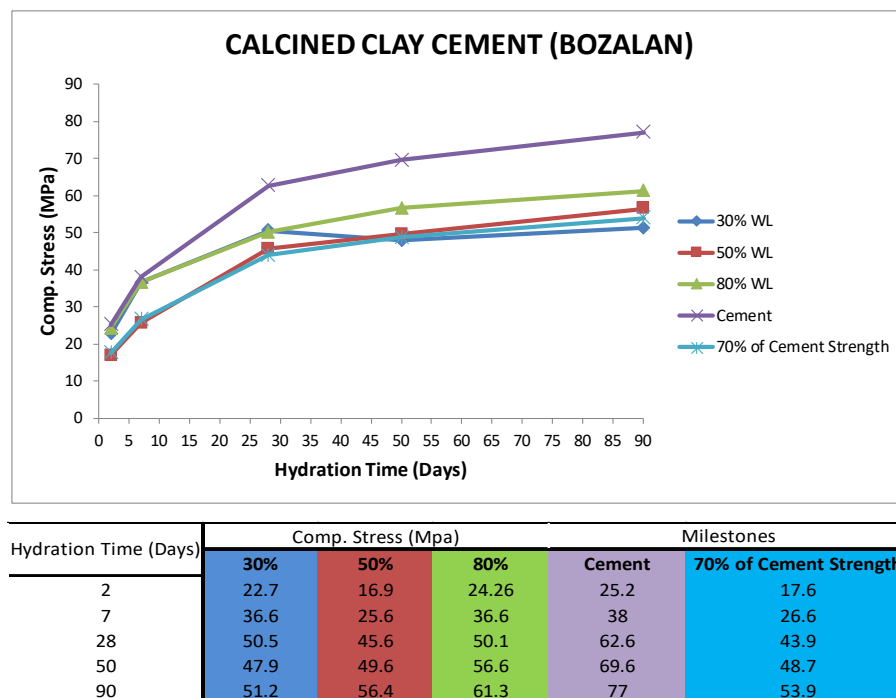


Figure 3. 100 Comparison of compressive strength of Bozalan sample subjected to different calcination temperatures with cement and 70% of cement compressive strength

For Bozalan sample, 30% and 80% samples have almost the same strength, while 50% of the sample is less than the others and is equivalent to 70% of cement strength. It is believed that there may be secondary reactions in the temperature range of 50% and these may alleviate the separation of phases. However, further heat treatment times need to be analyzed. Furthermore, these results can be indicative of how heterogeneous the powder samples can be.

Figure 3.101 shows the difference in the compressive strength behavior of Tastepe sample and pure cement.

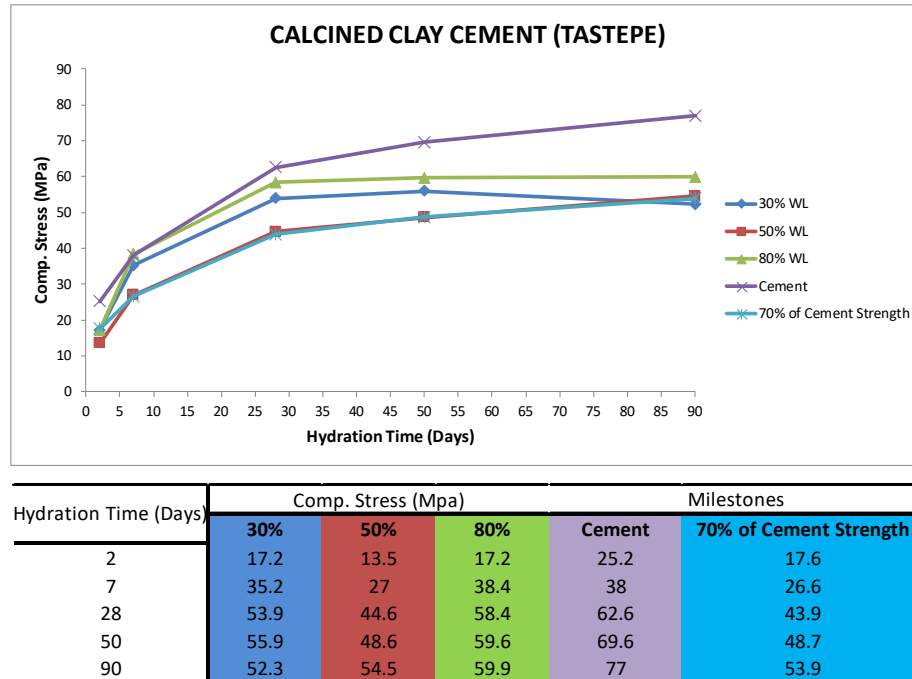


Figure 3. 101 Comparison of compressive strength of Tastepe sample subjected to different calcination temperatures with cement and 70% of cement compressive strength

It is seen that the same tendency is possible for Tastepe. 30% and 80% samples are similar, and 50% samples are lower than the others. In this case, the strength of 80% activation after 50 days indicates that Tastepe will decrease its strength in the long run, which would result in lower durability. However, it is necessary to measure the strength values after prolonged hydration in order to have more precise information about the behavior of the material. In the case of Tastepe, the reason behind the strength of 30% sample to be more than 50% is that the amount of clay in the sample is lower than the other phases. It should be considered that the decomposition of carbonate in the strength of the sample causes an increase in strength.

Figure 3.102 shows the difference in the compressive strength behavior of Ladik sample from pure cement.

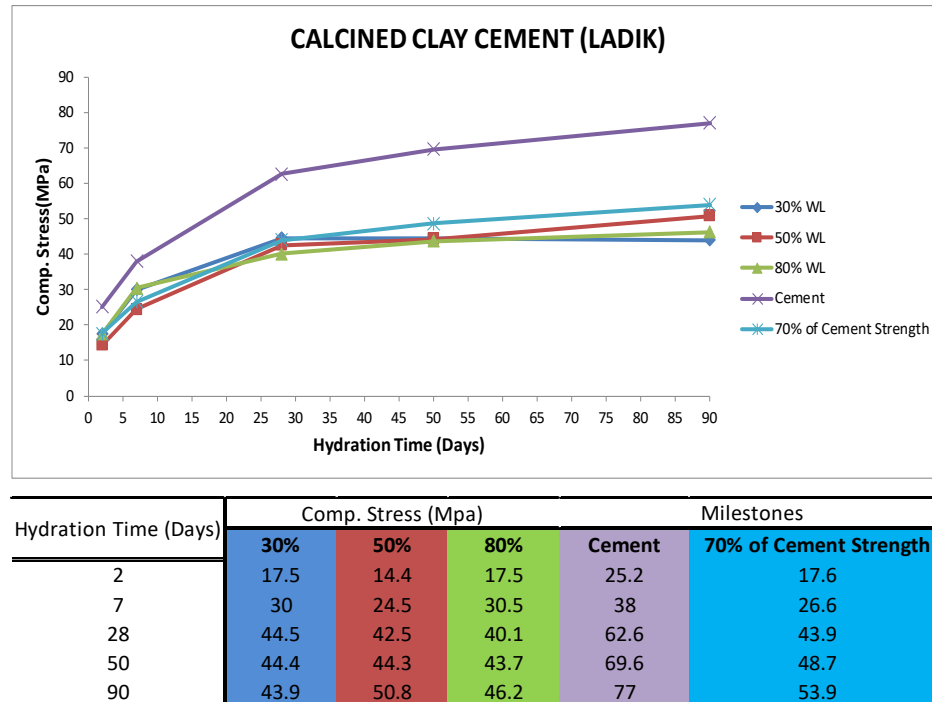


Figure 3. 102 Comparison of compressive strength of Ladik sample subjected to different calcination temperatures with cement and 70% of cement compressive strength

Ladik results are already known to have low values and as shown in the graph, the strength behavior of this sample during the different heat treatment periods was similar in the early days. However, after 28 days, the strength of the samples decreased, and these values were found to be lower than the 70% of cement strength. On the other hand, high heat treatment can adversely affect and reduce strength. It can be said that almost most of the reactive phases decompose before this temperature and a new stable structure is formed which alleviates the reactivity of calcined clay at higher temperature. It could be assumed that the main role of the obtained strength is due to the presence of Anorthite and Halloysite.

Figure 3.103 shows the difference in the compressive strength behavior of Kovukdere sample from pure cement.

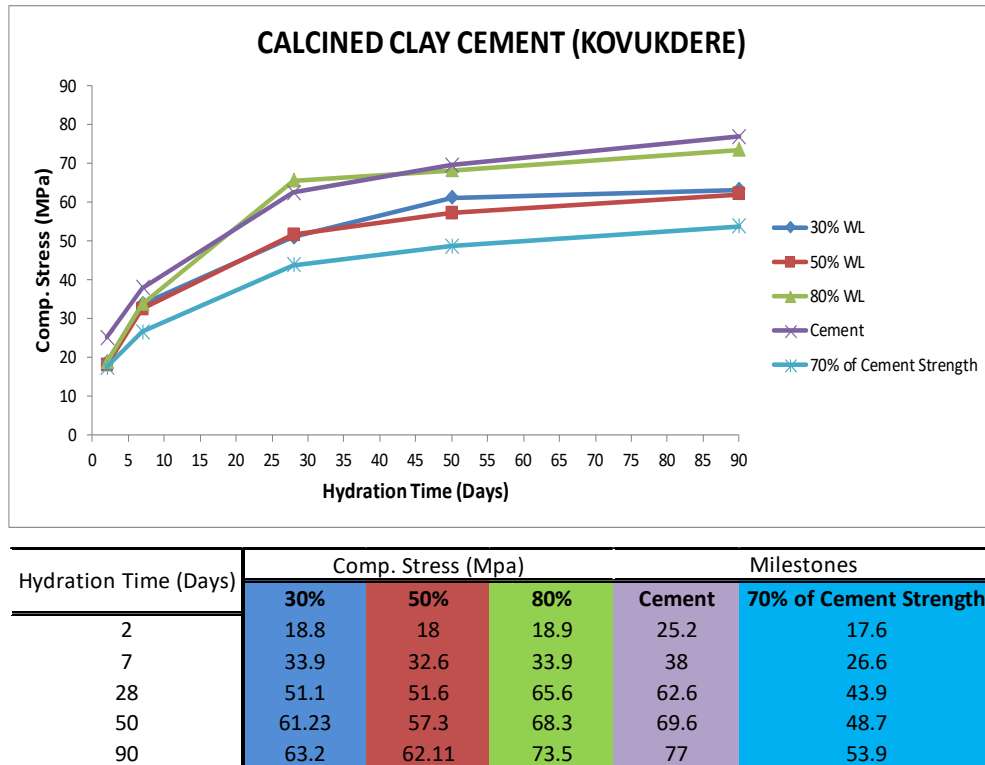


Figure 3. 103 Comparison of compressive strength of Kovukdere sample subjected to different calcination temperatures with cement and 70% of cement compressive strength

Kovukdere samples at all heat treatment temperatures show good pozzolanicity and acceptable strength values. All of them had almost the same behavior in the first days but 30% and 50% of samples had the same tendency, while the values of the 80% heat-treated sample had surprisingly increased. After 28 days the rise was reduced but still 50 days of pure cement amount is close to the value. The sudden change in 80% treated clay may be due to decomposition of the carbonates present in the powder composition. In addition, the more de-hydroxylation of the clay, the more reactive and better pozzolanicity of the material.

Figure 3.104 shows the difference in the compressive strength behavior of the Muratbey sample from pure cement.

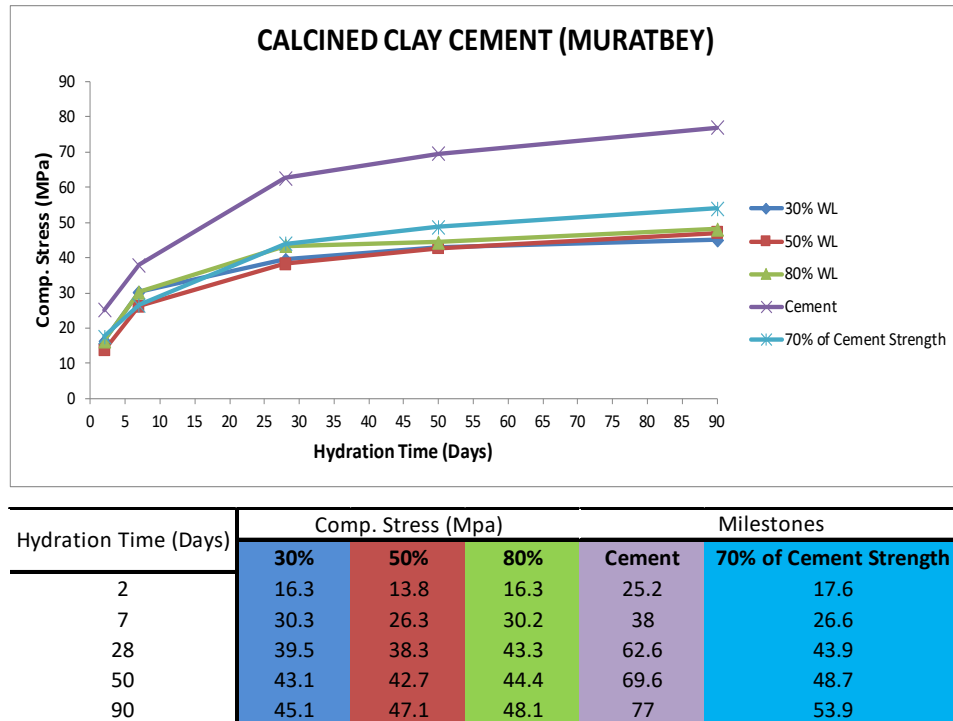


Figure 3. 104 Comparison of compressive strength of Muratbey sample subjected to different calcination temperatures with cement and 70% of cement compressive strength

The Muratbey sample was the sample with the lowest strength values among all samples. The strength behavior of the treated sample according to the strength measurements did not meet the expectation. This may be due to a small amount of decomposing clay and quartz, but all the strength curves are below 70% of cement strength. Therefore, it is very difficult to consider this sample as a potential candidate. The sample also includes some non-reactive silicate phases.

Figure 3.105 shows the difference in the compressive strength behavior of the Camlica sample from the pure cement.

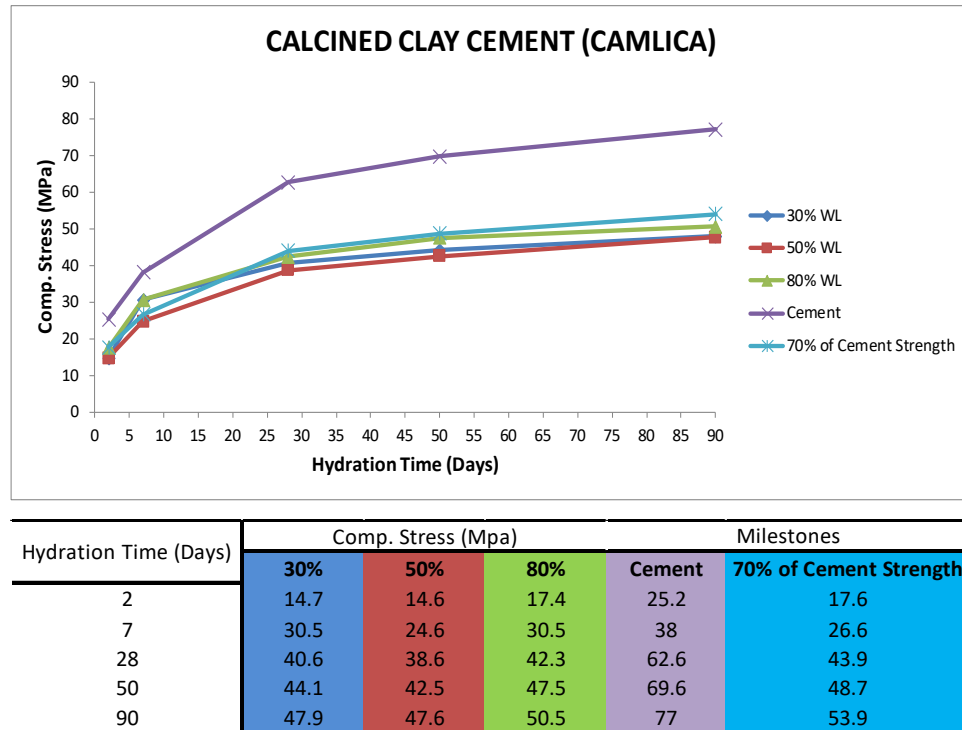


Figure 3. 105 Comparison of compressive strength of Camlica sample subjected to different calcination temperatures with cement and 70% of cement compressive strength

Although Camlica performs better than Muratbey, its values are not within the acceptable range. This sample showed an upward trend in the early days, but the rise was not permanent. As it is noted earlier about Camlica sample, there are various chemical phases, including clay and carbonates, but the amount of these phases is very small compared to the inert phases. As a result, despite having good pozzolonicity values, the strength property is very poor and is therefore not an acceptable candidate.

Figure 3.106 shows the difference in behavior of the Kaolinite sample in compressive strength from pure cement.

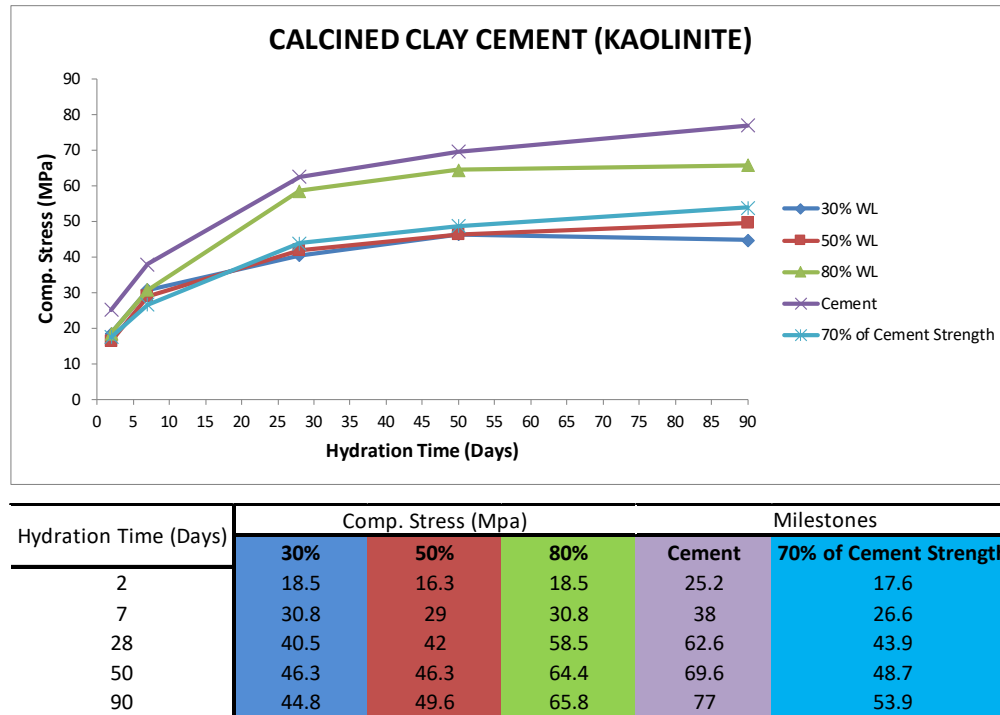


Figure 3. 106 Comparison of compressive strength of Kaolinite sample subjected to different calcination temperatures with cement and 70% of cement compressive strength

Kaolinite was chosen as a reference sample and its pozzolanicity and strength behaviors were already studied and discussed. Kaolinite also showed the acceptable strength performance as calcined clay, but the strength test results show the tangible difference between calcination temperatures of 80% to 50% or 80% to 30%. If more temperature effects on the pozzolanicity of the sample, it can be substituted cement as proper meta-kaolin. These results confirm the studies in the literature.

3.5 Discussion

To summarize, characterization of the samples and strength measurement were performed for all samples. For evaluation, six schist type powder received from mine quarries inside the Turkey. Studies on the transformation of Kaolinite into meta-kaolin by powder calcination have already been conducted. Therefore, Kaolinite was identified as a reference sample in this study. In the first stage, all raw powders were evaluated by pozzolanicity and some other characterization tests. The predefined heat-treatment was then applied to all samples in three steps. These steps were determined considering the temperature range for various mass loss of each sample. Then the accurate temperature corresponds to 30%, 50% and 80% of total weight loss was calculated for heat-treatment of samples. The heat treatment procedure was initiated by heating the samples to the specified temperatures, and after 120 minutes waiting, air-quenching was carried out to keep the decomposed phases stable. These measurements were also made for the treated materials considering the material properties and electrical conductivity, and finally the compressive strength measurements were considered as the most important criterion for the evaluation of the materials. Samples were prepared by substituting 30% of cement with calcined clay. The setting time for all samples was 2, 7, 28, 50 and 90 days. The compressive strength test confirmed some assumptions about samples with optimum values, but somewhat contradicted the pozzolanicity measurements. This contradiction was thought to come from the carbonate source of the materials. In addition, it results from the opposite reaction to increase the electrical conductivity. Carbonates regenerate ionized calcium and hydroxide and influence the reduction in electrical conductivity, while using calcium hydroxide causes a decrease in electrical conductivity.

As a result, Kovukdere and Tastepe were the main candidates for partial cement substitution. Other powders, however, could not show the appropriate results. It may be necessary to add minerals for the correct assessment of other candidates. This point will be addressed in the next section of the study. Since reservoir of Kovukdere and Tastepe clay powders will not be available for long periods of time, the empowerment of other raw powders may be important for applicability of this study in industrial scale. According to the results, it is seen that carbonate phase can play an important role in the hydraulic reactivity of raw materials.

Therefore, for non-reactive or semi-reactive materials, it may be necessary to assess the effect and application of the carbonate's additive.

In this part, it is tried to make inferences. Active aluminosilicate (hydrate) minerals could exist in different forms (crystal or amorphous), but not all clay phases are reactive. In addition, some of the raw materials contain carbonate compounds. The different characterization techniques were used during the studies. The XRD technique can only gather information about the phases in the crystal structure. However, it does not give clear information about amorphous phases. All mass loss (amorphous and crystalline clay phases and carbonates) from the material can be found in thermogravimetry studies, but due to the phases losing mass at the same temperatures, it cannot give a clear answer in the quantification of the phases separately. In order to determine the amount of clay that can be activated in the raw materials, the theoretical mass loss obtained from the amount of clay crystals obtained from XRD measurements and the mass loss observed in the TGA results were compared. If the TGA mass loss is higher than the theoretical mass loss, it means that the raw materials have an amorphous content which cannot be determined by XRD technique. If the TGA mass loss is less than the theoretical mass loss, this means that not all the aluminosilicate hydrate phases detected in the XRD can be activated. For the theoretical calculation of mass loss, it was accepted as the first approach that the clay structure in all raw materials was in the kaolinite structure. A layer of silica and an aluminum hydroxide layer are present in the kaolinite. During de-hydroxylation, one water release from the two hydroxide ions and remains in the structure for the function of active interface in an oxygen aluminum layer. In the calculations presented in the meantime, clays in all raw materials were accepted in kaolinitic structure. This may cause the mass loss to be expected to be ~ 30-40% larger than it may actually be. However, amorphous clayey will give important information about the phases. In the previous sections, it is tried to estimate the amount of amorphous material in the raw materials from the large peak that appeared in the XRD curves. It is found that this wide amorphous peak was different in various raw materials. This amorphous structure may be different glassy phases and may also include non-activated phases.

In the following tables, the focus is on decomposable phases especially the clay and carbonate that cause mass loss. In these tables, XRD and TGA results were re-shared. Table 3.38 shows these values for Kaolinite. No carbonate phase was detected in kaolinite. The amount of

kaolinite calculated by XRD Rietveld analysis is about 56% by weight. The mass loss observed in the same sample TGA is 7.55% of the total weight.

The theoretical mass loss from the activation of the clay phase in all samples was calculated based on the chemical formula of kaolinite ($\text{Al}_2\text{Si}_2\text{O}_5(\text{OH})_4$). That is, the mass loss resulting from the evaporation of theoretical water was calculated by counting an aluminum hydroxide layer to a silica layer. However, other clays, except kaolinite and its polymorphs, have an aluminum hydroxide layer on two silica layers. Some other clays (montmorillite and illite type), both molecular weights and relative structural water losses due to displacement of silicon / aluminum, Fe / Al or Mg / Al are different. The calculations given here should be considered as an initial estimation. For this calculation, the molecular weight of kaolinite was taken as 258 (Al = 27, Si = 28, O = 16, OH = 16 + 1 = 17 so K = 258). Considering that two water molecules will release from the kaolinite during activation, this mass is 34/258. Therefore, if the mass loss observed in TGA is more than $34/258 \times \text{kaolinite XRD\%}$, it means that there is activatable clay in the powder which XRD cannot detect. If this value is less than the theoretical one, it means that all kaolinite cannot be activated. The amount of clay that can be activated can be calculated from the TGA results. By employing this method, the amount of inactive clay in kaolinite powder is given in Table 3.41. Since there is no carbonate in this sample, it is assumed that all mass loss comes from clay.

Table 3. 41 Crystalline and inert portion of clay in Kaolinite

Sample	XRD Phase Amount (wt%)	TGA Mass Loss (wt%)	Explanation
Kaolinite	56% Clay	7.55% Clay	Amorphous Clay
Activatable Clay		57.5 Total Clay	1.50%

The amount of amorphous clay in kaolinite sample is about 1.5% by weight. The same calculations were carried out for Bozalan sample in Table 3.42. Calculations were done as if kaolinite was present as clay phase.

Table 3. 42 Crystalline and inert portion of clay in Bozalan

Sample	XRD Phase Amount (wt%)	TGA Mass Loss (wt%)	Explanation
Bozalan	40% Clay 8% Carbonate	1.48% Clay 3.55% Carbonate	Inactive Phase
Activatable Clay		11%	41-11=29%

It is assumed that only mass losses below 700 °C are due to clay since there is a portion of carbonate in the Bozalan sample. Based on calculation, the amount of clay that can be activated in Bozalan is 11% and the amount of clay that cannot be activated is 29%. Nevertheless, Bozalan performed relatively well in term of strength tests. This performance could be related to the carbonate phase and its reactivity. According to XRD results, there are no crystalline clay minerals in Tastepe powder sample. However, there is still a mass loss of 1.1% when the mass loss from the carbonate decomposition is omitted. This probably comes from the amorphous clays. Accordingly, in this sample, up to 9% of amorphous clays are not visible in XRD that is shown in Table 3.43.

Table 3. 43 Crystalline and inert portion of clay in Tastepe

Sample	XRD Phase Amount (wt%)	TGA Mass Loss (wt%)	Explanation
Tastepe	32% Carbonate	1.17% Clay 9.18% Carbonate	Amorphous Clay
Activatable Clay		11%	8.90%

According to these results, the proper performance of Tastepe powders in strength tests can be related to the high amount of carbonate phase in this powder. However, this may negatively affect the long-term strength of the composite cement. Corrosion and cracks, especially due to sulfate, can be a problem.

The Camlica powder contains almost equal amounts of carbonate and clayey material. By calculation of mass loss, the amount of clay that can be activated in Camlica schist decreases to 7% while 8% of clayey material is inactive. These results are shown in Table 3.44.

Table 3. 44 Crystalline and inert portion of clay in Camlica

Sample	XRD Phase Amount (wt%)	TGA Mass Loss (wt%)	Explanation
Camlica	15% Clay 14% Carbonate	6.58% Clay 3.82% Carbonate	Inactive Clay
Assumed Inactive Clay			15-7=8%

There is a small amount of active clay in Camlica. However, there is a considerable amount of carbonate in this powder. Camlica schist may be used as a source of carbonate for other schist samples.

The amount of clay that cannot be activated in the Kovukdere sample is shown in Table 3.45. As it can be seen from the Kovukdere strength tests, it is the clay containing schist that can be activated at the highest rate.

Table 3. 45 Crystalline and inert portion of clay in Kovukdere

Sample	XRD Phase Amount (wt%)	TGA Mass Loss (wt%)	Explanation
Kovukdere	54% Clay 16% Carbonate	6.42% Clay 9.84% Carbonate	Inactive Clay
Assumed Inactive Clay			56-48=6%

Moreover, Kovukdere schist carries its own carbonate. Therefore, it is not surprising that Kovukdere performs so well.

Muratbey schist has similarities with Kovukdere and comes from the same region as mine location. The amount of clay that can be activated in Muratbey schist is high with 32%. However, the carbonate phase in Muratbey schist did not found by XRD. Despite the relatively high amount of clay, the strength values of Muratbey schist as a supplementary cementitious material were disappointing. Table 3.46 shows the inactive phase amount in this sample.

Table 3. 46 Crystalline and inert portion of clay in Muratbey

Sample	XRD Phase Amount (wt%)	TGA Mass Loss (wt%)	Explanation
Muratbey	42% Clay	9.43% Clay	Inactive Clay
Assumed Inactive Clay			42-32=10%

Muratbey schist does not contain carbonate. Due to the possible potential of this schist sample, it would be beneficial to enrich it with the carbonate phase and re-evaluated.

The amount of non-activatable clayey phase of Ladik schist is shown in Table 3.47. Most Ladik clay can be activated, but it is not yet clear why this powder performs better than Muratbey.

Table 3. 47 Crystalline and inert portion of clay in Ladik

Sample	XRD Phase Amount (wt%)	TGA Mass Loss (wt%)	Explanation
Ladik	42% Clay	9.43% Clay	Inactive Clay
Assumed Inactive Clay			42-32=10%

Perhaps more performance can be obtained by adding carbonate to Ladik clay with the addition of Camlica.

3.6 Conclusion

So far, at least three of the six sample raw materials (Kovukdere, Tastepe and Bozalan) based on the results are proper substitute. Table 3.48 ranked the potential schist type raw materials. At the same time, it is possible to put theoretical calculations on better scenarios in order to better determine the potentials of schist samples. According to the obtained results, Kovukdere has outperformed expectations and study target. More than Kovukdere, Tastepe and Bozalan schists showed a performance close to the target of 28 days strength (at least 90% of the strength of the paste prepared with pure cement).

Table 3. 48 Sorting table of all sample in term of applicability of schist as possible potential for partial substitution of cement (Darker color = more potential)

Ranking	Sample
1st	Kovukdere
2nd	Tastepe
3rd	Bozalan
4th	Ladik
5th	Camlica
6th	Muratbey

CHAPTER 4

LIMESTONE CALCINED CLAY and CARBONATE CEMENT (LC⁴)

4.1 General

As it is stated, this study intends to evaluate the potential of a local schist mine as ordinary Portland cement substitution. In previous chapter, six different samples from various parts of Turkey were studied for their potential as a proper SCM material. They were from Kovukdere, Muratbey, Camlica, Bozalan, Ladik and Tastepe stone quarries. All of them were calcined up to temperatures that would provide 30, 50 and 80% of total weight loss associated with the de-hydroxylation of clay minerals contained in the schists. Calcined clay cement paste was prepared by replacing the OPC with 30 wt% calcined clay. The compressive strength measurement showed that the Kovukdere and Tastepe were the possible candidates for SCMs. According to the X-ray diffraction, the main difference of these two samples was

an increased amount of carbonate phases besides clayey minerals. In addition, the composition of Kovukdere and Muratbey resembled to each other strongly except for their carbonate content. These results necessitated further studies with engineered mine compositions.

Based on the availability and amount of the deposit, Muratbey was selected as the base schist whose composition will be tailored with carbonate additions. Four different samples were taken from different locations of the Muratbey mine quarry according to their appearance (colors). They were analyzed for their phase composition. The chemical and phase compositions of these four samples were similar while the amounts of carbonate were different. In addition, M₄ contained graphite and pyrite on top of clayey type materials and carbonate. All samples were topped off up with carbonate (calcite from Muratbey mine) such that their carbonate contents became 15 wt% like the phase distribution of Kovukdere schist. Based on the results obtained in the first phase of project, all tailored samples were later calcined up to corresponding temperatures that would yield 80% of the total weight loss. The four new custom-designed samples were called M₁ (Green), M₂ (Brown), M₃ (Pink) and M₄ (Black). Calcined unmodified samples were labelled as C³, and carbonate added, custom-designed and calcined samples were labelled as LC⁴.

The cube samples (4cm.4cm.4cm) were prepared for all calcined schist type powders. To ascertain the effect of carbonate, values of LC⁴ samples were compared to the values obtained from the same sets of C³ (Calcined Clay Cement). The results of the compressive strength measurement showed that the carbonate chemical phase could influence the strength of composite cement paste drastically. Among all four types of samples, calcined M₄ schist type powder showed the highest potential to be a partial cement substitute.

4.2 Experimental

4.2.1 Materials

The Muratbey mine is one of the mines that belong to AkcanSA cement manufacture in Istanbul near Catalca district. This mine includes around 2 km² as area. Figure 4.1 shows the approximate location and area of the Muratbey mine.



Figure 4. 1 Muratbey mine (Catalca District) – Google Earth

It is obvious from the appearance of different sections of the quarry that there would be a variation in chemical composition of Muratbey mine sections, inferred from the color variety. Therefore, four different samples were taken from the mine quarry. Figure 4.2 illustrates the chunks of the four schist type samples which were obtained from four parts of mine quarry.



Figure 4. 2 Four different samples from Muratbey mine quarry

The four approximately 40 kg rock samples were taken to AkcanSA cement manufacture for grinding and storage. Figure 4.3 shows the ground schist type samples that are classified according to their colors.

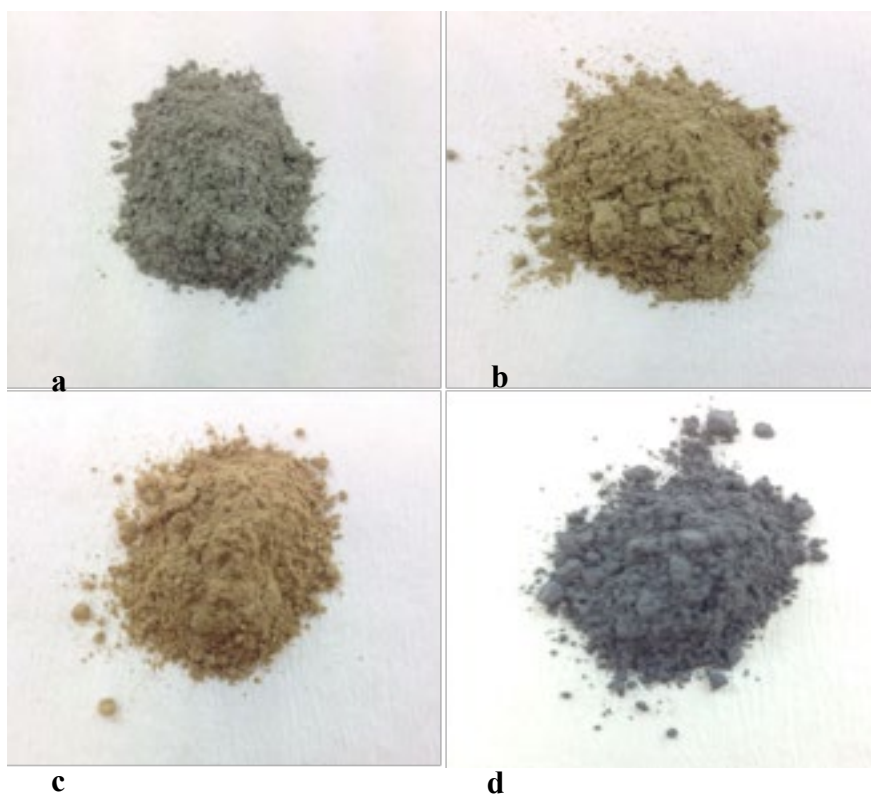


Figure 4. 3 Ground powder Muratbey schist type samples ready for calcination as (a) M₁-Green, (b) M₂-Brown, (c) M₃-Pink and (d) M₄-Black

The M₁ and M₂ were obtained from two neighboring locations in Muratbey mine that were only seven meters away from each other. The other two samples were from a short distance away from the green and brown labelled samples. It appeared that a sort of geological phenomena (faults) maybe the reason for the variations in the mine region. Regardless of topographical identification, chemical compositions, phase structure and potential of the all received virgin powders were evaluated with the help of the listed characterization methods. The Ordinary Portland Cement (OPC) is an ENS 197-1 CEM 42.5 R type which is provided by AkçanSA Cement Manufacturer. The limestone (\overline{CC}) with the particle size of $\leq 5 \mu\text{m}$ is also provided by AkçanSA.

4.3 Sample Preparation

4.3.1 Calcined Clay Cement (C³) Samples

The decomposition behavior of virgin schist with and without carbonate additions was obtained from the thermogravimetric analyses (not shown here but given in result section). Also, the total weight losses due to de-hydroxylation were calculated. Based on the experiences gained in the first phase of the project, it was determined that the optimum and safe calcination temperature is associated with 80% of the total weight loss. This temperature was experienced to be enough for the decomposition and activation of most of the clayey minerals in our schist samples and for avoiding overheating which causes dead-burning of clay. Hence, the proper activation temperatures for each sample were calculated as it will be described in the next section.

The accurate temperature associated to the 80% of total weight loss were calculated and all the powders were heat treated or in another term calcined up to this temperature with a heating rate of 10°C/min. The calcination method was determined to follow the stepped heating schedule. Powders (600 gr) were heat treated up to the starting point of the decomposition interval (300°C) in crucibles, followed by a dwell time of 1 hour and then heated up to temperature associated to 80% of total weight loss and keeping the temperature

constant at this temperature for 2 hours. These isothermal steps of heat treatment were applied to samples to homogenize the heat distribution within the powders of 600 grams. Then, crucibles containing heat treated materials were cooled down to the room temperature by air quenching.

4.3.2 Limestone Calcined Clay and Carbonate Cement (LC⁴) Sample

All the four schist mine powders were topped up to 15 wt% calcium carbonates content to obtain M₁, M₂, M₃ and M₄ with 15% CC. Indeed, these samples are obtained by adding a certain amount of calcium carbonate to virgin schist type material in a way that its total calcium carbonate content reaches to 15 wt%. After that, the same heat treatment and air quenching processes as C³ were performed on the LC⁴ samples.

4.3.3 Cement Paste Sample Preparation

After the calcination process and activation of the schist type materials with and without calcium carbonate, these activated samples were added to the Ordinary Portland Cement (OPC) such that 30 wt% of the solids (i.e composite cement mixture) is activated schist and 70 wt% is OP cement. For the strength measurement a series of cement paste samples with the w/solid ratio of 0.5 were prepared by mixing 700 g of cement, 300 g of one of the calcined materials and 500 g (500 mL) water. The samples for the compression test were then prepared by casting all the composite cement paste samples described earlier in the molds with the dimension of 40×40×40 mm. These composite cement samples were designed as M_x or M_x with 15% CC. The x subscript indicates the number of the calcined schist type material. Also, in order to compare the strength of the C³ and LC⁴ samples with OPC, a standard benchmarking cement paste sample was prepared by casting a mixture of 100% OP cement and water, with the same w/solid ratio in the same molds. After 24 h, the molded samples were separated from the molds, and put into circulating water with the temperature of 23°C and

kept there until the compression test days which were specified as 2, 7, 28, 50 and 90 days of hydration. Details of the compression test will be given in the characterization part.

4.4 Tests and Methods

4.4.1 Phase Analysis

The best phase identification for materials with unknown phase content is the x-ray diffraction analysis. Therefore, at the first step the x-ray spectrum from each virgin sample was analyzed. X-ray diffraction analyses are done using Bruker D8 Advance diffractometer utilizing Cu-K α ($\lambda=1.54$ Å) radiation. The divergence slit size is fixed and was 0.5° . Samples were scanned on the rotating stage between 5 to $90 [^\circ 2\theta]$ using step size of $0.02^\circ 2\theta$ and time per step of 1s. Rietveld analysis was carried out on samples to identify and quantify the amount of potentially pozzolanic and inert phases. Also, the amorphousness to crystallinity ratio of all virgin samples were determined by using the same software. The XRD diffractogram of all calcined powders were also analyzed and compared to the virgin powders to observe the effects of the calcination process. It should be mentioned that in case of LC⁴ powders, the comparison was performed between schist with 15% carbonate and the same mixtures after calcination. To test the accuracy of the XRD device and the software about the phase distribution of the samples and the crystallinity and amorphousness values, another experiment was designed. In fact, in order to correct the amount of graphite in one of the samples (which contained graphite), an experiment was done on a composite sample containing graphite and calcite with known amounts of the two phases. The same x-ray procedure was applied to this composite to determine the correct amount of graphite from x-ray analysis. In order to make a mixture with known amounts of graphite and calcite, 5 g of graphite powder was added to 95 g of calcite, and then the phase analysis was done on the mixture by using XRD. The results of the phase analysis and the proportion of two phases will determine the accuracy of the analysis.

4.4.2 Thermal Analysis

Thermal analysis [TG/DTA] (NETZSCH STA 449 JUPITER, Selb, Germany) of the samples were done in a temperature range between 30°C and 1000°C under Nitrogen gas. N₂ atmosphere was chosen in order to eliminate the possibility of oxygen in air reacting with some components of some samples (e.g. Sulfur and graphite). The heating rate was 10 K/min. For every run 50mg of as-received powder sample was used. This amount of specimen mass is a very small compared to the bulk powder samples which were calcined for preparing compressive test samples. Thermogravimetric analysis of each sample would extract an important data about the decomposition temperature range of virgin schist powder and the amount of weight loss that represent the potential reactivity of it. Based on the information extracted from the TGA graphs of the virgin samples, the proper temperatures for activating each of the schist type samples were determined. For each sample, the activation temperature is the temperature associated to 80% of total weight loss in the virgin sample's TGA graph. Additionally, in order to control the accuracy of calcination process, the virgin and heat-treated powders were also evaluated by thermogravimetric analysis. After calcination process, the total weight loss extracted from the TGA graph of the calcined sample should be 80% of the total weight loss of the virgin one. In order to define the reason for early decomposition of calcium carbonate when schist type material contains carbonate, another experiment was designed. Two TGA tests were done on 50 mg of calcium carbonate with two different heating rates of 1 K/min and 10 K/min. The comparison between these two TGA graphs will show the kinetic effect on the early decomposition of calcium carbonate.

4.4.3 Microstructure Analysis

In order to identify the differences between the virgin and calcined version of each sample, the microstructure of both virgin and calcined powders was characterized using a scanning electron microscopy coupled with energy dispersive X-ray microanalysis (SEM/EDS).

4.4.4 Compression Test

In order to evaluate the effect of activated samples on the early and late strength of cement, the compression test was done on all composite cement samples. The compressive strength measurement is the best indication to evaluate the potential candidates for cement substitution. This test was carried out on the 40×40×40 composite cement samples until failure using a MATEST E161N Servo-plus evolution compression test machine. For each composition and each hydration time, the given compressive strength values in the results section is the average of the strength of three samples. The compressive strength of the calcined clay cement (C^3) and limestone calcined clay and carbonate cement (LC^4) are then compared to indicate the effects of activated clay materials and also limestone on the early and late strength.

4.5 Results

4.5.1 Virgin Materials (Before Activation)

4.5.1.1 Phase Distribution

4.5.1.1.1 M₁ - Green

The main purpose of this study is to find the best potentially pozzolanic candidate for cement partial substitution. So, the schist virgin powders which contain higher amounts of potentially reactive phases deserve closer consideration in this study. Figure 4.4 illustrates x-ray diffractogram of virgin M₁-Green schist samples.

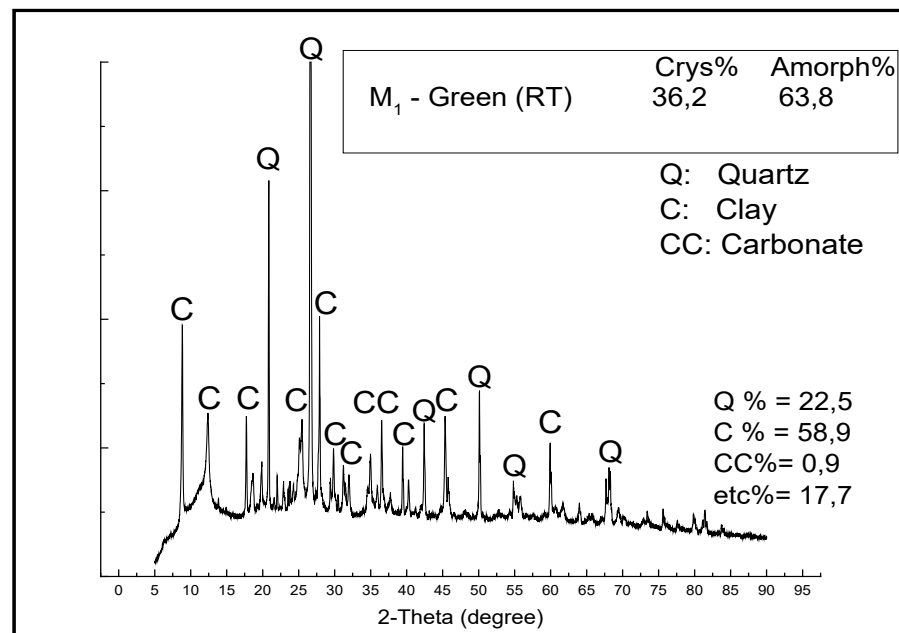


Figure 4. 4 M₁-Green schist type sample XRD spectrum and quantification

XRD analyses indicated that the virgin M₁ schist powder contains 36.2% crystalline and 63.8 wt% amorphous amounts. Crystalline phases included quartz, calcite and different types of

clayey minerals. The total amount of inert quartz phase was estimated as ~ 22.5 wt% and the total clayey content portion was around 58.9 wt%. The dominant clayey phase is illite (24.5 wt%). The amount of carbonate phase was calculated as 0.9 wt%. Other phases constituted 17.7 wt%. Table 1 lists the quantitative phase composition of M₁ sample. Their physical and chemical information (i.e. crystal structure and chemical formula) and weight percentages are also included.

Table 4. 1 The Phase distribution and detailed information about crystal structure and weight percentage for each chemical compound in M₁-Green virgin powder

Chemical Phases	wt%	Crystal Structure	Chemical Formula
Quartz	22,5	Hexagonal	SiO ₂
Calcite	0,9	Rhombo	CaCO ₃
illite	24,5	Monoclinic	(K , H ₃ O) Al ₂ Si ₃ Al O ₁₀ (O H) ₂
Muscovite	23,1	Monoclinic	K Al ₂ Si ₃ Al O ₁₀ (O H) ₂
Albite	3,8	Triclinic	(Na , Ca) (Si , Al) ₄ O ₈
Clinochlore	6,5	Monoclinic	(Mg _{2.96} Fe _{1.55} Fe _{.136} Al _{1.275}) (Si _{2.622} Al _{1.376} O ₁₀) (O H) ₈
Dickite	4,8	Monoclinic	Al ₂ Si ₂ O ₅ (O H) ₄
Anorthite	12,1	Triclinic	Na _{.25} Ca _{.71} (Al ₂ Si ₂ O ₈)
Titanium Oxide	1,8	Monoclinic	Ti ₃ O ₅

In addition to inert quartz phase, M₁ schist sample contained several clayey material phases (e.g. illite, Muscovite, Clinochlore and Dickite). During the calcination the amount of activation of these chemical phases could determine the reactivity of schist type sample. Besides the clays there are, phases like Albite and Anorthite which have compositions similar to natural glasses. The amount of carbonate phase was not significant.

4.5.1.1.2 M₂ – Brown

The locations where the brown sample and the green sample were neighboring each other. Therefore, these two samples were expected to have similar chemical and phase composition. However, there was a significant difference in their clayey contents. Figure 4.5 illustrates x-ray diffractogram of virgin M₂-Brown schist samples.

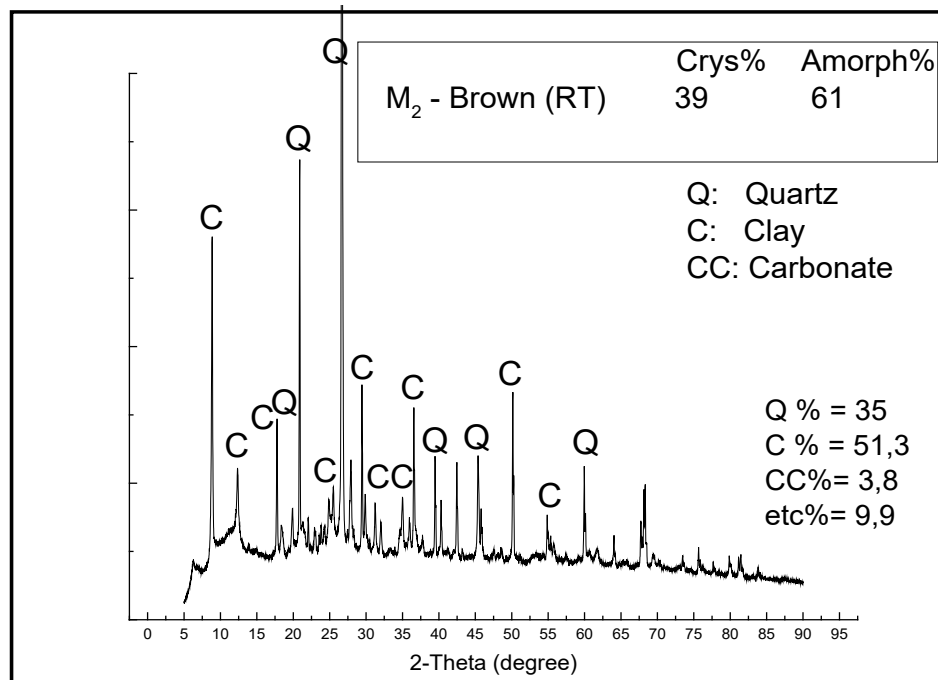


Figure 4. 5 M₂-Brown schist type sample XRD spectrum and quantification

The XRD program in house estimated from the X-ray diffractogram of M₂ sample 39% crystalline versus 61% amorphous content in this sample. Almost 35 wt% of this schist was quartz phase. The clayey portion of the schist was 51.3 wt%. A total of 3.8 wt% of it was carbonate phase. Other crystalline phases that have glass-like chemical compositions were around 9.9 wt%. Table 4.2 lists all existing chemical compounds of M₂ schist, their crystal structures and amounts.

Table 4. 2 The Phase distribution and detailed information about crystal structure and weight percentage for each chemical compound in M₂-Brown

Sample #	Chemical Phases	at%	Crystal Structure	Chemical Formula
1	Quartz	35	Hexagonal	SiO ₂
2	Calcite	3,8	Rhombo	CaCO ₃
4	Muscovite I	28,2	Monoclinic	K Al ₂ (Al Si ₃ O ₁₀) (O H) ₂
4	Muscovite II	16,1	Hexagonal	(K , Na) (Al , Mg , Fe) ₂ (Si _{3.1} Al _{0.9}) O ₁₀ (O H) ₂
9	Albite	4	Triclinic	(Na , Ca) (Si , Al) ₄ O ₈
5	Clinocllore	3,3	Monoclinic	(Mg ₅ Al) (Si , Al) ₄ O ₁₀ (O H) ₈
3	Kaolinite	3,7	Triclinic	Al ₂ (Si ₂ O ₅) (O H) ₄
7	Anorthite	5	Triclinic	Ca (Al ₂ Si ₂ O ₈)
8	Titanium Oxide	0,9	Orthorhombic	Ti ₃ O ₅

As a general statement, the chemical composition of M₂ schist resembled M₁, However, existing differences could vary their reactivity potential. The dominant crystalline clayey compound is Muscovite which is known as a complex clay crystal. The minor phases contained Albite, Anorthite and Titanium Oxide. Glassy content could take a part in reactivity. The carbonate phase amount is higher than the M₁ but still not enough to have significant effect on hydration processes.

4.5.1.1.3 M₃ – Pink

The Pink schist is another source of clayey materials in Muratbey mine region. Figure 4.6 shows the XRD diffractogram of virgin M₃ sample.

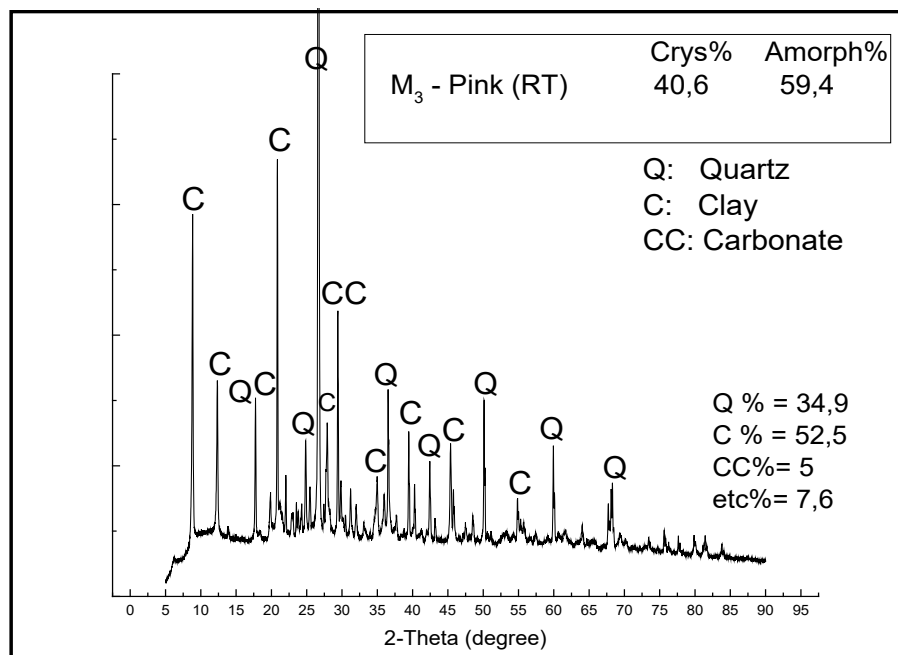


Figure 4. 6 M₃-Pink schist type sample XRD spectrum and quantification

The Rietveld analysis claims 40.6 wt% crystallinity and 59.4 wt% amorphous content of this schist sample. The inert quartz phase is estimated around 34.9 wt% while it contained 52.5 wt% of clayey structures. The calcite amount is almost 5 wt% that is still low for a strong

influence on hydration of pozzolans. Table 3 lists the phase composition of M₃ sample and their crystal structure and weight percentages.

Table 4. 3 The Phase distribution and detailed information about crystal structure and weight percentage for each chemical compound in M₃-Pink

Sample #	Chemical Phases	at%	Crystal Structure	Chemical Formula
1	Quartz	34,9	Hexagonal	SiO ₂
2	Calcite	5	Rhombo	CaCO ₃
4	Muscovite I	28,4	Monoclinic	$K (Al_{1.88}Fe_{0.12}) (Si_3Al) O_{10} (OH)_2$
4	Muscovite II	18,2	Hexagonal	$(K, Na) (Al, Mg, Fe)_2 (Si_{3.1}Al_{0.9}) O_{10} (OH)_2$
9	Albite	5,8	Triclinic	NaAlSi ₃ O ₈
3	Kaolinite	5,85	Triclinic	$Al_2 (Si_2O_5) (OH)_4$
8	Rutile	0,4	Tetragonal	TiO ₂

The clayey structures of M₃ sample is like M₂. According to the x-ray diffraction analysis results, the two mentioned samples projects a similar potential of reactivity.

4.5.1.1.4 M₄ – Black

The M₄ schist material appeared to be somehow different from the others. Based on visual inspection the color and appearance of this sample may put the reactivity of M₄ in question. Figure 4.7 illustrates the xrd spectrum of virgin M₄ schist sample.

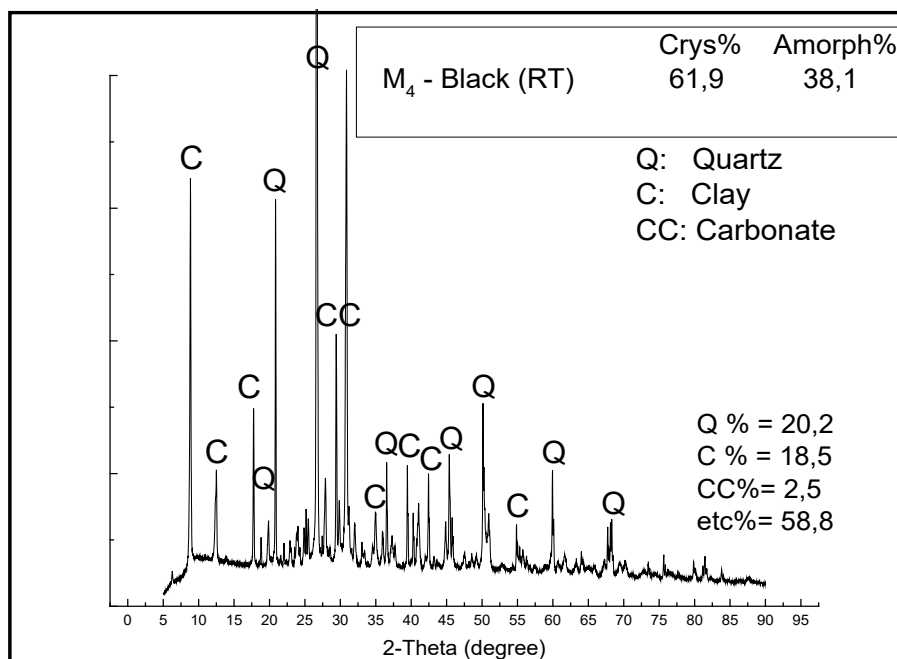


Figure 4. 7 M₄-Black schist type sample XRD spectrum and quantification

Table 4.4 lists the phases of M₄ sample and their crystal structure and weight percentages.

Table 4. 4 The Phase distribution and detailed information about crystal structure and weight percentage for each chemical compound in M₄-Black

Chemical Phases	wt%	Crystal Structure	Chemical Formula
Quartz	20.2	Hexagonal	SiO ₂
Calcite	2.5	Rhombo	CaCO ₃
Muscovite I	10.4	Hexagonal	(K , Na) (Al , Mg , Fe) ₂ (Si _{3.1} Al _{0.9}) O ₁₀ (O H) ₂
Ankerite	12.8	Rhombo	Ca (Mg _{0.67} Fe _{0.33} +2) (C O ₃) ₂
Albite	2	Triclinic	Na Al Si ₃ O ₈
Clinocllore	2	Monoclinic	(Mg _{2.8} Fe _{1.7} Al _{1.2}) (Si _{2.8} Al _{1.2}) O ₁₀ (O H) ₈
Mg-Annite	6	Monoclinic	K (Mg , Al) ₂ O ₄ (Si _{3.34} Al _{0.66}) O ₁₀ (O H) ₂
Graphite	42.7	Hexagonal	C
Titanium Oxide	0.8	Monoclinic	Ti ₃ O ₅
Pyrite	0.5	Cubic	Fe S ₂

A surprising phase of this sample was Pyrite that was 0.9 wt% of schist. According to the x-ray diffraction results for M₄ sample, it seems that there would less hope in terms of its activation.

Based on the quantification routine of the existing XRD software, in M₄ sample the amount of graphite exceeded 42.5 wt% of the powder. The peculiar property of graphite is the exaggerated peak intensity in x-ray diffractograms. In order to correct the exaggerated amount of the graphite, a known calibration experiment was conducted. The result of the experiment can be seen in Figure 4.8 that shows an unusually high intensity of graphite peak in a mixture of graphite and calcium carbonate with a mixing ratio of carbonate to graphite of 95 to 5 wt% respectively. The quantification routine of the XRD software showed 45% of graphite phase in the mixture that contained just 5% in reality.

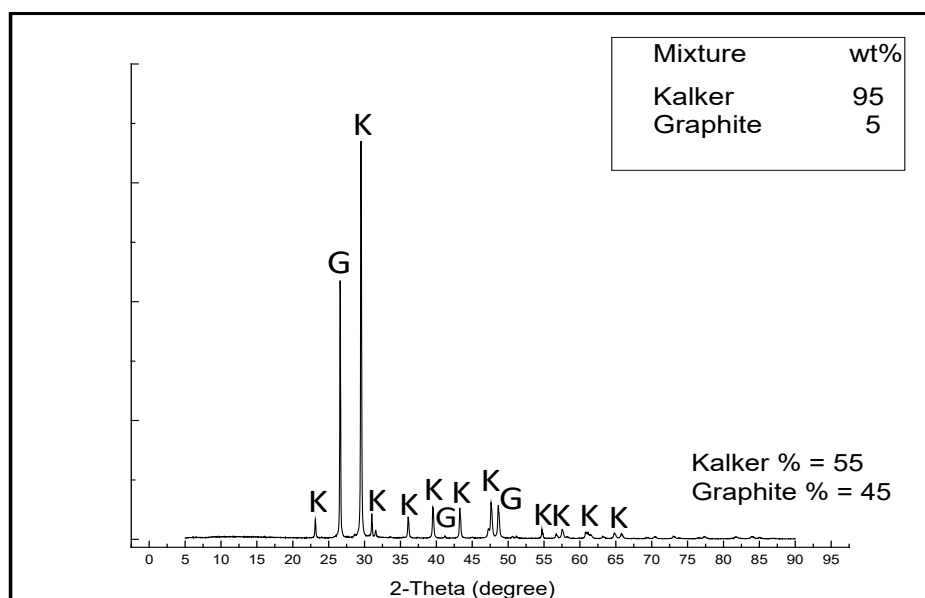


Figure 4. 8 Mixture of 95 wt% calcium carbonate and 5 wt% graphite XRD diffractogram

4.5.1.2 Activation Process

In order to determine the proper temperature for activation that should be applied to each sample, the TGA analysis were performed. The results threw light into the decomposition behavior of the samples.

4.5.1.2.1 M₁-Green

The M₁ schist thermogravimetric graph analysis is shown in Figure 4.9. The TG of the M₁ illustrated the decomposition temperatures associated with different chemical phases.

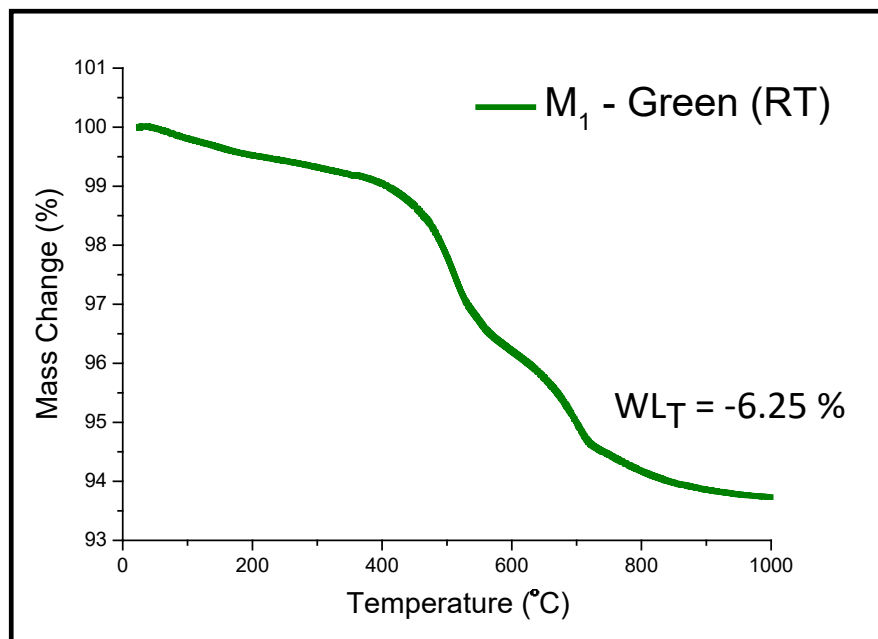


Figure 4. 9 TGA of M₁-Green virgin powder

Apparently, the low temperature weight loss was related to the non-structural water existing as moisture inside the powders. The total weight loss associated with clayey phases was around 5% that indicated a moderate reactivity of this schist. The main decomposition started around 350°C, and this decomposition reaction went up to 600°C. This early reaction was most likely related to the decomposition of one of the clayey materials which may be even in the amorphous portion of the powders. Since there are several clayey components in all schist samples, DTG showed a series of weight losses in the temperature range associated with the de-hydroxylation of clayey materials. Carbonate decomposition takes place in the 650°C to 850°C temperature interval. Some portion of weight loss could be related to the decomposition reactions of the amorphous phases of various chemistries.

4.5.1.2.2 M₂-Brown

The virgin brown sample thermogravimetric analysis represents the early decomposition of some clayey type component. Figure 4.10 illustrate the TG of the M₂-Brown schist.

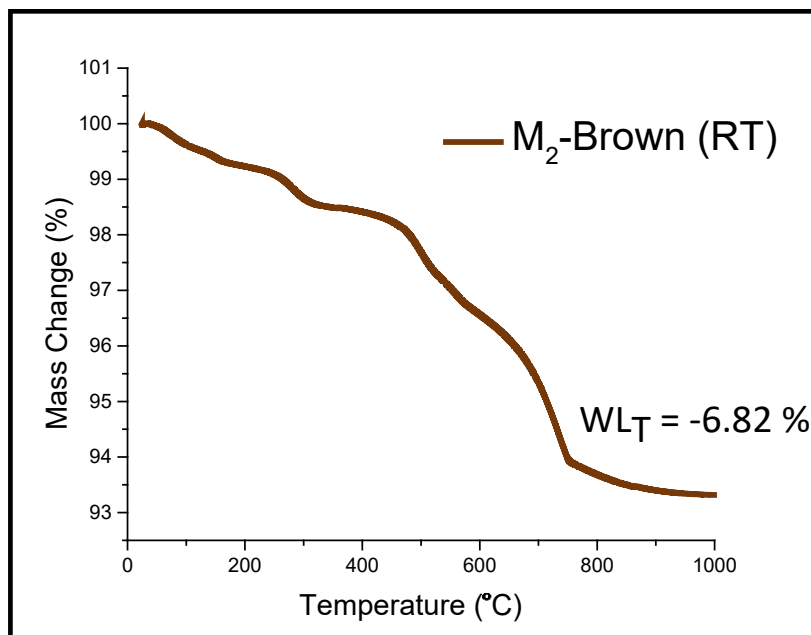


Figure 4. 10 TGA of M₂-Brown virgin powder

The decomposition started at around 250°C and the total weight loss was calculated as 5.29%. The clayey components de-hydroxylated in different temperature intervals up to 650°C. The carbonate decomposed between 650°C to 800°C. The total weight loss due to decomposition was not very different than M₁.

4.5.1.2.3 M₃-Pink

Figure 4.11 shows the TG graph of M₃-Pink schist. The decomposition temperature range and behavior resembled the one from M₂. The total weight loss that was around 6.43% confirmed this assumption that M₂ and M₃ are more similar to each other in their decomposable phase content than the two others.

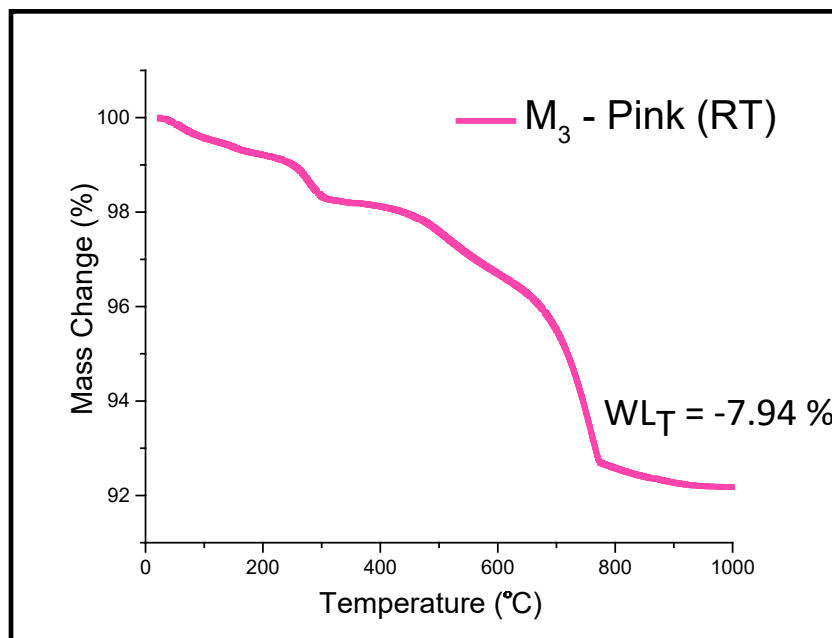


Figure 4. 11 TG of M₃-Pink virgin powder

The low temperature weight losses in TGA graph were related to the evaporation of non-structural water. The de-hydroxylation of clayey phases started around 450°C and continued until at least to 650°C. At this temperature, decomposition of carbonate phase started and lasted to 800°C at this heating rate.

4.5.1.2.4 M₄-Black

The thermogravimetric analysis of M₄-Black schist is illustrated in Figure 4.12.

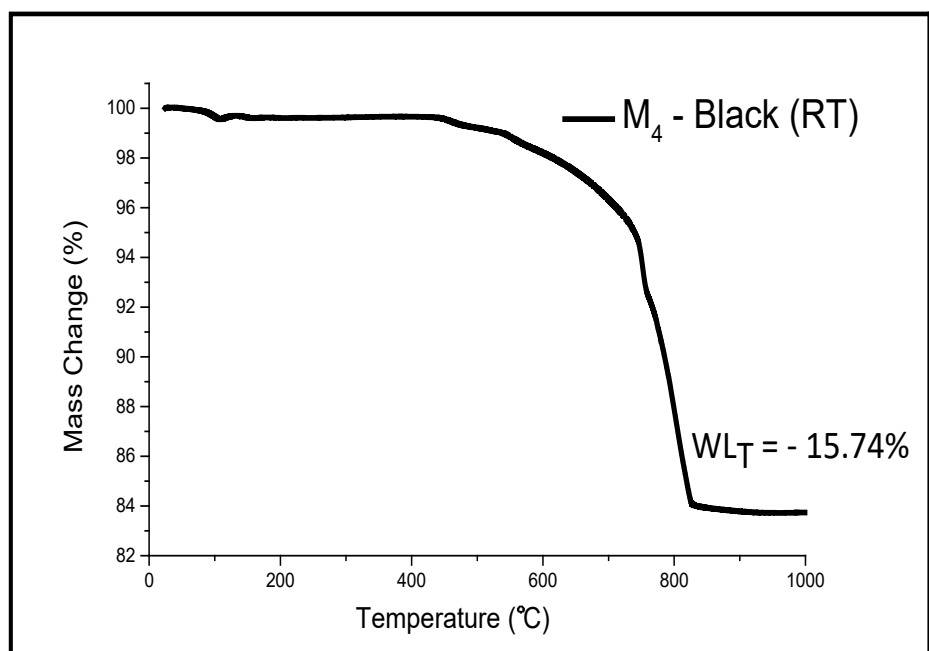


Figure 4. 12 TGA of M₄-Black virgin powder

The M₄ schist contained similar clayey components like the other samples from the same mine. However, the de-hydroxylation of these phases started at 500°C. It seemed as if that the crystal structure of the clayey phases in this sample were more stable. As indicated in the XRD phase analysis and was obvious from the color of this sample, it contained graphite which decomposed around 730°C. There were two different carbonate phases in M₄. Calcite and Ankerite decomposes in temperature range of 750°C to 830°C.

Temperature ranges that would correspond to 30%, 50% and 80% of the total weight losses due to de-hydroxylation or decomposition reactions were calculated based on the TG analyses of the schist and schist + carbonate samples. These temperature ranges are listed in Table 4.5.

Table 4. 5 Decomposition temperature intervals and total weight loss for schist powders w/o carbonate additive

Sample	Decomposition Starts @ (°C)	Decomposition End @ (°C)	80% of range (°C)	Total WL (mg)	Total WL (wt%)
M1 (Green)	350	760	640	2.48	-4.75
M2 (Brown)	300	780	680	2.52	-5.29
M3 (Pink)	300	800	740	3.32	-6.43
M4 (Black)	500	825	770	7.83	-15.64
M1 w/t 15% CC	300	825	770	5.51	-10.89
M2 w/t 15% CC	300	830	768	4.9	-11.32
M3 w/t 15% CC	300	825	770	5.24	-10.95
M4 w/t 15% CC	500	850	810	9.93	-18.51

As it can be seen in the table the accurate temperature associated to the 80% of total weight loss were calculated and all the powders were heat treated or in another term calcined up to this temperature. These temperatures are calculated based on the TGA analysis which 50 mg of each sample was used. In real experiments which the sample amount in the box furnace is at least 500 mg, the heat treatment of this massive amount may differ from the TGA analysis.

4.5.1.3 Microstructure Analysis

4.5.1.3.1 M₁ – Green

The electron micro-graphs helped to evaluate the M₁ schist phase distribution according to their appearance. Figure 4.13 shows the microstructure of green schist in different magnifications.

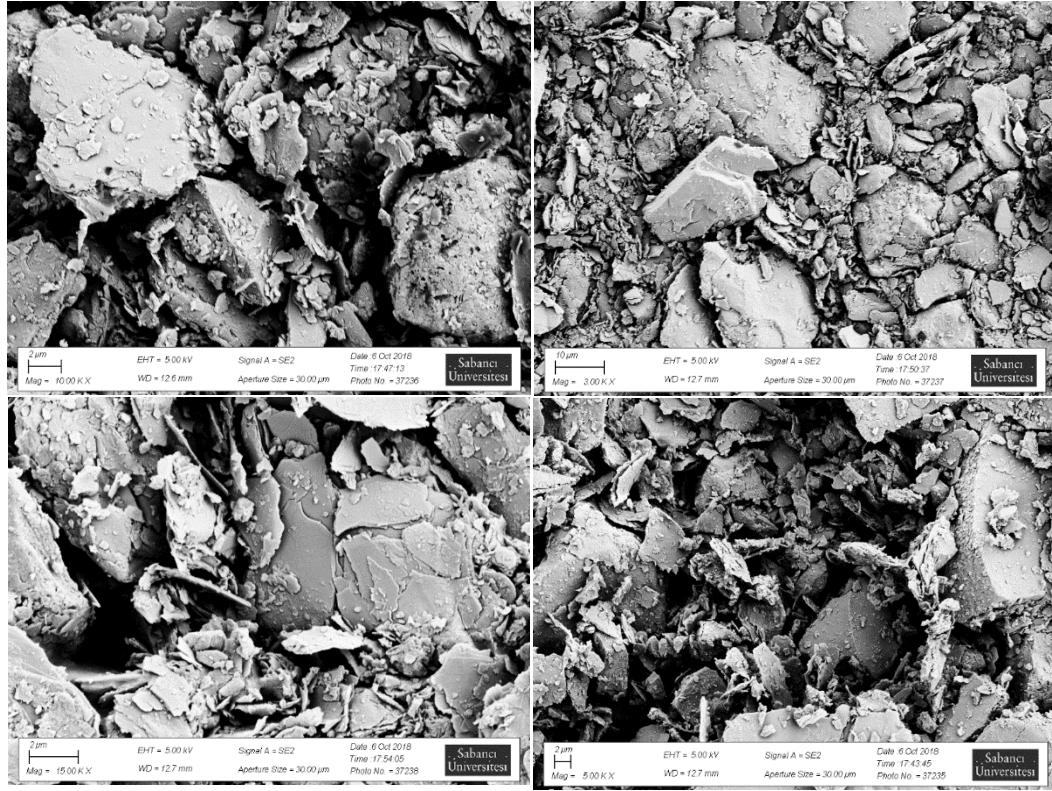
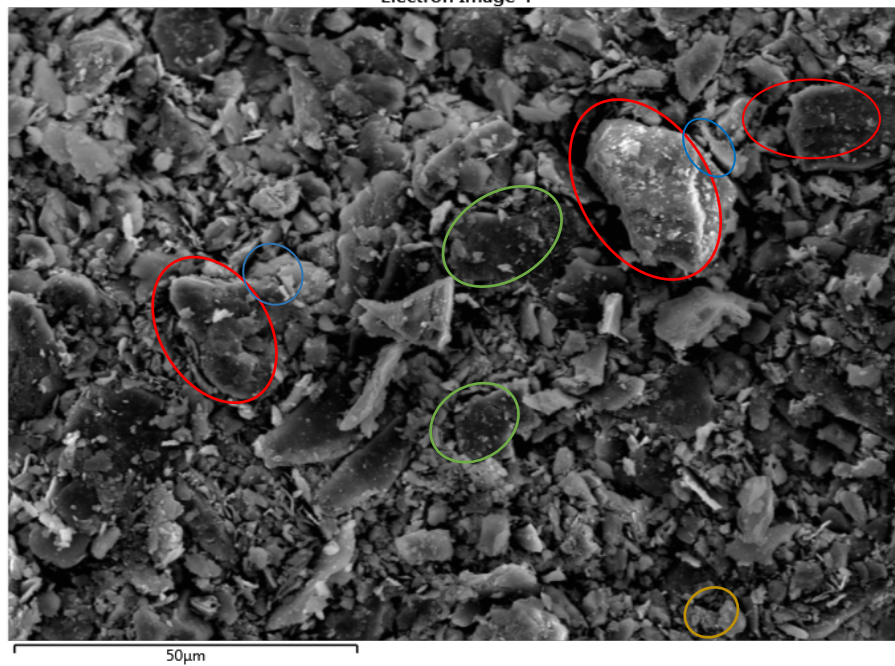


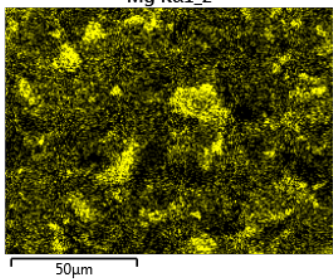
Figure 4. 13 M₁- Green schist type sample micrograph in different magnification

As it can be seen the M₁ micrograph, the main obvious components of this schist type material were quartz and clayey phases. The layered structure like non-symmetric sheets were interpreted to be clays. Also, the calculated average particle size for this sample was around 33 μm. For further identification of these various prismatic shapes, EDS analysis was carried out. Figure 4.14 represent the elemental distribution map in M₁ schist obtained with EDS.

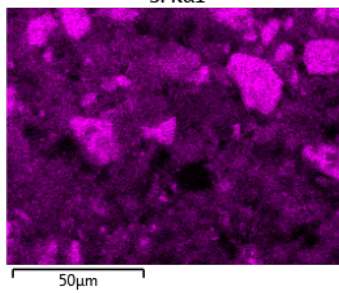
Electron Image 4



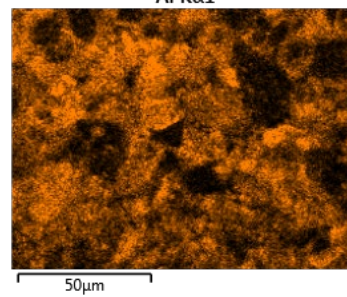
Mg K α 1_2



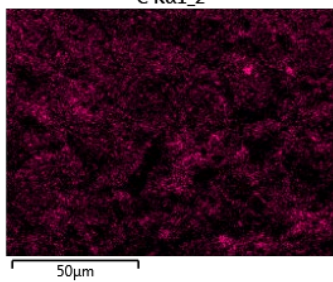
Si K α 1



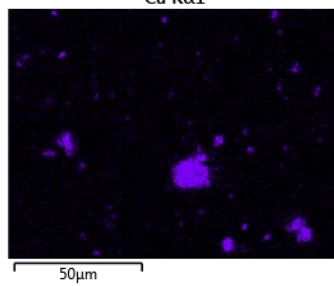
Al K α 1



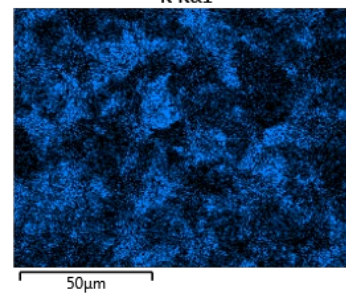
C K α 1_2



Ca K α 1



K K α 1



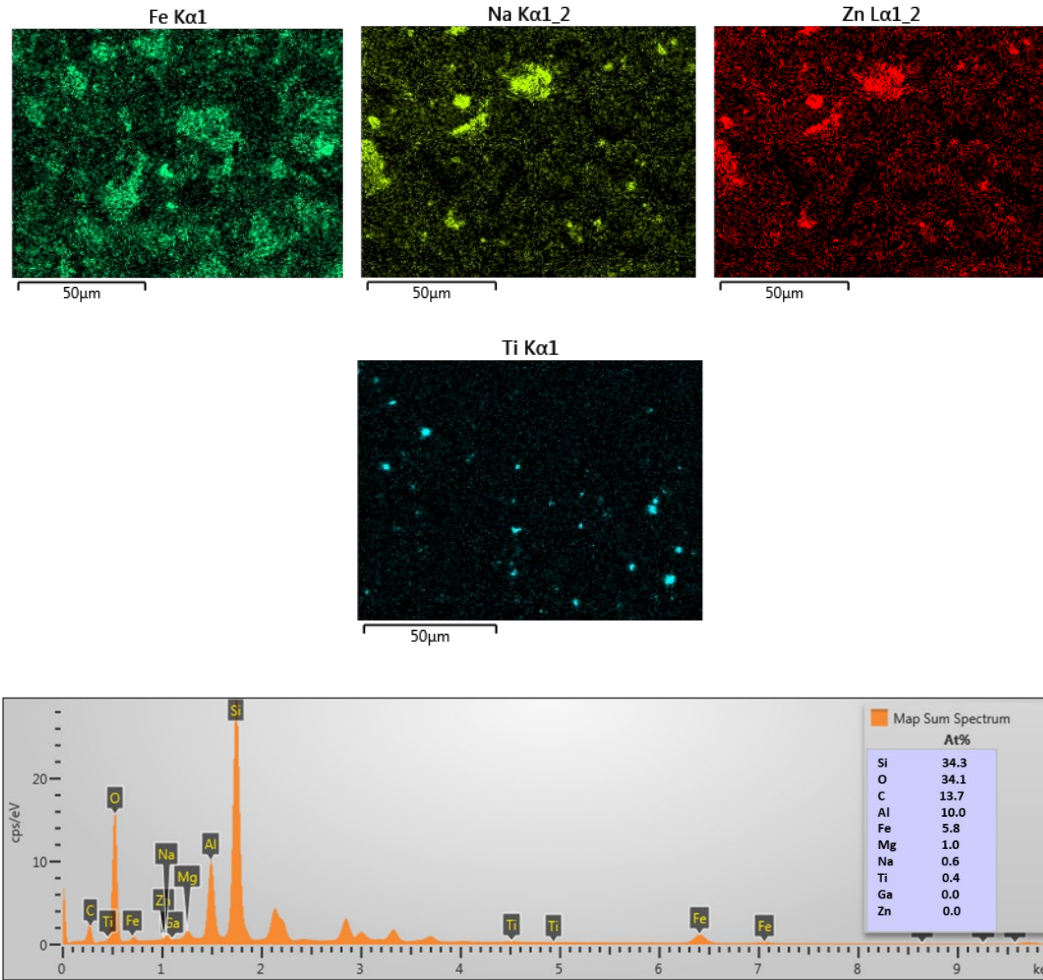


Figure 4. 14 EDS elemental analysis of M₁- Green Schist

The EDS analysis of M₁ – Green schist shows the larger particles of quartz and clayey compounds and minor phases as well. The Al/Si ratio in this sample is 0.3. The most dominant elements are O, Si and Al which indicated the existence of clays. Red circles represent the inert quartz particles and green circles illustrate the clayey phases like Illite, Muscovite and Clinchlore. The amount of carbon in this microstructure was around 14% which is shown as blue circles that are related to carbonate phase which is mainly calcite. Also, some pebble shape particles are shown with brown circles which would be titanium oxide.

4.5.1.3.2 M₂ – Brown

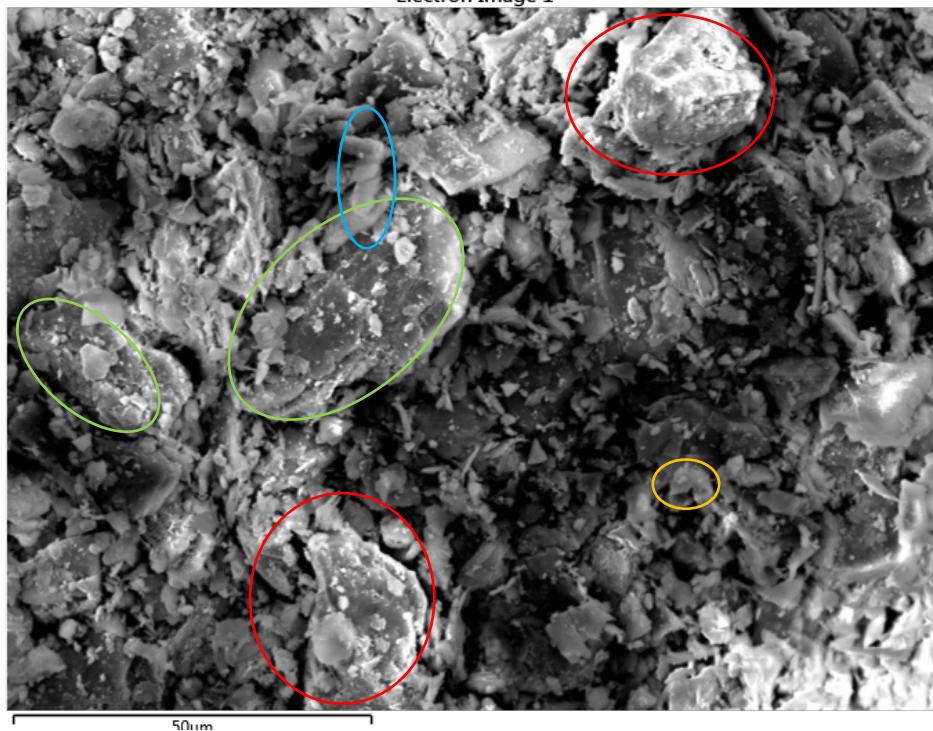
The microstructure of M₂ – Brown schist taken at different magnifications are shown in Figure 4.15.



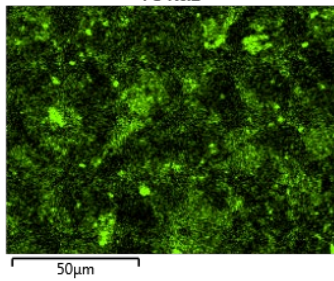
Figure 4. 15 M₂-Brown schist type sample micrograph in different magnification

M₂ microstructure resembles the one of M₁. Dominant mineral phases are quartz and clayey materials. The average particle size (35 μm) seems somehow close to M₁. Also, the layered structures in larger chunks appeared sturdier and thicker. Figure 4.16 illustrates the EDS elemental results.

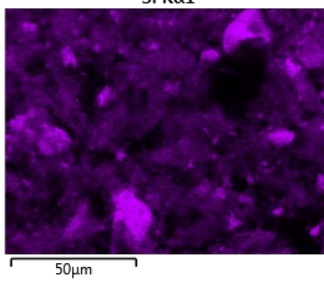
Electron Image 1



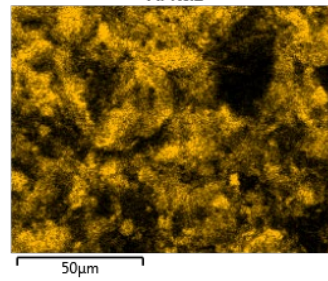
Fe K α 1



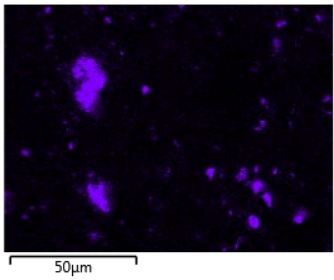
Si K α 1



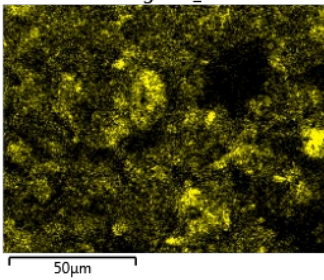
Al K α 1



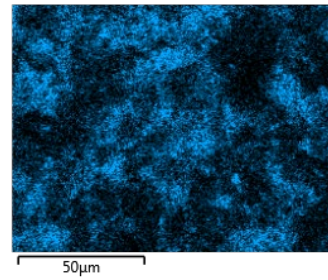
Ca K α 1



Mg K α 1_2



K K α 1



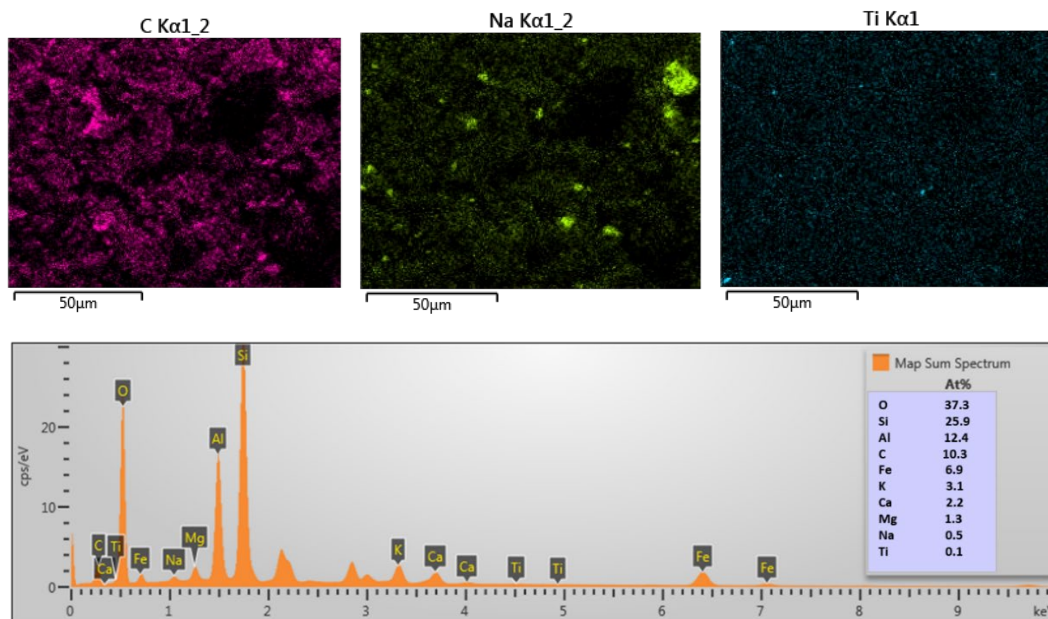


Figure 4. 16 EDS elemental analysis of M₂- Brown Schist

The microstructure of M₂ schist mainly consisted of quartz and clayey components. The Ca/Si ratio is 0.08 and Al/Si ratio is about 0.48. The ratios are like M₁ schist but the amount of quartz in this sample is higher while the total amount of clays is lower. Red circles show some particles of quartz and green circles represent clayey minerals. Other minor phases like carbonate illustrated by blue circle and titanium oxide with brown one.

4.5.1.3.3 M₃ – Pink

Figure 4.17 shows the microstructure analysis of M₃ schist sample. Based on the x-ray phase analysis, this sample was expected to show significant resemblance to M₂ and M₃ samples.

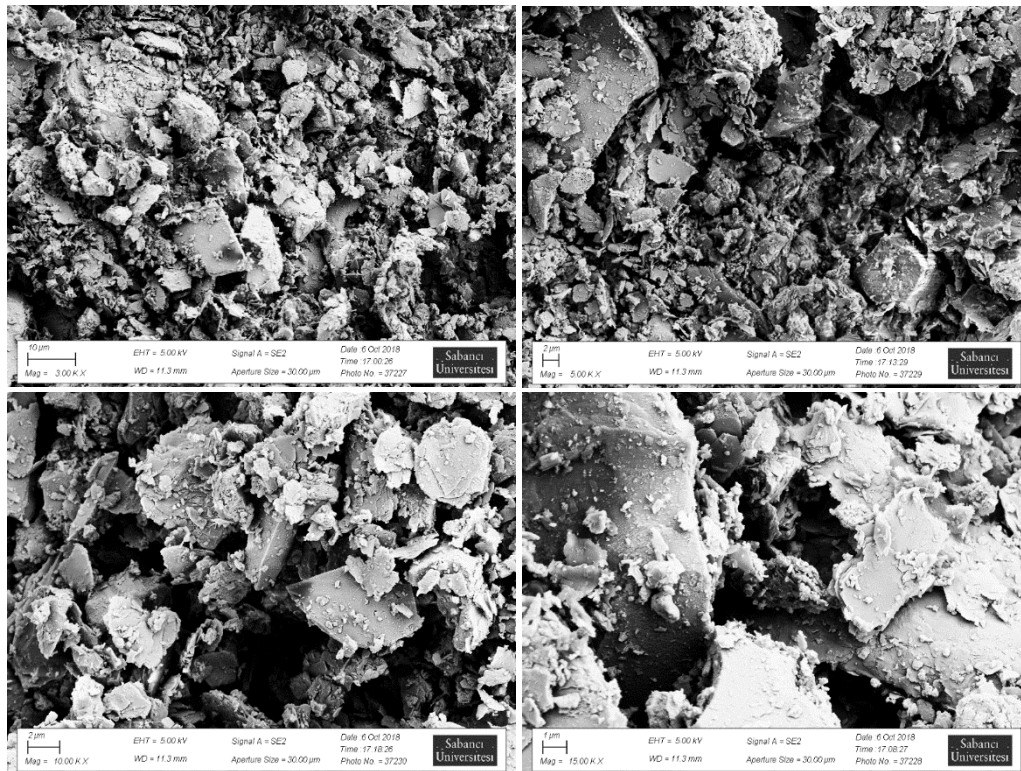
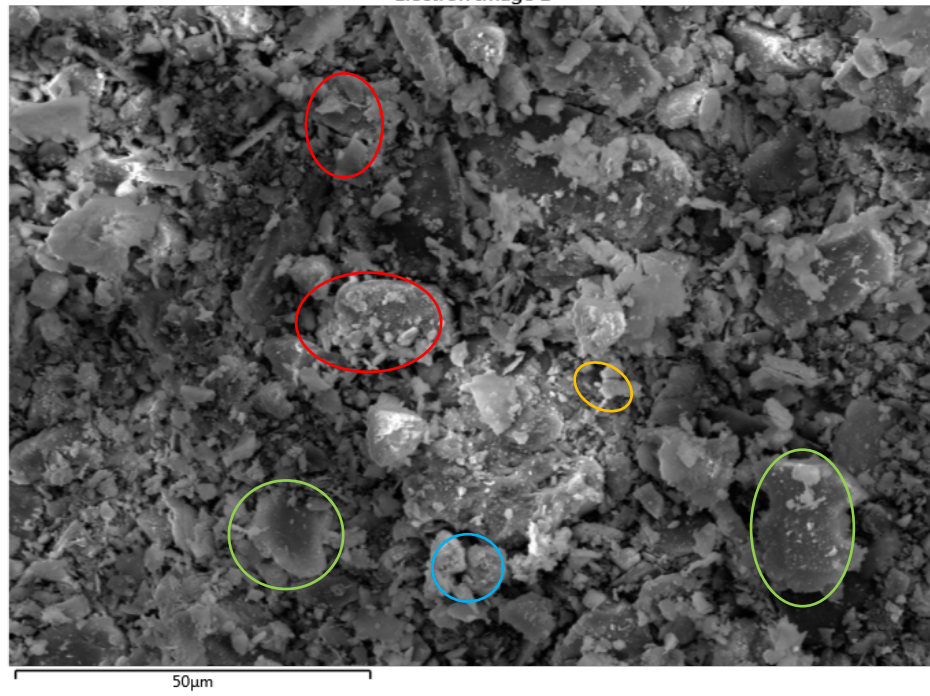


Figure 4. 17 M₃-Pink schist type sample micrograph in different magnification

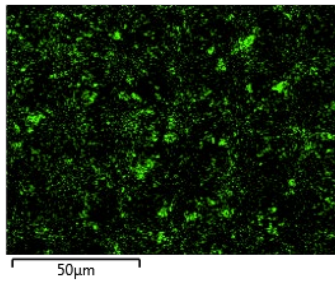
The microstructure of M₃ schist also contains quartz particles and obvious layered structures that were interpreted as clayey minerals. The particle sizes (30 μm) resembled M₂ sample and close to M₁.

Figure 4.18 illustrates the EDS elemental analysis of M₃ schist that would expose more detailed information.

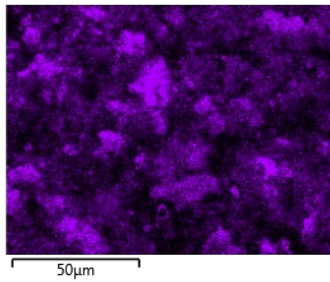
Electron Image 1



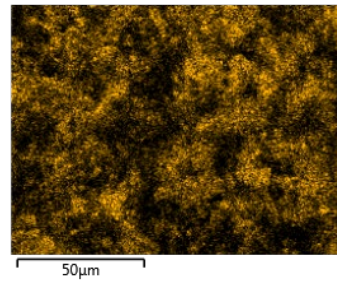
Fe K α 1



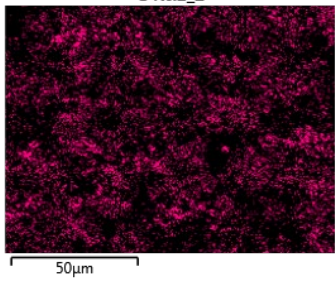
Si K α 1



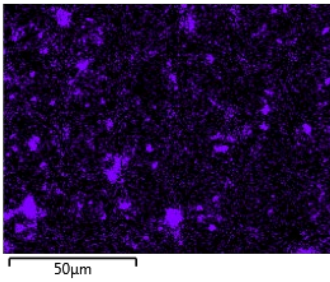
Al K α 1



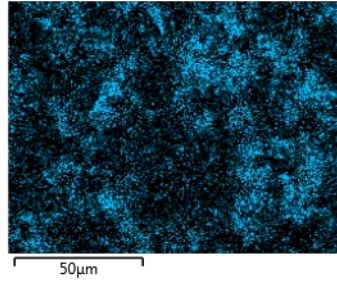
C K α 1_2



Ca K α 1



K K α 1



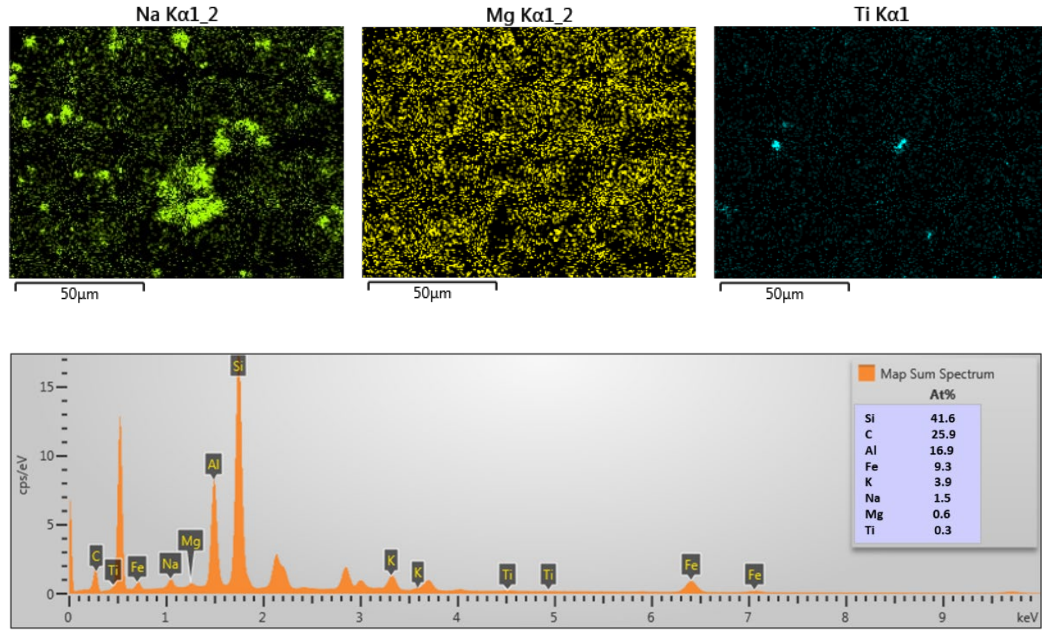


Figure 4. 18 EDS elemental analysis of M3- Pink Schist

The elemental analysis of M₃ material shows heterogeneous distribution of clay and quartz. The Al/Si ratio is almost 0.4. According to the colored map, the Si dominant regions mostly introduce silicon oxide or quartz. Combination of Al, Si and O may be accompanied by Fe, Na or Mg makes the region inscribed by clay components. Red circles declare the existence of quartz and green circle, clayey materials. As it is mentioned before the blue circle shows carbonate phase and brown one represents the titanium oxide.

4.5.1.3.4 M₄ – Black

Figure 4.19 displays the micrographs containing the microstructure of M₄–Black schist sample that. Based on the quantitative phase analysis with the help of XRD, this sample was expected to show some differences to other samples.

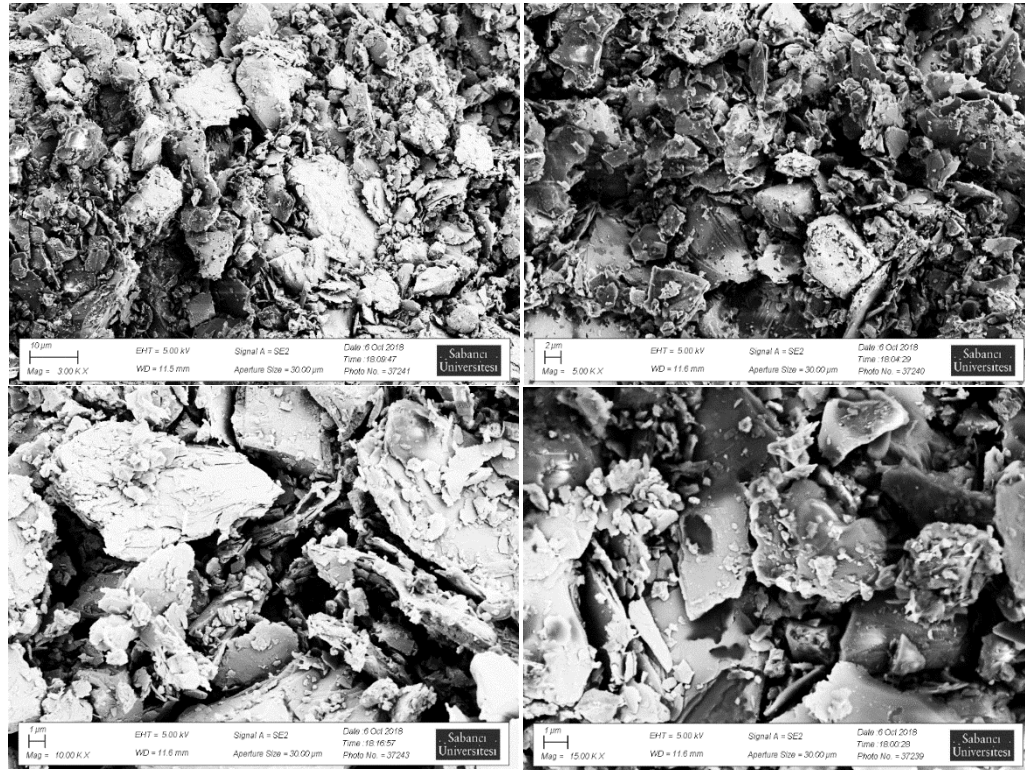
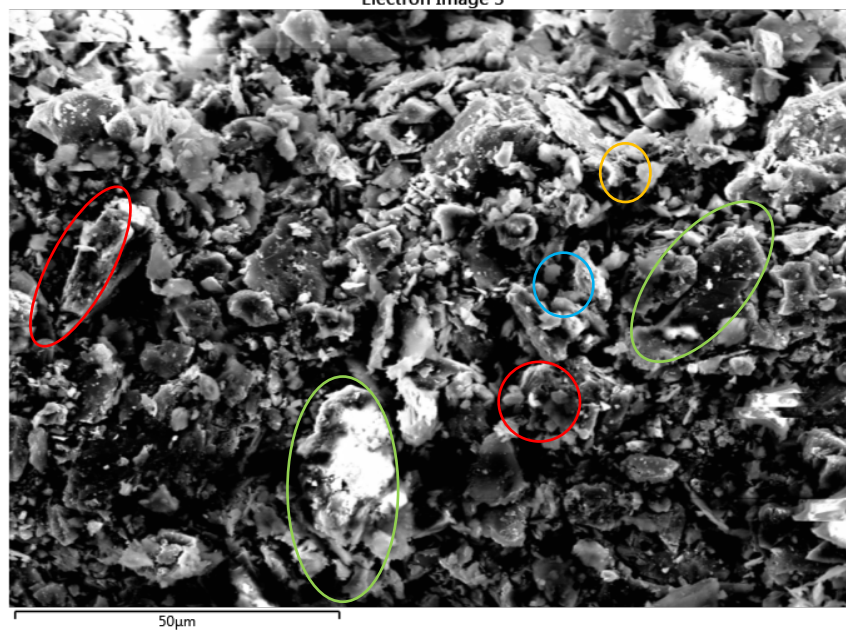


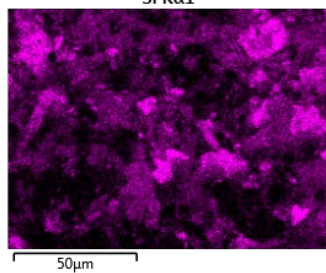
Figure 4. 19 M4-Black schist type sample micrograph in different magnification

The microstructure of M₄ sample revealed a larger fraction of plate-like particles than the other three samples. The particle sizes seem somehow smaller than M₁ in some parts, but the average particle size (35 µm) is close to other three samples. Figure 4.20 contains the elemental map analysis of the M₄ schist for better interpretation of phase distribution.

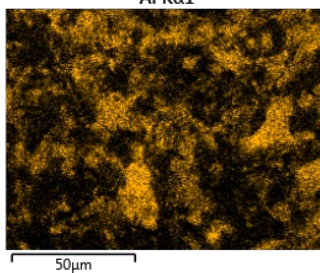
Electron Image 3



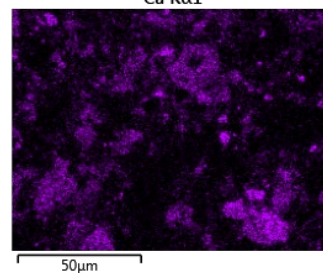
Si Kα1



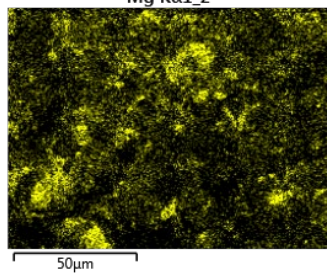
Al Kα1



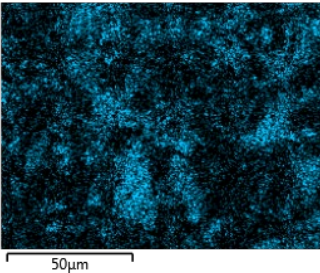
Ca Kα1



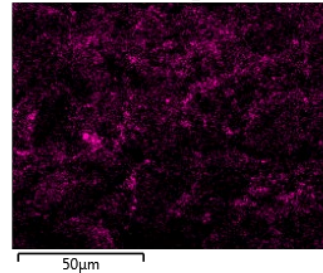
Mg Kα1_2



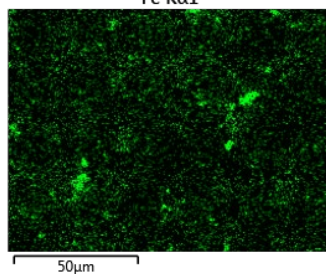
K Kα1



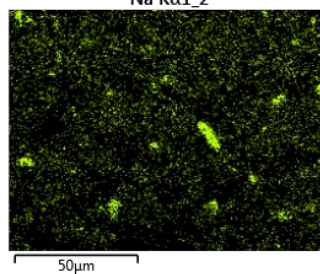
C Kα1_2



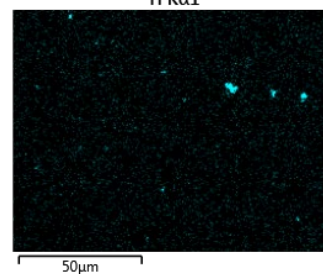
Fe Kα1



Na Kα1_2



Ti Kα1



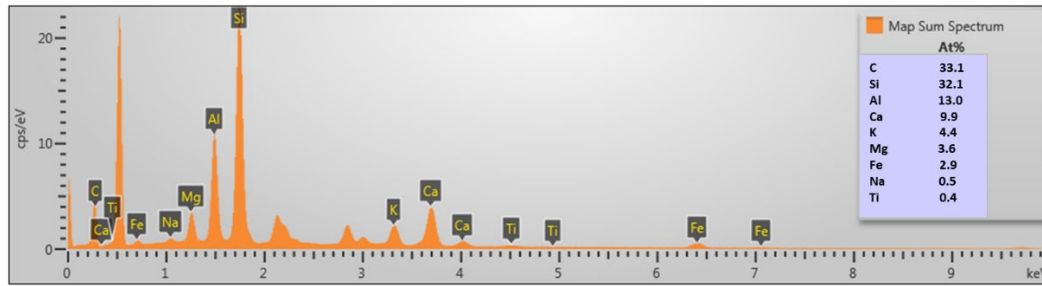


Figure 4. 20 EDS elemental analysis of M₄- Black Schist

The elemental analysis of M₄ samples shows a variety of phases which distributed heterogeneously. Ca/Si ratio is about 0.3 and Al/Si ratio is almost 0.4. The proportions reveal this fact that the clayey content of this powder is somehow lower than the others but not significantly.

4.5.2 Calcined Materials (C³ and LC⁴)

Phase distribution of the investigated virgin schist samples indicated that all of the schist type materials could have the possibility to be activated to be used as potential cement substitute. Therefore, we decided to evaluate their potential based on the two different recipes. One aim was to assess potential of various schist materials as there were mined, that this was the first phase of project. The second phase of the project was launched to investigate the effect of activated calcia additions to activated schists on composite cement hydration, strength and durability. We will now compare the calcined clay cement (C³) which had no carbonate additions; and calcined clay/carbonate mixtures added to cement (LC⁴). Therefore, in C³ phase, the samples included only virgin samples without carbonate addition. This means there is just the original carbonate content inside the schist composition. On the other hand, LC⁴ samples contained the virgin powders with the carbonate content topped off to 15 wt% of the total composition.

4.5.2.1 Phase Distribution and Evolution during activation process

The X-ray diffractogram of all calcined powders were analyzed and compared quantitatively to the phase distributions of virgin powders to observe the effects of the calcination process. For the LC⁴ powders whose carbonate amount was topped off to 15 wt%, the comparison was performed between schist with 15% carbonate and the same mixtures after calcination.

4.5.2.1.1 M₁ with and without 15% \overline{CC} Addition

According to the x-ray analysis before calcination, the M₁- Green schist powder contained about 0.9 wt% carbonate. This carbonate content was topped of to 15% and x-ray diffractograms of virgin and heat-treated powders were evaluated. Figure 4.21 shows both the virgin and calcined powders spectra on the same graph. Table 4.6 represents the chemical phase distribution and detailed information about their crystal structure.

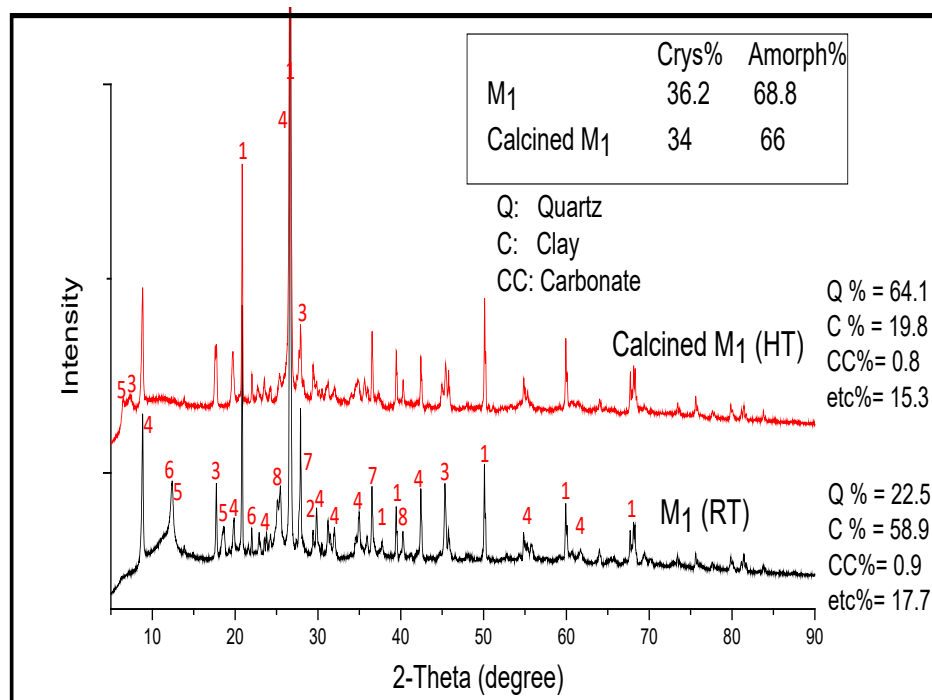


Figure 4. 21 X-ray spectrum of virgin vs. calcined M₁- Green schist powder

Table 4. 6 The Phase distribution and detailed information about crystal structure and weight percentage for each chemical compound in M1-Green virgin and calcined powder

Sample #	Chemical Phases	at%	Crystal Structure	Chemical Formula
1	Quartz	22.5	Hexagonal	SiO ₂
2	Calcite	0.9	Rhombo	CaCO ₃
3	illite	24.5	Monoclinic	(K , H ₃ O) Al ₂ Si ₃ Al O ₁₀ (O H) ₂
4	Muscovite	23.1	Monoclinic	K Al ₂ Si ₃ Al O ₁₀ (O H) ₂
9	Albite	3.8	Triclinic	(Na , Ca) (Si , Al) ₄ O ₈
5	Clinocllore	6.5	Monoclinic	(Mg _{2.96} Fe _{1.55} Fe _{.136} Al _{1.275}) (Si _{2.622} Al _{1.376} O ₁₀) (O H) ₈
6	Dickite	4.8	Monoclinic	Al ₂ Si ₂ O ₅ (O H) ₄
7	Anorthite	12.1	Triclinic	Na _{.25} Ca _{.71} (Al ₂ Si ₂ O ₈)
8	Titanium Oxide	1.8	Monoclinic	Ti ₃ O ₅

Based on the Rietveld analysis of virgin and calcined M₁ schist (LC⁴), the crystalline phases amount changed from 36.2 to 34% while the amorphousness increased by 2.2%. The amount of quartz as inert phase must be constant before and after calcination. However, it appeared to have increased during heat treatment. This apparent contradiction was seen before a clear understanding of will be again given in the discussion section. It should be sufficient to say that it is a misinterpretation of data by the quantification software. The quantification software calculates the total weight percentage from 100% and it is expected to add the decomposed percentage of other phases to quartz. So, the increase in inert phase is not accurate and important at this point. After a calcination at 640°C for 2 hours, the clay content of M₁ sample changed from 58.9 to 19.8 wt% and carbonate amount from 0.9 to 0.8 wt%. Some other phases decomposition took place and it was about 2.4 wt%. Based on this quantification, it can be argued that the clayey materials de-hydroxylate to 80% of their expected total weight loss. The percentage amount of decomposition by de-hydroxylation was about 67% of the possible total as estimated from XRD results.

Figure 4.22 shows the x-ray spectra of M₁ with up to 15% carbonate additions before (RT) and after heat treatment (HT).

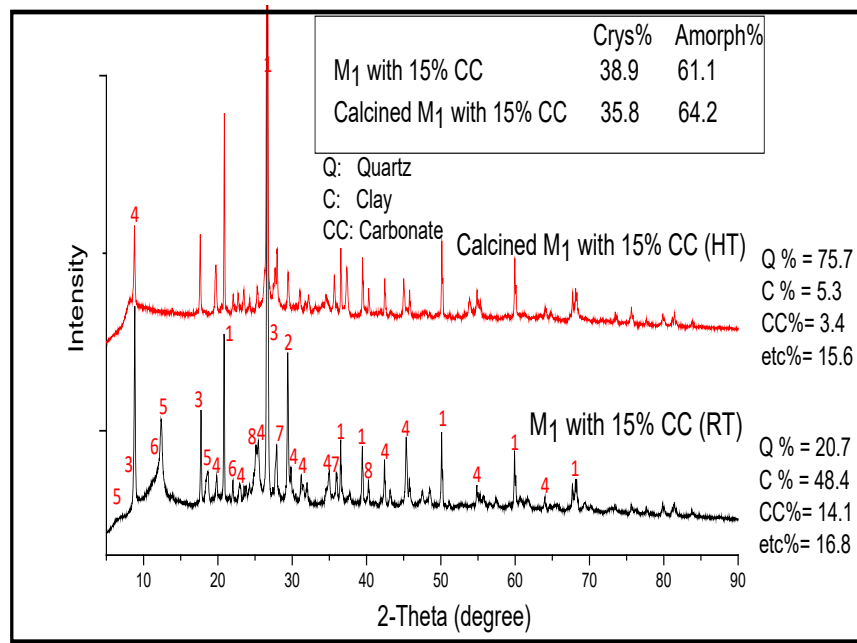


Figure 4. 22 X-ray spectrum of virgin vs. calcined M₁- Green with 15% (CC)

A similar interpretation can be made from the x-ray diffractograms of virgin and calcined M₁ with 15%. The crystallinity of virgin powder was about 38.9% prior to calcination and decreased to 35.8% and simultaneously the amorphousness changed from 61.1 to 64.2%. The clay phase weight percentage changed from 48.4 to 5.3% which means that 95% of total clay amount has been decomposed. Almost 76% of carbonates decomposed and the proper amount of clayey chemical phases were also decomposed.

4.5.2.1.2 M₂ with and without 15% \overline{CC} Addition

The x-ray analysis of the virgin M₂ – Brown powder illustrated that this schist type materials contained 3.8 wt% carbonate. To generate LC⁴ M₂ sample, we added enough calcite to this powder to top off the carbonate amount to 15%. Figure 4.23 shows the both virgin and calcined powders spectra without carbonate additions. Detailed information represented in Table 4.7.

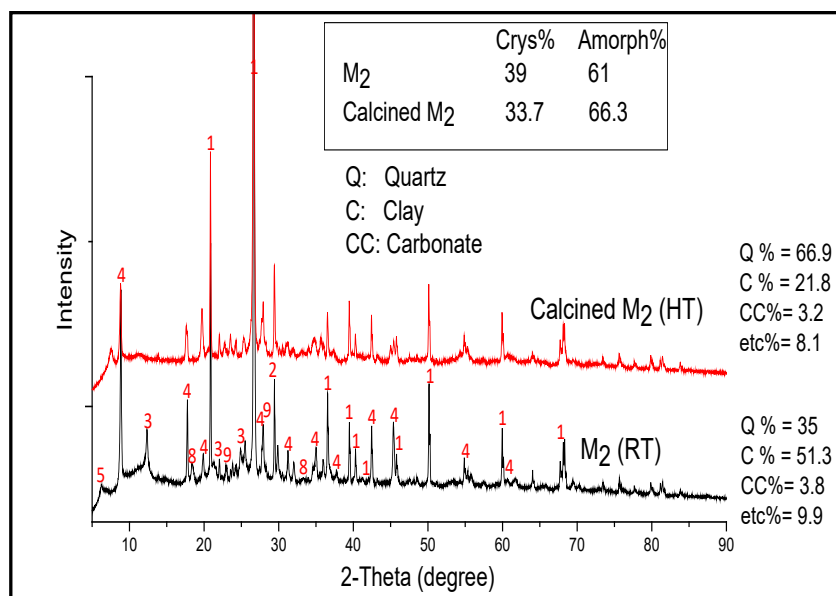


Figure 4. 23 X-ray spectrum of virgin vs. calcined M₂- Brown schist powder

Table 4. 7 The Phase distribution and detailed information about crystal structure and weight percentage for each chemical compound in M₂-Green virgin and calcined powder

Sample #	Chemical Phases	at%	Crystal Structure	Chemical Formula
1	Quartz	35	Hexagonal	SiO ₂
2	Calcite	3.8	Rhombo	CaCO ₃
4	Muscovite I	28.2	Monoclinic	K Al ₂ (Al Si ₃ O ₁₀) (O H) ₂
4	Muscovite II	16.1	Hexagonal	(K , Na) (Al , Mg , Fe) ₂ (Si _{3.1} Al _{0.9}) O ₁₀ (O H) ₂
9	Albite	4	Triclinic	(Na , Ca) (Si , Al) ₄ O ₈
5	Clinocllore	3.3	Monoclinic	(Mg ₅ Al) (Si , Al) ₄ O ₁₀ (O H) ₈
3	Kaolinite	3.7	Triclinic	Al ₂ (Si ₂ O ₅) (O H) ₄
7	Anorthite	5	Triclinic	Ca (Al ₂ Si ₂ O ₈)
8	Titanium Oxide	0.9	Orthorhombic	Ti ₃ O ₅

The crystallinity of powder decreased from 39 to 33.7% while the amorphousness increased from 61 to 66.3%. The 29.5 wt% of clayey materials de-hydroxylated (from 51.3 wt% to 21.8 wt%) which means the achieved decomposition was around 60% of total weight loss. None of the carbonate phase decomposed. Lack of decomposition of carbonate phase also confirmed that we did not reach the intended activation levels.

Figure 4.24 shows the x-ray spectra of virgin and calcined LC⁴ M₂ with 15% \overline{CC} to compare the decomposition magnitude of clayey and carbonate phases.

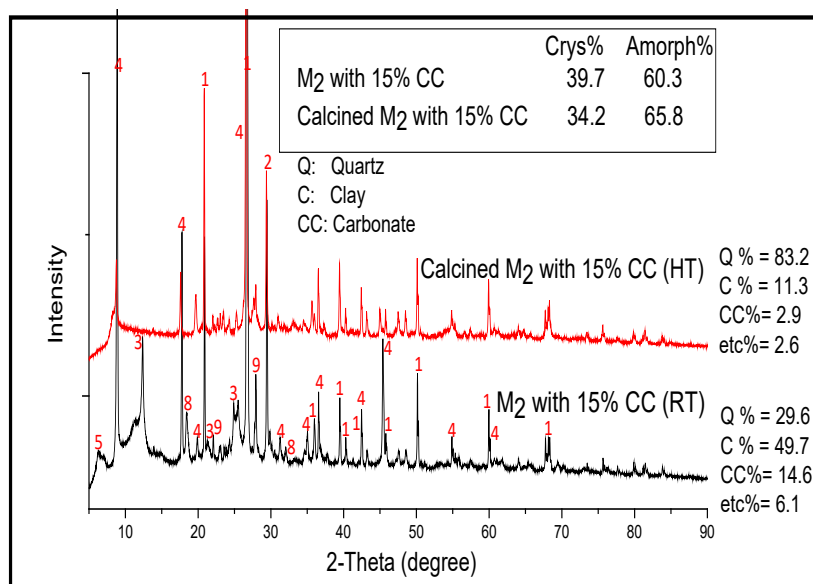


Figure 4. 24 X-ray spectrum of virgin vs. calcined M₂ - Brown with 15% (CC)

Clay components' de-hydroxylation changed the initial amount of 49.7% to 11.3%. In addition, 80% of the carbonate content was decomposed. Crystallinity of virgin powder dropped down for 5.5% while the amorphousness increased by the same amount. Calcination of the M₂ with 15% of carbonate phase is closer to the intended levels and produced higher amounts of reactive phases.

4.5.2.1.3 M₃ with and without 15% \overline{CC} Addition

Quantitative X-ray analysis of M₃ – Pink schist powder with and without carbonate additions was carried out in order to monitor the changes in the phase composition of the sample due to activation heat treatment. Figure 4.25 illustrates the x-ray diffractometer spectra of virgin and calcined M₃ without carbonate additions. Table 4.8 includes detail information about containing phases. The sample was heat treated to a temperature that would correspond to 80% of the total weight loss due to de-hydroxylation reactions.

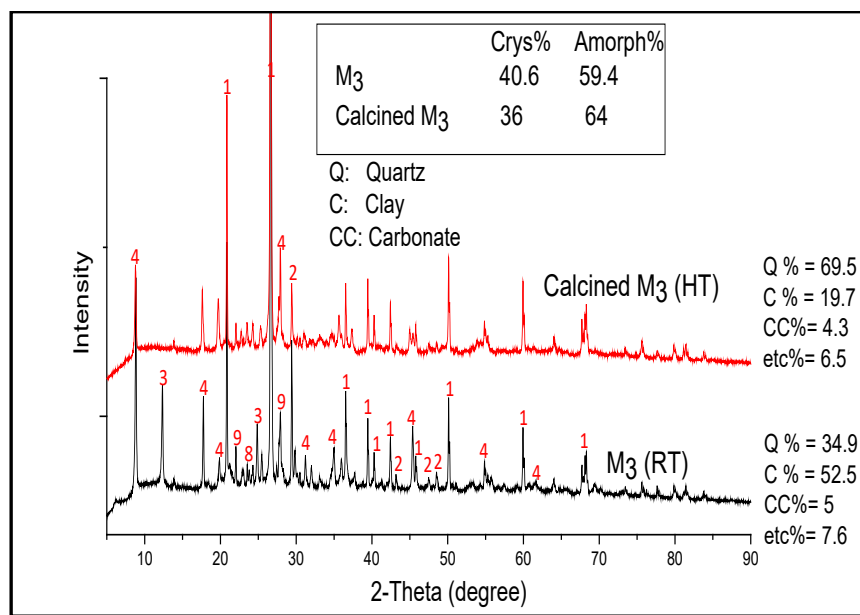


Figure 4. 25 X-ray spectrum of virgin vs. calcined M₃- Pink schist powder

Table 4. 8 The Phase distribution and detailed information about crystal structure and weight percentage for each chemical compound in M₃-Green virgin and calcined powder

Sample #	Chemical Phases	at%	Crystal Structure	Chemical Formula
1	Quartz	34.9	Hexagonal	SiO ₂
2	Calcite	5	Rhombo	CaCO ₃
4	Muscovite I	28.4	Monoclinic	$K (Al_{1.88}Fe_{0.12}) (Si_3Al) O_{10} (OH)_2$
4	Muscovite II	18.2	Hexagonal	$(K, Na) (Al, Mg, Fe)_2 (Si_{3.1}Al_{0.9}) O_{10} (OH)_2$
9	Albite	5.8	Triclinic	NaAlSi ₃ O ₈
3	Kaolinite	5.85	Triclinic	$Al_2 (Si_2O_5) (OH)_4$
8	Rutile	0.4	Tetragonal	TiO ₂

The de-hydroxylated clayey materials in M₃ powder after calcination is about 62% of the total clayey content of the sample. It was less than the intended 80% decomposition. The carbonate phases decomposed for 0.7% and other phases decomposed for 1.1%. The apparent crystallinity decreased from 40.6 to 36% while the amorphousness increased from 59.4 to 64%. The magnitude of changes observed in the phase composition in this schist source due to activation was similar to M₁ and M₂. Figure 4.26 illustrates the virgin and calcined M₃ with 15% carbonate.

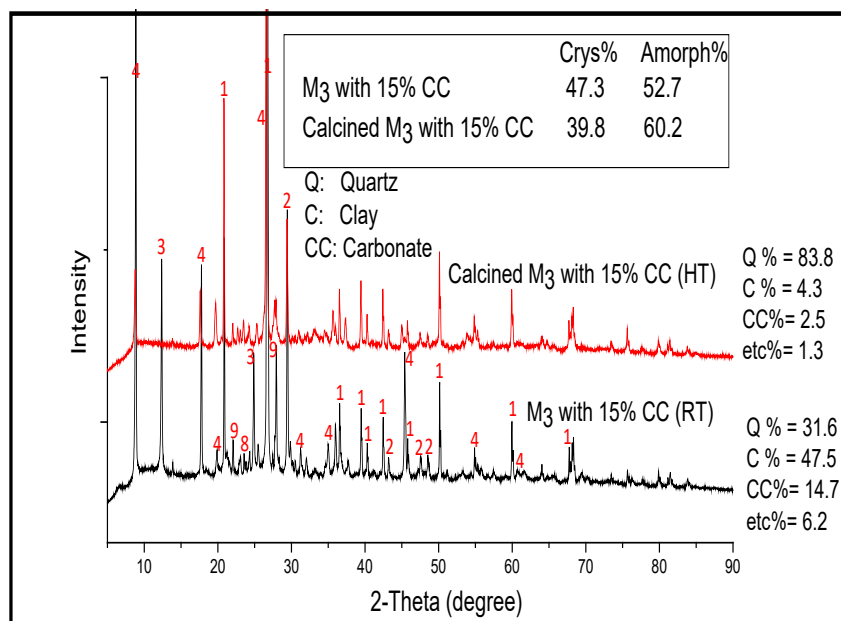


Figure 4. 26 X-ray spectrum of virgin vs. calcined M₃ - Pink with 15% (CC)

A comparison of the spectra before and after the activation heat treatment shows the reduction in some peaks' intensity indicating the decomposition of some some of the mineral phases. Due to the calcination, crystallinity decrease from 47.3 to 39.8% accordingly the amorphousness increased from 52.7 to 60.2%. The weight percentage of clayey phases changed from 47.5 to 4.3% and 82% of the carbonate content was decomposed. Therefore, the degree of reactivation coincides to expectation.

4.5.2.1.4 M₄ with and without 15% \overline{CC} Addition

The X-ray diffraction analysis were carried out for the virgin and calcined M₄ with and without carbonate additions. Figure 4.27 shows the diffractogram of virgin and calcined M₄ without any modification in its carbonate amount. Table 4.9 represents the detailed information about phases of this sample.

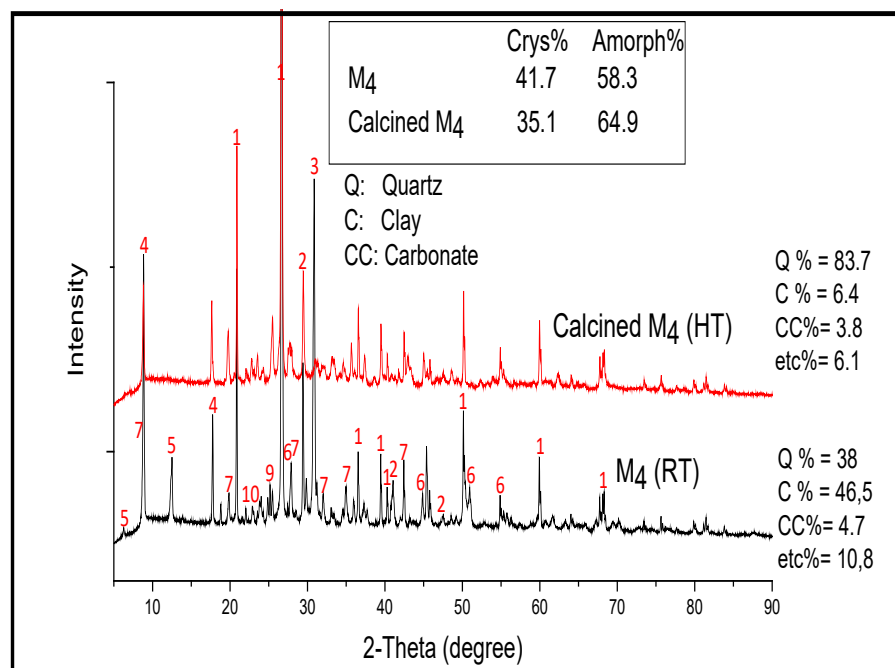


Figure 4. 27 X-ray spectrum of virgin vs. calcined M₄- Black schist powder

Table 4. 9 The Phase distribution and detailed information about crystal structure and weight percentage for each chemical compound in M₄-Green virgin and calcined powder

Sample #	Chemical Phases	at%	Crystal Structure	Chemical Formula
1	Quartz	38	Hexagonal	SiO ₂
2	Calcite	4.7	Rhombo	CaCO ₃
4	Muscovite I	19.7	Hexagonal	(K , Na) (Al , Mg , Fe) ₂ (Si _{3.1} Al _{0.9}) O ₁₀ (O H) ₂
3	Ankerite	14.3	Rhombo	Ca (Mg _{0.67} Fe _{0.33} + ₂) (C O ₃) ₂
9	Albite	3.7	Triclinic	Na Al Si ₃ O ₈
5	Clinocllore	3.7	Monoclinic	(Mg _{2.8} Fe _{1.7} Al _{1.2}) (Si _{2.8} Al _{1.2}) O ₁₀ (O H) ₈
7	Mg-Annite	8.77	Monoclinic	K (Mg , Al) ₂ O ₄ (Si _{3.34} Al _{0.66}) O ₁₀ (O H) ₂
6	Graphite	5	Hexagonal	C
8	Titanium Oxide	1.32	Monoclinic	Ti ₃ O ₅
10	Pyrite	0.9	Cubic	Fe S ₂

The XRD quantitative phase analysis indicated that the decomposition process of clayey materials, reached to 80% of total weight loss as it was intended for M₄ type schist. This is a marked difference in the decomposition behavior of this schist in comparison to the rest of the samples. The carbonate phase decomposed 0.9% and the other phases changed their crystalline amounts in the total composition by 19.1%. The calculated crystallinity of the sample decreased from 41.7 to 35.1%.

Figure 4.28 illustrates the x-ray spectra of virgin and calcined M₄ for which the original amount of carbonate phase in virgin powder which is about 4.7 wt% was increased to 15 wt% by adding calcite powders.

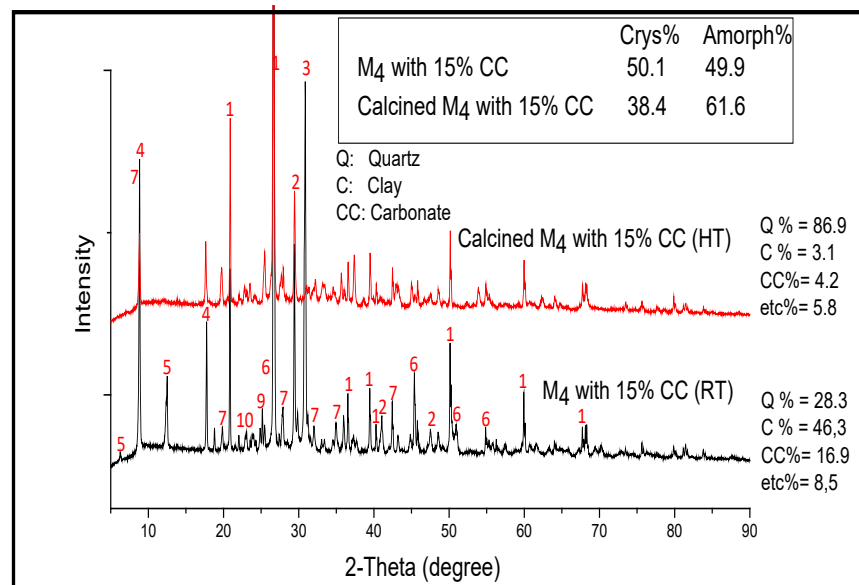


Figure 4. 28 X-ray spectrum of virgin vs. calcined M₄ - Black with 15% (CC)

The quantitative x-ray diffraction analyses indicated that the crystallinity of M₄ powder with modified carbonate decreased from 50.1 to 38.4%. More than 90% of clayey components and 80% of carbonate phase decomposed.

4.5.2.2 Scaling up the Activation Process

To control the accuracy of scaling up the calcination process to amount of powders that will be used in cement paste sample preparation, the virgin and powders heat-treated in industrial size furnaces were re-evaluated by thermogravimetric analysis. The graphs in this section include the TG diagrams illustrating the amounts of weight losses of virgin powders (as they are received) and weight losses indicating the remaining activation potential in calcined powders.

4.5.2.2.1 M_1 with and without 15% \overline{CC} Addition

The thermogravimetric analysis of as received M_1 schist material revealed that the temperature that would ensure the 80% of weight loss was around 640°C. Figure 4.29 shows the TG diagrams of virgin and M_1 powders calcined in a laboratory furnace at 640°C for comparison.

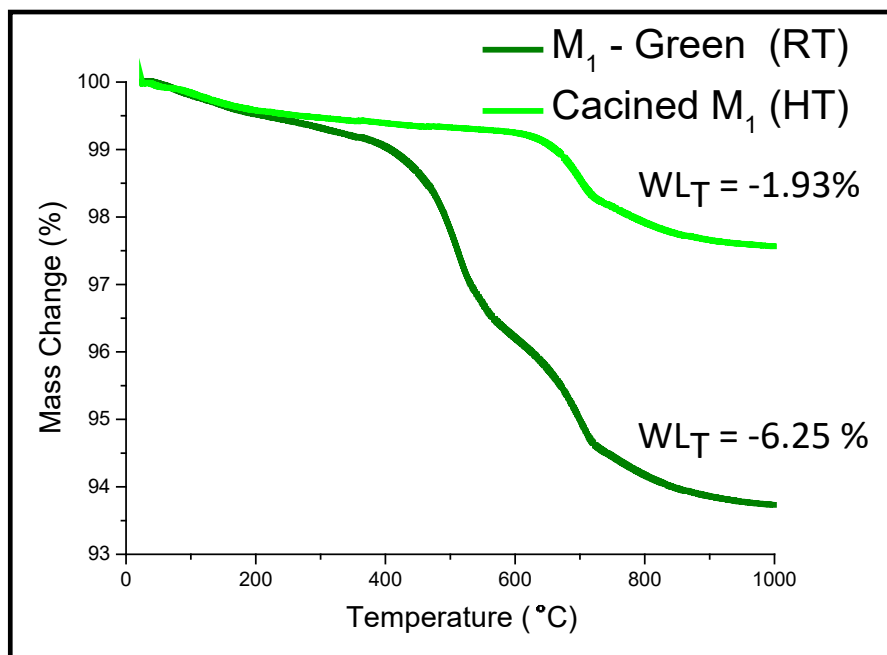


Figure 4. 29 Thermogravimetric analysis of virgin and calcined M_1

As it can be seen in TGA plot, the total weight loss of the virgin M_1 is about 6.25 wt% while this amount dropped down to 1.93 wt% after heat treatment. According to theoretical calculations the powders calcined for 80 wt% activation should show a remnant weight loss around 1.25 wt%. Therefore, the decomposition appeared to have happened insufficiently in the furnace when large amounts were calcined. Figure 4.30 illustrates the same mismatch in the targeted and realized weight losses for activated M_1 with 15% carbonate additions.

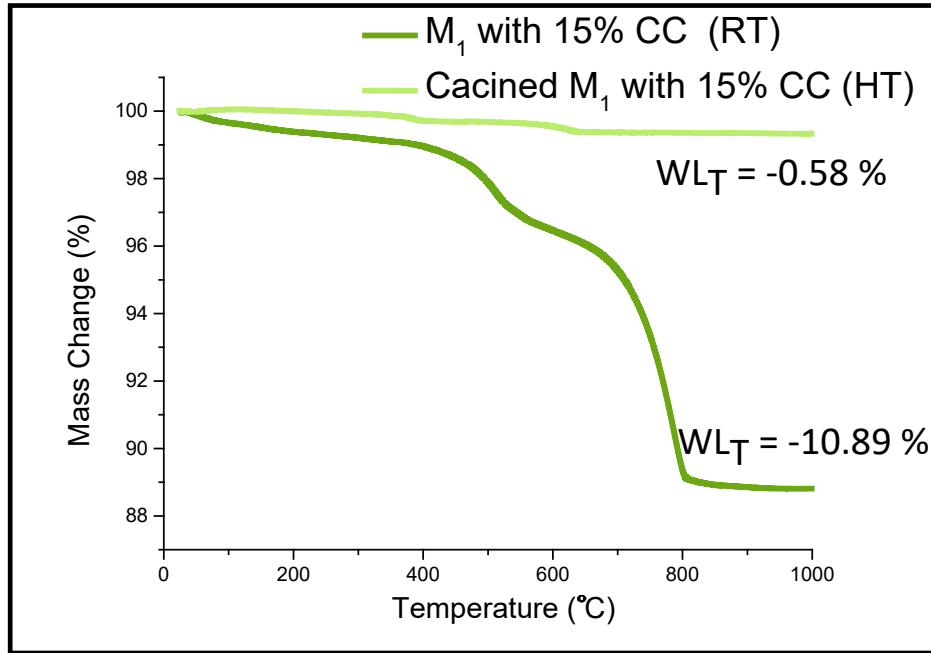


Figure 4. 30 Thermogravimetric analysis of virgin and calcined M₁ with 15% (CC)

In case of M₁ with 15% \overline{CC} , the total weight loss is about 10.89 wt% while the calcined sample weight loss is around 0.58 wt%. Even though the theoretical amount would be 2.17 wt%, the surplus amount reveals that the calcination temperature was high, or the carbonate distribution was not homogenous.

4.5.2.2.2 M₂ with and without 15% \overline{CC} Addition

As it was stated before the calculated temperature for 80% activation of M₂ sample was about 670°C. This temperature was applied to the virgin schist for calcination for 2 hours. Figure 4.31 shows the thermograms of as-received virgin M₂ schist and heat treated (activated) M₂ schist powders.

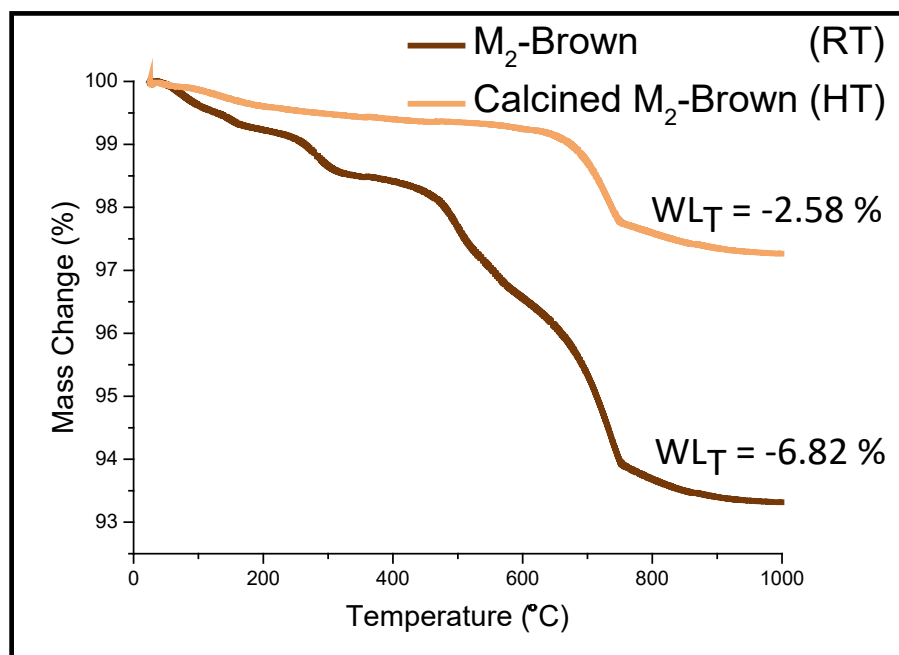


Figure 4. 31 Thermogravimetic analysis of virgin and calcined M_2

According to the theoretical calculations for an 80% activated M_2 schist, the remaining amount of weight loss should have been around 1.36 wt%, but the actual results showed that there was still 2.58 wt% possible in this heat-treated schist.

Figure 4.32 shows the results from the virgin and calcined M_2 with 15% \overline{CC} additions.

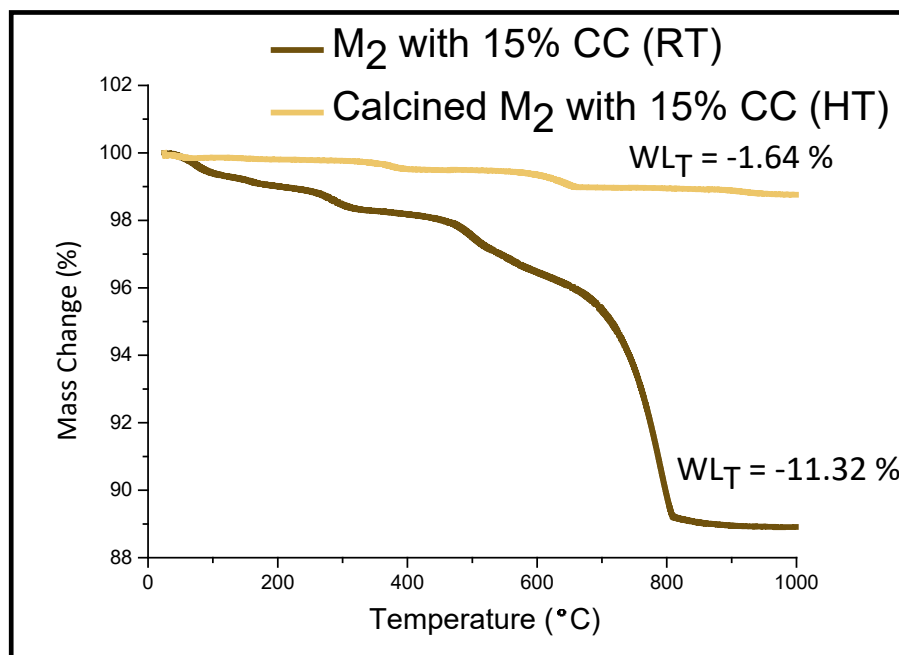


Figure 4. 32 Thermogravimetic analysis of virgin and calcined M₂ with 15% (CC)

The weight losses for virgin and activated M₂ with 15% \overline{CC} additions were about 11.32 wt% and 1.64 wt%, respectively. The calcined schist should have had a remaining weight loss of about 2.26 wt%. It appears that this mixture was over-activated to almost 86% of its potential. The calcination temperature was 768°C. This temperature range includes the decomposition of clayey minerals and carbonate in the mixture as well.

4.5.2.2.3 M₃ with and without 15% \overline{CC} Addition

Figure 4.33 shows the thermograms of as-received virgin M₂ schist and heat treated (80% activated) M₂ schist powders. According to x-ray analysis the M₃ schist powder resembled M₂ schist powders closely but their thermal responses were different during heat treatment.

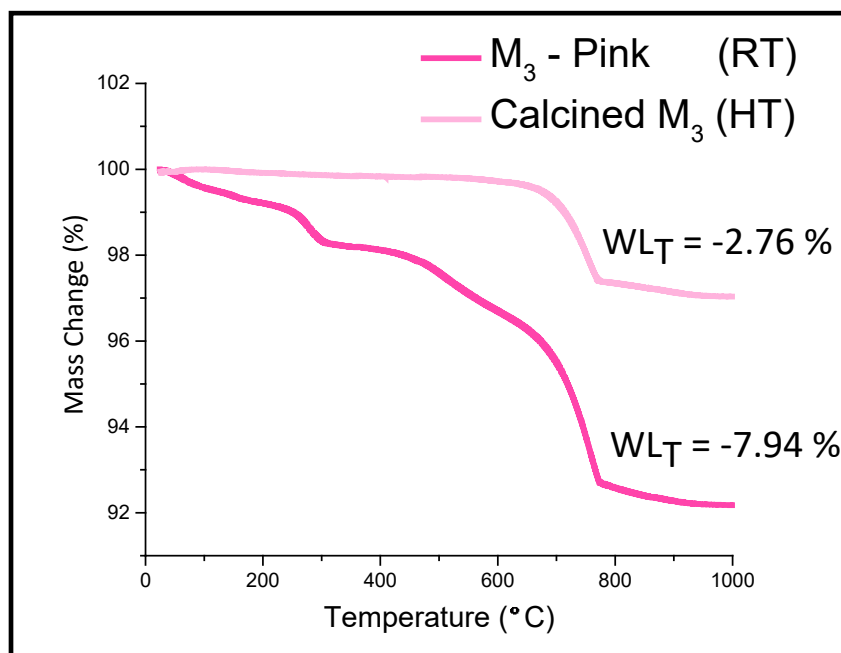


Figure 4. 33 Thermogravimetic analysis of virgin and calcined M₃

The calculated difference between the weight losses of as-received M₃ schist powder and activated powders should have been about 5.18 wt%. The TGA results showed that M₃ schist powders could only be activated to 66% of their potential when calcined in a laboratory furnace at temperatures determined by TGA analysis. Such discrepancies are important for the scale-up processes.

Figure 4.34 illustrates the TG curves for virgin and calcined M₃ schist powders that were mixed with calcium carbonate powders such that the mixture would contain 15 wt% \overline{CC} .

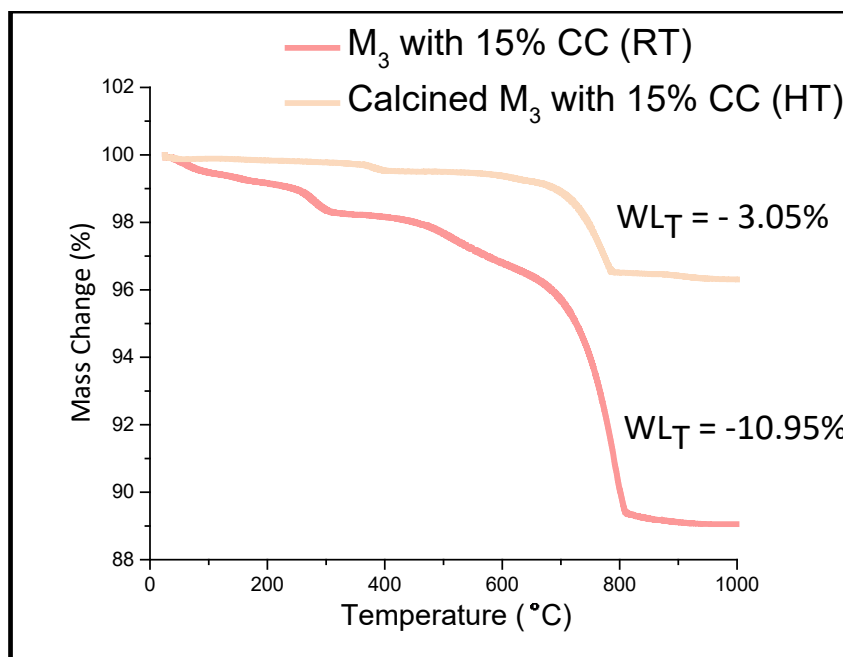


Figure 4. 34 Thermogravimetric analysis of virgin and calcined M₃ with 15% (CC)

The temperature that would achieve 80% activation for M₃ schist powders with 15% \overline{CC} was estimated from TG analysis as around 770°C. The associated remaining weight loss for 80% activated powders should have been about 2.19 wt%. The measured amount was again more than the expected weight loss for this sample indicating that the powders were not activated properly.

4.5.2.2.4 M₄ with and without 15% \overline{CC} Addition

Figure 4.35 compares the TG analysis results of as-received and 80% activated M₄ schist powders. M₄ – Black schist differed from the three other schist samples in terms of its chemical composition as it was detailed in earlier sections of this report. This sample had a significant amount of carbon (graphite~ 5 wt%) in its mineral blend.

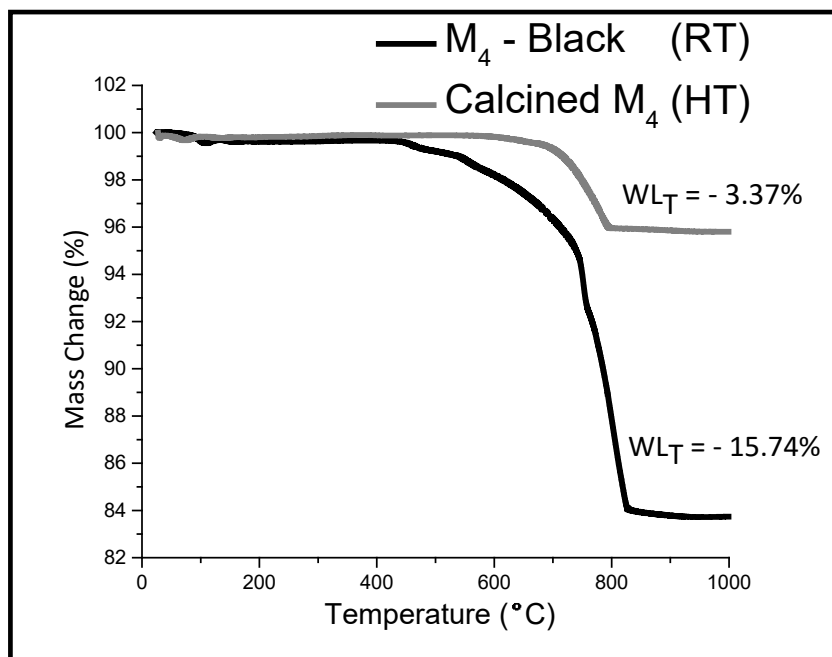


Figure 4. 35 Thermogravimetic analysis of virgin and calcined M₄

The calculated theoretical weight loss should be around 3.2 wt% and the obtained experimental value is very close to it.

Figure 4.36 illustrates the thermograms of M₄ with 15% calcium carbonate in its composition before and after 80% thermal activation process.

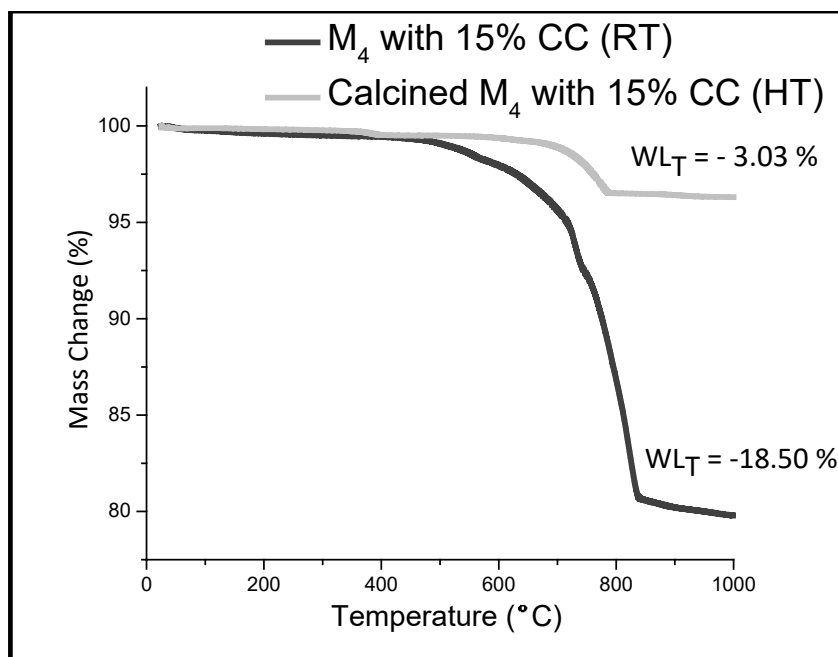


Figure 4. 36 Thermogravimetic analysis of virgin and calcined M₄ with 15% (CC)

The 80% activated powders would have had 3.7 wt% remaining weight loss (potential for further activation). The TGA results showed 3 wt% which is very close to the expected value.

4.5.2.3 Microstructure Analysis

The use of SEM to identify the changes incurring during calcination had two main purposes. The changes in microstructures of various minerals due to the calcination were observed. In addition, the changes, if any, in the chemistry of the phases which were caused by heat treatment were observed. The SEM micrographs illustrated the particle morphological changes and reduction in size in some parts and de-crystallization (the disappearance of prisms with ocular shapes was interpreted as such) in some others. A change in the visible color of the calcined powders in comparison to the virgin materials could be an indication of changes in phase composition in virgin powders. In the following section optical changes in the powders were presented before the results of SEM investigations are shown.

Figure 4.37 shows the M₁ – Green schist powder before and after calcination. Since, there would be no drastic changes in color on the macro scale by topping off the carbonate content

to 15 wt%, the pictures presented here are valid for virgin and calcined schists with and without calcite additions.



Figure 4. 37 M₁ – Green schist powder (a) before and (b) after calcination

Virgin M₁ sample was originally called “green” sample, however, when calcined M₁ powder changed its color to light brown. In most cases of the clayey materials the calcined powders turned to brownish red after treatment. Figure 4.38 includes the snapshot of virgin and calcined M₂ – Brown.



Figure 4. 38 M₂ – Brown schist powder (a) before and (b) after calcination

M₂ - brown schist changed to darker red-brown color after heat treatment. Figure 4.39 illustrates the M₃ – Pink schist powder before and after calcination.



Figure 4. 39 M₃ – Pink schist powder (a) before and (b) after calcination

The pink color of the M₃ schist powder changed to dark red-brown after calcination. For these three samples the color usually became darker and this would be due the oxidation of iron content in clays and other siliceous phases. This reddish-brown color is reminiscent to terra-cotta of bricks and roof tiles.

Figure 4.40 shows the change in color of M₄ – Black schist sample due to the calcination.



Figure 4. 40 M₄ – Black schist powder (a) before and (b) after calcination

For the M₄ powder which is so called black sample, its color changed to lighter grey through the calcination process. Because of the graphite content in this virgin material the color of it was dark grey to black. The heat-treatment process caused burning (oxidation) of graphite; and the color became a lighter grey.

4.5.2.3.1 M₁ with and without 15% \overline{CC} Addition

The micrographs of the virgin (left row) and calcined M₁ (right row) are shown in Figure 4.41 taken at two different magnifications. The SEM micrographs are only provided for virgin and calcined schist in their original composition without any additions of the carbonate phase.

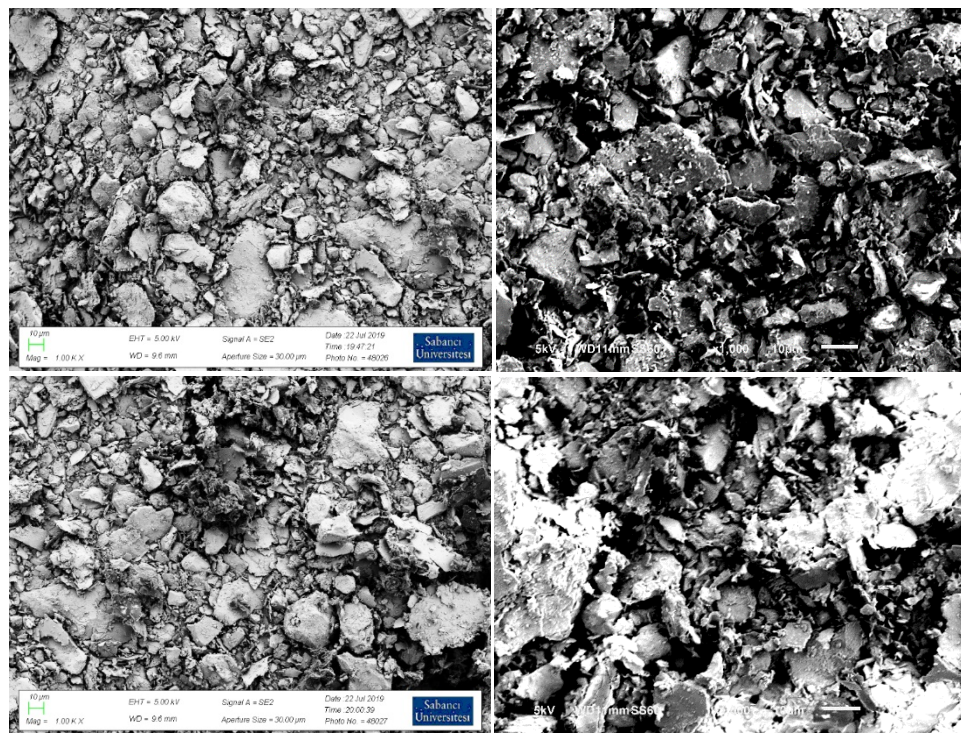
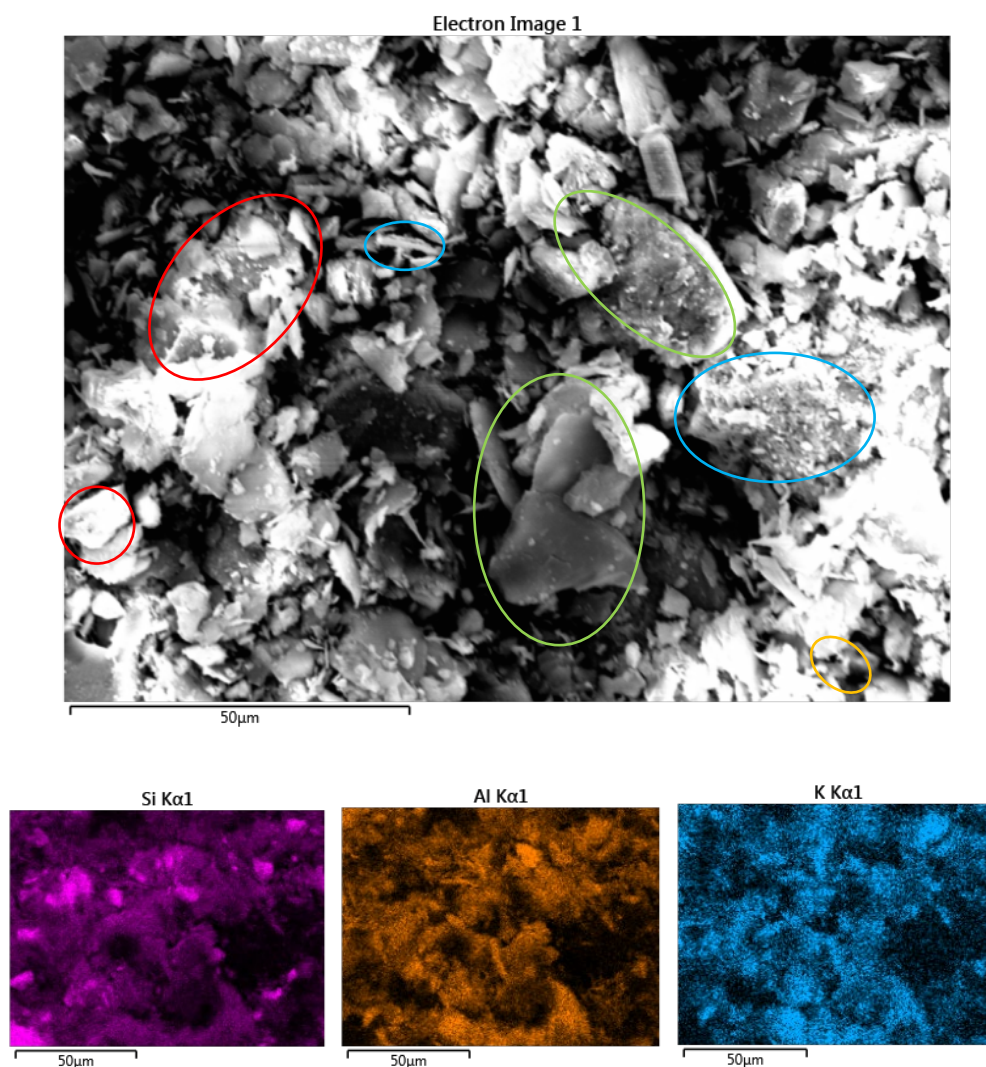


Figure 4. 41 M₁- Green schist micrographs for Virgin (Left) and Calcined (Right) Powders at the same magnification

The size and morphology of particles changed during calcination. Heat treatment caused a reduction in the average particle size from 33 to 10 μm. Morphology of the various particles

also changed as a result of calcination. Calcined powder particles had ruffled edges of the plate clay particles. For the chemical identification of the particles, EDS analysis was very useful. Figure 4.42 shows EDS elemental color maps of calcined M_1 powder sample alongside a micrograph where certain mineral phases are circled, The EDS spectrum below was collected from the whole exposed area of the imaged and gives a general idea about the overall composition of the powders.



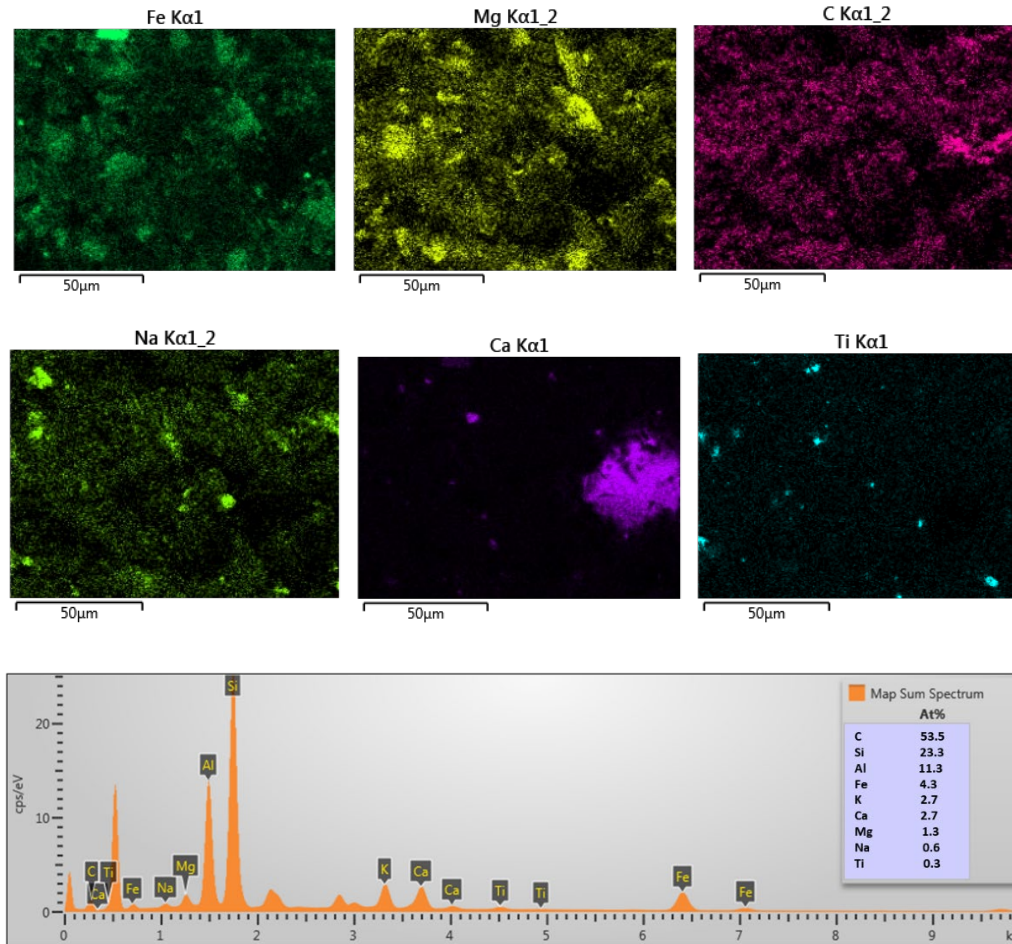


Figure 4. 42 EDS elemental analysis of calcined M₁- Green Schist

Based on the elemental analysis of calcined M₁ schist, there is some trace of carbonates circled in blue and appeared as the large magenta particle on the left in Ca-map-image and the remaining quartz particles circled in red in the figure. The Ca/Si atomic ratio is about 0.11 and Al/Si represent the ratio around 0.48.

4.5.2.3.2 M₂ with and without 15% \overline{CC} Addition

Micrographs taken at two different magnifications from virgin and calcined M₂ schist samples are shown in Figure 4.43 to identify the morphological changes that happened as a result of heat treatment (activation process).

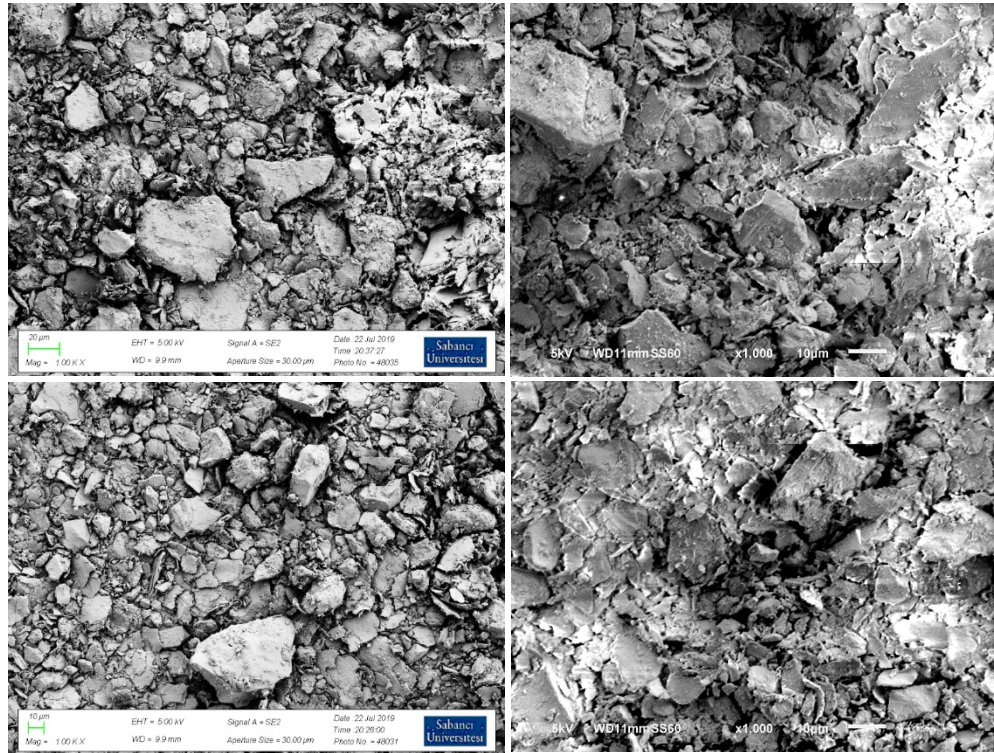
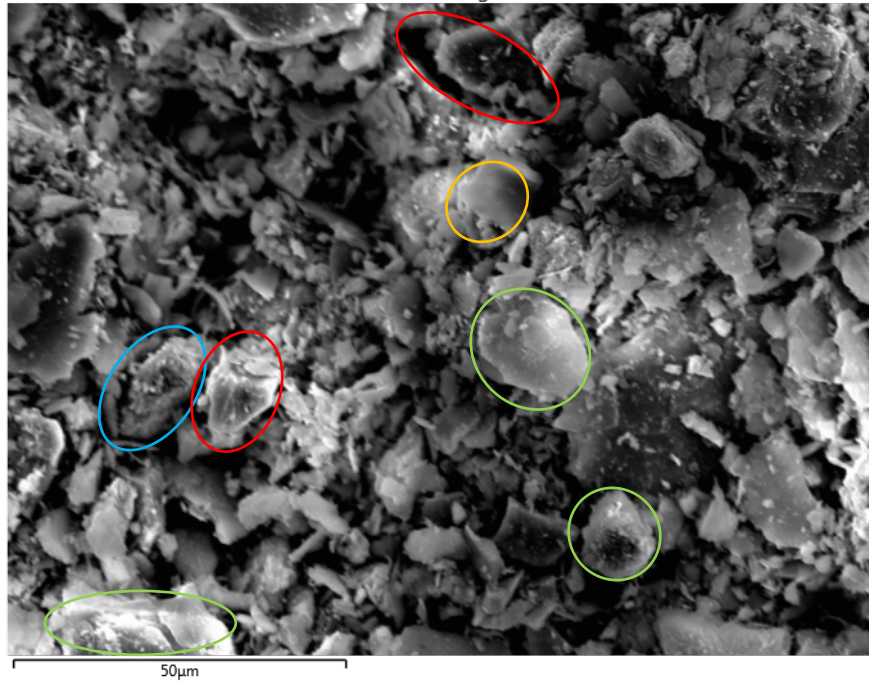


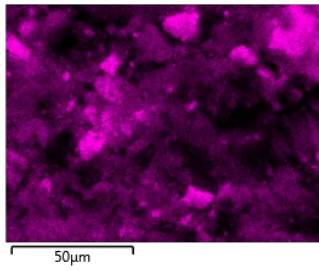
Figure 4. 43 M₂- Brown schist micrographs for Virgin (Left) and Calcined (Right) Powder

As it was the case with M₁ schist sample, the calcination affected the microstructure of some platy particles. The decomposition of clay minerals with plate-like morphologies can be recognized by ruffled edges. Also, the average particle size is reduced from 35 to 13 µm during calcination process. The quartz and carbonate particles were easy to recognize with the help of the EDS elemental mapping. Figure 4.44 illustrates the EDS elemental analysis results of the calcined M₂ powder.

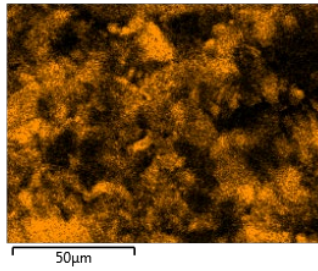
Electron Image 1



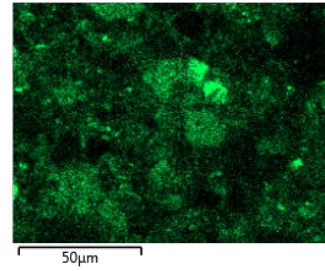
Si Kα1



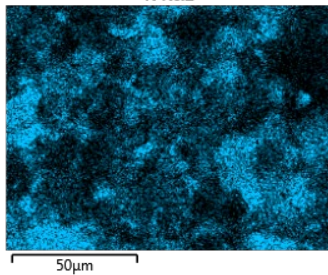
Al Kα1



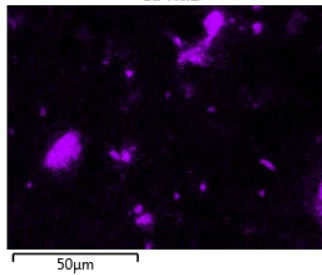
Fe Kα1



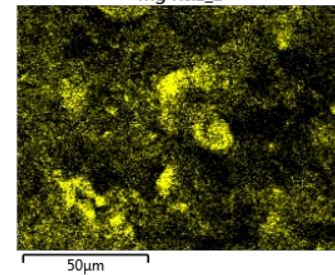
K Kα1



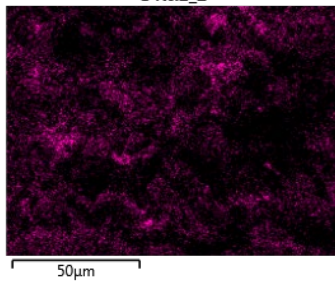
Ca Kα1



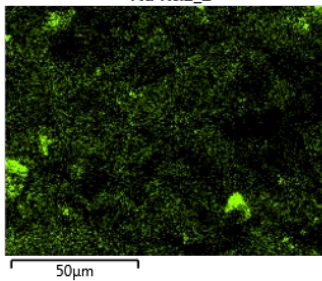
Mg Kα1_2



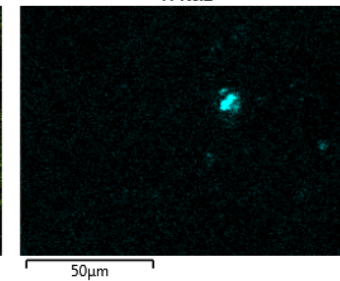
C Kα1_2



Na Kα1_2



Ti Kα1



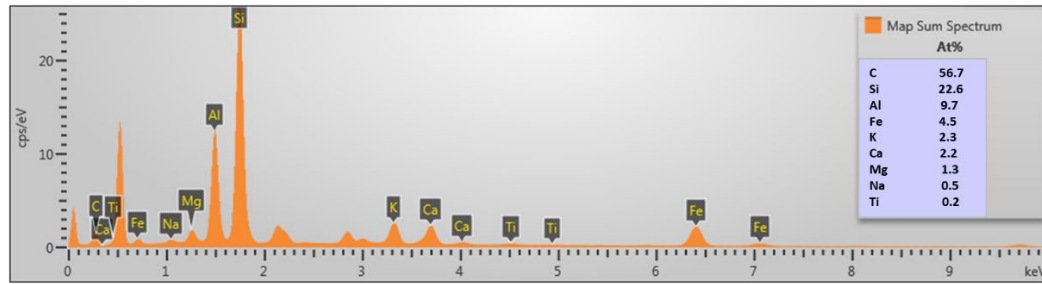


Figure 4. 44 EDS elemental analysis of calcined M₂- Brown Schist

The EDS elemental analysis shows that after calcination the Ca/Si ratio is about 0.1 and the ratio for Al/Si is 0.43. Therefore, there is partial dihydroxylation and destruction of clayey materials.

4.5.2.3.3 M₃ with and without 15% \overline{CC} Addition

Figure 4.45 shows the micrographs of virgin (left two images) and calcined M₃ (right two images) and the related changes that occurred through the heat treatment.

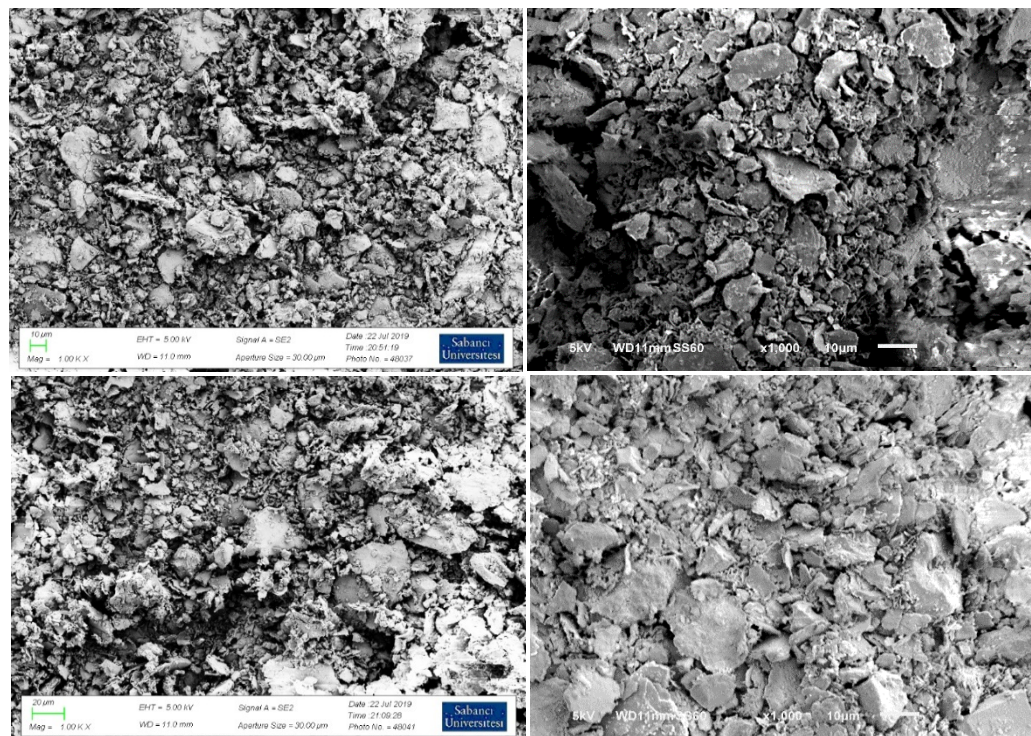
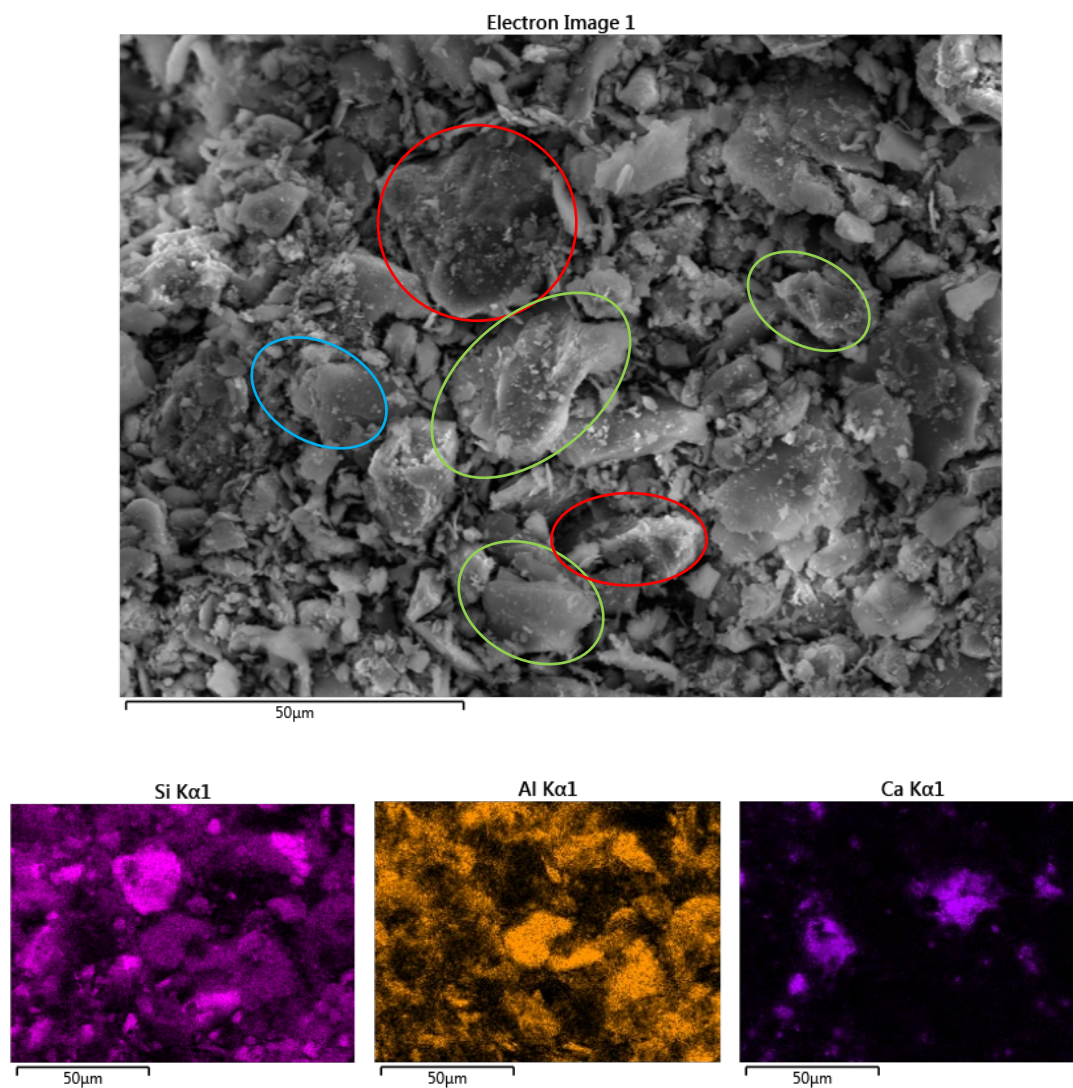


Figure 4. 45 M₃- Pink schist micrographs for Virgin (Left) and Calcined (Right) Powder

During the calcination, the particles of the M_3 components were destroyed and the edges were ruffled. The particle size was reduced from 30 to 14 μm . Also, the relative composition of them was deformed. More information can be obtained from the elemental analysis that is shown in Figure 4.46.



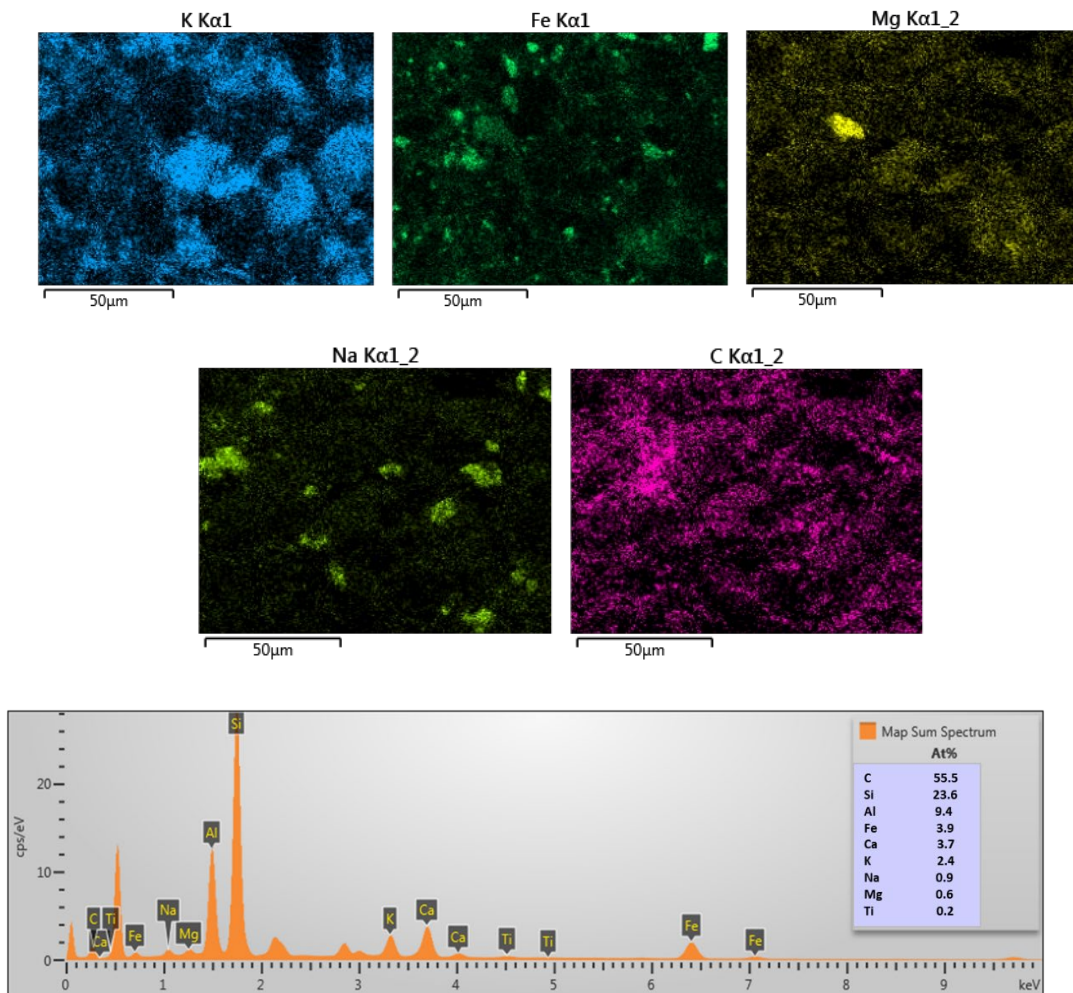


Figure 4. 46 EDS elemental analysis of calcined M₃- Pink Schist

The decomposition of M₃ clay after calcination resembles M₂ while the magnitude of dihydroxylation could be somehow more. The overall Ca/Si ratio in this sample is 0.15 and Al/Si ratio is around 0.4.

4.5.2.3.4 M₄ with and without 15% \overline{CC} Addition

Figure 4.47 represents the micrographs of M₄ – Black schist powder before and after the heat treatment.

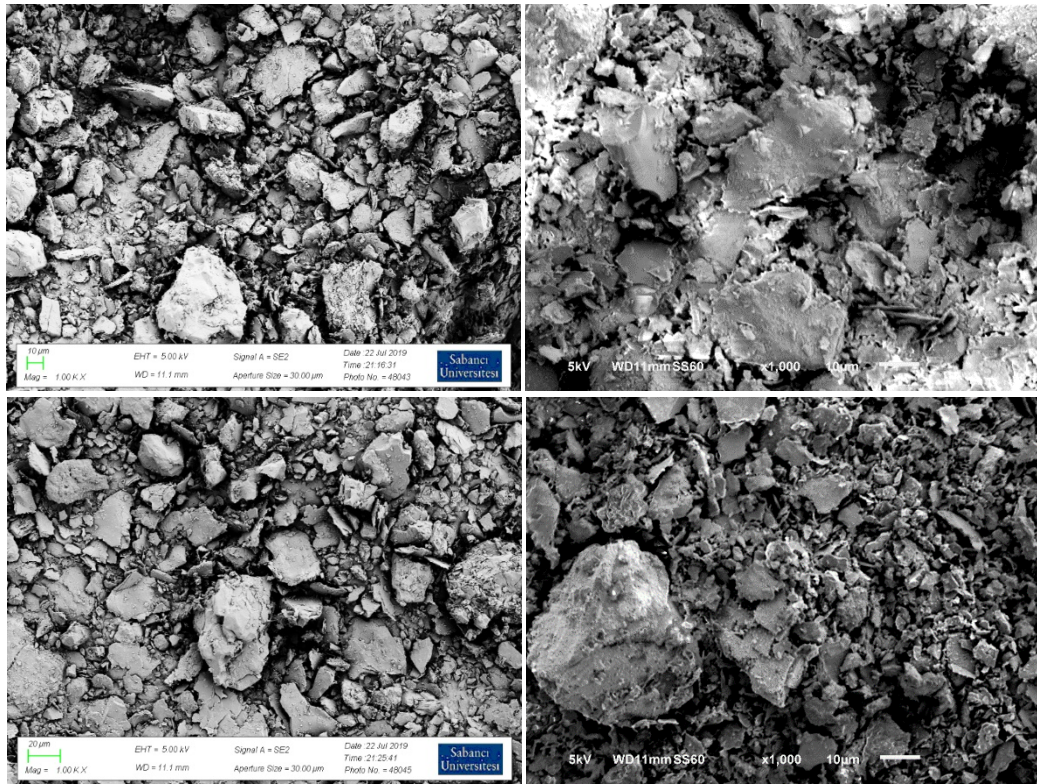
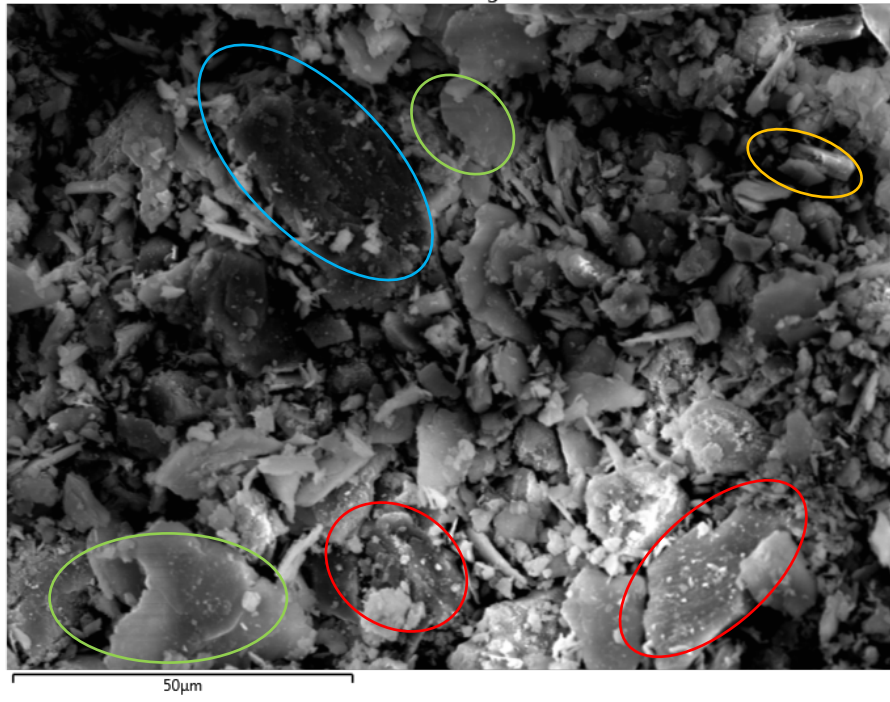


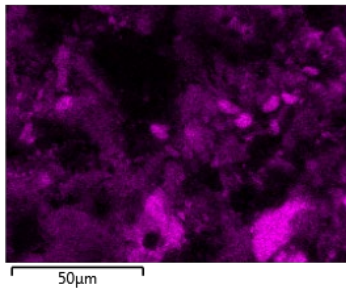
Figure 4. 47 M₄- Black schist micrographs for Virgin (Left) and Calcined (Right) Powder

The de-hydroxylated clayey particles be a ruffled edge particle in some parts of M₄ micrograph. The ruffled edged particles are more obvious in this sample after calcination. Moreover, during heat treatment process, the average particle size was reduced from 35 to 11 µm. Figure 4.48 shows the EDS analysis of the calcined material.

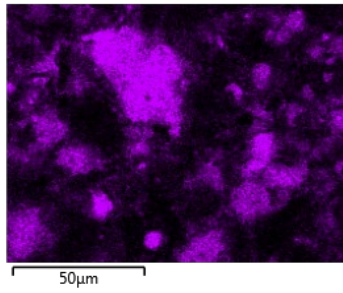
Electron Image 2



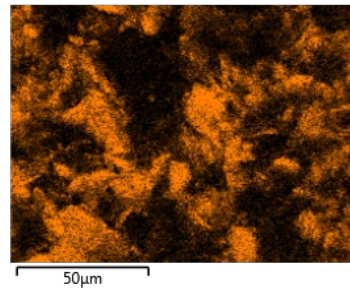
Si Kα1



Ca Kα1



Al Kα1



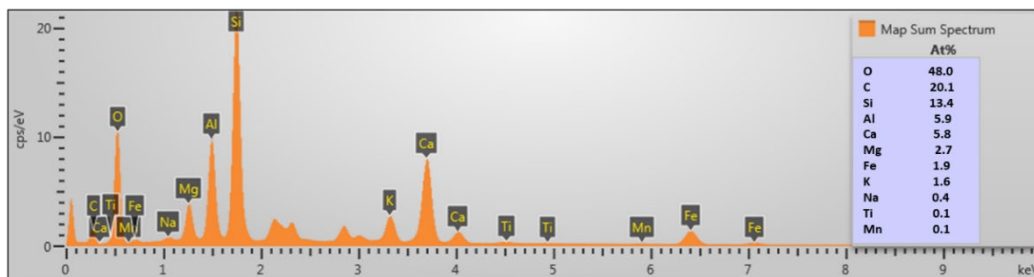
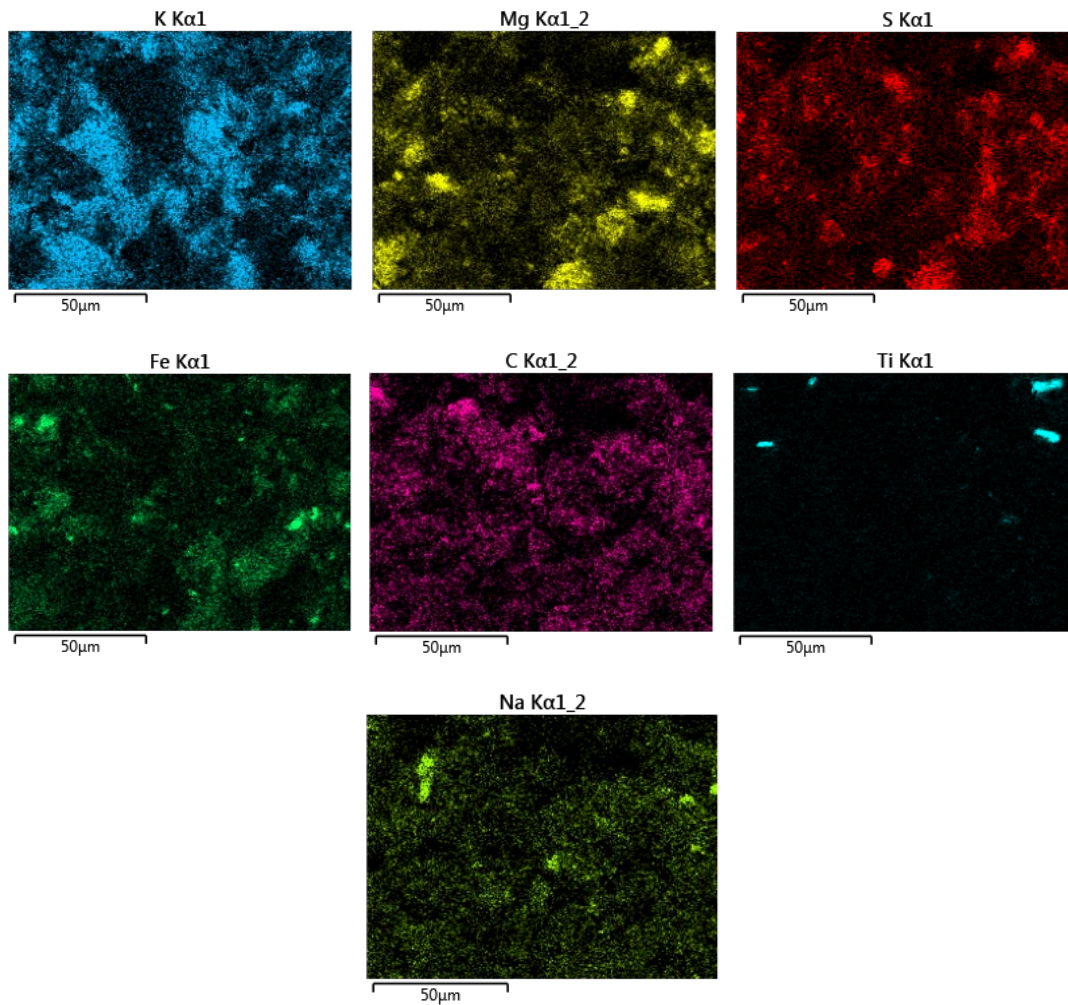


Figure 4. 48 EDS elemental analysis of calcined M₄- Black Schist

The EDS analysis of the calcined M₄ powder shows the Ca/Si ratio of 0.43 and Al/Si ratio of 0.44.

4.5.2 Compressive Strength Measurement

The compressive strength measurement is the best indication to evaluate the potential candidates for cement substitution. In this section, the compressive strength of the calcined clay cement (C^3) and limestone calcined clay and carbonate cement (LC^4) were compared. This comparison work is done to discern the effect of limestone or carbonate addition either as calcined carbonate (i.e. CaO) or virgin limestone ($CaCO_3$). The targeted strength criterium in this project was that the compressive strength of composite cement paste may not be less than 90% of the pure cement paste after 28 days of hydration.

Figure 4.49 illustrates the M_1 – Green schist compressive strength results when it is substituted 30 wt% of the cement as C^3 or LC^4 .

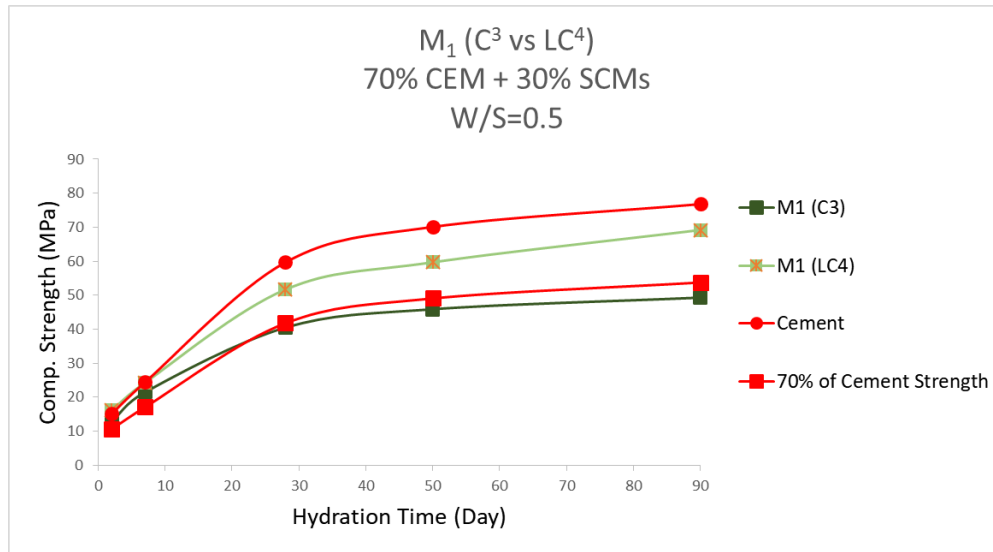


Figure 4. 49 M_1 - Green schist powder (calcined) compressive strength (C^3 vs. LC^4)

Based on the compressive strength results, the C^3 version of M_1 sample could not reach to the 70% of pure OPC strength. However, as it can be seen in the graph, added amount of carbonate to schist had the drastic effect on composite cement paste hydration. Generally, it is assumed that the pozzolanic reactions in composite cement pastes are slow take part in cement hydration. They contribute mostly to late strength. Therefore, it is safe to assume that the early strength values for 2 and 7 days of setting time are mostly associated with the

cement's contribution to the strength. Table 4.10 listed the compressive strength values of M_1 as C^3 and LC^4 to compare them to the ones of 100 wt% OP cement strength. The calculated strength values of 70 wt% cement (the rest assumed to be an inert filler) were given as a hypothetical inert substitution benchmark.

Table 4. 10 Compressive strength of composite cement paste prepared with calcined M_1 – Green as partial cement substitution (C^3 vs. LC^4)

Setting Time (Day)	M_1	M_1 with 15% CC	Cement	70% of Cement Strength
2	12.7	16.1	15.1	10.57
7	21.5	24.3	24.4	17.08
28	40.5	51.7	59.7	41.79
50	45.9	59.7	70.1	49.07
90	49.3	69.2	76.8	53.76

The 70 wt% of cement and 30 wt% hypothetical inert filler powder is chosen as benchmark to evaluate the role of calcined clay as cement substitution. The composite cement paste prepared with 70 wt% OPC and 30 wt% calcined M_1 schist (C^3) resulted in strength values that are much lower than the pure OP cement. Composite cement pastes prepared using M_1 as LC^4 samples resulted in strength values slightly below the predetermined criteria of 90% strength of pure OPC. On the other hand, the strength values for 90 days of setting are more than 90% of the pure OPC strength.

Figure 4.50 shows the compressive strength results for the composite cement pastes prepared with 30 wt% of either calcined M_2 (C^3) or calcined M_2 with 15 wt% carbonate (i.e. total carbonate amount before calcination (4.5 wt% of the composite cement powders)).

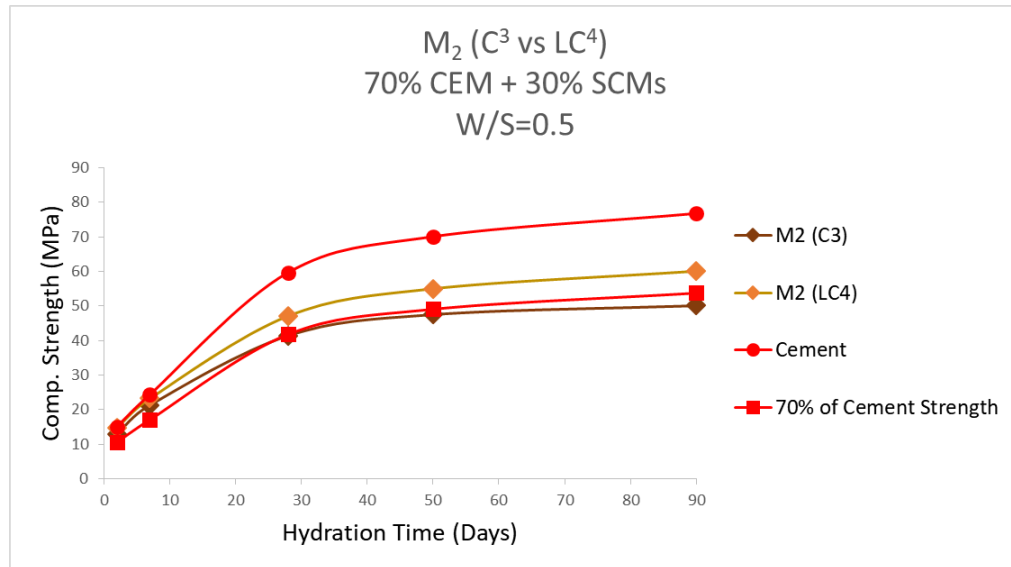


Figure 4. 50 M₂- Brown schist powder (calcined) compressive strength (C³ vs. LC⁴)

The compressive strength test results for M₂ sample either for C³ or LC⁴ did not satisfy the set goals. The obtained values are significantly lower than pure cement strength. Table 4.11 listed the values for M₂ composite cement paste sample in order to facilitate a comparison to the pure cement values.

Table 4. 11 Compressive strength of composite cement paste prepared with calcined M₂ – Brown as partial cement substitution (C³ vs. LC⁴)

Setting Time (Day)	M2	M2 with 15% CC	Cement	70% of Cement Strength
2	12.9	14.7	15.1	10.57
7	21.3	23.2	24.4	17.08
28	41.4	47.1	59.7	41.79
50	47.5	55	70.1	49.07
90	50.1	60.1	76.8	53.76

The achieved value for M₂ without the carbonate addition is almost 70% of cement strength that means the effect of pozzolanic reaction on strength of cement is not significant. In case of composite cement paste sample prepared with calcined schist/carbonate mixture (with 15

wt% of carbonate) the strength was only 80% of the OP cement strength. Therefore, both SCMs could not satisfy the chosen strength criteria.

Figure 4.51 shows the compressive strength results for composite cement paste mixture prepared with calcined M₃ without and with carbonate additions.

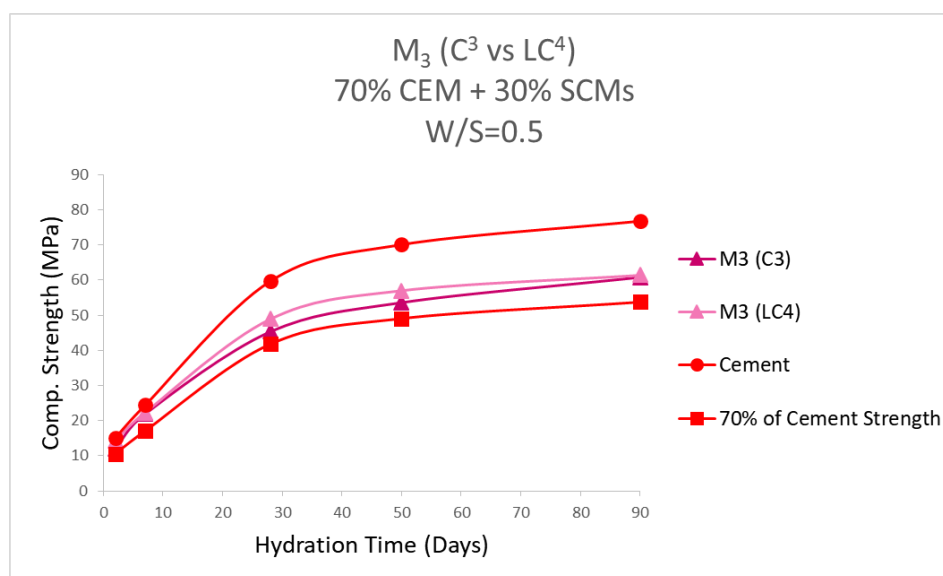


Figure 4. 51 M₃- Pink schist powder (calcined) compressive strength (C³ vs. LC⁴)

According to the strength graphs there is no substantial different between the C³ and LC⁴ for M₃ calcined schist. Both are considerably below the strength of 100 wt% OP cement paste. Table 4.12 represents the measured strength values for M₃ (C³) and M₃ (LC⁴) compressive strength tests.

Table 4. 12 Compressive strength of composite cement paste prepared with calcined M₃ – Pink as partial cement substitution (C³ vs. LC⁴)

Setting Time (Day)	M3	M3 with 15% CC	Cement	70% of Cement Strength
2	11.9	14.4	15.1	10.57
7	21.9	22.3	24.4	17.08
28	45.3	48.9	59.7	41.79
50	53.6	57	70.1	49.07
90	60.8	61.4	76.8	53.76

The compressive strength of M₃ schist as C³ and LC⁴ is lower than the determined threshold. For both cases the values are close to the 80% of the OP cement strength. This could be interpreted as that the pozzolan could not undertake the expected role in composite paste hydration and strength development.

Figure 4.52 shows the compressive strength of composite cement paste that was prepared with 30 wt% calcined M₄ with and without 15% carbonate additions.

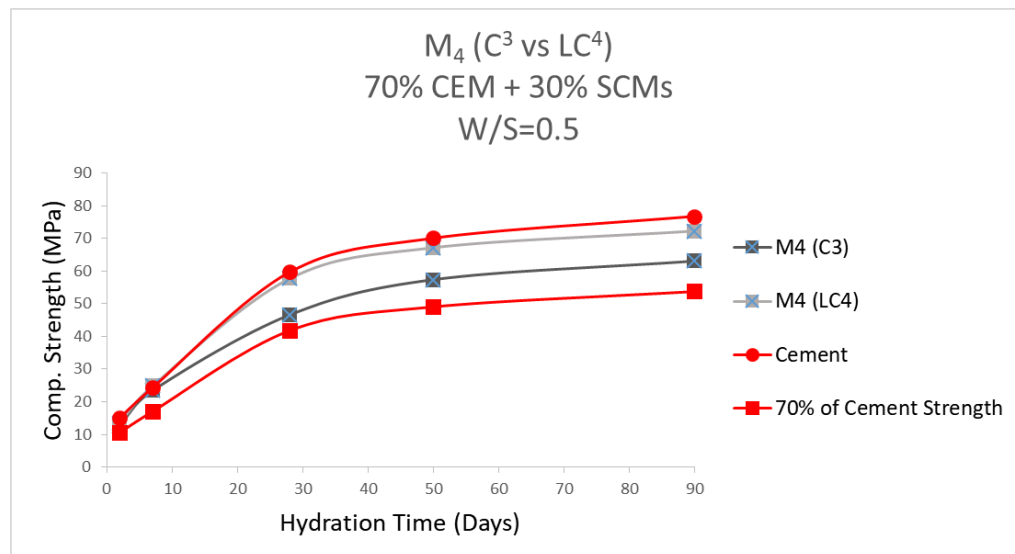


Figure 4. 52 M₄- Black schist powder (calcined) compressive strength (C³ vs. LC⁴)

The composite cement pastes which is made with calcined M₄ without any modification could not surpass the acceptable threshold but the LC⁴ samples astonishingly satisfied the criteria. Table 4.13 listed the strength values for the C³ and LC⁴ which was prepared with M₄ schist in order to be able to compare them to the strength values of pure cement paste.

Table 4. 13 Compressive strength of composite cement paste prepared with calcined M₄ – Black as partial cement substitution (C³ vs. LC⁴)

Setting Time (Day)	M4	M4 with 15% CC	Cement	70% of Cement Strength
2	12.6	13.5	15.1	10.57
7	23.42	24.8	24.3	17.01
28	46.6	57.7	59.7	41.79
50	57.4	67.2	70.1	49.07
90	63.1	72.3	76.8	53.76

As it can be seen in this table the compressive strength of the M₄ with 15% \overline{CC} was almost 97% of the pure cement strength. The compressive strength for M₄ sample without any 15% \overline{CC} additive was not satisfactory. The strength difference of these two samples must have been related to the effect of calcined carbonate.

Figure 4.53 illustrates the compressive strength values for all prepared composite cement paste samples comparing them to the pure OP cement. The most obvious interpretation about the results is to note the positive effect of carbonate additions to schists in compressive strength. For almost all schist samples except for M₃, the addition of carbonate to the virgin schist before calcination improved the strength of composite cements. Therefore, the highest ranked potential candidates are calcined M₁ and M₄ schists whose carbonate content in the original mixture was topped off to 15 wt% of carbonates in the total SCM mixture (i.e. schist + carbonate before calcination).

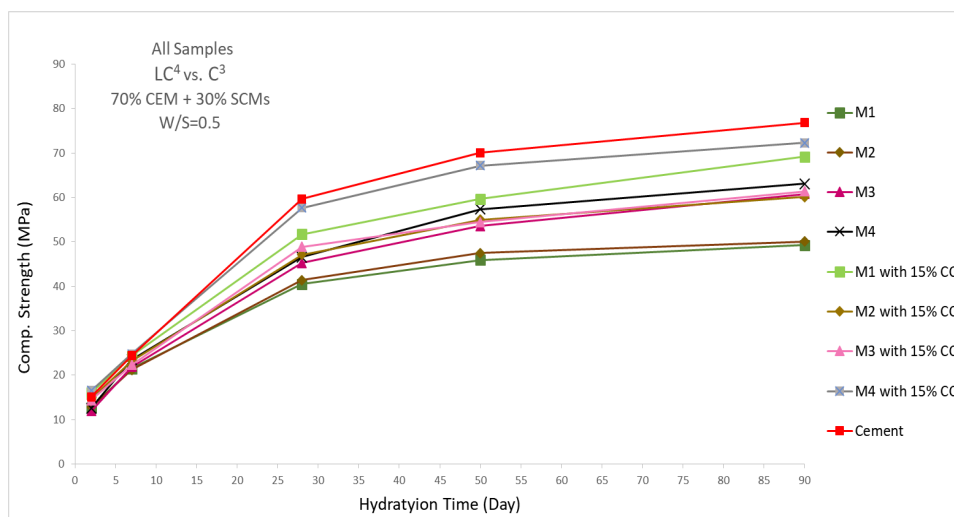


Figure 4. 53 The compressive strength test results for all samples (C^3 vs. LC^4 vs Cement)

Although M_1 and M_4 were the best candidates for SCMs, there is still hope for developing the potential of M_3 and M_2 if one can tailor their calcination temperature. Table 4.53 lists the compressive strength values of all samples for an easy comparison.

Table 4. 14 Compressive strength of composite cement paste prepared with calcined schists as partial cement substitution (C^3 vs. LC^4)

Setting Time (Day)	M1	M2	M3	M4	M1 with 15% CC	M2 with 15% CC	M3 with 15% CC	M4 with 15% CC	Cement
2	12.7	12.8	11.9	12.6	16.1	14.7	14.4	16.5	15.1
7	21.5	21.2	21.9	23.5	24.3	23.2	22.3	24.8	24.4
28	40.5	41.4	45.3	46.6	51.7	47.1	48.9	57.7	59.7
50	45.9	47.5	53.6	57.4	59.7	55	54.5	67.2	70.1
90	49.3	50.1	60.8	63.1	69.2	60.1	61.4	72.3	76.8

4.6 Discussion

The initial characterization of virgin schist materials was done to evaluate their clay contents and hence their potential for activation and cement substitution. According to XRD, SEM, EDS and TGA analysis, all 4 virgin materials have the proper phase compositions to be considered as viable cement substitution candidates. The chemical compositions of powders from first three mine overburden (M_1 , M_2 and M_3) were similar. Regardless of the amount of carbonate in their composition, the potentially reactive content of clayey phases was in acceptable weight percentage range. The quantitative XRD analysis of M_4 sample showed its graphite amount as 45 wt% in phase distribution. However, as we did the calibration experiment with an internal graphite standard, the same software program estimated the graphite phase amount as 45 wt% although only 5 wt% of graphite was added to a graphite-calcite mixture. Therefore, it is understood that the actual total amount of graphite in M_4 schist sample could be around 5 wt%. The rest 40 wt% of miscalculated graphite phase amount was distributed to other existing crystalline phases proportional to their original ratios. The corrected graphite phase amount in this sample is given in Figure 4.54 x-ray pattern and shown in Table 4.15 which lists the phase distribution.

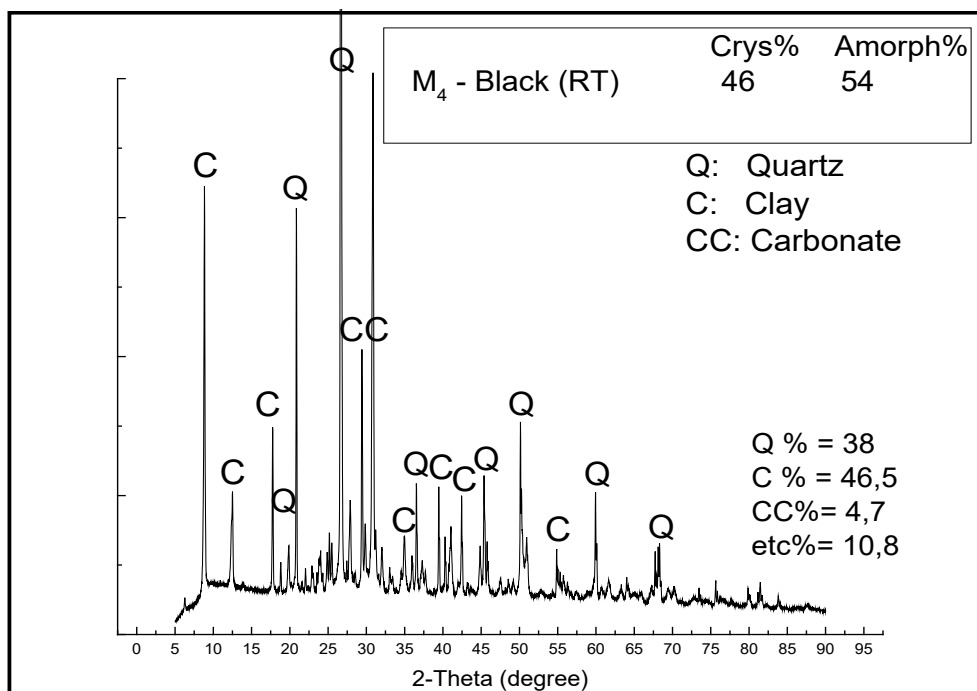


Figure 4. 54 M₄-Black schist type sample XRD spectrum and quantification

Table 4. 15 The Phase distribution and detailed information about crystal structure and weight percentage for each chemical compound in M₄-Black

Sample #	Chemical Phases	at%	Crystal Structure	Chemical Formula
1	Quartz	38	Hexagonal	SiO ₂
2	Calcite	4,7	Rhombo	CaCO ₃
4	Muscovite I	19,7	Hexagonal	(K , Na) (Al , Mg , Fe) ₂ (Si _{3.1} Al _{0.9}) O ₁₀ (O H) ₂
3	Ankerite	14,3	Rhombo	Ca (Mg _{0.67} Fe _{0.33} + ₂) (C O ₃) ₂
9	Albite	3,7	Triclinic	Na Al Si ₃ O ₈
5	Clinocllore	3,7	Monoclinic	(Mg _{2.8} Fe _{1.7} Al _{1.2}) (Si _{2.8} Al _{1.2}) O ₁₀ (O H) ₈
7	Mg-Annite	8,77	Monoclinic	K (Mg , Al) ₂ .04 (Si _{3.34} Al _{0.66}) O ₁₀ (O H) ₂
6	Graphite	5	Hexagonal	C
8	Titanium Oxide	1,32	Monoclinic	Ti ₃ O ₅
10	Pyrite	0,9	Cubic	Fe S ₂

After corrected graphite quantification, the amount of inert quartz amount changed to 38 wt%. M₄ sample contains 46% crystalline and 64% amorphous phases. These amounts before correction were 61.9 % crystalline and 38.1 % amorphous phases.

Figure 4.55 shows the comparison spectra and quantification of all four virgin samples.

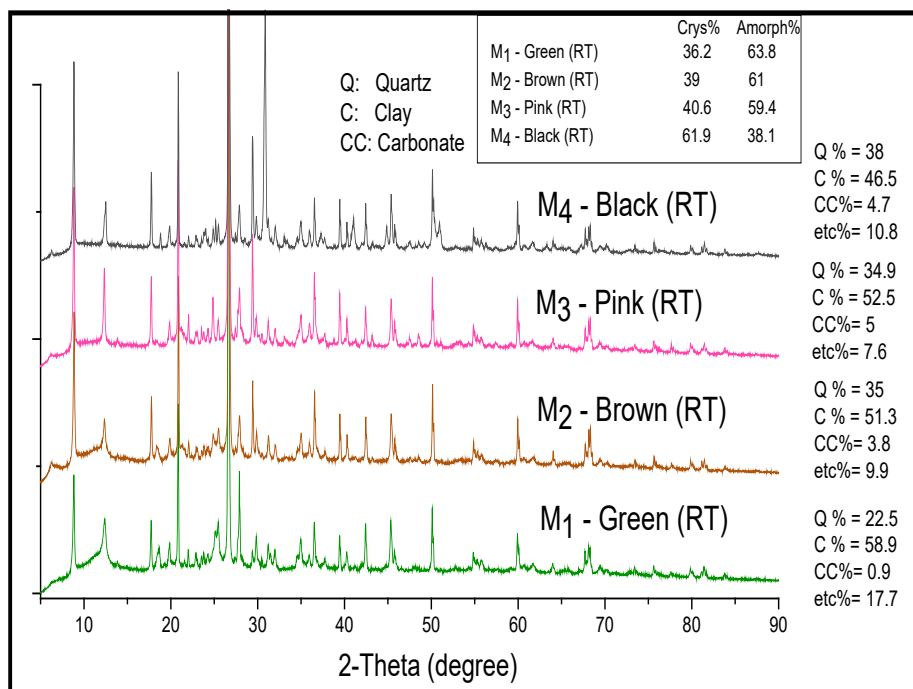


Figure 4. 55 X-ray diffractogram of all four samples and quantification

Table 4.16 provides the amounts of existing mineral phases in each schist sample for a proper comparison of all 4 candidate powders. Therefore, it also contains clues about which sample could be most appropriate one for activation.

Table 4. 16 Phase distribution and quantifications for all 4 samples

M ₁		Quartz: 22.5% Clay: 58.9% Carbonate: 0.9% etc: 17.7%	M ₂		Quartz: 35% Clay: 51.3% Carbonate: 3.8% etc: 9.9%
Chemical Phases	wt%	Crys%: 36.2 Amorph%: 63.8	Chemical Phases	wt%	Crys%: 39 Amorph%: 61
Quartz	22.5		Quartz	35	
Calcite	0.9		Calcite	3.8	
Illite	24.5		Muscovite I	28.2	
Muscovite	23.1		Muscovite II	16.1	
Albite	3.8		Albite	4	
Clinocllore	6.5		Clinocllore	3.3	
Dickite	4.8		Kaolinite	3.7	
Anorthite	12.1		Anorthite	5	
Titanium Oxide	1.8		Titanium Oxide	0.9	
M ₃		Quartz: 34.9% Clay: 52.5% Carbonate: 5% etc: 7.6%	M ₄		Quartz: 38% Clay: 46.5% Carbonate: 4.7% etc: 10.8%
Chemical Phases	wt%	Crys%: 40.6 Amorph%: 59.4	Chemical Phases	wt%	Crys%: 61.9 Amorph%: 38.1
Quartz	34.9		Quartz	38	
Calcite	5		Calcite	4.7	
Muscovite I	28.4		Muscovite I	19.7	
Muscovite II	18.2		Ankerite	14.3	
Albite	5.8		Albite	3.7	
Kaolinite	5.85		Clinocllore	3.7	
Rutile	0.4		Mg-Annite	8.77	
			Graphite	5	
			Titanium Oxide	1.32	
		Pyrite	0.9		

The general expectation is that the higher amounts of proper clayey phases a sample has the higher potential as an SCM the sample would have. However, the compression strength test results do not confirm this simple assumption. Obviously, there is a further parameter that has not been considered yet in our analysis that causes the strength of the cement pastes prepared with M₁, M₂ and M₃ samples to be lower than that of the composite cement prepared with M₄ powders. The clayey phase proportion in M₄ schist was lower than the others and consequently lower strength would be expected.

The answer for this apparent contradiction came by reviewing the thermogravimetry analysis of virgin and calcined schist powder samples. Table 4.17 lists a comparison of theoretical and experimental weight losses in M₁ after calcination.

Table 4. 17 Theoretical and Experimental weight loss amount of virgin M_1 after calcination

M_1	WL _T % (Experimental)	WL _T % (Theoretical)
Virgin	6.25	-
Calcined up to 80% WL_T	1.93 (31% WL)	1.25 (20% WL)

Our goal for calcination was that the calcination of schist type materials must be performed up to a temperature that would cause a decomposition that would correspond to 80% of the total weight loss that is possible in the schist (6.25 wt%). According to the calculated theoretical value the residual weight loss in M_1 schist after such a calcination should have been about 1.25%. However, the experimental amount is 1.93 wt%. This residual value would correspond to 69% of the total weight loss. It appeared that the heat treatment inside a box furnace to a massive amount of schist powders did not give the expected decomposition, the reason for this could be that the applied heat to a large amount (600 gr) of virgin powders was not distributed uniformly and transferred to all over the powder inside the furnace as well as it would be in a thermal analysis equipment with an extremely small amount of sample (50 mg).

A similar result was obtained for the same powder where the amount of carbonate in the schist was topped of to 15 wt% of the schist + carbonate mixture. Table 4.18 shows the calculated theoretical and experimental values for the M_1 with 15% \overline{CC} .

Table 4. 18 Theoretical and Experimental weight loss amount of M_1 with 15% CC after calcination

M_1 with 15% CC	WL _T % (Experimental)	WL _T % (Theoretical)
Virgin	10.89	-
Calcined up to 80% WL_T	2.72 (25%)	2.18 (20% WL)

As it can be seen, the residual decomposable materials were 25 wt% of the total decomposable material (clays' hydroxyl ions and carbonates' carbonate ions). The heat treatment resulted in a more successful activation in this powder mixture than the virgin M₁ schist powder. Probably the higher temperatures required for the decomposition of carbonate phase which was almost 100°C higher than the one of virgin powders helped the heat distribution within the bulky schist + carbonate powders. The better strength value of this material could have been influenced by the magnitude of properly calcined clayey phases and decomposed carbonate phase. Post mortem examination of the other schist samples yielded similar results and interpretations of strength development. Table 4.19 shows the comparison among the theoretical and experimental values for weight loss in term of M₂ with/without 15% \overline{CC} calcination.

Table 4. 19 Theoretical and Experimental weight loss amount of M₂ with/without 15% CC after calcination

M₂	WL _T % (Experimental)	WL _T % (Theoretical)
Virgin	6.82	-
Calcined up to 80% WL_T	2.58 (38% WL)	1.36 (20% WL)
M₂ with 15% CC	WL _T % (Experimental)	WL _T % (Theoretical)
Virgin	11.32	-
Calcined up to 80% WL_T	3.39 (30%)	2.26 (20% WL)

The difference between the magnitude of expected and actual weight losses of M₂ with and without carbonate confirmed the above-mentioned facts. The amount of calcination for bulk virgin M₂ powder was about 62 wt%. The actual weight loss was 70 wt% of the total weight loss for M₂ with 15% \overline{CC} . The similar observations were made for the two other samples. M₃

sample phase distribution is like M2. Table 4.20 shows the comparison for bulk M₃ powders with/without 15% \overline{CC} .

Table 4. 20 Theoretical and Experimental weight loss amount of M₃ with/without 15% CC after calcination

M₃	WL _T % (Experimental)	WL _T % (Theoretical)
Virgin	7.94	-
Calcined up to 80% WL_T	2.76 (35%)	1.59 (20% WL)
M₃ with 15% CC	WL _T % (Experimental)	WL _T % (Theoretical)
Virgin	10.95	-
Calcined up to 80% WL_T	3.05 (28%)	2.19 (20% WL)

The amount of calcination for bulk virgin M₃ was about 65 wt% and 72 wt% of the total weight loss for M₃ powder mixture with 15% \overline{CC} .

Table 4.21 represents the expected and actual magnitude of weight losses due to decomposition reactions for M₄ with and without 15% \overline{CC} .

Table 4. 21 Theoretical and Experimental weight loss amount of M₄ with/without 15%(CC) after calcination

M₄	WL _T % (Experimental)	WL _T % (Theoretical)
Virgin	15.74	-
Calcined up to 80% WL_T	3.37 (21%)	3.15 (20% WL)
M₄ with 15% CC	WL _T % (Experimental)	WL _T % (Theoretical)
Virgin	18.5	-
Calcined up to 80% WL_T	3.51 (19%)	3.7 (20% WL)

M₄ powders showed a different calcination behavior than the other schist samples. The heat treatment in a box furnace was more successful for bulk M₄ schist powders than the other schist powders. M₄ schist contained in its original composition graphite and pyrite which made it different from the others. The role of graphite among the other phases is somehow unusual. It was assumed that during the calcination, graphite could burn and provide more heat in addition to the furnace heat and cause further decomposition or de-hydroxylation. During the decomposition of graphite, the reaction with oxygen would cause further heat. Facilitating further decomposition of components.

Therefore, M₄ schist may have a better activation and more reactivity than the other schists. For other three samples, since the thermal conductivity of clay is very low and there is not any internal heat generator during calcination, the calcination process was not completed for the entire bulk samples. Again, in the M₄ with 15% \overline{CC} addition, burning of graphite provided extra heat for more decomposition. Based on the TGA analysis for virgin M₄ schist in previous section the graphite decomposition temperature range was lower than the carbonate decomposition temperature range. So, the excessive heat that was originated in graphite, mainly decomposed the carbonate component. In the elemental analysis of M₄ sample, It is not that easy to track footprint of graphite. But according to the x-ray analysis, the ascertained amount of graphite is diffused in all over the powder.

Pyrite will change to Pyrrhotite after 780°C that does not seem to have any drastic effect on reactivity. Also, the amount of these two components did not exceed 8 wt% of total composition which cannot make any other tangible effect.

The mentioned interpretation represents the importance of temperature and magnitude of calcination in reactivity of schist type powders. Hence, it should be possible to have better strength results after calcination schedule was modified.

Another topic that should be discussed is the relationship between the change in the amorphous content and the strength development and pozzalanicity. It is believed that high amorphous materials proportions in the original powders would help with the reactivity of the sample. Although it is likely that the non-crystalline aluminosilicate phases (reactive phases) could participate in pozzolanic reactions, it is not possible to be certain that the whole amorphous portion would be pozzalanically reactive material. It is possible to have non-reactive phases in the amorphous content.

The partial decomposition of carbonate phase provides an opportunity to take advantage of calcined or decomposed carbonate as a source of Ca^{2+} ion and the virgin carbonate may enter the reaction directly. As it is mentioned in the literature review section [5] that the excessive amount of carbonate in powder could react and/or provide filler effect, it is also claimed that it could influence the ettringite formation during the hydration process.[5] According to the theoretical calculations it seems that there is a possibility to increase the amount of carbonate portion more. The employed 15 wt% carbonate content in the schist was originating from the first phase of project. In the first phase, Kovukdere schist sample contained 15 wt% of calcium carbonates in its composition and showed the best compressive strength performance among all the tested samples. Therefore, it was decided to top off the carbonate amount up to 15 wt% to control the strength performance of the Muratbey schist which was identical in its phase composition except for the missing carbonate amount. However, according to the chemical formula of the C-S-H ($\text{Ca}_5\text{Si}_6\text{O}_{16}(\text{OH})_2 \cdot 4\text{H}_2\text{O}$) and C-A-S-H ($\text{Ca}_5\text{Al}_2\text{Si}_6\text{O}_{16}(\text{OH})_2 \cdot 4\text{H}_2\text{O}$) it is possible to top off the amount of carbonate up to 30wt% of total replacement.

We are extending our activation studies into also determining the proper calcination procedures, times and temperatures for the M1, M2, and M3 schist samples with and without CC additions. We will also conduct experiments to highlight the dangers of over-doing the calcination process to kill all the activity in the clay type pozzolans.

4.7 Conclusion

As it was mentioned before the purpose of the second phase of project is to evaluate the effect of carbonate either as “calcined-into-CaO” or virgin limestone powder on compressive strength. The effect of limestone as a source of virgin carbonate is already being discussed in several studies. Filler effect and the promotion of hemi-carboaluminates are the main application of carbonate in composite cement pastes. But in this study the application of carbonate mainly calcium carbonate or calcite, is discussed as a source of additional reactive Ca^{2+} ions. The idea is based on the fact that the extra calcium (2+) ions were going to react with activated Al-Si-O-H to provide further C-S-H or C-A-S-H. Hence, the existence of carbonate as calcined carbonate in raw materials for composite cement paste is going to be more beneficial. Moreover, proposed pozzolanic minerals could help avoid the excessive amount of portlandite in cement or concrete structure which can cause inevitable damages and mitigation of durability due to the late age’s reactions.

In this study, four different mine minerals were evaluated for possible potential of partial cement substitution. The virgin powders as received from the mine were indexed as M_1 – Green, M_2 – Brown, M_3 – Pink and M_4 – Black. The microstructure of them resembled to each other while there were some differences in their compositions. M_2 and M_3 were much closer to each other and M_1 was similar. But there were some differences between M_4 and the others. M_4 schist contained some small amounts of graphite and pyrite. The effect of graphite as a source of excessive heat during the calcination due to the burning was investigated. But there is no direct evidence about the influence of the iron sulfide or pyrite in this study.

All the schist types mine powders were calcined, according to the determined and calculated temperatures to activate them. The heat treatment temperatures corresponding to partial activation of possible pozzolanic phases were chosen accurately to avoid dead-burning the clayey materials. Therefore, calcination temperature was the temperature associated to the 80% of the total weight loss. These exact temperatures were determined for the virgin schist powders with the help of a thermal analysis equipment. The schist powders were investigated for their potential for activation in as-received form and as modified mixed-powders with

their weight percentage of the carbonate was topped off to 15%. The calcined materials partially substituted the cement powder when preparing composite cement pastes.

Three sets of cube samples (4cm x 4cm x 4cm) were prepared for each setting time which were 2, 7, 28, 50 and 90 days. The portion of cement replacement was 30 wt%. The cube samples were cured in full moisture condition and the uniaxial compressive strength measurement were applied to all of them.

The strength measurement results revealed that the M₄ with 15% \overline{CC} was the best potential candidate and M₁ with 15% \overline{CC} took the second place. M₄ with 15% \overline{CC} surpassed the determined criteria which was the compressive strength to be not less than 90% of the pure cement paste during the 28 days. The study also illustrated the importance of proper heat treatment to reach the targeted activation amount in the schist powder mixtures. It appeared to be possible to further increase the strength of hydrated composite cement pastes by properly adjusting the amount of Ca²⁺ ion in the SCM.

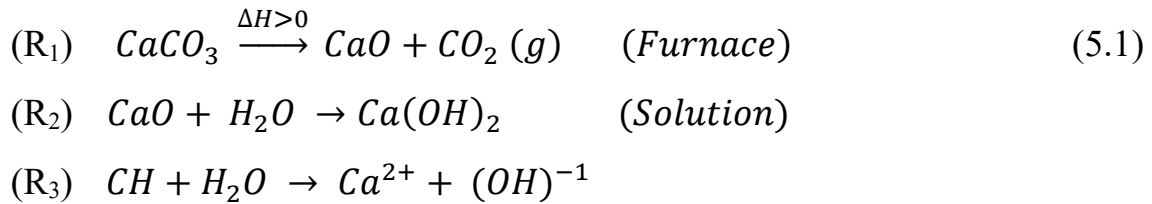
CHAPTER 5

CONCLUSION

Several groups [171, 172] have previously claimed that calcined clay can be used as SCM and would ensure an improved durability of concrete made from the substituted cement. Most successful candidate among the clay minerals was Kaolinite which worked as a proper material for cement substitution when activated by heat to [meta-Kaolinite]. However, kaolinite is one of the least available clay minerals. Few other studies with other types of clays reported less successful results when compared meta-kaolinite. In this study, we illustrate successful activation of minerals containing various types of clays as SCMs when properly heat treated. These minerals were natural mines containing quartz, clays, carbonates, glassy structures and some minor phases. Previous studies with the Kaolinite powders indicated that activation of Kaolinite to meta-kaolinite happens through the de-hydroxylation which renders the clayey structure semi-amorphous and unstable. It is postulated [171] that the de-hydroxylated aluminum sites provide a point of attack during hydration reactions. Therefore, the more active sites of attack that we provide the more reactive is the clay mineral. There are two types of basic clay structures. Kaolinite is the simpler one with one tetrahedral sheet of silicate and one octahedral sheet of aluminate while in more complex layered structures (e.g. Illite and Smectite) aluminum hydroxide layer is sandwiched between

two silicate layers. In our study, schist-derived virgin materials contain different types of clays which decompose at various temperatures. By releasing the hydroxyl bond through heat treatment, or de-hydroxylation, these various clay minerals are de-stabilized to various degrees. The strongly alkaline solution of cement hydration can attack these unstable structures to initiate pozzolanic reactions. Consequently, C-S-H and C-A-S-H will form gradually through the polymerization process of dissolved silicate and aluminate mers with calcium ions. Ordinary Portland cement would provide almost 5% free lime as a source of calcium ions. Based on this reaction scenario the effectiveness of a pozzolan is related to the amount of de-hydroxylated aluminum. To confirm this postulate, the received materials activated to 30%, 50% and 80% of the total de-hydroxylation (i.e. the total amount of weight loss due to de-hydroxylation) for the first phase of study. The applied activation temperature was kept on purpose at a value that would correspond to 80% of total weight loss in order to avoid dead burning of the clay minerals by overheating. The pozzolanic potential of our sources were evaluated through two common methods described in literature. The first method is the so-called pozzolanicity method which relates the change in electrical conductivity of a saturated calcium hydroxide solution to the pozzolanic activity of a sample. Electrical conductivity of the solution decreases as the active clay minerals react with calcium ions. The change in electrical conductivity is therefore correlated to the pozzolanic activity of the sample. The second method is the observation of strength development in blended cement pastes that are prepared with activated schist minerals treated for different curing time. Although levels of pozzolanic activity obtained from pozzolanicity and compressive strength measurements paralleled each other for meta-kaolinite and carbonate free schist minerals there was an open contradiction between the results of these two methods for schist type sample with some portion of carbonate. For Kaolinite and schist type samples without carbonate as the activation level was increased pozzolanicity as well as strength of the blended cements made from them increased. However, although pozzolanicity measurements indicated a decreasing pozzolanic effectiveness beyond 50% activation for sample with carbonate like Kovukdere schist, the blended cement prepared with this sample continued to increase in its strength for all curing times. Decomposition temperature range of clays usually starts around 400°C and ends around 800°C. The preceding weight losses correspond to non-structural (maybe absorbed) water [111-115]. Best known example, Kaolinite decomposes

through the de-hydroxylation in the temperature range of 450°C to 750°C. The temperature that corresponds to 80% of weight loss of schist type powder without carbonate phase is within this temperature range. However, for other investigated samples (e.g. Kovukdere) contained carbonate phases which decomposed in the temperature range of 710°C to 850°C. The temperature required for 80% weight loss of these sample corresponded to the upper end of this temperature range. Therefore, sample samples with calcite contained some amounts of decomposed calcium carbonate when treated up to 80% weight loss. This extra source of calcium ions in these schist type sample is the cause of error in pozzolanicity measurements. Temperature ranges that correspond up to 50% of weight loss are below the decomposition temperature of the carbonate phase. Therefore, for these samples pozzolanicity measurements were not tempered by calcium ions from them. Hence the pozzolanicity measurements and strength development gave parallel results for all samples up to 50% activation. As the samples with carbonate heat treatment impinged into decomposition temperatures of the existing carbonate the inconsistency between the two types of test emerged according to the reaction scheme described below:



Calcium carbonate decomposition during activation produces calcium oxide. As this sample was put in the aqueous solution, additional calcium and hydroxyl ions would form which in turn would increase the pH as well as the electrical conductivity of the solution negating the effect of activated clays. Therefore, pozzolanicity measurement by electrical conductivity may not be suitable for activated schist minerals containing carbonate phases. To clarify this contradiction, it would be beneficial to compare three samples. Kovukdere as a schist type material with some portion of carbonate, Muratbey as a schist without carbonate and Kaolinite clay as a benchmark.

Compressive test results are the most trusted indicator of cement paste strength. Figure 5.1 represents the compressive strength of the Kovukdere, Muratbey and Kaolinite samples after 28 days of curing as function of their activation level. Pozzolanicity and strength development, paralleled each other for Muratbey type schist and Kaolinite. Both increased as activation level of the clay type materials increased. However, there is an apparent contradiction between the pozzolanicity and strength development of Kovukdere schist material at highest level of activation (80 wt%).

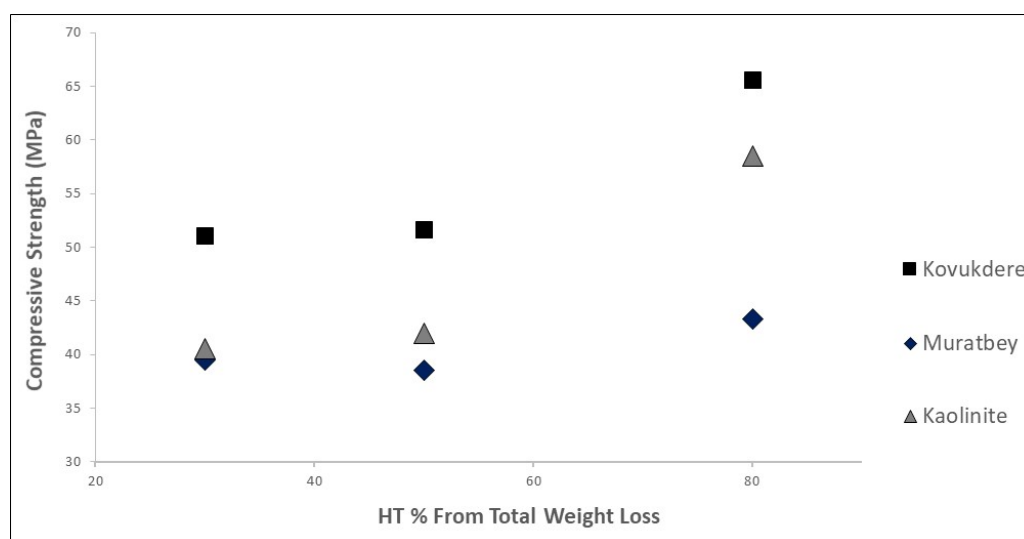


Figure 5. 1 Compressive strength of Kovukdere, Muratbey and Kaolinite (28d) vs. magnitude of heat treatment (30, 50 and 80% of WL_T)

The measured pozzolanicity of the Kovukdere schist decreased after 50 wt% heat treatment although the compressive strength increased even for 80 wt% activation. As it was determined by the X-ray phase analysis, Kovukdere schist contained 16 wt% calcium carbonates in addition to the clay minerals and quartz. The temperature that corresponded to 80 wt% weight loss for Kovukdere schist sample encompasses also the decomposition of calcite in to calcia. This calcium oxide converts to calcium hydroxide in aqueous solution obscuring the validity of the pozzolanicity test for the reactivity of the sample. Therefore, pozzolanicity measurement shall not be taken as an indicator of reactivity for samples containing carbonate phases. Figure 5.1 also reveals an important fact about the potential of

natural clay resources as SCMs. Combination of quantitative X-ray and EDS elemental analysis of Kovukdere and Muratbey schist materials indicated that the Kovukdere contained a higher amount of amorphous aluminosilicate and calcium content. This difference in the phase composition of Kovukdere schist sample indicated itself also in strength development of the cement paste prepared with it. Despite the similar crystalline clay phases content of Kovukdere and Muratbey samples, Kovukdere-schist/cement composite paste gave a higher strength even for non-activated SCM additions. This is believed to be due to the extra active amorphous aluminosilicates in this sample participating in pozzolanic reactions.

The comparison of the results obtained from these three samples revealed an important aspect of activated clay sources. Carbonate phases in such clay minerals when calcined provides an extra source of calcium ions for pozzolanic reactions. Such aluminosilicate based SCMs therefore resulted in higher compressive strength when incorporated in to composite cement pastes as seen in the case of Kovukdere schist material.

Previous studies [171-175], claimed that the combination of limestone and calcined clay was an effective partial substitute for cement. In this study, we furthered the existing knowledge about clay based SCMs by showing that calcined carbonate phases alongside with activated clay is a better substitute for OPC. The positive influence of having additional active calcium ions in the composition of a pozzolanic SCM is motivated the launching of the second phase of study intensively of the sequel on activated clays by addition or topping up the amount of carbonate to the pre-determined portion. According to the obtained results for the second phase of study, it could be claimed that any natural resources containing clay minerals are possible to activate as pozzolanic SCM for OPC substitution. The amount of pozzolanic activity is directly related to the level of de-hydroxylation of clay minerals as manifested by the weight losses in the temperature range from 400 to 800°C. The de-hydroxylation reaction leaves behind an amorphous and active aluminosilicate structure that will react with the available calcium ions in an aqueous solution. Clay minerals containing calcium carbonate phases resulted in higher strength composite cement pastes for all curing times when the carbonate phases were co-activated by thermal treatment. The pozzolanicity measurements by electrical conductivity are rendered inaccurate for SCMs containing activated carbonate phases.

REFERENCES

- [1] R. Andrew, "Global CO₂ emissions from cement production," CICERO Center for International Climate Research, Oslo, 2017.
- [2] C. D. Keeling, "Industrial production of carbon dioxide from fossil fuels and limestone," *Tellus*, 25, no. <https://doi.org/10.3402/tellusa.v25i2.9652>, pp. 174-198, 1973.
- [3] USGS, "Cement statistics, in: Historical Statistics for Mineral and Material Commodities in the United States," U.S. Geological Survey Data Series 140, Virginia, 2015.
- [4] H. G. Van Oss, "Cement, in: 2014 Minerals Yearbook," USGS, Virginia, 2017.
- [5] T. A. Boden, R. J. Andres and G. Marland, "Regional and National Fossil-Fuel CO₂ Emissions," U.S. Department of Energy, Tennessee, 2017.
- [6] B. Vanderborght and U. Brodman, "The Cement CO₂ Protocol: CO₂ Emissions Monitoring and Reporting Protocol for the Cement Industry," World Business Council for Sustainable Development, New York, 2001.
- [7] F. C. Lai, "Innovative cement additives quality improves in sustainable cement and concrete," *Sains Malaysiana*, vol. 11, no. 44, pp. 1599-1607, 2015.
- [8] J. Ke, M. McNeil, L. Price, N. Z. Khanna and N. Zhou, "Estimation of CO₂ emission from China's Cement production: Methodologies and uncertainties," *Energy Policy*, vol. 57, pp. 172-181, 2013.
- [9] Q. Zhu, "CO₂ abatement in the cement industry," IEA Clean Coal Centre-CCC/184, 2011.
- [10] F. M. Lea, *The chemistry of cement and concrete* 3rd edition, New York: Chemical Publishing Company, 1971.
- [11] S. L. Znackzko Jaworski, *Oczierki Historii Wiazuszczich Wieszczestw (History of Binding Materials)*, Moscow: Izd. Akadeimii Nauk SSSR, 1963.
- [12] R. H. Bouge, *The Chemistry of Portland Cement*, New York: Reinhold Publication Corporation, 1947.
- [13] R. Malinowski and Y. Garfinkel, *Concrete Intern*, London, 1991.

- [14] J. Bensted and C. Nichola , Cement Wapno Beton, Beograd, 2003.
- [15] P. K. Mehta, "ASTM Publication," Special Technical Publication, New York, 1953.
- [16] H. F. Gonnermann, W. Lerch and M. W. Whiteside, "PCA Research Labortory Bulletin," Cement Inc., Chicago, 1953.
- [17] H. F. W. Taylor , Cement Chemistry, Washington: T. Telford, 1997.
- [18] A. C. A. Muller, K. L. Scrivener, A. M. Gajewicz and P. J. McDonald, "Densification of C-S-H measured by H NMR relaxometry," *Journal of Physical Chemistry* , vol. C117, no. 1, pp. 403-412, 2013.
- [19] P. F. G. Banfill, "7th ICCC Paris," ICCC, Paris, 1980.
- [20] W. Kurdowski , Cement and Concrete Chemistry, London: Springer , 2014.
- [21] E. CEN, "Composition, specifications and conformity criteria of common cements," European Standards, Zurich, 2000.
- [22] W. Gaca, "Cement Wapno Gips," ICO, Berlin, 1963.
- [23] R. Kovacs, "8th ICCC Rio de Janeiro," Rio Pub , Rio de Janeiro, 1986.
- [24] N. B. Winter, Understanding Cement, Suffolk: WHD Microanalysis Consultants Ltd, 2009.
- [25] T. C. Powers and T. L. Brownyard, "Studies of the physical properties of hardened portland cement paste," in *American Concrete Ins.*, Miami, 1946.
- [26] A. M. Neville, "Properties of Concrete," Prentice Hall - 4th Edition , Princeton, 1995.
- [28] W. A. Gutteridge and J. A. Dalziel, "Filler cement: The effect of the secondary component on the hydration of Portland cement. Part I. A fine non-hydraulic filler," *Cement and Concrete Research* , vol. 20, no. 2, pp. 778-782, 1990.
- [29] M. Regourd and P. Barnes , "Structure and Performance of Cements," *Applied Science* , vol. 12, no. 1, p. 109, 1983.
- [30] W. Kurdowski and S. N. Ghosh, Advances in Cement Technology, Oxford: Pergamon Press, 1983.
- [31] P. K. Mehta, "Concrete Technology for Sustainable Development," Concrete International , Boston, 1999.

- [32] M. Schneider, M. Romer, M. Tschudin and H. Bolio, "Sustainable Cement Production - Present and Future," *Cement and Concrete Research* , vol. 41, no. 5, pp. 642-650, 2011.
- [33] H. Pollmann , "Composition of cement phases, in structure and performance of cements," Taylor Pub, New York, 2009.
- [34] K. J. Wang, M. S. Konsta-Gdoutos and S. R. Shah, "Hydration, rheology, and strength of ordinary Portland cement (OPC)-Cement kiln dust (CKD) - Slag binders," *ACI Mater*, vol. 99, no. 3, pp. 173-179, 2002.
- [35] B. Lothenbach, K. Scrivener and R. D. Hooton, "Supplementary cementitious materials," *Cement and Concrete Research* , vol. 41, no. 3, pp. 217-229, 2011.
- [36] M. Thomas, "Supplementary Cementing Materials in Concrete," in *Durability of Concrete* , CRC Press, 2013, p. Chap. 9.
- [37] M. D. A. Thomas and et al. , "Supplementary cementitious materials on chloride binding in hardened cement paste," *Cement and Concrete Research* , vol. 42, no. 1, pp. 1-7, 2012.
- [38] K. De Weerdt and et al. , "Hydration mechanism of ternary Portland cements containing limestone powder and fly ash," *Cement and Concrete Research* , vol. 41, no. 3, pp. 279-291, 2011.
- [39] R. W. Mielenz and O. Glantz, "Effect of calcination on natural Pozzolans," in *Symposium on use of Pozzolanic Materials in Mortars and Concrete*, New York, 1950.
- [40] B. Marsh and R. Day, "Pozzolanic and cementitious reactions of fly ash in blended cement pastes," *Cement and Concrete Research*, vol. 41, no. 3, pp. 301-310, 1988.
- [41] M. Ghrici, S. Kenai and M. Said-Mansour, "Mechanical properties and durability of mortar and concrete containing natural pozzolana and limestone blended cement," *Cement and Concrete Composites*, vol. 29, no. 7, pp. 542-549, 2007.
- [42] K. Weerdt, "Hydration mechanism of ternary Portland cements containing limestone powder and fly ash," *Cement and Concrete Research* , vol. 41, no. 3, pp. 279-291, 2011.
- [43] M. Moesgaard, "Physical performance of blended cements containing calcium aluminosilicate glass powder and limestone," *Cement and Concrete Research* , vol. 41, no. 3, pp. 359-364, 2011.

- [44] K. Vance and et al., "Hydration and strength development in ternary Portland cement blends containing Limestone and fly ash or metakaolin," *Cement and Concrete Composites* , 2013.
- [45] L. Vizcaino, A. Alujas, F. Martirena and K. Scrivener, "Low clinker cements made with ternary blends of calcined clay and limestone: Influence of grinding procedures on mechanical properties," *Cement and Concrete Composites*, 2013.
- [46] S. Kumar and et al. , "Mechanical activation of granulated blast furnace slag and its effect on the properties and structure of Portland slag cement," *Cement and Concrete Composites* , vol. 30, no. 1, pp. 679-685, 2008.
- [47] S. Murgier, H. Zanni and D. Gouvenot, "Blast furnace slag cement: a ^{29}Si and ^{27}Al NMR study," *2004*, vol. 7, no. 2, pp. 389-394, *Comptes Rendus Chimie*.
- [48] S. Pal, A. Mukherjee and S. Pathak, "Investigation of hydraulic activity of ground granulated blast furnace slag in concrete," *Cement and Concrete Research* , vol. 33, no. 4, pp. 1481-1486, 2003.
- [49] K. Yeau and E. Kim, "An experimental study on corrosion resistance of concrete with ground granulated blast-furnace slag," *Cement and Concrete Research* , vol. 35, no. 2, pp. 1391-1399, 2005.
- [50] S. Kosmatka , B. Kerkhoff and W. C. Panarese, "Fly ash, slag, silica fume, and natural pozzolans in design and control of concrete mixtures," Portland Cement Association , Washington D.C, 2003.
- [51] K. D. Hoang, "Hardening accelerator for fly ash blended cement," NTNU - Norwegian University of Science and Technology , Trondheim , 2012.
- [52] T. Ostnor, "Alternative Pozzolans as supplementary cementitious materials in concrete," SINTEF, Trondheim, 2007.
- [53] W. A. Gutteridge, "On the dissolution of the interstitial phase in Portland cement," *Cement and Concrete Research* , vol. 9, no. 3, pp. 319-324, 1979.
- [54] H. Cement, "<https://www.hanson.co.uk/en/products/cement>," Hanson Cement - Under Heidelberg Cement , Liverpool, 2004.
- [55] J. S. Damtoft, J. Lukasik , D. Herfort, D. Sorrentino and E. M. Gartner , "Sustainable development and climate change initiatives," *Cement and Concrete Research* , vol. 38, pp. 115-127, 2008.
- [56] R. J. Lauf, L. A. Harris and S. S. Rawlston, "Pyrite framboids as the source of magnetite spheres in fly ash," *Environmental Science and Technology* , vol. 16, pp. 218-220, 1982.

- [57] P. Mounanga and et al. , "Improvement of the early-age reactivity of fly ash and blast furnace slag cementitious system using limestone filler," *Material and Structures* , vol. 44, no. 2, pp. 437-453, 2011.
- [58] M. E. A. Thiery , "Influence of carbonation on the microstructure and moisture properties of cement-based materials case of materials prepared with fly ash," 2011.
- [59] T. Bier, J. Kropp and H. Hilsdorf, "Formation of silica gel during carbonation of cementitious system containing slag cements," in *Natural Pozzolan in Concrete*, Paris, 1989.
- [60] M. A. Czerewko, J. C. Cripps, J. M. Reid and C. G. Duffel, "The development of a new testing protocol for sulphur compounds in structural backfills," *Quarterly Journal of Engineering Geology and Hydrogeology* , vol. 36, pp. 133-142, 2003.
- [61] J. Schieber and G. Baird, "On the origin and significance of Pyrite spheres in Devonian black shales of north america," *Journal of Sedimentary Research*, vol. 71, pp. 155-166, 2001.
- [62] P. S. Mozley, "Relation between depositional environment and the elemental composition of early diagenetic siderite," *Geology*, vol. 17, pp. 704-709, 1989.
- [63] R. Talero and V. Rahhal, "Calorimetric comparison of portland cements containing silica fume and metakaolin," *Journal of Thermal Analysis and Calorimetry* , vol. 96, pp. 383-393, 2009.
- [64] P. Greil, "Structure and Mechanical Properties," in *Glass and Ceramics* , Nuernberg, University of Erlangen, 2002.
- [65] H. Justnes, "Condensed silica fume as a cement admixture," in *Structure and Performance of Cements* , Taylor and Francis, 2009.
- [66] C. J. Mueller, "Pozzolanic activity of natural clay minerals with respect to environmental geotechniques," ETH , Zuerich , 2005.
- [67] S. H. Kosmatka , B. Kerkhoff and W. C. Panarese, "Fly ash, slag, silica fume, and natural pozzolans," Portland Cement Association , 2003.
- [68] F. Massaza, "Pozzolanic Cements," *Cement and Concrete Composites*, vol. 15, pp. 185-214, 1993.
- [69] C. S. Poon, S. C. Kou and L. Lam, "Compressive strength, chloride diffusivity and pore structure of high performace metakaolin and silica fume concrete," *Construction and Building Materials*, vol. 20, pp. 858-865, 2006.
- [70] D. Herfort, "Portland limestone cements," ECRA , Dusseldorf, 2012.

- [71] A. Ipavec and et al., "Chloride binding into hydrated blended cements: The influence of limestone and alkalinity," *Cement and Concrete Research* , vol. 48, no. 0, pp. 74-85, 2013.
- [72] K. D. Ingram and K. E. Daugherty, "A review of limestone additions to Portland cement and concrete," *Cement and Concrete Composites* , vol. 13, no. 3, pp. 165-170, 1991.
- [73] T. Vuk , V. Tinta, R. Gabrovsek and V. Kaucic, "The effect of limestone addition, clinker type and fineness on properties of Portland cement," *Cement and Concrete Research* , vol. 31, no. 1, pp. 135-139, 2001.
- [74] S. Tsivilis , G. Batis, E. Chaniotakis, G. Grigoriadis and D. Theodossis, "Properties and behavior of limestone cement concrete and mortar," *Cement and Concrete Research*, vol. 30, no. 10, pp. 1679-1683, 2000.
- [75] I. Elkhadiri, A. Diouri, A. Boukhari, J. Aride and E. Puertas , "Mechanical behavior of various mortars made by combined fly ash and limestone in Portland cement," *Cement and Concrete Research* , vol. 32, no. 10, pp. 1597-1603, 2002.
- [76] F. Bergaya and G. Legaly, "General Introduction: clays, clay minerals, and clay science," in *Handbook of clay science* , Developments in clay science, Elsevier, 2006.
- [77] S. Guggenheim and R. T. Martin, "Definition of clay and clay minerals: Joint report of the AIPEA nomenclature and CMS nomenclature committees," *Clay and Clay Minerals* , vol. 43, pp. 255-256, 1995.
- [78] D. M. Moore and R. C. Reynolds , X-ray diffraction and identification and analysis of clay minerals, New York: Oxford University Press , 1989.
- [79] C. K. Wentworth , "A scale of grade and class terms for clastic sediments," *Journal of Geology*, vol. 30, pp. 377-392, 1922.
- [80] H. L. Alling , "A metric grade scale for sedimentary rocks," *The journal of Geology* , vol. 51, pp. 259-269, 1943.
- [81] D. Heim, "Tone und Tonminerale - Grundlagen der sedimentologie und mineralogie," Ferdinand Enke Verlag, Stuttgart, 1990.
- [82] H. H. Murray, "Applied clay mineralogy - occurrences, processing and application of Kaolins, Bentonites, Palygorskite-Sepiolite, and common clays," *Developmenets in Clay Science*, vol. 2, 2007.
- [83] E. Galan, "Genesis of clay minerals," in *Handbook of clay science* , Elsevier, 2006, p. Vol.1.

- [84] M. Okrusch and S. Matthes, Mineralogie - ein einfuehrung in die spezielle mineralogie petrologie und lagerstättenkunde, Heidelberg: Springer Verlag, 2005.
- [85] E. H. De Carlo , G. M. McMurtry and H. W. Yeh, "Geochemistry of hydrothermal deposits from loihi submarine volcano," *Earth and Planetary Science Letters* , vol. 66, pp. 438-449, 1983.
- [86] H. Kristmannsdottir, "Alteration of basaltic rocks by hydrothermal-activity at 100-300C," *Developments in Sedimentology* , vol. 27, pp. 359-367, 1979.
- [87] K. Marumo and K. H. Hattori, "Seafloor hydrothermal clay alteration at Jade in the back-arc Trough: mineralogy, geochemistry and isotope characteristics," *Geochimica et Cosmochimica Acta* , vol. 63, pp. 2785-2804, 1999.
- [88] G. M. McMurtry, W. Chung-Ho and Y. Hsueh-Wen , "Chemical and isotopic investigations into the origin of clay minerals from Galapagos hydrothermal mounds field," *Geochimica et Cosmochimica Acta*, vol. 47, pp. 475-489, 1983.
- [89] F. Press and R. Siever, Allgemeine geologie - Einfuehrung in das system erde, Heidelberg: Spektrum Akademischer Verlag, 2003.
- [90] www.mindat.org.
- [91] R. Grim, "Applied clay mineralogy," McGraw-Hill , I.S.I.T.E, 1962.
- [92] F. Bergaya, B. K. Theng and G. Lagaly, Handbook of clay science, Vol.1 : Elsevier , 2011.
- [93] J. K. Mitchell, Fundamentals of soil behavior, 3rd Edition : John Wiley & Sons Inc. , 2005.
- [94] P. S. L. Souza and D. C. C. Dal Molin, "Viability of using calcined clays, from industrial by-products, as pozzolans of high reactivity," *Cement and Concrete Research* , vol. 35, no. 10, pp. 1993-1998, 2005.
- [95] R. Fernandez Lopez, "Calcined clayey soils as a potential replacement for cement in developing countries," EPFL, Laussane, 2009.
- [96] A. C. Dunham, "Development in industrial mineralogy: I. The mineralogy of brick-making," *Proc. Geo. Soc, Yorkshire*, 1992.
- [97] L. Stoch, "Application of thermal analysis methods in studies of siliciclastic rocks of various levels," *Geologiczne*, Warsaw, 1974.
- [98] H. Justnes, I. Meland , J. O. Bjorgum, J. Krane and T. Skjetne, *Advance Cement Research*, vol. 3, p. 105, 1990.

- [99] T. R. Jones, J. Bensted and P. Barnes , "Metakaolin as a pozzolanic addition to concrete," Spon Press, London, 2002.
- [100] A. Palomo, M. T. Blanco-Varela, M. L. Granizo, F. Puertas , T. Vazquez and M. W. Grutzeck, "Chemical stability of cementitious materials based on metakaolin," *Cement and Concrete Research* , vol. 29, pp. 997-1004, 1999.
- [101] J. Davidovits , "High alkali cements for 21st century concretes," in *Concrete Technology, Past, Present and Future*, ACI-V, 1994, pp. 383-397.
- [102] G. Malquori, "Portland-pozzolana cement," in *4th international symposium on the chemistry of cement* , Washington , 1962.
- [103] W. Kurdowski and H. Pomadowski , "Selected properties of concretes modified with varying content of metakaolinite additive," *Silicates Ind.*, Warsaw, 2001.
- [104] P. s. De Silva and F. P. Glasser, "Phase relations in the system $\text{CaO-Al}_2\text{O}_3\text{-SiO}_2\text{-H}_2\text{O}$ relevant to metakaolincalcium hydroxide hydration," *Cement and Concrete Research* , vol. 23, pp. 627-639, 1993.
- [105] J. A. Larbi and J. M. Bijem, "Effect of mineral admixtures on the cement paste aggregate interface," in *4th CANMET/ACI International Conference on fly ash, silica, fume, slag, and natural pozzolans in concrete*, Istanbul , 1992.
- [106] G. A. Chadbourn, "Chloride resistance and durability of cement paste and concrete containing metakaolin," University of Aston, Aston, 1997.
- [107] H. Xu and J. S. J. Van Deventer, "The geopolymerisation of alumino-silicate minerals," *International Journal of Mineral Processing* , vol. 59, no. 3, p. 247, 2000.
- [108] Q. Mohsen and N. Y. Mostafa, "Investigating the possibility of utilising low kaolinitic clays in production of geopolymer bricks," *Ceramic. Silik* , vol. 54, no. 2, p. 160, 2010.
- [109] H. H. Murray, "Applied clay mineralogy: Occurences, Processing and Application of Kaolins, Bentonites, Palygorskite-sepoilite, and common clays," *Development in Clay Science*, vol. 2, 2007.
- [110] A. Shvarzman, K. Kovler, G. S. Grader and G. E. Shter, "The effect of dehydroxylation/amorphization degree on pozzolanic activity of kaolinite," *Cement and Concrete Research* , vol. 33, pp. 405-416, 2003.
- [111] C. He, E. Makovicky and B. Osbaeck, "Thermal stability and pozzolanic activity of calcined illite," *Applied Clay Science*, vol. 9, no. 5, pp. 337-354, 1995.

- [112] C. He, E. Makovicky and B. Osbaeck, "Thermal stability and pozzolanic activity of raw and calcined mixed-layer mica-smectite," *Applied Clay Science* , vol. 17, no. 3, pp. 141-161, 2000.
- [113] C. He, E. Makovicky and B. Osbaeck, "Thermal treatment and pozzolanic activity of sepiolite," *Applied Clay Science* , vol. 10, no. 5, pp. 337-349, 1996.
- [114] C. He, E. Makovicky and B. Osbaeck, "Thermal treatment and pozzolanic activity of Na-and Ca-montmorillonite," *Applied Clay Science* , vol. 10, no. 5, pp. 351-368, 1996.
- [115] C. He, E. Makovicky and B. Osbaeck, "Thermal stability and pozzolanic activity of calcined kaolin," *Applied Clay Science* , vol. 9, no. 3, pp. 165-187, 1994.
- [116] C. He, B. Osbaeck and E. Makovicky, "Pozzolanic reactions of six principal clay minerals: Activation, reactivity assessments and technological effects," *Cement and Concrete Research* , vol. 25, no. 8, pp. 1691-1702, 1995.
- [117] B. B. Sabir, S. Wild and J. Bai, "Metakaolin and calcined clay as pozzolans for concrete: a review," *Cement and Concrete Composites*, vol. 23, no. 1, pp. 441-454, 2001.
- [118] R. Siddique and J. Klaus, "Influence of metakaolin on the properties of mortar and concrete: A review," *Applied Clay Science* , vol. 43, no. 4, pp. 392-400, 2009.
- [119] R. C. Mielenz, K. T. Greene and N. C. Schieltz, "Natural pozzolan for concrete," *Economic Geology*, vol. 46, no. 3, pp. 311-328, 1951.
- [120] C. Bich, J. Ambroise and J. Pera, "Influence of degree of dehydroxylation on the pozzolanic activity of metakaolin," *Applied Clay Science* , vol. 44, no. 3, pp. 194-200, 2009.
- [121] M. Murat, "Hydration reaction and hardening of calcined clays and related minerals: II. influence of mineralogical properties of the raw-kaolinite on the reactivity of metakaolinite," *Cement and Concrete Research* , vol. 13, no. 4, pp. 511-518, 1983.
- [122] A. Chakouk, B. Samet and T. Mnif, "Study on the potential use of Tunisian clays as pozzolanic material," *Applied Clay Science* , vol. 33, no. 2, pp. 276-281, 2006.
- [123] A. Tironi and et al. , "Kaolinitic calcined clays: Factors affecting its performance as pozzolans," *Construction and Building Materials* , vol. 28, no. 1, pp. 276-281, 2012.
- [124] B. Samet , T. Mnif and M. Chaabouni, "Use of a kaolinitic clay as a pozzolanic material for cements: Formulation of blended cement," *Cement and Concrete Composites*, vol. 29, no. 10, pp. 741-749, 2007.

- [125] G. Habert and et al., "Effects of the secondary minerals of the natural pozzolans on their pozzolanic activity," *Cement and Concrete Research* , vol. 38, no. 7, pp. 963-975, 2008.
- [126] S. Salvador , "Pozzolan properties of flash-calcined kaolinite: A comparative study with soak-calcined products," *Cement and Concrete Research* , vol. 25, no. 1, pp. 102-112, 1995.
- [127] G. I. Cadoret , "Method and installation for the dehydroxylation treatment of aluminium silicate," SGMCM, Paris , 2004.
- [128] P. Ptacek, F. Frajkorova, F. Soukal and T. Opravil, "Kinetics and mechanism of three stages of thermal transformation of kaolinite to metakaolinite," *Powder Technology* , vol. 264, pp. 439-445, 2014.
- [129] R. C. Mackenzie and M. Society , "The differential thermal investigation of clays," Mineralogical Society (Clay Mineral Group), 1957.
- [130] B. R. Ilic, A. A. Mitrovic and L. R. Milicic, "Thermal treatment of kaolin clay to obtain metakaolin," *Hemijaska Industrija*, vol. 64, pp. 351-356, 2010.
- [131] A. Souiri, H. Kazemi Kamyab , R. Snellings , R. Naghizadeh, F. Golestani-Fard and K. Scrivener , "Pozzolan activity of mechanochemically and thermally activated kaolins in cement," *Cement and Concrete Research* , vol. 77, pp. 47-59, 2015.
- [132] A. Shvarzman, K. Kovler, G. S. Grader and G. E. Shter, "The effect of dehydroxylation/amorphization degree on pozzolanic activity of kaolinite," *Cement and Concrete Research* , vol. 33, pp. 405-416, 2003.
- [133] A. Alujas, R. Fernandez, R. Quintana , K. L. Scrivener and F. Martirena , "Pozzolan reactivity of low grade kaolinite clays: Influence of calcination temperature and impact of calcination products on OPC hydration," *Applied Clay Science* , vol. 108, pp. 94-101, 2015.
- [134] M. Murat and C. Comel , "Hydration reaction and hardening of calcined clays and related minerals. III. Influence of calcination process of kaolinite on mechanical strength of hardened metakaolinite," *Cement and Concrete Research* , vol. 13, pp. 631-637, 1983.
- [135] K. J. D. Mackenzie and D. E. Rogers, "Thermal and Mossbauer studies of iron-containing hydrous silicates : I. Nontronite," *Thermochimica Acta*, vol. 18, pp. 177-196, 1977.

- [136] G. W. Brindley and M. Nakahira, "The Kaolinite-Mullite reaction series: II, metakaolin," *Journal of the American Ceramics Society* , vol. 42, no. 7, pp. 314-318, 1959.
- [137] G. W. Brindley and M. Nakahira, "The Kaolinite-Mullite reaction Series: I, A survey of outstanding problems," *Journal of the American Ceramic Society*, vol. 42, no. 7, pp. 311-314, 1959.
- [138] G. W. Brindley and M. Nakahira, "The Kaolinite-Mullite reactions series: III, the high-temperature phases," *Journal of the American Ceramic Society* , vol. 42, no. 7, pp. 319-324, 1959.
- [139] R. C. Mielenz, N. C. Schieltz and M. E. King, "Thermogravimetric analysis of clay and clay-like minerals," *Clays and Clay Minerals* , vol. 2, pp. 285-314, 1953.
- [140] R. San Nicolas , "Approche performantielle des beton avec metakaolins obtenus par calcination flash," Universite Paul Sabatier-Toulouse III, Toulouse, 2011.
- [141] J. Sanz and et al., "Aluminum-27 and Silicon-29 Magic-Angle spinning nuclear magnetic resonance study of the kaolinite-mullite transformation," *Journal of the American Ceramic Society* , vol. 71, no. 10, pp. C418-C421, 1988.
- [142] R. Fernandez, F. Martirena and K. L. Scrivener, "The origin of the pozzolanic activity of calcined clay minerals: A comparison between kaolinite, illite and montmorillonite," *Cement and Concrete Research* , vol. 41, no. 1, pp. 113-122, 2011.
- [143] C. E. White and et al. , "Density functional modeling of the local structure of kaolinite subjected to thermal dehydroxylation," *Journal of Physical Chemistry A*, vol. 114, no. 4, pp. 4988-4996, 2010.
- [144] C. E. White and et al . , "Structure of kaolinite and influence of stacking faults: Reconciling theory and experiment using inelastic neutron scattering analysis," *Journal of Chemical Physics*, vol. 138, no. 19, 2013.
- [145] J. Lambert, W. Millman and J. Fripiat, "Revisiting kaolinite dehydroxylation: A silicon-29 and aluminum-27 MAS NMR study," *Journal of the American Chemical Society* , vol. 111, pp. 3517-3522, 1989.
- [146] E. M. J. Berodier, "Impact of the supplementary cementitious materials on the kinetics and microstructural development of cement hydration," EPFL, Laussane, 2015.

- [147] A. Tironi, M. A. Trezza, A. N. Scian and E. F. Irassar, "Assessment of pozzolanic activity of different calcined clays," *Cement and Concrete Composites*, vol. 37, pp. 319-327, 2013.
- [148] A. S. Silva, A. Gameiro, J. Grilo, R. Veiga and A. Velosa, "Long-term behavior of lime-metakaolin pastes at ambient temperature and humid curing condition," *Applied Clay Science*, Vols. 88-89, pp. 49-55, 2014.
- [149] J. Ambroise, M. Murat and J. Pera, "Hydration reaction and hardening of calcined clays and related minerals. IV. Experimental conditions for strength improvement on metakaolinite minicylinders," *Cement and Concrete Research*, vol. 15, pp. 83-88, 1985.
- [150] K. De Weerd, M. B. Haha, G. Le Saout, K. O. Kjellsen, H. Justnes and B. Lothenbach, "Hydration mechanism of ternary Portland cements containing limestone powder and fly ash," *Cement and Concrete Research*, vol. 41, pp. 279-291, 2011.
- [151] M. Zajac, A. Rossberg, G. Le Saout and B. Lothenbach, "Influence of limestone and anhydrite on the hydration of Portland Cements," *Cement and Concrete Composites*, vol. 46, pp. 99-108, 2014.
- [152] V. L. Bonavetti, V. F. Rahhal and E. F. Irassar, "Studies on the carboaluminate formation in limestone filler-blended cement," *Cement and Concrete Research*, vol. 31, pp. 853-859, 2001.
- [153] B. Lothenbach, G. Le Saout, E. Gallucci and K. Scrivener, "Influence of limestone on the hydration of Portland cements," *Cement and Concrete Research*, vol. 38, pp. 848-860, 2008.
- [154] G. Kakali, S. Tsivilis, E. Aggeli and M. Bati, "Hydration products of C3A, C3S and Portland cement in the presence of CaCO₃," *Cement and Concrete Research*, vol. 30, pp. 1073-1077, 2000.
- [155] T. Matschei, B. Lothenbach and F. P. Glasser, "The role of calcium carbonate in cement hydration," *Cement and Concrete Research*, vol. 37, pp. 551-558, 2007.
- [156] O. Chowaniec, "Limestone addition in cement," EPFL 5335, Lausanne, 2012.
- [157] C. E. Tsivilis, S. E. Badogiannis, G. Pathoulas and A. Ilias, "A study on the parameters affecting the properties of Portland limestone cements," *Cement and Concrete Composites*, vol. 21, pp. 107-116, 1999.
- [158] T. Ramlochan and M. Thomas, "Effect of metakaolin on external sulfate attack," ACI Special Publication, 2000.

- [159] N. M. Al-Akhras, "Durability of metakaolin concrete to sulfate attack," *Cement and Concrete Research*, vol. 36, no. 9, pp. 1727-1734, 2006.
- [160] C. Shi, D. Wang and A. Behnood, "Review of Thaumasite sulfate attack on cement and concrete," *Journal of Materials in Civil Engineering*, vol. 24, no. 12, pp. 1450-1460, 2012.
- [161] A. Skaropoulou and et al., "Use of mineral admixtures to improve the resistance of limestone cement concrete against thaumasite from of sulfate attack," *Cement and Concrete Composites*, 2013.
- [162] F. Bellmann and J. Stark, "Prevention of thaumasite formation in concrete exposed to sulphate attack," *Cement and Concrete Research*, vol. 38, no. 10, pp. 1154-1161, 2007.
- [163] F. Bellmann and J. Stark, "The role of calcium hydroxide in the formation of thaumasite," *Cement and Concrete Research*, vol. 38, no. 10, pp. 1154-1161, 2008.
- [164] T. Chappex and K. L. Scrivener, "The influence of aluminium on the dissolution of amorphous silica and its relation to alkali silica reaction," *Cement and Concrete Research*, vol. 42, no. 12, pp. 1645-1649, 2012.
- [165] M. N. Saad, W. P. De Andrade and V. A. Paulon, "Properties of mass concrete containing an active pozzolan made from clay," *Concrete International*, vol. 4, no. 07, pp. 59-65, 1982.
- [166] K. De Weerd, K. Kjellsen, E. Sellevold and H. Justnes, "Synergy between fly ash and limestone powder in ternary cements," *Cement and Concrete Composites*, vol. 33, no. 1, pp. 30-38, 2011.
- [167] B. Lothenbach, T. Matschei, G. Moschner and F. P. Glasser, "Thermodynamic modelling of the effect of temperature on the hydration and porosity of Portland cement," *Cement and Concrete Research*, vol. 38, no. 1, pp. 1-18, 2008.
- [168] W. P. Inskeep and P. R. Bloom, "An evaluation of rate equations for calcite precipitation kinetics at less than 0.01 atm and pH greater than 8," *Geochimica et Cosmochimica Acta*, vol. 49, no. 10, pp. 2165-2180, 1985.
- [169] B. Lothenbach, G. Le Saout, E. Gallucci and K. Scrivener, "Influence of limestone on the hydration of Portland cements," *Cement and Concrete Research*, vol. 38, no. 6, pp. 848-860, 2008.
- [170] G. Menendez, V. Bonavetti and E. F. Irassar, "Strength development of ternary blended cement with limestone filler and blast-furnace slag," *Cement and Concrete Composites*, vol. 25, no. 1, pp. 61-67, 2003.

- [171] M. Antoni, J. Rossen, F. Martirena and K. Scrivener, "Cement substitution by a combination of metakaolin and limestone," *Cement and Concrete Research* , vol. 42, pp. 1579-1589, 2012.
- [172] M. Antoni, "Investigation of Cement substitution by blends of calcined clays and limestone," Ecole Polytechnique Federale de Lausanne , Thesis 6001, 2013.
- [173] H. H. Murray, "Applied clay mineralogy today and tomorrow," *Clay Minerals* , vol. 34, pp. 39-49, 1997.
- [174] D. Herfort and J. S. Damtoft, "US Patent WO 2010/130511 A1 - Portland Limestone Calcined Clay Cement," World Intellectual Property Organization , 2010.
- [175] G. Habert, N. Choupay , G. Escadeillas, D. Guillaume and J. M. Montel , "Clay content of argillites: Influence on cement based mortars," *Applied Clay Science* , vol. 43, pp. 322-330, 2008.
- [176] C. L. Christ , J. C. Hathaway , P. B. Hostetler and A. O. Shepard , "Palygorskite: new X-ray data," *American Mineralogy*, vol. 54, pp. 198-205, 1969.
- [177] F. Bullerjahn, M. Zajac and D. Nied, "US Patent 2017/0267586 A1 - Supplementary cementitious materials made of aluminium silicate and dolomite," 2017.
- [178] J. Dupuis and D. Chazay, "US 2007/028925 A1 - Installation and process for calcining a mineral load containing a carbonate in order to produce a hydraulic binder," 2007.
- [179] G. Meynardi, "US patnet 1988/4737191 - Process for manufacturing hydraulic binders," 1988.
- [180] D. J. Cook and R. N. Swaing , "Cement Replacement Materials," *Concrete Technology and Design*, pp. 40-72, 1985.
- [181] IPCC, "Revised 1966 IPCC Guidelines for national greenhouse gas inventories," IPCC/OECD/IEA, Paris, 1997.
- [182] WBCSD, "World business council for sustainable developmenet - Cement industry energy and CO2 performance " Getting the numbers right", " CSI, Washington DC, 2009.
- [183] "Environmental characteristics of clays and clay mineral deposite (usgs.gov)," 2015.
- [184] E. Benhelal , G. Zahedi , E. Shamsaei and A. Bahadori, "Global strategies and potentials to curb CO2 emissions in cement industry," *Journal of Cleaner Production* , vol. 12, pp. 142-161, 2013.

- [185] G. Kalkali and et al. , "Thermal treatment of kaolin: the effect of mineralogy on the pozzolanic activity," *Applied Clay Science* , vol. 20, pp. 73-80, 2001.
- [186] S. Wild and et al. , "Relative strength, pozzolanic activity and cement hydration in superplasticised metakaolin concrete," *Cement and Concrete Research*, vol. 26, no. 10, pp. 1537-1544, 1996.
- [187] M. A. Caldarone, K. A. Gruber and R. G. Burg, "High reactivity metakaolin : a new generation mineral admixture," *Concrete International*, vol. 1, pp. 37-40, 1994.
- [188] D. S. Snell, "Review of synthesis and properties of Tobermorite, C-S-H (I), and C-S-H gel," *Journal of American Ceramic Society* , vol. 58, no. 7-8, pp. 272-295, 1975.
- [189] G. L. Kaousek, "Crystal chemistry of hydrous calcium silicates: (I) substitution of aluminum in lattice of Tobermorite," *Journal of American Ceramic Society* , vol. 40, no. 3, pp. 74-80, 1957.
- [190] M. Jackson, E. Landis , P. Brune , M. Vitti and Q. Li, "Mechanical resilience and cementitious processes in imperial roman architectural mortar," *PNAS*, pp. 18484-18489, 2007.
- [191] M. Luxan, F. Madruga and J. Savedra, "Rapid evaluation of pozzolanic activity of natural products by conductivity measurements," *Cement and Concrete Research* , vol. 4, pp. 63-68, 1989.
- [192] H. Murray, "Traditional and new application for Kalinite, smectite, and palygorskite: a general overview," *Applied Clay Science* , pp. 207-221, 2000.
- [193] R. Rodriguez-Camacho and R. Uribe-Afif, "Importance of using the natural pozzolans on concrete durability," *Cement and Concrete Research* , vol. 2, pp. 441-454, 2002.
- [194] K. Scrivener , M. Antoni , A. Favier and F. Martirena , "Low carbon cement based on clinker, calcined clay and limestone," *Journal of the American Ceramic Society* , pp. 1901-1910, 2011.
- [195] A. Ipavec and et al. , "Carboaluminate phases formation during the hydration of calcite-containing portland cement," *Journal of the American Ceramic Society* , vol. 94, no. 4, pp. 1238-1242, 2011.
- [196] J. Pera , S. Husson and B. Guilhot, "Influence of finely ground limestone on cement hydration," *Cement and Concrete Composite*, vol. 21, no. 2, pp. 99-105, 1999.
- [197] E. Worrell, L. Price, N. Martin , C. Hendriks and L. Ozawa Meida, "Carbon dioxide emission from the global cement industry," *Annual Review of Energy and The Environment* , pp. 303-329, 2001.

